The Dynamic Simulation and Control of Aluminium Smelting Cells

by

A. Wright B.Sc.

Department of Chemical and Process Engineering
University of Newcastle-upon-Tyne
Newcastle-Upon-Tyne, NE1 7RU
England

Submitted in partial fulfilment of the requirements for the degree of Doctor of Philosophy at the University of Newcastle-Upon-Tyne

June, 1993

ABSTRACT

The Hall-Héroult process for the electrolytic production of aluminium from alumina is a costly and difficult to control process that has remained little changed since the early 1900's. A decreasing trend in the real profitability of the process since 1930 has made it necessary for aluminium smelting companies to reduce the expenditure in all aspects of the process in order to remain viable. The most significant proportion of the costs of production is the utilisation of the electrical energy required to produce the aluminium but improvements such as the rebuilding of the cell superstructure in modern low resistance materials are precluded by the capital costs involved. It is generally only possible to make improvements by changes in operational procedure and the control strategy.

The introduction of computer control and data logging systems has reduced the manual involvement in cell operation and has allowed control strategies to be standardised on all cells within a smelter. Although the data logging facilities have increased the amount of data that can be collected and improved the understanding of the operation of aluminium smelting cells, the control of remains difficult due to the lack of data that can be continuously monitored, in particular the alumina concentration in the electrolyte.

In this work, a mathematical model for the dynamic simulation of aluminium smelting cells is developed. A simulation program is then written incorporating the exact control algorithms from Anglesey Aluminium's CELTROL computer control system for half-break cells. The aim of the simulation is to study the effects of different operating conditions and control strategies upon the operation of the cell. The simulation is developed to be modular in nature allowing different control systems and cell models to be easily incorporated and tested.

The model is evaluated against data from Anglesey Aluminium's half-break cells and is successful in predicting the behaviour of these cells. The simulation is also used in plant trials to investigate the effects of different metal tapping schedules.

Acknowledgements

I would like to express my sincere thanks to the following people who have enabled me to carry out this research:

My supervisor, Dr Allen Wright for his continual support, encouragement and advice during the course of this research.

The staff of the Department of Chemical and Process Engineering for their help and advice.

George Guelfo, David Salt, Tony Sargent and Mike Wilson of Anglesey Aluminium for their support and practical assistance in developing the model and their patience when showing me the ropes of aluminium production.

The technical staff of Anglesey Aluminium also for their advice and assistance.

The UK Science and Engineering Research Council and Anglesey Aluminium for financial support.

Finally, I would like to thank my wife, Suzanne for her moral support and encouragement during the overly long course of this research.

To my wife, Suzanne and our son, Toseland...

Contents

List of Figures

List of Tables

1.0 History of the Hall-Héroult Process

The electrolytic process for the industrial production of aluminium was patented in 1886 by P.L.T Héroult in France and, independently, by C.M. Hall in the U.S.A. The process involves the electrolysis of a molten solution of alumina in cryolite and utilises the reaction

$$2Al_2O_3 + 3C \rightarrow 3CO_2 + 4Al$$

The carbon anode is oxidised during the reaction and aluminium is produced at the cathode. The function of the cryolite is as a solvent for the alumina and is required because of the high melting point of pure alumina.

The electrolytic production of aluminium increased from about 40 tonnes in 1890 to 450 tonnes in 1895. The first commercial cells were operated with a current of 4000 A and an energy consumption of 42 kWh per kg aluminium. Even under these conditions, the price of aluminium was only half that of the cheapest aluminium produced by the Ste.-Claire Deville process which was based upon the chemical reduction of aluminium by sodium. Improvements in cell construction were quickly made and by 1893 the energy consumption had already dropped to 25 kWh per kg aluminium. The Hall-Héroult process had been shown to be commercially viable and remains little changed to the present day.

1.1 Main Costs Of Production

Figure 1.1 shows how the cost of production and the price commanded for aluminium has changed over the 55 years prior to 1985.[1] It is clear that overall there has been a trend of decreasing real profitability since 1930. This is not due to a similar trend in capital costs but rather to the increase in world production especially due to the building of large smelting plants in developing nations to utilise cheap electricity and labour.

For a smelter to remain in business it is necessary to reduce the expenditure of all cost centres. The typical percentage cost of each stage is shown in order of priority in table 1.1. The actual values may vary significantly from smelter to smelter especially with regard to comparisons between developed and developing countries.

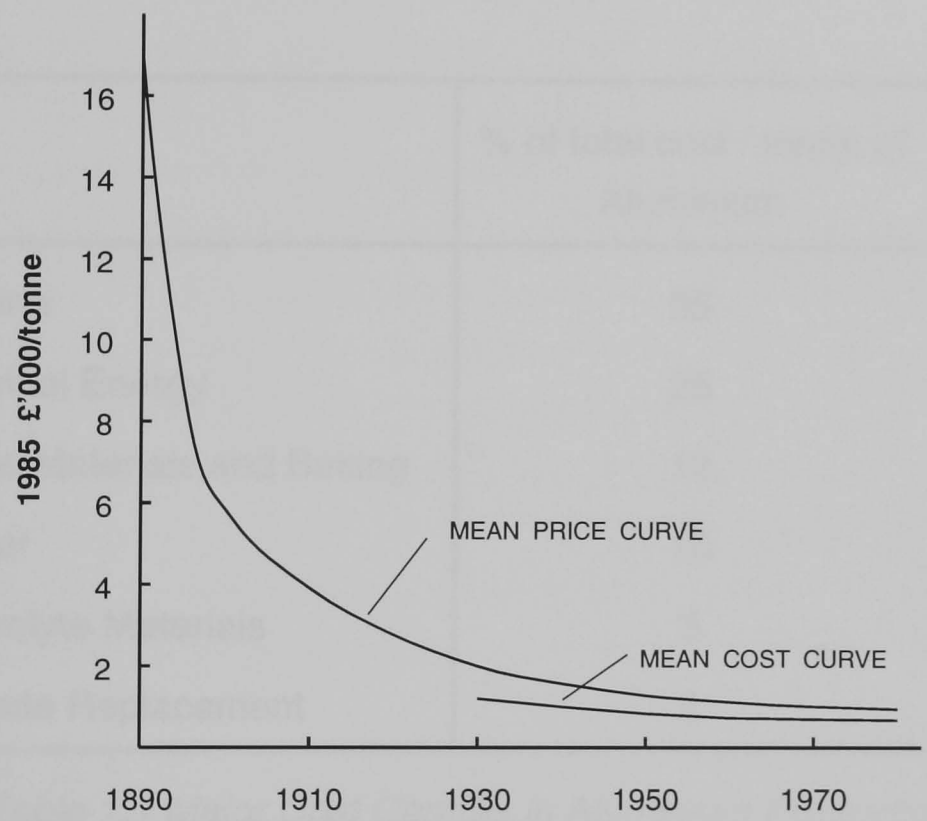

Figure 1.1 Cost of Production against Time

	% of total cost / tonne of Aluminium
Alumina	35
Electrical Energy	25
Anode Materials and Baking	12
Labour	10
Electrolyte Materials	3
Cathode Replacement	2

Table 1.1 Major Cost Centres in Aluminium Production

The cost for replacement of the carbon cathode shown in table 1.1 is based upon a cathode life of at least 3 years. If operation of the cell results in the cathode life being much less than this, then replacement costs can become highly significant.

It can be seen that the cost of the alumina fed to the cell constitutes the largest percentage of the cost of producing aluminium. In the case of Anglesey Aluminium, the alumina is purchased upon the open market and, although alumina quality affects the operation of the cell, control over alumina costs does not rest directly with the smelter.

The most significant area for improvement is therefore in the utilisation of electrical energy. The other costs, anode, cathode and electrolyte materials, are all inter related with energy costs. Minimum energy consumption cannot be achieved without good quality anodes which depends upon efficient baking. A well designed cathode and a properly maintained electrolyte composition are also essential. The key area within this section is the day to day operation and control strategy of the cell. Increased computerisation has not only reduced the manual involvement in cell operation, thus saving on labour costs, but has also allowed control to be standardised on all cells within a smelter. The data logging facilities have increased the amount of data collected for individual cells aiding in the understanding of the process.

The capital costs involved preclude such methods of improvement of energy utilisation as the rebuilding of the cell superstructure with modern low resistance materials. With a computer control system already installed in a smelter, as at Anglesey Aluminium, it is cheaper to make improvements by changes in the control strategy for a cell. The aim of this work is to produce a fully dynamic model of an aluminium production cell to study the effects of different operating conditions and control strategies upon the operation of the cell.

1.1.1 Fundamental relationships

There are three fundamental relationships that dictate the way in which an aluminium cell should be operated. These are

increasing current and increasing current efficiency gives increased productivity

$I \uparrow + CE \uparrow \rightarrow$ productivity $\uparrow$

increasing current efficiency and decreasing voltage gives decreased energy usage

$CE \uparrow + V \downarrow \rightarrow$ energy $\downarrow$

increasing current density gives increased energy usage

$cd \uparrow \rightarrow$ energy $\uparrow$

In order to increase current for improved productivity without increasing the energy consumption of the cell it is therefore necessary to maintain the same current density by increasing the anode area.

The economic climate will dictate which of these relationships are the most important. At times when aluminium can command a high price it is desirable to increase productivity at the expense of energy efficiency, while at times when the price of aluminium is low it is most important to reduce production costs by increasing energy efficiency. Any control strategy must be able to accommodate both these situations without the need for major changes to the hardware.

1.2 Types of Cell

A commercial aluminium cell operates by passing a current through an electrolyte consisting primarily of alumina dissolved in molten cryolite. The ratio of the mass of sodium fluoride to aluminium fluoride in the electrolyte is modified from the natural 1.5 of cryolite by the addition of excess aluminium fluoride. Other additives, such as calcium and lithium fluorides may be used to reduce the melting point of the electrolyte and to improve the operability of the cell. The electrolyte, or "bath", is therefore a complex mixture of molten salts.

The aluminium cell or "pot" consists of a steel box lined with a refractory brick. A carbon cathode block lies on top of this and forms the floor of the cell. The cell is partially filled with the molten electrolyte and carbon anodes are immersed in the electrolyte. A layer of molten aluminium, the "pad" forms at the surface of the cathode block protecting the carbon from the corrosive action of the electrolyte and taking over the role of the cathode.

The sidewalls of the cell are designed to allow a crust or "ledge" of frozen cryolite to form around the cell. This contains the molten electrolyte and is very important in protecting the cell lining from corrosion and in maintaining the thermal stability of the cell.

The only really fundamental technological change to the Hall-Héroult process has been the development of the Soderberg anode. Unlike the original cells which used an anode manufactured from coke and pitch baked in a separate process, the Soderberg anode uses the heat generated within the operating cell to bake these materials in situ. Coke and pitch are fed in the top of the anode and by the time they reach the reacting surface they have baked into solid carbon. The two types of cell are shown schematically in figures 1.2 and 1.3.

The Soderberg anode was first patented in 1923 by the Norwegian company Elektrokemisk and utilised a horizontal stub that entered the anode from the sides. It was later shown that the fumes from the top of the anode might be carcinogenic and the difficulty of containing them put the Soderberg cell out of fashion. All new smelters since the middle of the 1970's have used the older 'pre-bake' anode technology. Research has however continued on the Soderberg cell and methods of operation have been developed that make this type of cell safe to use although it has not gained widespread popularity.

As its name implies, the pre-bake anode is manufactured in a separate process to that of electrolysis of aluminium. Whilst this may not be so energy efficient, it does have advantages in that the anode quality may be more easily controlled and poor anodes rejected before they are used in the cell. An aluminium reduction cell contains banks of anodes made up of individual units, in the case of an Anglesey Aluminium cell, two banks of

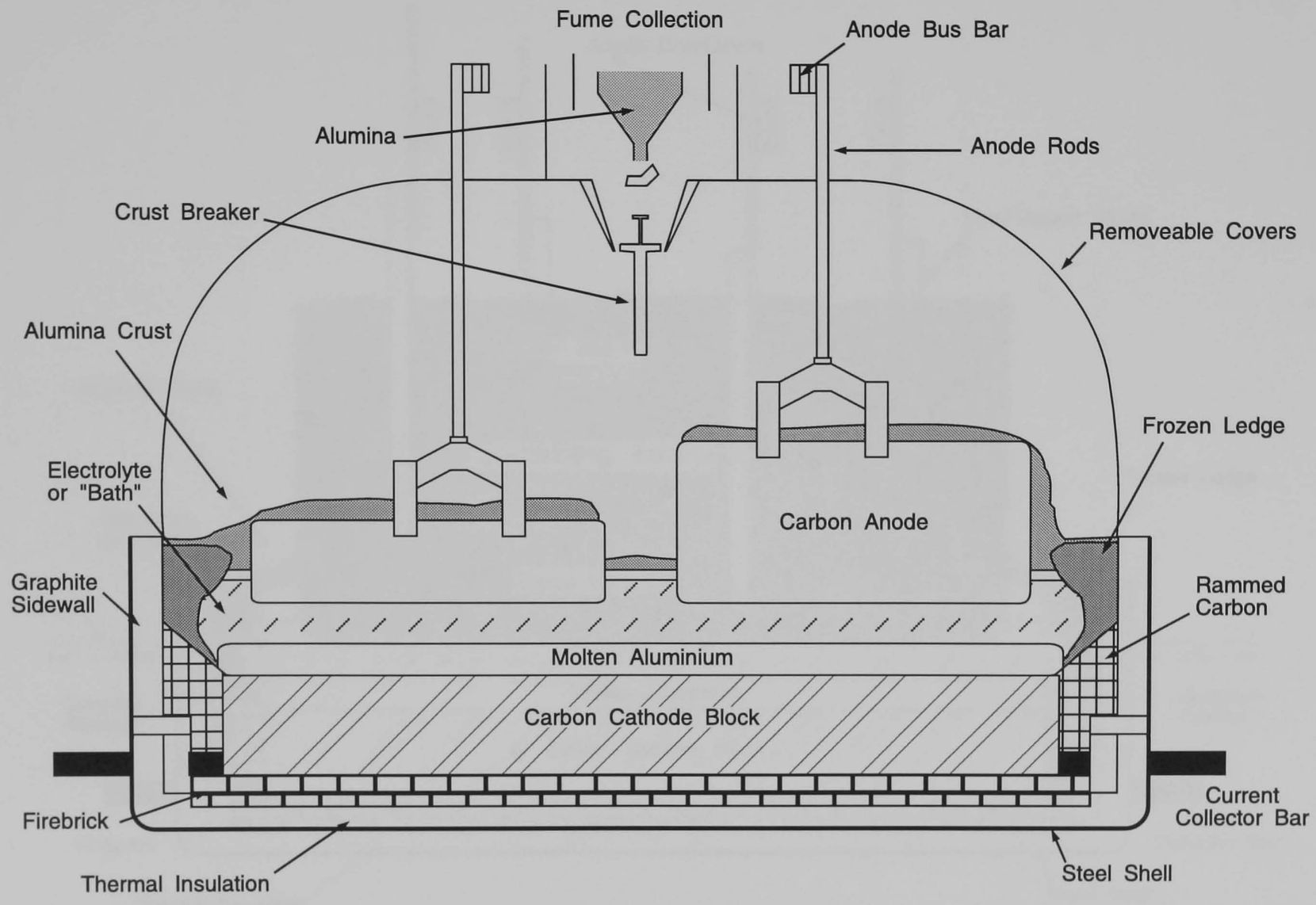

Figure 1.2 Schematic Diagram of the Hall Héroult Cell

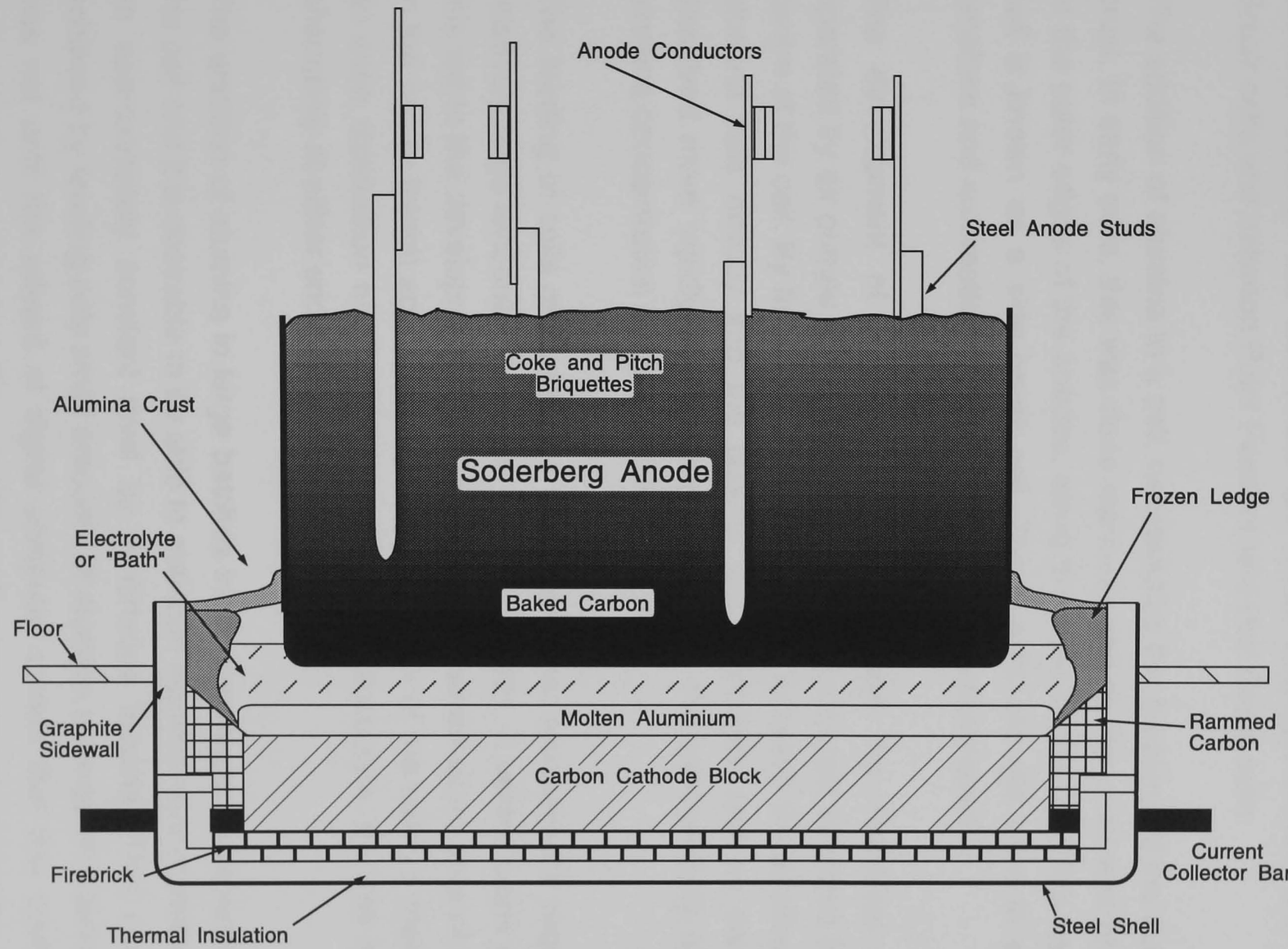

Figure 1.3 Schematic Diagram of the Soderberg Cell

nine anodes making a total of eighteen in all. As the anode carbon is consumed by the reaction, individual anodes must be changed at periodic intervals.

Pre-bake cells are further classified by the method and frequency of alumina feeding. The distinctions are made between Centre and Side Break cells and between Point Feeders and Half Break cells.

The addition of alumina to a cell, necessitates the breaking of the surface crust. In early cells, this was done manually and so the crust was broken at the outer edges of the anodes, along the sides of the cell. This type of cell is known as a side break cell. These cells are still used in some smelters and automatic crust breakers have been developed.

The development of mechanical crust breakers for individual cells operated by air pumps allowed for the positioning of crust breakers in the centre of the cell. By feeding in the centre trench between the anodes, the alumina falls directly into the bulk of the electrolyte and so can be dissolved more rapidly giving some increase in the controllability of the alumina concentration within the cell.

The feeding of cells manually and by simple timer mechanisms required relatively large amounts of alumina fed infrequently. In centre break cells, this led to the development of half breakers. These break an area of crust in the centre trench approximately half the length of the cell. To maintain an even distribution of alumina throughout the electrolyte, the cell is fed alternately at either end.

The addition of alumina in large batches introduces large disturbances to the cell and it is desirable to be able to maintain alumina concentrations at an approximately constant level by continuous feeding. This can be achieved by feeding only small amounts of alumina at frequent intervals. It was not until the advent of digital computer control that this could be successfully implemented. The resulting cell is termed a point feeder since it only breaks a small area of crust in the centre trench, sufficient for the addition of small amounts of alumina in the electrolyte.

1.3 Operation of a Prebake Cell

The day to day running of an aluminium smelting cell consists of a number of operations that must be performed at different intervals. The actions may be carried out either automatically or manually and the decision as to which action to take may be based upon measured data, as in the case of voltage control, or upon the experience of the cell room operator, as in the case of voltage set point changes.

1.3.1 Data Sampling

In order for decisions to be made on what actions to take in the operation of an aluminium cell, information on the cell behaviour must be collected. This consists of data obtained both by chemical analysis and by observation by the operators of the general appearance of the cell. The data can then be divided into two categories, one which can be measured and one which is observed.

Measured data

Measurable data includes such information as electrolyte composition, cell voltage and electrolyte temperature. These can be measured with different degrees of accuracy and frequency. For example, cell voltage can be measured almost continuously and with good accuracy. At Anglesey Aluminium, the control computer, CELTROL, samples individual cell voltages at a 100 ms interval to 4 significant figures accuracy. Bath composition, on the other hand, is measured by mass spectroscopy methods which are time consuming and cannot be performed continuously. Although the accuracy of this method is good for individual samples, it is not necessarily representative of the whole cell.

Observed data

Appearance of the cell. eg flame colour, crust cover, movement of the electrolyte. This type of data is subjective and depends upon the experience of the operator for its usefulness.

1.3.2 Alumina feed

Alumina is fed to a cell by breaking the surface crust and allowing the crust along with a mass of alumina to fall into the electrolyte. The alumina on the surface is then replenished and a new crust allowed to form.

In early cells, the crust was manually broken using metal bars and alumina was shovelled onto the surface. The process was first mechanised by the development of large vehicular crust breakers that were driven along the sides of the cells breaking the crust by means of a cogged wheel. Alumina was replenished from a following truck.

Mechanisation of individual cells used mechanical crust breakers activated by simple timers or, more recently, digital computers. At Anglesey Aluminium, the breakers are suspended over the centre trench and are operated by air motors. The motors are operated with compressed air that is controlled by a solenoid activated either by a control computer or manually. The motors control both the breaking of crust by movement of the breaker beam and the dumping of alumina onto the surface by operation of a gate in the alumina hopper suspended above the cell. There are two sets of motors allowing individual feeding at both the tap end and duct end of the cell.

1.3.3 Voltage control

The control of voltage drop across the aluminium reduction cells is by movement of the anodes, thus altering the inter electrode gap. Continuous voltage control has only been possible with the advent of computers that can continuously monitor the cell resistance. The inter electrode gap is adjusted by movement of the anode bus bar. Thus the anodes are moved as a block and there is no facility for the automatic movement of individual anodes. As with the feed system, the bus bars are moved by air motors using compressed air. The solenoid switches may be activated either by computer or manually with the anode movement being measured in time rather than distance.

1.3.4 Anode effect termination

Anode effect occurs when the alumina concentration in the electrolyte falls below a critical level. During anode effect, the composition of the bath results in dewetting of the anodes and the formation of large bubbles on the anode surface. The bubbles are predominately carbon tetrafluoride and present a physical barrier to the passage of current into the electrolyte. Anode effect cannot, therefore, be terminated by the simple addition of alumina to the melt thus increasing the alumina concentration above the critical level, but requires the breaking of the gas bubble layer for alumina addition to be effective. This may be achieved by a number of methods.

The first stage in anode effect termination is to agitate the electrolyte by movement of the anodes. This works by both pumping the gas from under the anodes and by bringing the anodes in contact with streamers of aluminium from the metal pad. This causes momentary short circuiting and allows the gas to disperse without being replenished by electrolysis. Other methods of dispersal of the gas by anode movement have involved the tilting of the anodes[2].

Should anode movement not be successful in terminating anode effect then a green wood pole is pushed into the electrolyte. As the pole burns violently the combustion gases cause a great deal of turbulence in the electrolyte. This both physically breaks up the bubble and causes shorting due to the throwing up of aluminium streamers from the pad allowing the bubble to dissipate.

In Anglesey Aluminium's cells, operated under the CELTROL control system, anode effects are terminated automatically. The computer performs a sequence of the following actions:

raise anode
lower anode
break duct end
break tap end
feed duct end
feed tap end

A typical sequence for a half break cell is shown in figure 1.4. Actions may be repeated a number of times by means of a loop construct or bypassed on the condition of the anode effect being terminated by means of a jump. These sequences are very effective with a 95% kill efficiency on point feed cells. If the sequence fails in terminating anode effect, however, the traditional method of using a green pole is still used.

1.3.5 Metal tapping

Molten aluminium metal is removed from the cell by a process known as tapping. The process has changed little over the years and is still performed manually.

In the early aluminium cells, aluminium was removed by simply breaking a hole in the cell wall, allowing the molten metal to pour out and plugging the hole with clay. This was hot and dangerous work and later methods made use of compressed air to siphon the aluminium into a receptacle known as a crucible.

Aluminium is still tapped by this method. A hole is broken in the surface crust of the cell at the tap end and the spout of the crucible lowered into the molten metal. The crucible is attached to the compressed air line on the cell superstructure and aluminium is siphoned off until a desired amount has been removed. The crucible is then moved on to the next cell that requires tapping and the procedure is repeated. At Anglesey, one crucible is used to tap four cells before it is taken across to metal servicing to be formed into ingots. This amounts to a total mass of metal of about 4000 kg.

The method of measuring the aluminium collected remains crude, although electronic scales have recently been introduced to the pot room. The depth of aluminium in the cell is measured by means of a dipstick and the difference between this measurement and the desired depth determines the amount of metal to be tapped. Until recently, the metal tapped into the crucible was also measured using a dipstick but the introduction of electronic scales has seen a change over to tapping by weight. This has seen some improvement in the accuracy of tapping as the scales can be reset between each cell. Using the dipstick method, the

	0	1	2	3	4	5	6	7	8	9
0	BRAK	LOWR	7.0	W006	JUMP	15	RAIS	5.0	DUMP	BRAK
1	LOWR	5.0	W006	LOP0	1 6	~RAIS	3.0	W005	RAIS	3.0
2	W006	BRAK	W005	DUMP	DUMP	DUMP	DUMP	----	----	----
3	----	----	----	----	----	----	----	----	~----	----
4	----	----	~----	----	----	----	----	W005	BRAK	W010
5	DUMP	DUMP	DUMP	DUMP						

Failure Location at: 15
Plus seconds up at: 2
Acc. Feed Point at: 50
AVC on at: 38

Feed loop start at: 38
Failure feed seq at: 0
Max feed allowed at: 34
Feed loop end at: 42

Sequence for Half Break Cell

	0	1	2	3	4	5	6	7	8	9
0	DUMP	BRAK	LOWR	2.0	DUMP	BRAK	JUMP	13	LOWR	2.0
1	DUMP	BRAK	W001	LOP0	1 8	JUMP	24	RAIS	3.0	DUMP
2	BRAK	LOWR	3.0	W001	LOP1	217	BRAK	DUMP	~RAIS	2.0
3	BRAK	DUMP	W002	RAIS	2.0	W002	RAIS	0.0	~W045	BRAK
4	DUMP	DUMP	~----	----	----	----	----	----	----	----
5	----	----	----	----						

Failure Location at: 28
Plus seconds up at: 2
Acc. Feed Point at: 50
AVC on at: 38

Feed loop start at: 38
Failure feed seq at: 0
Max feed allowed at: 34
Feed loop end at: 42

Sequence for Point Feed Cell

Nomenclature

BRAK	activate crust breaker, both ends
DUMP	activate alumina dump, both ends
LOWR n.n	lower anode bus for n.n seconds
RAIS n.n	raise anode bus for n.n seconds
JUMP nn	jump to location nn if anode effect terminated
Wnnn	pause nnn periods of 6 seconds = nnn × 6 seconds
LOPn xxyy	loop to position yy allowed xx times if AE not terminated eg LOP0 1 6 loops to 6. Loop is allowed only once
~	decision point

Figure 1.4 Anode Effect Termination Sequences

aluminium tapped was measured cumulatively with the result that if one cell was over tapped then subsequent cells would be under tapped.

1.3.6 Addition of raw materials other than alumina

As well as replenishing alumina being consumed by electrolysis it is necessary to maintain the composition of the electrolyte by the addition of other raw materials. The principal of these is aluminium fluoride which is added to maintain the ratio of sodium fluoride to aluminium fluoride in the bath. This ratio fluctuates for a number of reasons:

1. Sodium oxide in the alumina feed reacts with aluminium fluoride in the melt to form sodium fluoride.

2. Aluminium fluoride is consumed by electrolysis during anode effect.

3. Both sodium fluoride and aluminium fluoride are volatilised off the bath surface. This becomes more severe at higher temperatures.

4. The melting and freezing of the ledge causes changes in the ratio. This is because the electrolyte freezes with a ratio closer to that of pure cryolite at about 1.40. In an electrolyte with a ratio less than that of cryolite this effectively means that sodium fluoride freezes preferentially to aluminium fluoride with the result that freezing causes the ratio to decrease and vice versa.

This tends to result in a ratio greater than that desired and it is necessary to add aluminium fluoride to the bath. This is simply done by adding bagged aluminium fluoride to the cell at a fixed interval. A typical example would be 25 kg aluminium fluoride per day. The bag of aluminium fluoride is simply thrown into the centre trench of the cell and broken into the electrolyte by the action of the crust breakers.

The overall mass of electrolyte in the cell may also need replenishing. This can be due to volatilisation of the electrolyte in a hot or poorly covered cell or due to the splashing of bath out of the cell by anode movements. The need to add electrolyte is not common in mature cells but is necessary in cells shortly after start up. This is done by siphoning electrolyte from a

mature cell using the same method and crucible as for metal tapping and blowing it into the receiving cell using compressed air.

1.3.7 Anode change

During electrolysis, the carbon anodes are consumed by the formation of carbon dioxide. In a pre bake cell, it is therefore necessary to replace the anodes periodically. The time between anode changes depends upon the size of the anodes and the operational current of the cell. At Anglesey, with the cells operating at 151 kA and with anode dimensions of 80×134× 80 cm, the 18 anodes in a cell are all replaced over a 21 day period. Problems in cell operation or poor quality anodes may cause spiking, in which an anode short circuits to the aluminium pad due to uneven consumption of the anode, or burn offs, where poor covering of the top of the anode allows surface oxidation around the metal stub allowing the anode to break free and fall into the electrolyte, which necessitates un-scheduled anode changes.

A spent anode is pulled from the cell by a small 'crane'. If necessary, the hole is then enlarged to take the new anode by drilling out the frozen sidewall. The new cold anode is then placed in the electrolyte and bolted to the bus bar. The positioning of the anode on the bus bar is adjusted to give a uniform inter electrode gap within the cell. As the metal pad has a humped profile due to the electromagnetic forces in the cell, the depth of the anode relative to the bus bar is determined by its position within the cell.

A new anode is much colder than the electrolyte into which it is being placed, about 200 °C compared to 970 °C. A layer of frozen electrolyte immediately forms around the anode effectively insulating it both electrically and thermally. This frozen layer melts as the anode warms over the next 30 hours but in order to increase the speed of melting it is common practise to set a new anode low so that the frozen layer can contact the metal pad. This prevents the freeze from growing and heat is then conducted more speedily through the freeze and into the anode. On the day following the anode change, the new anode is raised to the correct position.

1.3.8 Sampling

Many of the parameters important to the operation of an aluminium cell cannot be determined continuously or with great accuracy. Such parameters are the bath and metal compositions, liquid levels, cathode and ledge profiles and cell temperatures.

The bath and metal compositions are determined on a daily or weekly basis by mass spectroscopy. Samples are removed from the cell in small crucibles and processed in the laboratory. Impurity levels in the aluminium, as well as being important for quality control can indicate whether the aluminium is corroding the cathode or sidewalls leading to a cell failure. The bath composition results can be strongly affected by the sample point in the cell if, for example, the sample is taken close to a sludge pocket. Alumina concentrations are not available from mass spectroscopy but may be determined by chemical analysis. It is not possible, however, to distinguish between dissolved and undissolved alumina.

Liquid levels are determined on a daily basis by inserting an iron rod into the bath and metal. When the rod is removed from the cell, the aluminium and electrolyte freeze, the metal forming a thinner layer. The depth of each section may then be read off against a rule on the side of the cell and the values used to decide the amount of metal that should be tapped.

The corrosive environment of the electrolyte makes the use of permanent thermocouples for the continuous measurement of temperature unsuitable. Temperatures are measured on a daily basis using a hand held thermocouple enclosed in an iron sheath. The sheath is slowly dissolved by the bath and must be periodically replaced. The temperature of a cell varies throughout the feed cycle and depends upon the position of the thermocouple in the electrolyte. Temperature measurements taken by this method are therefore more useful in indicating that the cell is operating in the correct temperature range than giving an absolute temperature measurement. Continuous temperature measurement has been attempted by embedding thermocouples in the cathode structure when the cell is built. This can give a better indication of temperature fluctuations but has a number of drawbacks. An additional hardware interface is required for each cell to monitor the thermocouples and this is

expensive. If a thermocouple fails, it cannot be replaced, and some means of discarding the results from failed thermocouples is therefore necessary.

The determination of cathode and ledge profiles is labour intensive but can be useful in evaluating the performance of a cell. The covers are removed from the cell and holes punched through the crust between the anodes and in the centre trench. Iron rods are then inserted in these holes and the height of a reference marker is determined with a theodolite.

In the absense of high quality quantitative data regarding the operation of a cell, an exception oriented process control system can be developed. Such a system is described by S Manaktala [3] and is designed to assign numerical severity values to visually monitored process exceptions in the reduction cell. These exceptions are compiled as a potline survey and action taken through specifically designed follow up procedures.

The severity indices for individual cells are stored and can be used in conjunction with quantitative results to isolate and control chronic cell operation problems.

The potline survey can be carried out by the line supervisor and cell operators and includes an assessment of the flame coloration, pot voltage and stability, carbon dusting in the bath and liquid levels. A severity index of 0.5 to 3 is assigned to a cell having one or more abnormal attributes and the required corrective action may then be taken.

References

1 Kent, J. H., *"A Review of the Hall-Héroult Process"*, Aluminium and Energy, A 100 Year Partnership Conference and Exhibition, Bangor, Sept 18-19, 1986

2 Saksvikronnig, T., Valsvik, G., and Hove, S. J., *"Anode Effect Quenching by Anode Tilting"*, AIME Light Metals, 1982, p553-558

3 Manaktala, S., "Process Control Techniques for Reduction Cell Operation", AIME Light Metals, 1971, pp165

2.0 Process Modelling

The usual method for evaluating the effect of changes in operating parameters upon a system is by actual physical experimentation. This type of experimentation can be very successful but its range is limited by cost and safety. An alternative approach is to construct a mathematical model of the process and experiment with the model instead of reality. This has a number of advantages:

1) Understanding of the system

The development of the model demands an understanding of the process to be gained. This insight enables extraneous "confusion factors" to be stripped away from the problem allowing relationships between variables to be seen more easily. Examples of confusion factors include changes in raw materials or in ambient temperatures.

2) Economics

In industry, the cost of raw materials, labour etc can restrict extensive experimentation. A suitably detailed process model however, is able to quantitatively describe the behaviour of a system under a variety of different operating conditions. Simulation studies can provide large amounts of data at little cost and in a fraction of the time required for experimentation. The cost of simulation of an experiment that results in failure is no more than for one that is successful.

3) Optimisation and design

Simulation studies make it possible to study the effects of changes in operational parameters easily and under reproducible conditions, which is not always guaranteed in practise. Operation of the process can therefore be optimised with respect to these parameters. The effect of changes in design of the process may also be evaluated.

As fewer people need to be involved, especially at shop floor level, this allows for the precise evaluation of designed operating procedure and operational targets.

4) Safety

Mathematical models can be used to simulate process behaviour under extreme conditions that cannot be practically or safely reproduced in the laboratory.

5) Computer control

The advent of cheap powerful computers in the past few years has permitted vastly more detailed and realistic analysis to be carried out for a reasonable degree of effort and cost. More complex and fundamental physical principles have been employed to formulate mathematical models of processes. This has resulted in many processes being comprehensively better monitored and controlled and has allowed control systems to be designed without undue disturbance to the process.

6) Operator training

Process modelling makes possible the training of process operators using simulation rather than real plant. Operators can gain first hand experience in dealing with conditions that may occur only infrequently in process operation as well as the implementation of safety procedures.

2.1 Model Development

The development of a process model will usually progress through a number of stages:

1) Problem formulation and data acquisition

The first stage in model development is to decide upon the ultimate requirements of the model. Following this, it necessary to obtain a detailed knowledge of the complete system. This is usually achieved by using literature data together with some experimental measurements. In formulating a complete process model the complete process must be studied, including such aspects as operator intervention. This last is best investigated by spending a period on-site involved in the day to day operation of the process.

2) Model description

Once comprehensive data on the system has been accumulated, the process can be broken down into a number of relevant inter-reacting sub-systems. From this a verbal description or conceptual model of the complete process can be constructed.

3) Constructing the model

Each block in the conceptual model represents a system of algebraic and differential equations. These equations are based on mass and energy balances incorporating the appropriate kinetic expressions for the rates of all relevant reactions and the rates of transport of mass and energy within the system.

4) Model evaluation

Once the model has been developed it is necessary to evaluate it against experimental data. If the models predictions do not compare favourably under all operating conditions then it is unlikely to be correct. In this case, either the model must be modified or a new model developed.

5) Application

If the model is able to accurately describe the system, it can then be used to simulate process behaviour under a wide range of conditions. Any assumptions made in development of the model must be taken into consideration, however, as the model may not be valid if these do not apply.

In practise, real problems are often ill defined and difficult to specify. Lack of experimental data often makes it difficult to construct a model that provides a balanced image of reality. Too simple a model may fail because it does not adequately describe the process, while too complex a model will contain a great number of unknown parameters and variables and may not be mathematically tractable. The complexity of model constructed therefore depends upon the accuracy required and the application for which the model is intended.

2.2 Types of Model

The simplest form of process model is an empirical relationship between a number of process variables. This type of model is usually developed by regression analysis of experimental data and does not consider the mechanisms of the process. These relationships can be extremely accurate but are strictly only valid for conditions that lie within the range of experimental data used in analysis. Empirical relationships cannot adequately describe the dynamic effects of a complete process but are invaluable in describing the individual blocks. For example, in an aluminium reduction cell, the relationship between electrolyte density and composition and temperature is well described by an empirical relationship[1]. However, a similar equation relating cell current efficiency to a number of process variables[2] is unsuitable for use in a dynamic model as it is based upon average conditions in the cell over a period of time and does not take account of the actual mechanism of current efficiency loss.

2.2.1 Lumped parameter models

A lumped parameter model makes the assumption that process variables are uniform throughout space. This allows the dynamics of a system to be represented by ordinary, rather than partial, differential equations. A classic example is the assumption that a stirred tank reactor is well mixed. The temperature throughout the reactor can then be assumed uniform. All resistance to heat transfer from the reactor to the jacket is 'lumped' together in the stagnant film at the vessel wall. In many applications this treatment is highly successful.

2.2.2 Distributed parameter models

In a distributed parameter model, consideration is taken of the variation of process variables in space. This can allow for greater accuracy but the number of calculations, and hence time, required for solution will also be increased. The modelling of a tubular reactor provides a good example of a distributed model. The composition and temperature of the reactants flowing through the reactor vary both axially and radially. A complete dynamic model requires the solution of partial differential equations in both directions.

The complexity of distributed parameter models may be reduced by reducing the model dimensionally. In the tubular reactor example, if flow through the reactor is turbulent then the system may be assumed well mixed in the radial direction. Only one set of differential equations, representing conditions along the length of the reactor, need then be solved. What is lost in neglecting the radial distribution may be gained in the simplicity of the resulting model.

2.2.3 Static and dynamic models

The major distinction that must be made in describing process models is that between static and dynamic models. A static model describes a steady state system or system at a given instant with a defined average of states. A dynamic model describes the changing states of the system through time as the process is subject to internal and external disturbances. The application for which the model is required determines the type of model that should be used.

For example, static models have been developed for the cathode lining of an aluminium cell. These models are complex and can accurately predict the temperature profiles for a particular set of conditions. The model is used to design cathode linings based upon average conditions expected in operating the cell.

In practise, these conditions vary throughout time. It would be possible to construct a dynamic model of the heat balance and use it to simulate the changes in temperature profiles through time. However, the inter-relationships of all factors involved are extremely complex and the resulting model would provide little improvement over the present method of cathode design.

Dynamic models on the other hand, often sacrifice high levels of detail accorded by multi dimensional distributed models for the sake of both mathematical tractability and computation time. An obvious example of this approach is that used in classical control system analysis where linear ordinary differential equations are used throughout. These equations are often 'fitted' to process responses to known disturbances. Although this approach may provide sufficient detail for controller tuning, it provides little data for other engineering design.

2.3 Choice of Model

A large model of a complete system, such as that of an aluminium reduction cell, consists of many sub-models representing balance and rate equations. The choice of model for a particular sub-system, e.g. dynamic, static, lumped, distributed etc, is, however, more often the subjective choice of the model builder and is partly based upon the experience and skill in model building and partly upon the computing power available. The recent advent of more powerful computers has allowed the accuracy and complexity of dynamic models to be increased.

The following chapter describes some of the models available in literature for the simulation of aluminium reduction cells.

References

1 Kvande, H. and Rorvik, H., *"The Influence of Bath Density in Aluminium Electrolysis"*, AIME Light Metals, 1985 pp671-678

2 Grjotheim, K., Haupin, W. E. and Welch, B. J., *"Current Efficiency--Relating Fundamental Studies to Practice"*, AIME Light Metals, 1985 pp679-694

3.0 Mathematical Models of Aluminium Reduction Cells

Process models may be divided into two main groups, static and dynamic models. A static model represents a steady state system, or a system at a given instant in time, for a defined average of states.

For example, many static models exist for the heat balance in a cell. In fact the heat flows will vary with changes in temperature, instantaneous cell voltage, electrolyte composition and depth, cell design and ambient temperature. These models assume constant values for all such parameters.

3.1 Static Models

3.1.1 Model of M.C. Richard [1]

M.C. Richard developed a model in 1975 to predetermine the effect of operating parameters resulting from design changes to the anode and cathode configurations. The model is essentially a steady state analysis of the cell and was designed to define the Revere cell in the range 102 to 122 kA only. As the model was designed for use only in a narrow range on either side of the existing operating conditions first order equations were used to describe many of the physical effects. The model made no attempt to model many non-steady state and human factors such as metal tapping. Heat losses were calculated by treating the cell as a furnace and fixing a desired operating temperature from which the losses could be calculated by a steady state heat balance.

Whilst this simple approach is adequate for the investigation of the long term effects of changes within some operational parameters it cannot be used to describe the dynamic effect of a cell to frequent changes such as alumina feed and anode effect.

3.1.2 Model of B. Sulmont and G. Hudault [2]

Sulmont and Hudault developed a two dimensional thermoelectric model for all categories of prebake pots. The model can be employed to determine the equilibrium profile of frozen electrolyte, determine temperatures and voltages at any point and calculate current densities in

both the electrolyte and metal pad and peripheral heat flows. The pot is represented by a cross section of unit thickness and divided into a number of elements. In the particular instance published, 1683 intersections were necessary for the required accuracy. Temperatures and potentials are determined at each intersect by iterative calculation from an arbitrary initial solution.

This type of model is very accurate in the simulation of steady state profiles but the number of equations involved make it unsuitable for use in dynamic simulation. Its primary use is therefore in the design or modification of pots.

3.2 Dynamic Models

3.2.1 Model of S.R Blake [3]

S.R Blake developed a model for the variation of alumina concentration in industrial Hall-Heroult cells. The model did not attempt a full solution of the heat balance as this was outside the scope of the study. Variations in the heat balance were accounted for by a random variation in the dissolution rate of the alumina into solution. The model is based upon a simple, but quantitative, picture of the mass transfer processes whereby alumina passes from the solid to the dissolved state.

This model is quite successful at predicting the trends of alumina concentration for different methods of feeding but is not complex enough to investigate control strategies based upon the heat balance as well as the mass balance. It also cannot predict the power usage of a cell and so an optimum alumina concentration must be assumed.

3.2.2 Model of A. Ek and G. E. Fladmark [4]

A. Ek and G. E. Fladmark developed a model for calculating the dynamic behaviour of a complete cell. The cell is divided into a number of coarse elements for which the the energy and mass balances are formulated. The effect of the chemical reactions, supply of materials to the bath and the freezing and melting of the side freezes are included in the model. This model cannot produce such accurate profiles across the cell as multi-

nodal models like that presented by Sulmont and Hudault but accurately describes the working of the cell. The accuracy of this type of model depends upon the accuracy of the individual assumptions and expressions used within it.

3.2.3 Model of T. Hashimoto and H.Ikeuchi [5]

T. Hashimoto and H. Ikeuchi also developed a dynamic model of a complete cell similar to that developed by Ek. In this case the cell was divided into eight parts and partial differential equations with regard to heat flux were solved by the finite difference equation. In addition to the calculations in Ek's model the boundary layer between the melts and the side freezes was treated as a diffusion layer giving a more accurate estimation of bath composition in this section.

3.3 Models for the Dissolution of Alumina

Although the mechanism for the dissolution of alumina in cryolite is not clear, much work has been done on the measurement of the dissolution rate of alumina. The experiments have all been done on a lab scale and the methods of adding alumina and measuring the dissolution rate have varied considerably.

Thonstad et al[6] introduced alumina into a well stirred cryolite melt at 1030 °C and measured the dissolution ie the time required for the disappearance of alumina particles in the melt by a visual method. Gerlach[7] put a tablet of alumina into a stirred melt at 1015 °C and removed samples at regular intervals which were analysed for alumina content. At the International Course on Process Metallurgy of Aluminium in Trondheim[8], Thonstad cites four different types of experimental technique

1. Vigorous stirring causing effective dispersion of alumina (Thonstad[6], Winkhaus[9])
2. Moderate stirring allowing formation of agglomerates with the electrolyte

3. Dissolution from a stagnant bottom layer of loose alumina or sintered alumina (Gerlach[7])
4. Rotating discs of sintered alumina

Experiments have also been done on the effect of the alumina feeding method. Maeda et al[10] did bench scale experiments using industrial composition bath at 970 °C. Alumina was poured into the melt through a funnel and the dissolution time measured visually. No stirring was done and a large number of alumina samples were collected world wide.

The rate determining step for alumina dissolution in industrial cells has not been clarified. According to the Thonstad[8] it may be

- mass transfer
- heat transfer
- chemical reaction

Mass transfer models fall into two categories

1. Zeroth order models - dissolution rate independent of alumina concentration

2. First order models - dissolution rate proportional to alumina concentration

3.3.1 Zeroth order models

Both Gerlach[7] and Thonstad[6] postulate a zeroth order mechanism at low concentrations of alumina of the type

$$r = k_0 \cdot \exp\left(\frac{E}{RT_0} \cdot \left(1 - \frac{T_0}{T}\right)\right) \qquad [g\ cm^{-2}\ min^{-1}] \qquad (1)$$

where r = rate of dissolution of alumina g cm^{-2} min^{-1}
k_0 = reaction rate constant cm min^{-1}
E = activation energy kcal $mole^{-1}$
R = universal gas constant kcal $mole^{-1}$ K^{-1}
T_0 = reference temperature °K
T = reaction temperature °K

For concentrations greater than 3-6 wt% alumina they seem to agree with a first order model. The accuracy of measurement by both visual and chemical methods is not very great and it may be that at low concentrations the driving force for dissolution is such that a first order mechanism is involved. Other workers[9] have found first order correlations at all concentrations.

3.3.2 First order models

A first order model for dissolution rate is given by Asbjornsen[11] after Kachanovskaya[12] as

$$r = k_0 \cdot \exp\left(\frac{E}{RT_0} \cdot \left(1 - \frac{T_0}{T}\right)\right) \cdot (c^* - c) \qquad \left[g\ cm^{-2}\ min^{-1}\right] \qquad (2)$$

where c^* = saturation concentration of alumina in melt g cm^{-3}

c = concentration of alumina in melt g cm^{-3}

This is agreed with by a number of workers (Winkhaus[9], Jain[13]) and Thonstad[6] and Gerlach[7] at higher concentrations. The experimental work by Maeda et al[10] showed the dissolution rate of alumina to be proportional to the concentration for the slow feeding method.

Much work has also been done on the dissolution of alumina from sludge[14,15,16,17,18]. All workers agree that the rate of dissolution from sludge is slower than the initial rate for dispersed alumina particles in suspension. This would be expected as the specific area of particles in suspension will be many times greater than that of sludge but may also be due to sub cooling and the formation of agglomerates. The rate of dissolution is also reduced by the presence of aluminium between the sludge and bath forming a physical barrier. Thonstad[14] determined that sludge dissolved by a first order reaction when exposed to bath with 4-5 % alumina by weight at 1020 °C.

3.3.3 Heat transfer models

In heat transfer control models the rate of dissolution is determined by the rate at which frozen cryolite melts from around clusters of particles of alumina powder. A.N. Bagshaw et al[19] investigated the effect of operating

conditions on the dissolution of alumina by using a voltammetric technique for the in-situ measurement of dissolved alumina. Alumina was fed to molten cryolite in a crucible by a variety of different methods and the alumina concentration measured at five second intervals. The temperatures of the bath and the crucible were also monitored. In many cases a two stage dissolution pattern was observed, indicative of fast initial dissolution followed by the formation, melting and dissolution of agglomerates. The time for remelting of the agglomerates seen as a delay in the dissolution of alumina can be calculated from

$$h_b \cdot 4 \cdot \pi \cdot r^2_{Al_2O_3} \cdot (T_b - T_l) \cdot t_{remelt} = M_f \cdot \Delta H_{fus} \qquad (3)$$

where
h_b = heat transfer coefficient from bath to agglomerate
$r_{Al_2O_3}$ = radius of Al_2O_3 agglomerate
T_b = bath temperature
T_l = bath liquidus temperature
t_{remelt} = time for remelt of agglomerate
M_f = mass of bath frozen into agglomerate
ΔH_{fus} = latent heat of fusion of bath

The right hand side of the equation is given as

$$M_f \cdot \Delta H_{fus} = \int_{25}^{T_b} (MCp)_{Al_2O_3} dT \qquad (4)$$

where $(MCp)_{Al_2O_3}$ = mass of alumina × specific heat capacity of alumina

The time for remelt is highly dependent upon the mass of the agglomerate and its position in the cell. Bagshaw has calculated times of 4-6 seconds for individual particles exposed to turbulent bath with high heat transfer coefficient and 10 °C superheat. Under the same conditions a much larger aggregate of 1.2 g alumina would take 230 seconds to melt. However, in a stagnant zone with a consequently lower heat transfer coefficient this time would be doubled. The circulation of bath would also be required to break up the agglomerate to prevent further freezing.

These experiments show the validity of a multi-stage model. The freezing effect may be simplified by assuming a lower specific area of alumina in suspension than the powder to account for the presence of agglomerates. This approach would reduce the accuracy of a multi-nodal model but will be adequate for a well mixed model in which an average heat transfer coefficient will be assumed throughout the bath zone. This negates the necessity of determining the sizes and flow patterns of agglomerates.

3.3.4 Addition of alumina to electrolyte.

It has been assumed by most modellers that on introduction to the bath the alumina goes into a number of different states. This is borne out by a number of experimental studies where the type of alumina and the method of feeding have been found to effect the dissolution rate and formation of sludge. Many models(Ek[4], Hashimoto[5]) assume alumina to exist in the electrolyte in two states, dissolved and undissolved. A proportion of alumina is assumed to go directly into solution and the rest into a buffer from which it dissolves according to a first order model. This assumption is likely to be valid when alumina is added to a cell with an alumina concentration well below the saturation concentration. In this case the concentration gradient would be great and the rate of dissolution very fast. However this will not simulate accurately abnormal conditions such as the effect of over feeding a pot unless the proportion dissolving instantly is made a function of the concentration gradient within the electrolyte.

Blake[3] and Entner et al[20] assume three states of existence. These are as dissolved alumina, dispersed alumina or suspension and bottom sludge. Entner assumes that alumina is first dispersed into suspension from which it dissolves by a first order model dependent upon the mass of alumina in suspension, the temperature of the electrolyte and the time since anode effect. The latter factor is to account for the enhanced dissolution of alumina due to the perturbation of the bath during anode effect. Alumina in suspension also sediments out to form a bottom sludge from which it dissolves into solution. The rate at which it dissolves from sludge is unclear but appears to have the same form as dissolution from suspension.

Blake also defines the same three states as Entner but a proportion of the alumina introduced is added to each of these states. Mass transfer is

assumed to occur sequentially from sludge to suspension and from suspension to solution. Alumina sludge is transferred to suspension according to the relationship

$$R_1 = k_1.M_1^{K_2} \qquad (5)$$

where R_1 = the rate of transfer of alumina from sludge to suspension

k_1 is a function of the average bath velocity

M_1 = the mass of alumina as sludge

K_2 represents the sludge geometry. This final term allows for the simulation of different designs of cell and feed strategies.

Alumina dissolves from suspension by a first order model as above.

Blake's model was primarily designed for a side break cell in which feeding takes place mainly from the sludge. In centre break cells where the amount of sludge should not be so great and alumina crusts may form at the metal/bath interface, the rate at which alumina can dissolve directly from sludge may be greater than the dispersion of alumina in suspension by the movement of electrolyte over the sludge. This would account for the difference between the models of Blake and Entner.

3.4 Models for the Evolution of Fluorine from Reduction Cells

Fluoride is lost from the cell during normal operation as well as by the production of fluorocarbons during anode effect. The fluoride is often classified as gaseous and particulate. Gaseous fluorides are those that continue to be gases at ambient temperature, namely HF, SiF_4 and fluorocarbons. Entrained and volatilised electrolyte becomes particulate on cooling. The exhaust gases are captured by the cells hood and passed through the baghouse where a proportion of the fluoride is trapped and recycled to the cells with the feed. Haupin[21] developed a mathematical model for the prediction of fluoride evolution from Hall-Heroult cells using thermodynamics, kinetics and the physical properties of the electrolyte.

3.4.1 Model of W.E. Haupin

Haupin derives relationships for three types of evolution of fluoride; gaseous, particulate by volatilisation and particulate by entrainment of bath.

3.4.2 Gaseous fluoride

The major gaseous fluorides are HF and fluorocarbons. The loss of fluoride as fluorocarbons can be calculated from the rate of reaction of anode effect. The evolution of fluorocarbons during anode effect is not considered in Haupin's model.

Haupin assumes HF to be the major gaseous fluoride evolved from the bath during normal operation. This is generated by hydrolysis of the molten electrolyte, water being introduced to the bath by

1. the water content of the alumina
2. burning of hydrocarbons from the anodes
3. moisture in the anodes
4. moisture in other bath additions

Fortunately only a small percentage of this moisture is converted to HF, measurements by Alcoa indicating that only some 8.7% of this moisture actually reacted.

The water is assumed to react with AlF_3 in the bath by the reaction

$$^1/_3AlF_3 + {}^1/_2H_2O \rightarrow HF + {}^1/_6Al_2O_3 \qquad [1]$$

since the equilibrium constant for H_2O reacting with AlF_3 is 10^3 times greater that for H_2O reacting with Na_3AlF_6 and 10^8 times greater than that for H_2O reacting with NaF.

The partial pressure of HF gas for this reaction is given by

$$p_{HF} = \exp\left(-\frac{\Delta G}{6 \cdot R \cdot T}\right) \cdot p_{H_2O}^{\frac{1}{2}} \cdot a_{AlF_3}^{\frac{1}{3}} \cdot a_{Al_2O_3}^{\frac{1}{6}} \qquad (6)$$

where p_{HF} = partial pressure of HF gas
ΔG = Gibbs free energy of reaction
R = universal gas constant
T = temperature of electrolyte
p_{H_2O} = partial pressure of H_2O in pot gas
a_{AlF_3} = activity of AlF_3 in electrolyte
$a_{Al_2O_3}$ = activity of Al_2O_3 in electrolyte

Expressing ΔG as a linear function of temperature and inserting appropriate literature data for activity coefficients into this equation, a good match was obtained to Alcoa test data when it was assumed that the reaction proceeded between 26.6 and 28.8% of the way to completion. This resulted in the following equation for the evolution of gaseous fluoride

$$F_G = \frac{2310000}{\%CE} - \frac{955000}{P_b} \cdot R_b \cdot \left[\exp\left(7.553 - \frac{8444}{T} \right) \right] \cdot$$

$$\left[\frac{\%H_2O \text{ in } Al_2O_3}{37.44} + \frac{\%H \text{ in anodes}}{21..5} \right]^{1/2} \cdot$$

$$\exp\left(0.44199 - 3.1733R_b + 0.78127R_b^2\right) \cdot \left[\frac{C_{Al_2O_3}}{C_{Al_2O_3}^{sat}} \right]^{-0.462} \qquad (7)$$

where F_G = gaseous fluoride evolved per metric ton aluminium produced kg F/ tonne Al
%CE = current efficiency as percentage
R_b = weight ratio NaF/AlF_3
P_b = barometric pressure kPa
$C_{Al_2O_3}$ = concentration of alumina in bath wt%
$C_{Al_2O_3}^{sat}$ = saturation concentration of alumina wt%

This model shows a very good fit to the Alcoa measurements at concentrations of alumina above 3 wt%. Below this value however the prediction diverges rapidly from the measured relationship. One reason for this could be that the measured relationship was derived by multiple regression analysis with a linear relationship assumed between fluoride evolution and each variable. The comparison is therefore being made

between the model and an extrapolation of a relationship derived by linear regression.

3.4.3 Particulate fluoride by volatilisation

It has been demonstrated that the vapour over the electrolyte is $NaAlF_4$ with a small but significant amount of dimerisation[22]

$$2NaAlF_4 \rightleftarrows Na_2Al_2F_8 \qquad [2]$$

The mass spectrographic measurements of the equilibrium constant can be correlated

$$K_d = \frac{P_d}{P_m^2} = \exp\left(-\frac{21414}{T} + 15.6\right) \qquad (8)$$

where K_d = equilibrium coefficient for dimerisation
P_d = partial pressure of $Na_2Al_2F_8$ kPa
P_m = partial pressure of $NaAlF_4$ kPa
T = temperature °K

From the data of a number of investigators Haupin has derived the following formula for vapour pressure over electrolyte

$$P_V = \exp\left(B - \frac{A}{T}\right) \qquad (9)$$

where

$$A = 7101.6 + 3069.7 \cdot Ratio + 635.77 \cdot Ratio^2 + 51.22 \cdot (\%LiF) - 24.638 \cdot Ratio \cdot (\%LiF) + \frac{764.5 \cdot (\%Al_2O_3)}{[1 + 3.2029 \cdot (\%Al_2O_3)]} + 13.2 \cdot (\%CaF_2)$$

$$B = 7.0184 + 0.6844 \cdot Ratio + 0.08464 \cdot Ratio^3 + 0.01085 \cdot (\%LiF) - 0.005489 \cdot Ratio \cdot (\%LiF) + \frac{1.1385 \cdot (\%Al_2O_3)}{[1 + 3.2029 \cdot (\%Al_2O_3)]} + 0.0068 \cdot (\%CaF_2)$$

% = wt% of species in electrolyte

Assuming that the pot gas is saturated with $NaAlF_4$ and $Na_2Al_2F_8$ at their calculated vapour pressures Haupin arrives at the following equation for the evolution of particulate fluoride

$$F_{Vp} = \frac{204000}{\%CE} \cdot \frac{(P_m + P_d)}{P_b} \qquad \text{kg F / tonne Al} \qquad (10)$$

where %CE = current efficiency of cell %

The calculated value of particulate fluoride by this method was always less than that measured. The difference between the calculated and measured values was assumed to be entrained electrolyte and was correlated against bath composition and temperature.

3.4.4 Particulate fluoride by entrainment

Although some investigators have described mechanisms for the entrainment of electrolyte[23,24,25] there is little published data on the subject. Evidence of significant entrainment include the fact that the NaF/AlF_3 weight ratio of the particulate fluoride is intermediate between that of bath vapour ($NaAlF_4$) with a ratio of 0.5 and that of the electrolyte itself. The presence of calcium fluoride in the particulate also suggests entrainment since calcium species in the bath have a negligible vapour pressure.

The differences between the calculated and measured particulate was assumed therefore to be due to entrained electrolyte. The data was correlated empirically with bath ratio, alumina concentration and temperature by multiple regression analysis and the following relationship obtained

$$F_E = \frac{\left[-17030 + 29800 \cdot R_b - 13000 \cdot R_b^2 + 67 \cdot (\%Al_2O_3) - 173 \cdot t - 0.389 \cdot t^2 + 141.6 \cdot R_b \cdot t\right]}{\%CE} \qquad (11)$$

where F_E = Entrained fluoride kg F/ tonne Al

t = T - 1243 °K

Being derived by difference this correlation contains all the errors of measurement and the predictive error of the other models. Additionally it predicts negative entrainments for electrolytes with bath ratios above 1.4 at temperatures greater than 990 °C. This demonstrates the danger of extrapolating an empirical correlation.

The total fluoride evolution is given by the sum of the gaseous and particulate evolution

$$F_{tot} = F_G + F_{Vp} + F_E \qquad (12)$$

This is the total fluoride evolved from the cell into the exhaust gases. These gases are passed to scrubbers where much of the fluoride is recaptured and recycled. The total fluoride irrevocably lost from the cell is therefore given by

$$F_{lost} = [1-HE] \cdot \left[(1-GE) \cdot F_G + (1-PE) \cdot \left(F_{Vp} + F_E \right) \right] \qquad (13)$$

where: F_{lost} = Fluoride irrevocably lost from the cell kg F/tonne Al
HE = Hooding efficiency of pot
GE = Scrubber efficiency for gaseous species
PE = Scrubber efficiency for particulate species

3.5 Models for the Loss of Current Efficiency

The current efficiency of an aluminium reduction cell is defined as the ratio of the actual production of aluminium to the theoretical production of aluminium by the current passing through the cell. In their review of current efficiency modelling, Grjotheim et al[26], state that the deviation from 100% current efficiency can be caused by all or one of the following

1) Other materials being co-deposited. This would be due to the reduction of other metal ions in the melt such as sodium, calcium, iron etc. This results in the presence of impurities in the aluminium.

2) Some of the product reduced at the cathode may remain in the electrolyte phase and be subsequently reoxidised.

3) Electronic conductivity of the electrolyte and physical short circuiting reduces the actual current used for electrolysis.

4) The formation of other heterogeneous compounds. Such an effect is the formation of aluminium carbide at the cathode by reaction between the aluminium pad and the cathode material.

5) Metal being removed from the product before the amount formed can be assessed. Aluminium could be reoxidised in the electrolyte either by dissolution from the metal pad or as a dispersion of droplets.

Obviously the effect of some of these mechanisms will be small and may be ignored in the modelling of the process. The purity of the metal produced is typically greater than 99.8% indicating that process (1) has only a small effect on current efficiency.

Process (2) is likely to be important through impurities in electrolytes that exhibit stable multiple valance states such as phosphorus and vanadium[27]. These form reduced species in the electrolyte and are cyclically reoxidised at the anode. This reduces current efficiency by providing competing reactions at the cathode. The importance of this effect will depend upon the concentration of these species in the electrolyte. If it can be assumed that the amount remains constant, ie these species are not present in the feed, then the effect can be modelled as a constant reduction in the current efficiency of the cell.

The dissolution of a metal in a molten salt imparts an electronic conductivity and lowers the current available for electrolysis. Physical shorting of the anode and cathode due to poorly set anodes will have the same effect. Although it is difficult to assess the loss due to electronic conductivity it is clear that the effect is small. Physical shorting is an exception to the normal running of the cell and is generally of a short time duration. It could, however, represent a significant loss particularly if the cell is to be operated at short anode to cathode distances.

The formation of aluminium carbide is the major reaction accounting for process (4). The effect on current efficiency is self limiting due to the slow diffusion of reactants through the carbide layer and is therefore limited to

the rate of dissolution of aluminium carbide in the metal and electrolyte with which it comes in contact. Although it has a significant solubility in the electrolyte, its solubility in metal is very low. Under normal conditions the cell sidewalls are protected by a ledge of frozen electrolyte and carbide on the cathode surface is protected from the bath by the metal pad. The effect upon current efficiency is therefore limited by the rate of dissolution into the metal and is very small. If the sidewalls become exposed, as after an extended anode effect, then aluminium carbide will form and dissolve causing erosion of the sidewall and loss of current efficiency until the frozen ledge is once more established. These effects are of great significance during the very early life of a cell or in a sick pot, but can be considered negligible during normal operation.

The effects of all the above processes are fairly small and it is universally accepted that the irreversible removal of metal by process (5) is the primary loss mechanism. It occurs through the dissolution of one or both of the electrode products and transportation to a reaction zone.

The most common method for the measurement of current efficiency is to compare the metal produced by a cell over a long period of time, typically a month or more, with the theoretical production based upon the average current during this period. This method is used to assess the current efficiency of industrial cells on a quarterly and yearly basis but is not suitable for current efficiency analysis over a short time scale.

The alternative method of measurement is by analysis of the pot gases. In 1947 Waddington and Pearson[28] discovered the following relationship for the ratio of CO_2 to CO in the anode gases and cell current efficiency

$$\%CE = \frac{1}{2} \cdot \frac{CO_2}{CO + CO_2} + 50 \qquad (14)$$

This relationship allows instantaneous current efficiencies to be measured although it has not so far been possible to monitor this ratio continuously on a plant wide basis. The method can be used to determine the instantaneous effects of operational parameters on current efficiency. The correlation demonstrates that CO_2 is the primary oxidant and CO the

byproduct of the oxidation reaction. The metal reoxidation reaction is usually depicted

$$Al(soln) + 1.5CO_2 = 0.5Al_2O_3(soln) + 1.5CO(g) \qquad [3]$$

The reaction may be assumed to occur between CO_2 as a gas or in solution. Studies of CO_2 solubility in the electrolyte[29] indicate that it is an order of magnitude lower than then solubility of aluminium. For this reason mechanistic explanations have assumed that the reaction was dominated by gaseous rather than dissolved carbon dioxide. The interfacial area between gas bubbles and electrolyte is much greater than that between the metal pad and electrolyte and despite the much lower solubility of carbon dioxide it is probable that dissolved carbon dioxide plays an important role in the reoxidation mechanism. The interfacial area of carbon dioxide as a function of alumina concentration determined by the observation of gas bubbles in an experimental cell has been published by Haupin[30]. The relationship is given by

$$A_{CO_2} = \frac{\left(\begin{array}{l} 0.02723 + 1.003 \cdot wt - 0.3208 \cdot wt^2 - 0.05874 \cdot wt^3 \\ + 0.03268 \cdot wt^4 - 0.001817 \cdot wt^5 \end{array}\right)}{\left(1 - 0.4715 \cdot wt + 0.06247 \cdot wt^2\right)} \times I_O \qquad (15)$$

where A_{CO_2} = interfacial area of CO_2 gas/electrolyte

wt = wt% of alumina in solution

I_O = current associated with the oxide reaction

Unfortunately, no relationship has been derived for the dependence of bubble surface area upon bath composition, anode properties and temperature.

Laboratory studies of the reoxidation reaction have generally been aimed at evaluating the reaction mechanism, especially the rate determining steps. In Grjotheim's review[26] he states that there is a lack of agreement as to the mechanism. However, under conditions similar to those found in operating cells mass transfer appears to play an important role although the rate determining step is not clear. There are several consecutive steps for the dissolution and loss of aluminium. These have been documented by Qiu [31] as being 3 steps

1. Dissolution-diffusion step. The dissolution of metal at the metal-electrolyte interface and the diffusion of the dissolved species through a stagnant cathodic layer. As the cathodic layer is usually very thin these two steps may be considered together.

2. Transfer of the dissolved metal through the bulk of the electrolyte to a reaction zone. Convective transport limited.

3. Reoxidation of the dissolved species by anode gases or dissolved anode gases. Reaction rate limited.

Qiu also lists various viewpoints presented in the literature for the rate determining step. This is duplicated in table 3.1.

These widely different conclusions have been explained by Grjotheim et al[26] as possibly being due to the differences in the experimental conditions and the way in which convection in the melts has been achieved ie. by means of a temperature gradient, mechanical stirring or gas bubbling. Where the melt is vigorously mixed the reaction is dissolution rate controlled whilst convective transport is the slow step in quiet melts. In industrial cells a combination of these steps may be responsible, dependent upon local conditions within the melt.

3.5.1 Empirical relationships

A number of investigators have correlated current efficiency with operational characteristics for reduction cells[26,32,33,34,35]. These correlations are generally obtained by multiple regression analysis of current efficiency measurements for a number of cells, the operational parameters being noted at the time of measurement. The current efficiencies may be obtained by metal inventory measurements or anode gas analysis techniques. An example correlation is that derived by Berge et al[36]

$$CE = 0.1388 \cdot T + 0.59 \cdot X_{AlF_3} + 58.9 \sin(3h) - 0.032 \cdot A + 163.7 \quad (16)$$

where CE = current efficiency %
T = bath temperature °C
X_{AlF_3} = excess AlF_3 in the electrolyte wt%

authors	year	experimental method	rate determining step
laboratory cells			
Abramov	1953	determine the metal loss in the bath with different depths	convective transport
Revazyan	1960	determine the metal loss of Cu-Al alloy in the bath	dissolution
Gjerstad and Welch	1964	determine the metal loss in the bath with different depths, by passing CO_2 over the bath surface.	convective transport
Gerlach	1974	determine the rate of oxidation of metal by passing CO_2 over the bath surface	dissolution
Thonstad and Rolseth	1981	passing CO_2 over cryolite melts in contact with metal	dissolution reaction
Qiu and Fan	1984	an electroanalytical method to assess the metal concentration in bath	convective transport
Industrial cells			
Arthur	1974	determine the metal concentration in different zones of bath	convective transport
Thonstad and Rolseth	1976	an electroanalytical method to assess the metal concentration in different zones in the bath	reaction
Qiu and Fan	1984	determine the metal concentration at different zones in the bath	dissolution

Table 3.1 Viewpoints on the Rate Determining Step for Alumina Dissolution

h = depth of metal pad cm

A = cell age months

Current efficiencies were obtained from metal inventory measurements by an isotope dilution method on a pot line of 34 cells. In the bulk of the cells one value of current efficiency was determined each week. The operating parameters must needs be the weekly averages for each cell.

Whilst multiple regression models can be used to predict average current efficiencies under target or average operating conditions they cannot provide the detailed information required for a dynamic model in which operating conditions are constantly changing.

3.5.2 Model of Robl et al

Robl et al[37] presented a model for the calculation of steady state current efficiency in terms of such geometrical and operating factors as anode-cathode distance, bath temperature, current density and bath composition. Hydrodynamic parameters are also included in the model.

The model is based upon the assumption that the reoxidation reaction occurs between dissolved CO_2 and aluminium dissolved or suspended in the bath. The two products are brought together by diffusion and mass transport in the bath. The model is illustrated by figure 3.1. The anode to cathode gap is divided into five regions

1. metal dissolution zone assumed to have constant metal concentration less than or equal to the metal solubility in the bath

2. convective transport zone for metal assumed to have constant gradient of metal concentration

3. reaction zone with overlap of metal and gas concentration gradients

4. convective transport zone for dissolved gas assumed to have constant gradient of gas concentration

5. gas dissolution zone assumed to have constant gas concentration less than or equal to the gas solubility in the bath

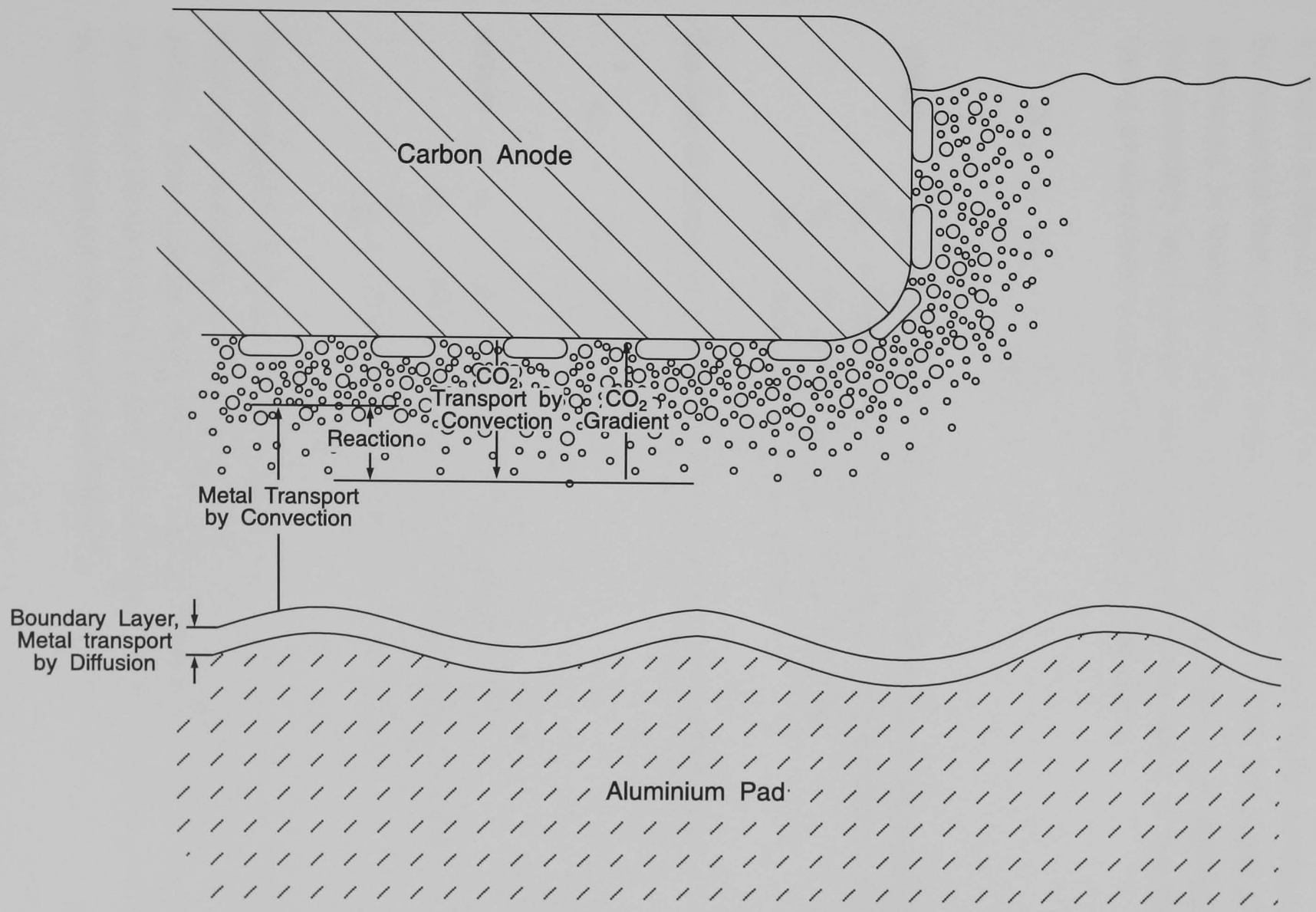

Figure 3.1 Schematic of the Current Efficiency Model

A hydrodynamic model of the cell was developed to allow the calculation of differing current efficiencies in different zones of the cell since distinctive flow regimes may be identified throughout the bath. The turbulent flow pattern of the bath within the inter electrode gap is likened to that in a channel whose walls are the anode and metal surfaces. It can be assumed that a thin boundary layer exists at both the metal and gas interfaces. In these boundary layers mass transport is by diffusion only, the boundary layers being small compared to the depth of the channel. Using an equivalent convective diffusivity as defined by

$$D_{em} = D_m + \frac{u_t}{Sc_t} \qquad (17)$$

where D_{em} = equivalent convective diffusivity for metal species
D_m = mean molecular diffusivity of metal species in bath
u_t = turbulent viscosity of the electrolyte
Sc_t = turbulent Schmidt number

the rate of convective transport can be calculated by Fick's Law

$$r_m = -D_m \cdot \frac{dC}{dz} \qquad (18)$$

where r_m = rate of convective transport of metal
D_m = diffusivity of metal through the boundary layer
$\frac{dC}{dz}$ = concentration gradient across boundary.

The turbulent Schmidt number may be related to the Schmidt and Reynolds numbers but the calculation of turbulent viscosity is more difficult. This is dependent upon the shear velocity, the friction factor, the skewness of the velocity profiles and surface roughness. Robl derived the following equation for equivalent diffusivity

$$D_{em} = D_m + \frac{\left[0.42 \cdot C_f^{\frac{1}{2}} \cdot \frac{z}{d} \cdot D_m \cdot U^2 \cdot \rho^2 \cdot d_c^2 \cdot \left(1 - C_s \cdot \frac{z}{d}\right)\right]}{\left[0.9 \cdot D_m \cdot U \cdot \rho \cdot d_c + \mu^2\right]} \qquad (19)$$

where μ = viscosity of the electrolyte
ρ = density of the electrolyte
U = average velocity of electrolyte reference to metal
d = interelectrode distance
d_c = critical dimension for Reynolds number
z = distance normal to interface
C_f = friction factor
C_s = factor for skewness of velocity profile due to unequal surface roughness

In the steady state, if the reaction between the two species is assumed to be instantaneous then the rate of metal loss is equal to the rate at which metal is transported to the reaction zone. The current efficiency is then calculated as

$$CE = 100 \times \left(1 - \frac{r_m}{r_t}\right) \qquad (20)$$

where r_t = theoretical maximum production of aluminium

$$= \frac{I}{z_{Al} \cdot F}$$

I = current flow through cell
z_{Al} = charge number for aluminium
F = Faradays constant

If the rate of convective transport is greater than the dissolution rate of metal into the electrolyte then it will become dissolution rate limited otherwise it will be equal to the convective transport rate. No mathematical model is presented for the dissolution rate although it is stated that an analytical expression for this should include the relative turbulences and surface tensions of the bath and metal pad.

Although this model can predict current efficiencies in differing zones of the cell many of the factors in equation (19), such as C_f and C_s, are difficult to determine. Whilst metal pad velocity is relatively easy to measure in industrial cells this is not the case for the electrolyte velocity. The accuracy of the hydrodynamic model also depends greatly upon the regional division of the metal and bath flow patterns.

An advantage of the model is that it is not restricted to the assumption of any particular rate determining step. However, for known conditions in certain Alcoa cells, the model without dissolution rate limits applied predicted current efficiencies that were too low. Robl concluded that in many instances it is likely that the dissolution rates for metal and/or gas are the limiting factors.

3.5.3 Model of Evans et al

Evans[38] assumed that the rate controlling step for the reoxidation reaction is transport through a surface tension induced boundary layer at the aluminium electrolyte interface. Using a relationship derived by Levich[39] they correlated the rate of transport through the interface to the turbulent kinetic energy. The kinetic energy was obtained from their k-e model used to calculate fluid flow. This lead to the relationship

$$r_m = \left(\frac{D_m \cdot \rho}{\sigma_m}\right)^{0.5} \cdot C^* \cdot k_t^{0.75} \qquad (21)$$

where r_m = rate of metal transport through boundary layer
D_m = molecular diffusion coefficient of dissolved metal
ρ = electrolyte density
σ_m = surface tension at aluminium surface
C^* = saturation concentration of metal in electrolyte
k_t = turbulent kinetic energy of the system

k_t is obtained by averaging the k-distribution obtained in their velocity calculations. In calculating the electrolyte velocity gas bubble induced forces are ignored, electromagnetic forces only being considered. The steady state current efficiency is again calculated as

$$CE = 100\left(1 - \frac{r_m}{r_t}\right) \qquad (22)$$

As with Robl's current efficiency model this includes a hydrodynamic model. Although this may increase the accuracy and allow the calculation of local current efficiencies, the number of calculations required make it cumbersome for dynamic simulation and the need to make

approximations for many of the unknown parameters reduces these benefits.

3.5.4 Model of B. Lillebuen et al

Like the previous models Lillebuen[40] assumed that the reaction between aluminium and carbon dioxide was solely responsible for current efficiency losses. In addition he makes the following assumptions:

1) the reaction takes place between dissolved reagants

2) simple film theory is valid and transportation of the heat of reaction and the reaction products is disregarded

3) the chemical reaction is instantaneous and the rate of reaction is considered to be controlled by the dissolution of reactants through stagnant films

The dissolution rates for aluminium and carbon dioxide taking into account the reaction can be written

$$r_{Al} = A_{Al} \cdot k_{Al} \cdot \left(1 + \frac{k_{CO_2} \cdot C_{CO_2}}{k_{Al} \cdot C^*_{Al}}\right) \cdot \left(C^*_{Al} - C_{Al}\right) \qquad (23)$$

$$r_{CO_2} = A_{CO_2} \cdot k_{CO_2} \cdot \left(1 + \frac{k_{Al} \cdot C_{Al}}{k_{CO_2} \cdot C^*_{CO_2}}\right) \cdot \left(C^*_{CO_2} - C_{CO_2}\right) \qquad (24)$$

where r = rate of dissolution of species
A = interfacial area of species and electrolyte
k = dissolution rate constant
C = concentration of species
C^* = saturation concentration of species
suffix Al refers to aluminium
CO_2 refers to carbon dioxide

An implication of assumption (3) is that if $C_{Al}>0$ then $C_{CO_2}=0$ and vice versa $C_{CO_2}>0$ requires $C_{Al}=0$. In line with experimental data[41] Lillebuen assumes that there is always dissolved metal present in the electrolyte.

As in the previous models the steady state current efficiency is given by

$$CE = 100 \cdot \left(1 - \frac{r_{Al}}{r_t}\right) \tag{25}$$

The stoichiometry of the reaction requires that

$$r_{CO_2} = \tfrac{3}{2} r_{Al} \tag{26}$$

combining equations (23), (24) and (26) gives

$$C_{Al} = \frac{k_{Al} \cdot A_{Al} \cdot C^*_{Al} - \frac{2}{3} \cdot k_{CO_2} \cdot A_{CO_2} \cdot C^*_{CO_2}}{\frac{2}{3} \cdot k_{Al} \cdot A_{CO_2} + k_{CO_2} \cdot A_{Al}} \tag{27}$$

Calculation of the steady state concentration of aluminium in the electrolyte allows the calculation of the rate of dissolution and hence the current efficiency.

3.5.5 Calculation of mass transfer coefficients

Attempts to calculate the mass transfer coefficient for gas bubbles, k_{CO_2}, by correlations proved unsuccessful due to lack of experimental data for CO_2 diffusivity and bubble diameters. Lillebuen therefore assumes that $k_{CO_2} = k_{Al}$ based upon the work of Aarebrot[42] with the ratio of gas bubble area to aluminium area being estimated as 0.1.

The mass transfer coefficient for aluminium is calculated from

$$Sh = 0.023 \cdot Re^{0.83} \cdot Sc^{0.33} \tag{28}$$

where Sh = Sherwood number $= \dfrac{k_{Al} \cdot 2\ell}{D_{Al}}$

Re = Reynolds number $= \dfrac{\rho \cdot v \cdot 2\ell}{\mu}$

Sc = Schmidt number $= \dfrac{\mu}{\rho \cdot D_{Al}}$

ℓ = interelectrode gap

ρ = density of electrolyte

D_{Al} = diffusivity of aluminium in the electrolyte

ν = interfacial velocity between electrolyte and metal pad

μ = viscosity of electrolyte

This then gives

$$k_{Al} = 0.023 \cdot \left(\frac{D_{Al}}{2\ell}\right) \cdot Re^{0.83} \cdot Sc^{0.33}$$

$$= 0.02044 \cdot D_{Al} \cdot \ell^{-0.17} \cdot \mu^{-0.5} \cdot \rho^{0.5} \cdot \nu^{0.83} \qquad (29)$$

Lillebuen and Mellerud[41] then calculated how the current efficiency should vary with the concentration of dissolved alumina in the electrolyte. In order to do this it was necessary to know how all parameters vary with alumina concentration. Using the following relationships the graph in figure 3.2 was obtained for current efficiency vs alumina concentration.

D_{Al} seems relatively insensitive to changes in alumina concentration and is assumed constant. Values taken from work by Vetyukov[29].

Haupin's relationship for A_{CO2} is used as given above.

The solubility of CO_2 in cryolite melts was measured by Bratland[43] and is given as

$$C^*_{CO_2} = \frac{0.03027 - 0.0006985 \cdot wt}{1 - 0.08989 \cdot wt} \quad kg\,m^{-3} \qquad (30)$$

where wt = wt% of alumina dissolved in electrolyte.

This expression is valid for alumina concentrations between 1 and 8 wt%.

The solubility of aluminium has been measured by Vetyukov[44] and is given as a weight percentage

$$C^*_{Al} = -0.2877 + 0.0268 \cdot R + 0.0003 \cdot T - 0.0019 \cdot CaF_2 - 0.0043 \cdot (wt - 12.5) \qquad (31)$$

where R = wt ratio of NaF to AlF_3 in electrolyte

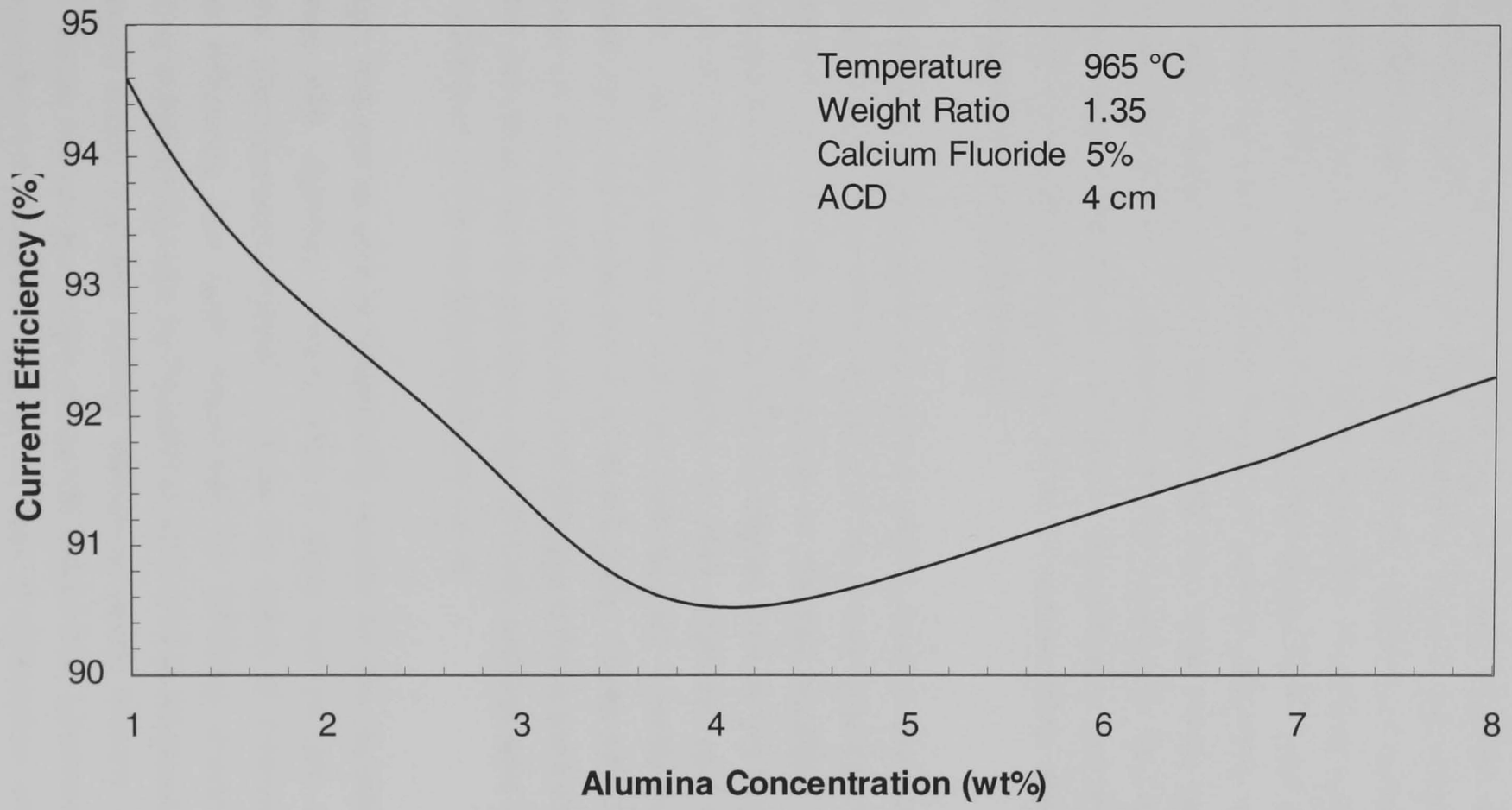

Figure 3.2 Cell Current Efficiency vs Alumina Concentration

T = temperature in degrees Celsius

CaF_2 = wt% CaF_2 in electrolyte

The calculated current efficiency shows a minimum at 4% Al_2O_3 and the presence of a minimum is borne out by many studies on laboratory cells[40,45,46,47,48,49,50,51,52,53,54]. The literature data is summarised in table 3.2. No data seems to be available for the variation of current efficiency with alumina concentration in modern computer controlled point feed cells. General operating conditions indicate that these cells need to operate at low alumina concentrations for maximum current efficiency and do seem able to attain higher current efficiencies than side break cells at higher alumina concentrations. Comparison of the model with data obtained from side break cells is difficult as it is virtually impossible to separate the effect of alumina concentration from the effect of temperature which rises with decreasing alumina concentration.

The model assumes a perfectly uniform distribution of alumina in the bath. In practise oxygen ions are consumed at the anode and therefore alumina concentration will be low in the vicinity of the gas bubbles. At the metal pad the alumina concentration may be higher than in the bulk due to the ability of alumina-bath agglomerates to float upon the pad surface. The bath film near the metal is enriched with sodium fluoride increasing the local bath ratio and hence the alumina solubility. These effects will reduce the metal solubility at the cathode and the gas bubble area at the anodes. This will decrease the dissolution rates of both species and cause a shift in the minimum of the current efficiency curve.

Although this model shows reasonable results for the variation of current efficiency with alumina concentration it does not include a sufficiently accurate hydrodynamic model to show the effect of interelectrode gap. Current efficiency has been measured for differing anode to cathode distances in industrial cells by Rolseth et al[55] and at Anglesey Aluminium. Both have found that the current efficiency varies linearly with ACD at values above 3-4 cm but drops off rapidly below this. Lillebuen's model for the dissolution of aluminium shows the rate of dissolution and hence the current efficiency to be virtually independent of the anode cathode distance. It may be that there are two mechanisms responsible for current efficiency dependent upon the distance between the electrodes. At low

Reference	Type of Cell	Correlation	Range
Gjerstad[46]	Laboratory Cell	Linearly increasing	0.5 - 12%
Belyaev[47]	Laboratory Cell	Minimum at 5%	1 - 11%
Grjotheim[48]	Laboratory Cell	Minimum at 4.5%	0 - 11%
Firsanova[49]	Laboratory Cell	Minimum at 9%	4 - 10.5%
Bersimenko[50]	Laboratory Cell	Linearly increasing	3 - 12%
Szekér[51]	Laboratory Cell	Minimum at 4.5%	2 - 12%
Abramov[52]	Laboratory Cell	Linearly increasing	5 - 12%
Schmitt[53]	Side-break Cell	Increasing	2 - 7%
Thonstad[54]	Side-break Cell	Increasing	2 - 7%
Poole[55]	Side-break Cell	Increasing	2 - 7%
Lillebuen[40]	Side-break Cell	Increasing or const	0.5 - 6%

Table 3.2 Current Efficiency vs Alumina Concentration: Literature Data

ACDs it is possible that the reaction is between carbon dioxide gas and aluminium or that waves in the metal pad come in contact with the anode and cause loss of current efficiency due to shorting.

The correlation for the dissolution rate constant is unsatisfactory for a number of reasons.

Firstly it is strictly applicable to mass transfer at the solid/liquid interface for the case of fluid flow through a tube which has little in common with the three-phase circulating fluid system of an aluminium cell. It also seems unlikely that the definition of Reynolds number using twice the ACD as the critical dimension is capable of describing the hydrodynamics of the cell.

Secondly it is only appropriate to turbulent flow. Employing values of electrolyte density of 2050 kg m^{-3}, viscosity of 3×10^{-3} Ns m^{-2}, anode cathode distance of 0.04 m and interfacial velocity of 0.10 m s^{-1} (Lillebuen uses a value of 0.06) the Reynolds number is of the order 5,000 which falls well short of the figure of 10,000 usually quoted for the onset of turbulence in pipe flow.

Thirdly, as with previous models, no account is taken of the turbulent effect of the gas bubbles. As a term the interfacial velocity is undesirable as it is extremely difficult to measure in industrial cells.

The model would therefore be improved by the use of a mass transfer correlation determined for a system more closely analogous both to the geometry and hydrodynamics of an aluminium cell.

3.5.6 Model of Vasiliadis

Vasiliadis[56] undertook the determination of an improved mass transfer correlation by investigation of the system Hexan-1-ol and Water. This system had the advantage of being observed at room temperature and could be analysed by refractive index measurements. The aqueous phase, analogous to aluminium, was rotated by a disc stirrer and the evolution of carbon dioxide simulated by introducing air or nitrogen into the hexan-1-ol / electrolyte phase through a porous plate. The liquid phases were contained in a cylindrical vessel.

The experiments resulted in the following correlation

$$k_{Al} = 2.24\times10^{-5}\cdot\left(\frac{v_f}{\ell}\right)^{1.42}\cdot\left(1+103\cdot N^{2.5}\right)\cdot\left(\frac{Sc_{Al}}{Sc_W}\right)^{0.33}\cdot\left(\frac{D_{Al}}{D_W}\right) \quad (32)$$

where v_f = velocity of anode gases
N = stirrer speed revs/s
suffix W refers to water

The volumetric flowrate of anode gases may be determined from the rate of electrolysis at the anode. The number of moles of gas formed

$$n_g = \frac{1}{2}\cdot\frac{i_o}{z_o\cdot F} + \frac{1}{4}\cdot\frac{i_F}{z_F\cdot F} \quad \text{mol s}^{-1} \quad (33)$$

where i = partial current
z = charge number
F = Faradays constant
suffix O refers to electrolysis of oxide ions
F refers to electrolysis of fluoride ions

The electrolysis of oxide and fluoride are the only reactions at the anode so

$$i_O + i_F = I \quad (34)$$

where I = total current

$z_O = 2$ and $z_F = 1$ so the equation reduces to

$$n_g = \frac{I}{4\cdot F} \quad \text{mol s}^{-1} \quad (35)$$

Assuming that the gases behave ideally then according to the universal gas law

$$V_g = n_g\cdot\frac{R\cdot T}{P} \quad m^3\ s^{-1} \quad (36)$$

where V_g = volumetric flowrate $m^3\ s^{-1}$
R = universal gas constant $J\ mol^{-1}\ K^{-1}$
T = temperature of gas °K
P = Pressure of gas $N\ m^{-2}$

The velocity of the anode gases is the volumetric flowrate for unit surface area of anode

$$\nu_f = \frac{V_g}{A_A} = \frac{I}{4 \cdot F} \cdot \frac{R \cdot T}{P} \cdot \frac{1}{A_A} = \frac{i \cdot R \cdot T}{4 \cdot F \cdot P} \quad m\,s^{-1} \qquad (37)$$

where A_A = Total anode area m2
i = anodic current density $A\ m^{-2}$

The speed of the stirrer has no direct counterpart in the cell but the velocity at its tip may be equated to the maximum velocities found in the metal pad.

Inserting the relationships and the values for the physical properties of water into the equation gives

$$k_{Al} = 2.147 \times 10^{-11} \cdot \left(\frac{i \cdot T}{\ell}\right)^{1.42} \cdot \left(1 + 313.3 \cdot \nu^{2.5}\right) \cdot \left(\frac{\mu}{\rho}\right)^{0.33} \cdot D_{Al}^{0.67} \qquad (38)$$

where ν = maximum velocity in the metal pad

This model is more attractive as it will directly relate current efficiency to parameters that are known to affect it in practice. It also has the advantage that it contains only parameters that are documented or may be relatively easily measured. Unfortunately, no correlation was made relating the depth of the metal pad to the dissolution rate constant although the metal pad velocity should be a function of metal pad depth. The experiment was also not strictly geometrically analogous as a cylindrical rather than rectangular geometry was used.

3.5.7 Model of Haupin

At the Trondheim course Haupin[30] presented the following model for mixed rate control. The model uses correlations formulated in both Lillebuen's and Robl's models. No assumption is made as to which step is controlling although the reaction between species is assumed to be instantaneous. As in Lillebuen's model this requires that for $C_{Al} > 0$, $C_{CO_2}=0$. The reaction is assumed to take place at the carbon dioxide boundary layer and the concentration profile is shown in figure 3.3.

The rate of dissolution of metal through the metal boundary layer is given

$$r_{Aldiss} = A_{Al} \cdot k_{Al} \cdot \left(C^{*}_{Al} - C_{Al(1)}\right) \qquad (39)$$

where r_{Aldiss} = dissolution rate for aluminium
$C_{Al(1)}$ = concentration of aluminium at electrolyte/ aluminium boundary.

The rate of convective transport of metal from the metal to carbon dioxide boundary layers is given by

$$r_{Alconv} = A_{conv} \cdot k_{conv} \cdot (C_{Al(1)} - CAl_{(2)}) \qquad (40)$$

where r_{Alconv} = rate of convective transport of aluminium
A_{conv} = interfacial area for aluminium/electrolyte in convective zone
k_{conv} = convective rate constant
$C_{Al(2)}$= concentration of aluminium at carbon dioxide boundary layer

The dissolution of carbon dioxide is enhanced by the reaction that is assumed to take place at the carbon dioxide boundary layer. The rate of dissolution is given by

$$r_{CO_2} = A_{CO_2} \cdot k_{CO_2} \cdot \left(1 + \frac{k_{Al} \cdot C_{Al(2)}}{k_{CO_2} \cdot C^{*}_{CO_2}}\right) \cdot \left(C^{*}_{CO_2} - C_{CO_2}\right) \qquad (41)$$

where r_{CO_2} = rate of dissolution of carbon dioxide

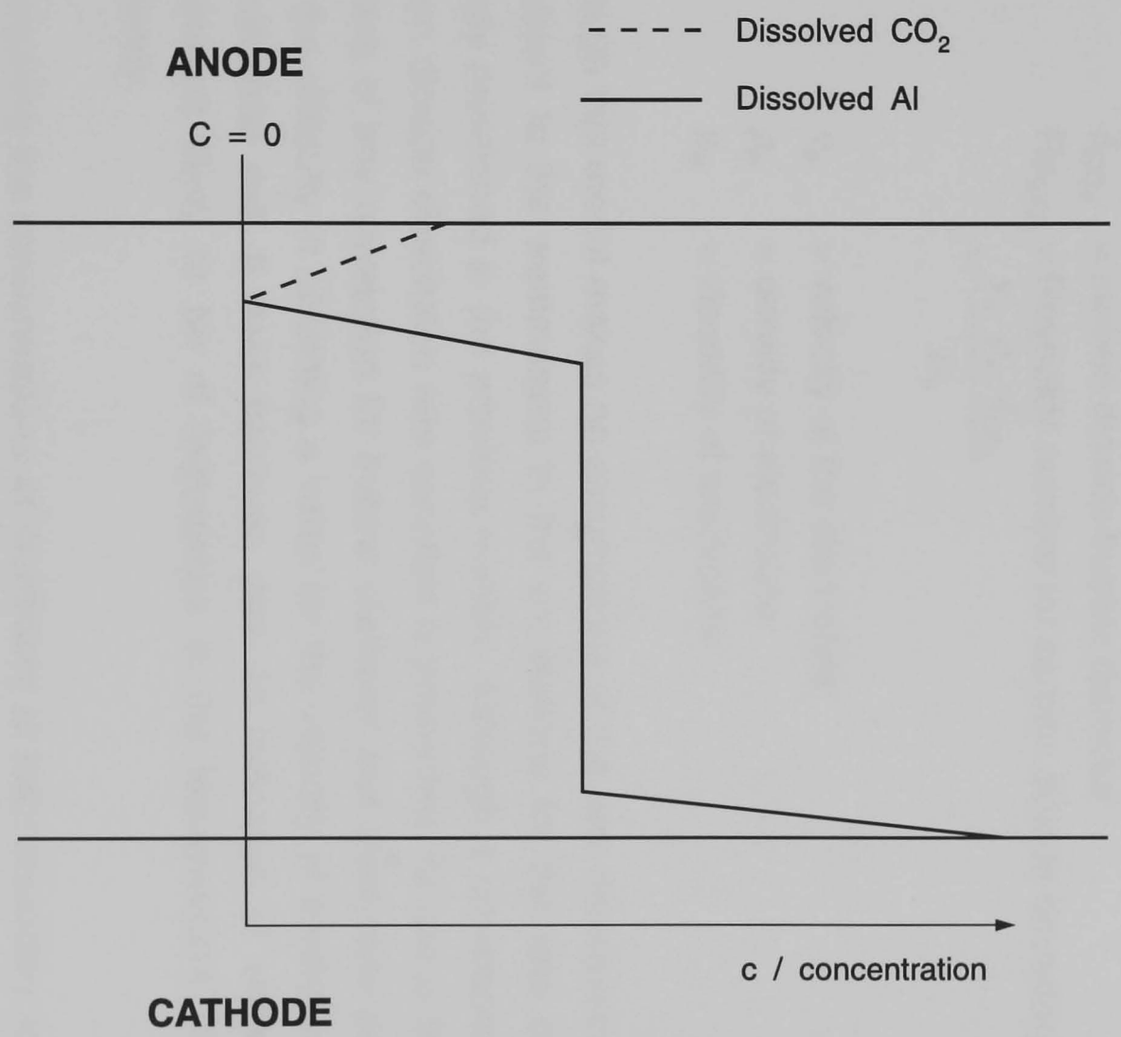

Figure 3.3 Aluminium Concentration across CO_2 Boundary Layer

Haupin uses the correlation presented by Lillebuen for the aluminium dissolution rate constant and the correlation presented by Robl for the convective rate constant. The rate constant for the dissolution of carbon dioxide is given as

$$k_{CO_2} = \frac{D_{CO_2}}{\delta_{CO_2}} \cdot \frac{1.703 - 0.7630 \ln Re_{CO_2}}{1 - 0.6272 \ln Re_{CO_2}} \cdot Re_{CO_2}^{0.5} \cdot Sc^{0.5} \qquad (42)$$

where D_{CO_2} = diffusivity of carbon dioxide in electrolyte

δ_{CO_2} = carbon dioxide bubble diameter

Re_{CO_2} = Reynolds number for carbon dioxide boundary layer

$$= \frac{\nu_e \cdot \rho_e \cdot \delta_{CO_2}}{\mu_e}$$

ν_e = velocity of the electrolyte

ρ_e = density of electrolyte

μ_e = viscosity of electrolyte

Although this model makes no assumptions of the rate determining step it is subject to the weaknesses in the correlations for the rate constants already mentioned in the previous models. Although a correlation for the carbon dioxide dissolution rate constant is presented, its use is limited by the lack of any correlation for bubble diameter and electrolyte properties and the difficulty in obtaining a value for the velocity of electrolyte within an industrial cell. It does however, give an indication of some of the parameters likely to be of importance in the improvement of current efficiency.

By requiring the concentrations of aluminium at both boundary layers the uniform distribution of alumina throughout the bath may not be assumed. Although this will lead to a more accurate model, its use is not so desirable in a dynamic simulation as it increases the number of equations required and the complexity of the solution. If the electrolyte may be assumed to be turbulent then the rate of convective transport may be very much greater than the dissolution rate and so the model will approximate that presented by Lillebuen.

3.6 Models for the Estimation of Frozen Bath Shape

Aluminium reduction cells are designed such that a layer of frozen bath forms around the sidewalls of the cell. This protects the material of the sidewalls from the corrosive effects of the electrolyte and the metal pad. The frozen layer also helps to regulate the temperature of the cell by freezing and melting. The freeze profile also affects the flow patterns within the cell and the current distribution.

Models for the precise estimation of freeze shapes have been developed by a number of workers[57,58,59]. These involve the division of the cell into a number of triangular elements for which the temperature distribution can be calculated by a finite difference method. The accuracy of the simulation depends upon the number of lattice points used. This type of model is therefore unsuitable for dynamic simulation due to the time required for these calculations.

A simpler model for heat transfer through the side walls assumes unidirectional heat flow through the walls. This model has been used by a number of workers for the calculation of steady state freeze thicknesses[60,61] and for the dynamic behaviour of freezes[2,5,62]. The heat flow and temperature gradients are shown schematically in figure 3.4.

The fundamental equations for the flow of heat through the side walls are

$$q_m = A_m \cdot h_m \cdot (t_m - t_1) \tag{43}$$

$$q_n = A_n \cdot \frac{k_n}{x_n} \cdot (t_n - t_{n+1}) \tag{44}$$

$$q_s = A_s \cdot h_s \cdot (t_s - t_a) \tag{45}$$

where
- q_i = heat flow from section i
- h_i = heat transfer coefficient from section i
- k_i = thermal conductivity of section i
- x_i = thickness of section i
- t_i = temperature at surface of section i or in the case of the melt and the surroundings, the bulk temperatures
- A_i = area for heat transfer from section i

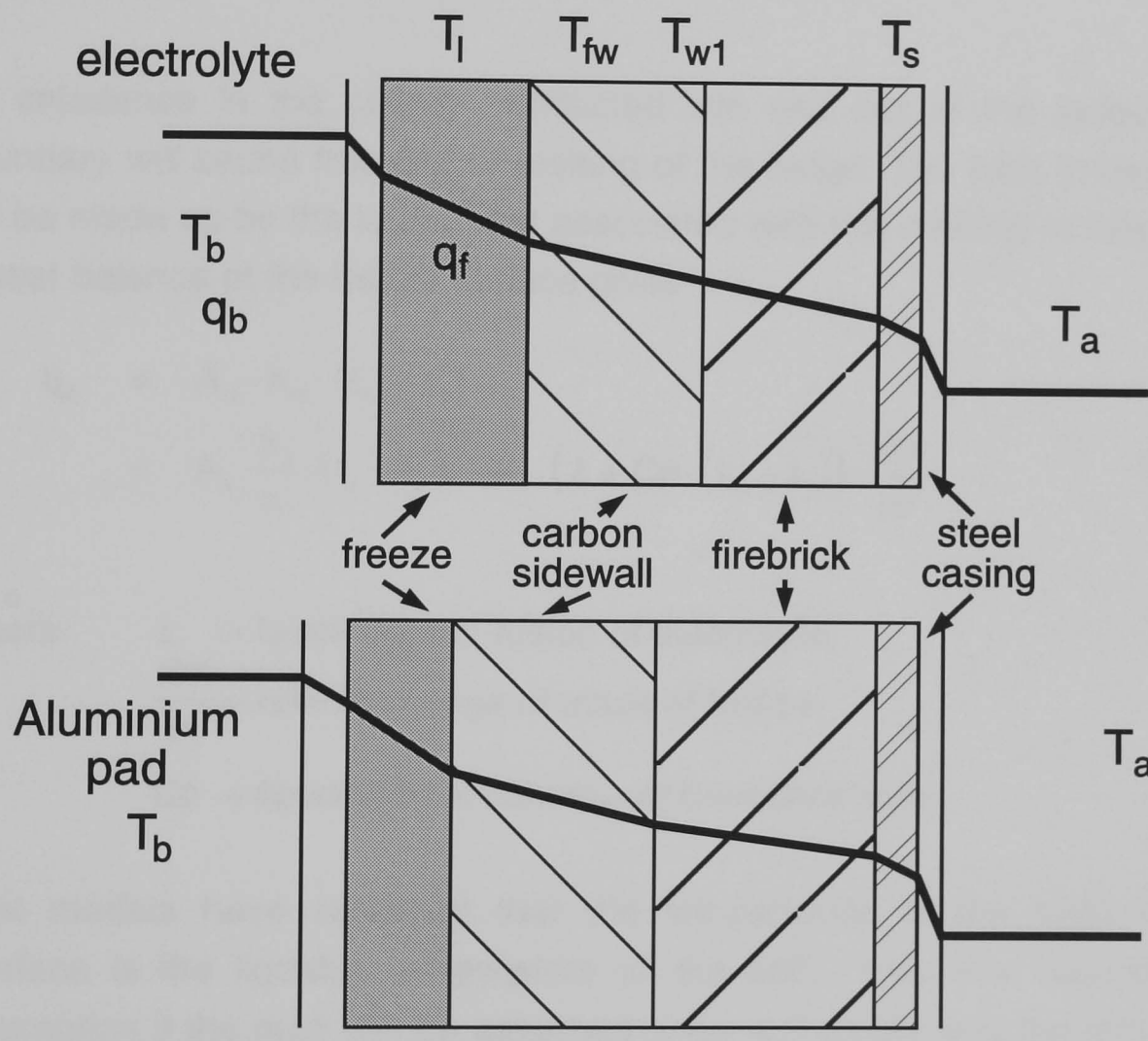

Figure 3.4 Heat Flow and Temperature Gradient across Frozen Sidewalls

and suffix

m represents the melt (bath or metal)

n represents a section of the wall or ledge with n=1 being the freeze and n=m being the outer shell

s represents the outer shell

a represents the cell surroundings

The heat transfer at the inner and outer surfaces is assumed to be purely by convection.

An imbalance in the energy conducted into and out of the ledge/melt boundary will cause freezing or melting of the ledge. The heat imbalance will be made up by the latent heat associated with this melting or freezing. A heat balance at the freeze surface gives

$$q_m = A_m \cdot h_m \cdot (t_m - t_1)$$

$$= A_1 \cdot \frac{k_1}{x_1} \cdot (t_1 - t_2) + (\lambda + Cp \cdot (t_m - t_1)) \cdot \frac{dm}{dt} \qquad (46)$$

where λ = latent heat of fusion of electrolyte

$\frac{dm}{dt}$ = rate of change of mass of freeze

Cp = specific heat capacity of boundary layer

Most models have assumed that the temperature at the bath ledge interface is the liquidus temperature of the bath. This is a reasonable assumption if the melt can be assumed to be well mixed and the diffusion of components away from the boundary layer fast.

If the electrolyte behaves as a simple eutectic system then the frozen ledge will consist of one pure solid compound or solid solution. If, however, freezing is much faster than the diffusion of species from the boundary layer. Chemical analysis of ledge in industrial cells by Thonstad[61] has shown it to consist of rather pure cryolite with smaller quantities of alumina and calcium fluoride than were present in the bath. Samples taken from the metal and bath ledges in a number of 'dead' cells at Anglesey had a weight ratio of 1.36-1.41 irrespective of the ratio in the

bath. This indicates that there is diffusion of individual components from the boundary layer to the melt.

This effect has been modelled by Hashimoto[5]. The diffusion of species i is given by

$$\frac{\partial C_i}{\partial t} = D_i \cdot \frac{\partial^2 C_i}{\partial x^2} - U \cdot \frac{\partial C_i}{\partial x} \qquad (47)$$

where D_i is the diffusion coefficient of species i and U is the velocity of solidification and is assumed constant. This equation was solved by applying the following approximations.

(a) The mass of the components moving between the freeze and the boundary layer is calculated from the amount of the electrolyte which freezes or melts.

(b) The concentrations of the components are represented by their average values in the boundary layer.

The mass of the components moving between the bulk electrolyte and the boundary layer is then calculated

$$W_i = -f \cdot W_f \cdot (C_{i,f} - C_{i,l}) \qquad (48)$$

where W_i = the amount of species i entering the boundary layer from the bulk
W_f = the amount of bath in the boundary layer per unit area
f = a fittable constant related to the diffusivity
$C_{i,f}$ = average concentration of species i in the boundary layer
$C_{i,l}$ = average concentration of species i in the bulk

The boundary layer is bath that is freezing or melting and W_f is calculated from equation (48). The value of f is estimated by Hashimoto from measurements in commercial cells and ranges between 0.1 and 0.00001. The exchange of mass between the layer and the bulk is taken to be relatively rapid for the layer in the bath but slow for the metal zone. The value of f has a marked effect upon the freeze thickness as is shown in figure 3.5. In this case it appears that the diffusivity of the specific

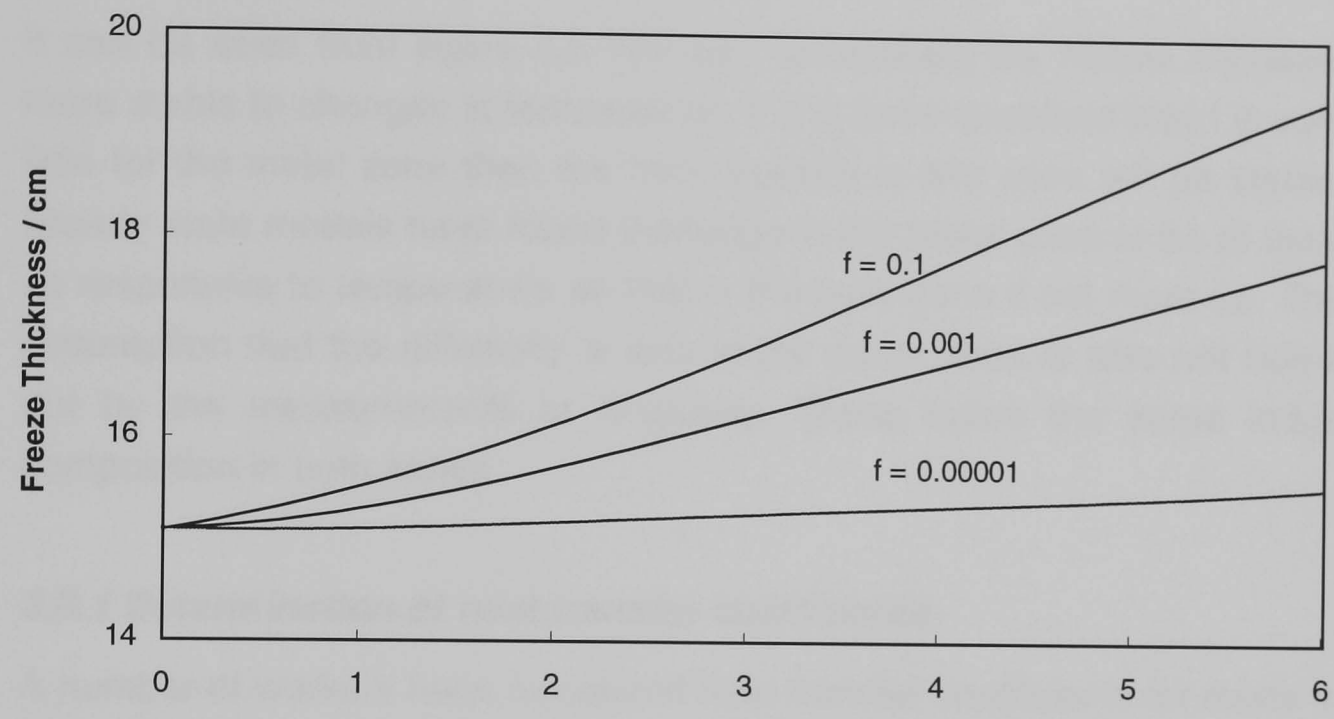

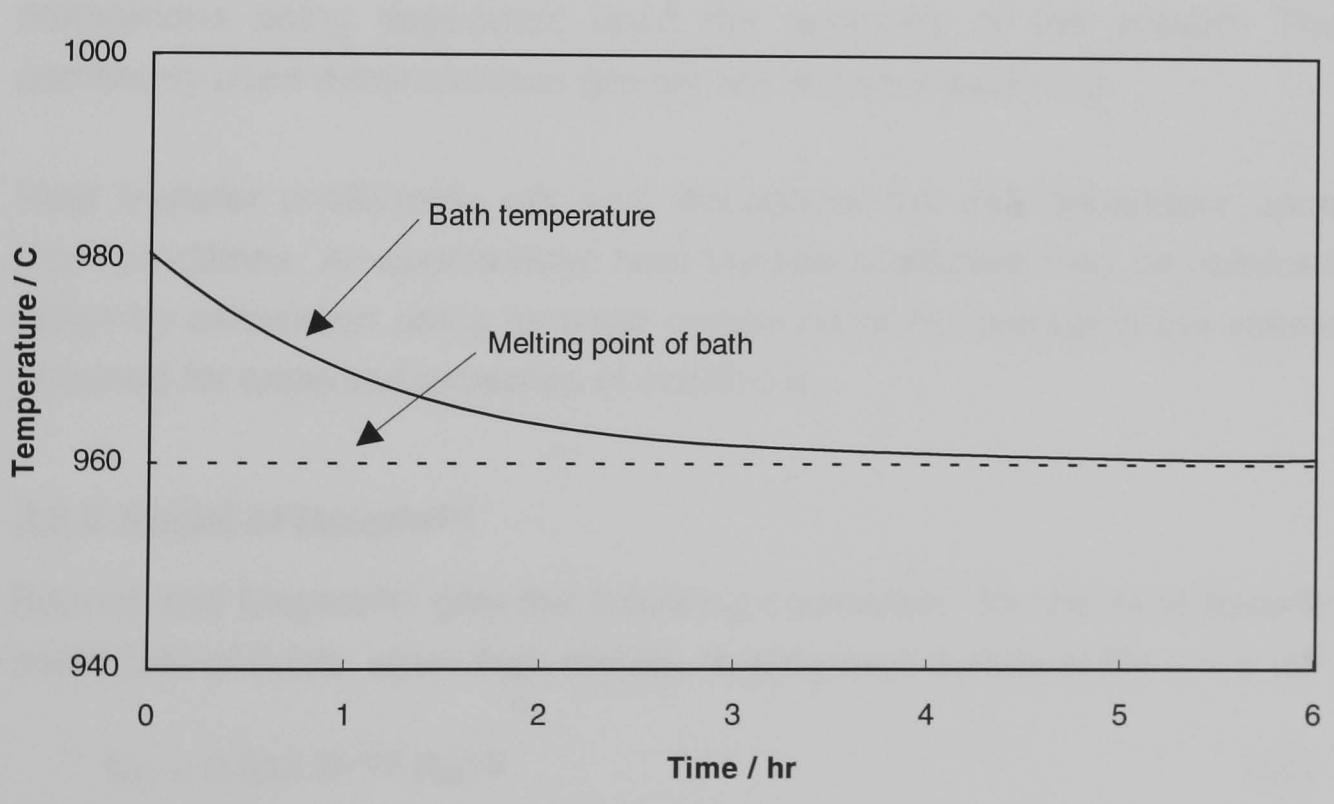

Figure 3.5 Variation of Freeze Thickness with Parameter f

components have been used to limit the amount of freeze formed by equation (48). In fact, the imbalance of heat flow at the boundary layer must be provided as latent heat by freezing or melting of the layer. Equation (47) cannot limit the total mass of the boundary layer that freezes or melts, but limits the composition that this layer can attain.

It can be seen from figure 3.5 that as f is reduced the freeze becomes more stable to changes in temperature. If it is to be assumed that f is very little for the metal zone then the freeze profile in this zone will be stable. Steady state models have found the ledge in the metal zone to be at least as responsive to temperature as that in the bath zone if not more so. The assumption that the diffusivity is less in the metal zone is also not borne out by the measurements at Anglesey. These found the same ledge composition in both zones.

3.6.1 Determination of heat transfer coefficients

A number of workers have calculated heat transfer coefficients for melts to sidewalls based upon correlations between dimensionless groups, the correlations being dependent upon the geometry of the system. The commonly used dimensionless groups are shown in table 3.3.

Heat transfer coefficients will vary throughout the cell dependent upon local conditions. An approximate heat transfer coefficient may be obtained either by calculation using average conditions or by averaging the values obtained for expected extremes of conditions.

3.6.2 Model of Haupin[60]

Bennet and Meyers[63] give the following correlation for the heat transfer coefficient of fluids, other than metals, flowing over a plate at $Re < 5 \times 10^5$.

$$Nu = 0.664\ Pr^{1/3}\ Re^{1/2} \qquad (49)$$

where the physical dimension for evaluating the Nusselt and Reynolds numbers is the interface dimension parallel to the fluid flow.

For aluminium flowing through a pipe Filimonov et al[64] gives the following correlation

Number	Symbol	Equation
Nusselt	Nu	$\frac{h \cdot L}{k}$
Grashof	Gr	$\frac{L^3 \cdot \rho^3 \cdot g \cdot \Delta T}{\mu^2}$
Prandtl	Pr	$\frac{Cp \cdot \mu}{k}$
Rayleigh	Ra	Gr·Pr
Reynolds	Re	$\frac{L \cdot \nu \cdot \rho}{\mu}$

where
- h = heat transfer coefficient of fluid
- L = physical dimension for description of system
  diameter in pipes of circular cross-section
- k = thermal conductivity of fluid
- ρ = density of fluid
- g = acceleration due to gravity
- ΔT = temperature gradient across fluid
- μ = viscosity of fluid
- Cp = specific heat capacity of fluid
- ν = velocity of the fluid

Table 3.3 Commonly Used Dimensionless Groups for Determination of Heat Transfer Coefficients

$$Nu = 5 + 0.025\,(Pr \cdot Re)^{0.8} \qquad (50)$$

Using these correlations, Haupin calculated the heat transfer coefficients for the metal pad to ledge and the bath to ledge. The critical dimension for the electrolyte was taken to be the bath depth measured at an angle to account for electromagnetic stirring and the drag force of swirling metal.

The equivalent diameter for fluid flowing in a shallow stream is used in the correlation for the metal. This is given by

$$L = \frac{4 \cdot H_m \cdot R_m}{2 \cdot H_m + R_m} \qquad (51)$$

where H_m = the depth of the metal pad
R_m = is the radius of rotation of molten metal

Applying typical properties for the metal and electrolyte at 980 °C Haupin obtained values of $h_b = 370\ W\,m^{-2}\,K^{-1}$ and $h_m = 1500\ W\,m^{-2}\,K^{-1}$. The result for h_b compares well with values calculated from measured heat fluxes but the calculated heat flux in the metal zone was 30-40% high. This discrepancy was attributed to the additional thermal resistance of the film of molten electrolyte always present at the metal / ledge interface. The effective heat transfer coefficient is then given by

$$\frac{1}{h_{me}} = \frac{1}{h_m} + \frac{x_e}{k_e} \qquad (52)$$

where h_{me} = effective heat transfer coefficient in metal zone
h_m = calculated heat transfer coefficient
x_e = thickness of electrolyte film
k_e = thermal conductivity of electrolyte

Assumption of a film thickness of 0.03 cm resulted in an effective heat transfer coefficient of $1100\ W\,m^{-2}\,K^{-1}$.

3.6.3 Model of A.Solheim and J.Thonstad[65]

Solheim and Thonstad used a low temperature model cell with gas induced flow to study the effect of gas flowrate, anode immersion depth

and anode-ledge distance on the heat transfer coefficient between the bath and ledge. This resulted in the relationship

$$h_{b(gas)} = k1 \cdot \left(\frac{GF \cdot AI}{ALD} \right)^{k2} \qquad (53)$$

where $h_{b(gas)}$ = heat transfer coefficient due to gas induced flow only
GF = gas flow rate per unit length of anode periphery
AI = anode immersion depth
ALD = anode-ledge distance
k1,k2 depend upon the position down the sidewall. For the middle position k1 = 140, k2 = 0.42.

This gives heat transfer coefficients in the region of 200-500 W m^{-2} K^{-1} but does not include the rotational effect of the bath due to electromagnetic forces. By applying a correction factor to account for horizontal flow the equation becomes

$$h_b = h_{b(gas)} \left[1 + \left(\frac{v_h}{v_v} \right)^2 \right]^{0.25} \qquad (54)$$

where h_b = heat transfer coefficient from bath to ledge
v_h = horizontal component of resultant fluid velocity
v_v = vertical component of resultant fluid velocity

Increasing the horizontal component from 0 to v_v results in a 19% rise in the value of h_b giving heat transfer coefficients of between 250–600 W m^{-2} K^{-1} in the middle region of the cell. This compares well with other published data.

3.6.4 Model of B.J. Welch

Welch[66] assumes a Nusselt correlation for natural convection superimposed with forced convection. Experimental data for heat flux measurements on immersed rotatable graphite cylinders giving flow patterns similar to those expected in industrial cells shows a straight line relationship between the Nusselt and Rayleigh numbers. The data for both

natural convection and natural convection plus superimposed velocity of approximately 0.15 m s^{-1} is shown in figure 3.6. Whilst it probably represents the most reliable data published, the accuracies for the heat transfer coefficients is only ±20%.

For natural convection involving parallel plates the form of correlation is

$$Nu = \alpha \cdot (Gr \cdot Pr)^m = \alpha \cdot Ra^m \qquad (55)$$

where α and m vary with orientation and size. Typically α varies between 0.2 and 1.3 and m is usually between 0 and 0.33.

For forced convection with laminar flow the correlation is usually of the form

$$Nu = \alpha \, Re^m Pr^n \qquad (56)$$

depending upon the geometry, α varies between 0.1 and 1 m between 0.33 and 0.8 and n about 0.33.

Using these correlations and parameters obtained from the experimental data Welch estimates ranges of heat transfer coefficient throughout the cell. For a bath with 10 °C superheat, that is 10 °C above the liquidus temperature of the bath, the local heat transfer coefficient for situations where only natural convection occurs is calculated as

$$450 < h_b < 480 \quad W\,m^{-2}\,K^{-1}$$

For the combined model with fluid velocities up to 0.15 m s^{-1} the range in heat transfer coefficient is

$$650 < h_b < 830 \quad W\,m^{-2}\,K^{-1}$$

This data shows that the heat transfer coefficient can vary by a factor of two for various locations on a cell's sidewall. Although these values are higher than other estimates published in literature Welch claims them to have been substantiated by independent unpublished data.

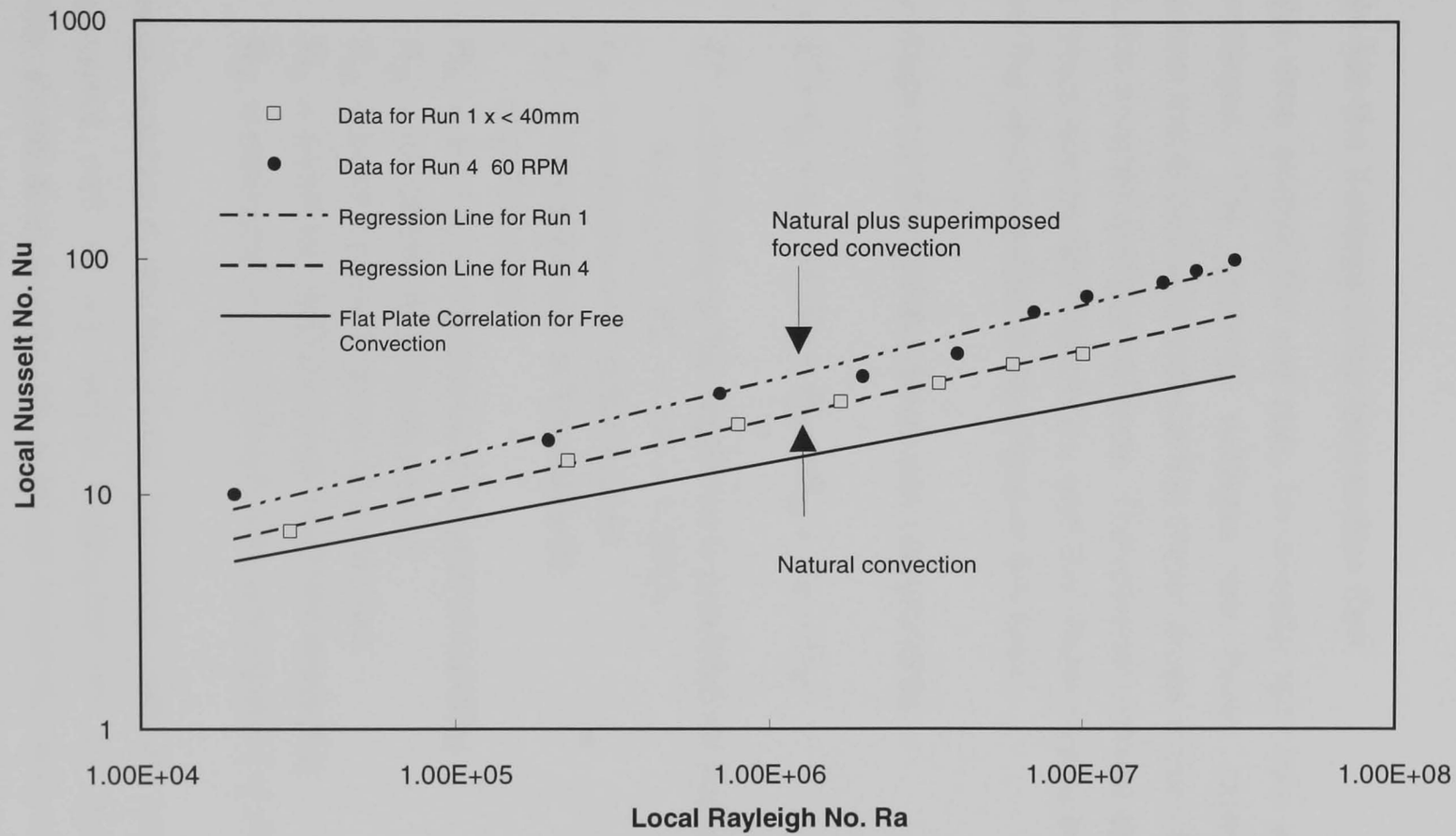

Figure 3.6 Local Nusselt Numbers as a Function of Local Rayleigh Number

This model does not include a specific correlation for gas induced turbulence in the cells. This is accounted for by the choices of the coefficients used in the two correlations, the velocity and critical dimension used in the calculation of the Reynolds number and degree to which the two models are superimposed.

3.7 Models for the Voltage Drop across the Cell

The voltage drop across the cell may be broadly split into external and internal voltages. The external voltages are those external to the electrolyte and metal pad and include the ohmic drops across the buswork of the cell, the anodes and the cathode. The internal voltage drops include the ohmic drops across the electrolyte and the metal pad and the voltage required for the electrochemical reactions in the bath.

The cell voltage can be broken down into components

$$E_{cell} = E^{\phi} + \eta_A + \eta_C + I\cdot(R_A + R_B + R_M + R_C + R_X) \qquad (57)$$

where E^{ϕ} = thermodynamic equilibrium potential for the reaction
$Al_2O_3 + 1.5C \rightarrow 2Al + 1.5CO_2$
η_A = overpotential at the anode
η_C = overpotential at the cathode
I = cell current
R_A = electrical resistance of anode assembly
R_B = electrical resistance of bath
R_M = electrical resistance of metal pad
R_C = electrical resistance of cathode assembly
R_X = electrical resistance of buswork external to the cell

The electrical resistance for the anode assembly, cathode assembly and external buswork can all be simply measured on an operating cell. Although the ohmic drop across the external buswork does not affect the heat balance on the cell, it must be included to determine the power efficiency of the cell.

The general equation for the resistance for a homogenous material with uniform temperature is

$$R = \frac{\kappa \cdot \ell}{A} \qquad (58)$$

where R = resistance of object
κ = electrical conductivity of material
ℓ = length of object
A = cross-sectional area for current flow

The resistance of the bath and metal pad may be approximated by the above relationship when an effective area for current flow is used. The effective area is an approximation to the true current distribution of the cell. Accurate models for the calculation of current distribution and voltage profiles are too complex for use in dynamic simulation. In models where the temperature and composition of the electrolyte is assumed to be uniform throughout, the current may be assumed to flow uniformly through an effective area based upon the area of the electrode. Haupin[67] correlated the effective anode cross sectional area with anode environment by determining the isopotential planes under and along the sides of each anode in a laboratory cell. This was done using an aluminium coated tungsten reference electrode and a micrometer positioning device. The effective area was correlated to anode enviroment by fanning factors, defined as an additional length or width added to the actual dimensions of the anode. The effective area of an anode is then

$$A_i = (L_A + F_{L1} + F_{L2}) \cdot (W_A + F_{W1} + F_{W2}) \qquad (59)$$

where A_i = effective area for current flow under anode i
L_A = actual length of anode
W_A = actual width of anode
F_{L1}, F_{L2} = fanning factors in the two directions of length
F_{W1}, F_{W2} = fanning factors in the two directions of width

A typical set of fanning factors determined against anode-cathode distance is shown in figure 3.7.

Haupin assumes that the effective area for the bath is equal to the total effective area of the bank of n anodes and is given by

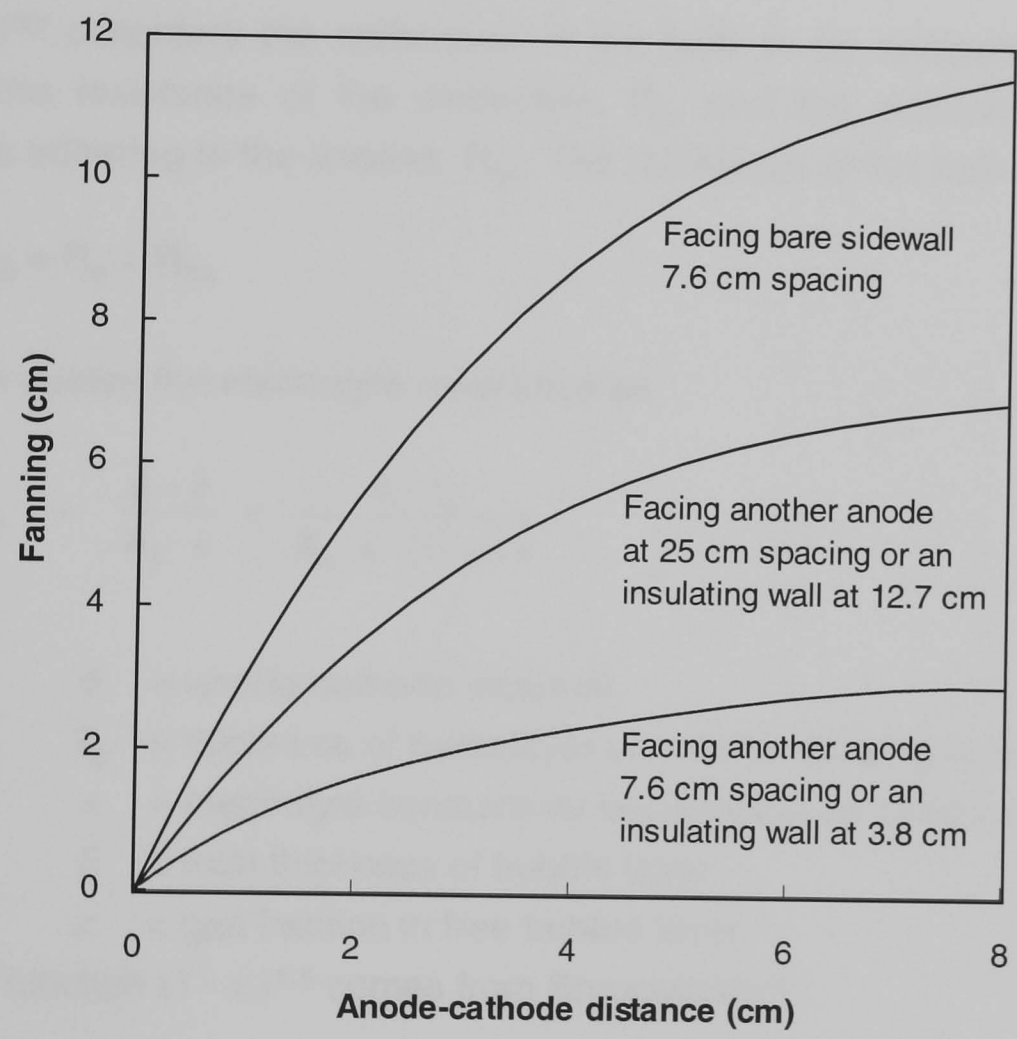

Figure 3.7 Fanning Factors for Determination of Effective Anode Area

$$A_A = A_B = \sum_{i=1}^{n} A_i \qquad (60)$$

where A_A = effective area for current flow through bank of anodes
A_B = effective area for current flow through bath
n = number of anodes in cell

This value is used to calculate the current density at the anode and the electrical resistance of the electrolyte.

Haupin[30] considers the resistance of the bath to be composed of two parts, the resistance of the electrolyte, R_e, and the resistance due to bubbles adhering to the anodes, R_{ba}. The resistance of the bath is then

$$R_B = R_e + R_{ba} \qquad (61)$$

Haupin quotes the electrolyte resistance as

$$R_e = \frac{d-\delta}{A_B \cdot \kappa} + \frac{\delta - t_a}{A_B \cdot \kappa \cdot (1-\varepsilon)^{1.5}} \qquad (62)$$

where d = anode-cathode distance
t_a = thickness of monolayer of bubbles ahering to anode
κ = electrolyte conductivity uncorrected for bubbles
δ = total thickness of bubble layer
ε = gas fraction in free bubble layer
and the function $(1 - \varepsilon)^{1.5}$ comes from Bruggeman[68]

The resistance of bubbles adhering to the anode derived from data reported by Sides and Tobias[69] is

$$R_{ba} = \frac{t_a}{\kappa \cdot (1-1.26 f_c) \cdot A_A} \qquad (63)$$

where f_c = fraction of the anode surface covered with bubbles

Haupin quotes this equation valid up to f_c = 0.65. This model for the electrolyte resistance is shown schematically in figure 3.8.

$$R_B = R_e + R_{ba}$$

$$R_e = \frac{d - \delta}{A_B K} + \frac{\delta - t_a}{A_B K (1-\varepsilon)^{1.5}}$$

$$R_{ba} = \frac{t_a}{K (1 - 1.26 f_c) A_A}$$

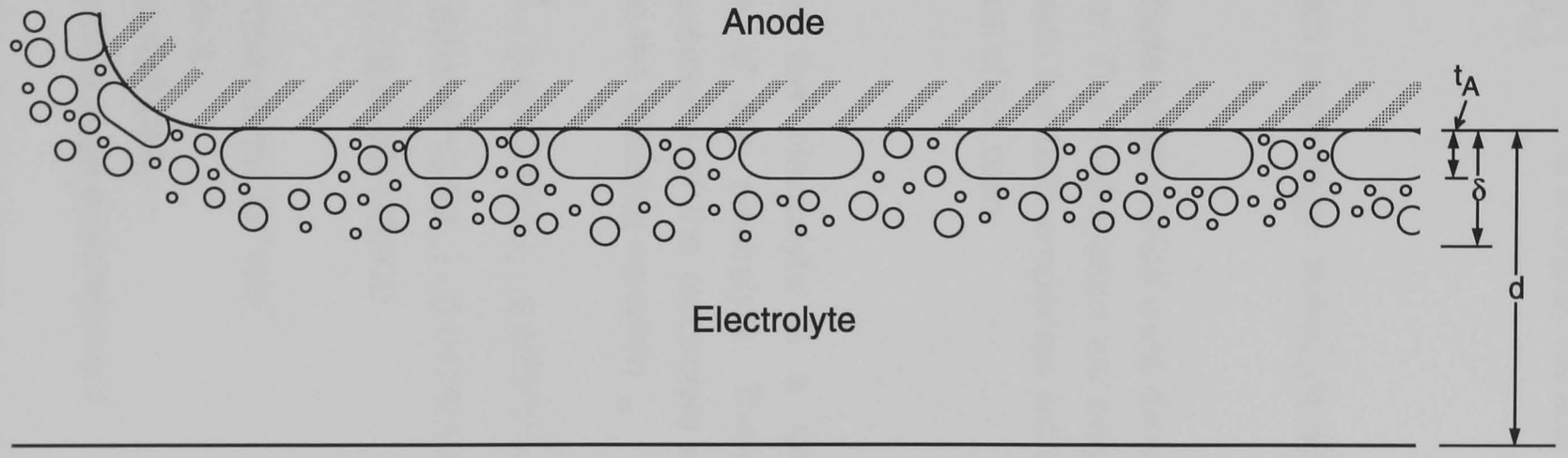

Figure 3.8 Schematic Diagram of the Model for Resistance across the Bath

The accuracy of this model is dependent upon the relationships used for f_c, ε, t_a and δ. In calculations at the Trondheim course the following relationships for f_c and ε are used and t_a and δ are assumed constant.

$$f_c = \frac{100}{(1 + 0.75 \times \%Al_2O_3)} \quad \% \text{ of anode surface} \qquad (64)$$

$$\varepsilon = 0.02 \times \%Al_2O_3$$

where $\%Al_2O_3$ is the weight percentage of Al_2O_3 in solution in the electrolyte

No indication is given of how these relationships were derived or the type of cell that they were derived for. The relationships are only related to the alumina concentration in the bath but both properties will be affected by the composition and temperature of the bath.

3.7.1 Electrical conductivity

The electrical conductivity of the electrolyte is a function of the composition and temperature of the electrolyte. There have been numerous experimental measurements of the electrolyte and regression analysis by Choudhary[70] led to the following equation

$$\begin{aligned} \ln\kappa = {} & 2.0156 - \frac{2068.4}{T} + 0.4349(\text{Ratio}) - 0.0207(\%Al_2O_3) \\ & - 0.005(\%CaF_2) - 0.0166(\%MgF_2) + 0.0178(\%LiF) \\ & + 0.0077(\%Li_3AlF_6) + 0.0063(\%NaCl) \end{aligned} \qquad (65)$$

where k = electrical conductivity $\Omega^{-1}\,cm^{-1}$
T = temperature K
Ratio = weight ratio NaF/AlF_3
% refers to weight percentage of component

This equation is claimed to give values of electrical conductivity with an accuracy better than ± 4%.

Three theoretical models have been presented by P. Fellner et al[71]. The first model is based on the assumption that the conductivity is proportional

to the number density of the effective electrical charges in the melt. In cryolite melts with large complex anions the current is carried mainly by cations which may be assumed to move by the influence of an electric field relative to the framework formed by the anions.

As a first approximation to the conductivity Fellner obtained

$$\kappa_{mix} = 93.5 \frac{\sum x_i \cdot z_i}{\sum x_i \cdot v_i^{\phi}} \qquad (66)$$

where k_{mix} = conductivity of melt
x_i = mol fraction of component i in the melt
z_i = effective charge of the current carrying species
v_i^{ϕ} = molar volume of species i

The numerical value of 93.5 Ω^{-1} cm^2 mol^{-1} for the proportionality factor was determined experimentally from the conductivity of pure cryolite by extrapolation to its value at 1273 K. This factor is assumed constant when the anion framework is not significantly affected by the additions.

The two other models assume that the charge-carrying species do not mutually influence each other. The conductivity is then the sum of the contributions of the pure melts placed in two conductivity cells connected in series or parallel. A schematic diagram of these two models is shown in figure 3.9. For two melts with conductivities κ_1 and κ_2 and volumes V_1 and V_2 in conductivity cells with cross sectional area A the resistivities R_1 and R_2 are given

$$R_1 = \frac{V_1}{\kappa_1 \cdot A} \qquad R_2 = \frac{V_2}{\kappa_2 \cdot A} \qquad (67)$$

In the series model, the conductivity cells are connected in series and the total resistivity, R_{total} is the sum of R_1 and R_2

$$R_{total} = \frac{V_1}{\kappa_1 \cdot A} + \frac{V_2}{\kappa_2 \cdot A} = \frac{V_1 + V_2}{\kappa_{mix,s} \cdot A} \qquad (68)$$

where $\kappa_{mix,s}$ denotes the conductivity of the system for the two cells connected in series and is equal to the ideal conductivity of the mixture of

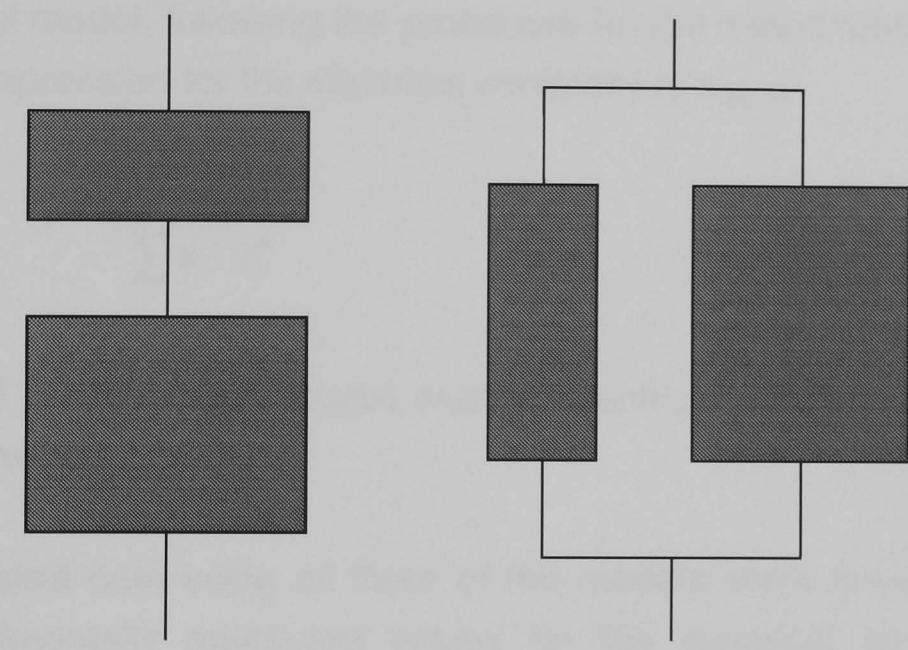

Schematic illustration of models for the calculation of conductivity of a binary mixture with volume fractions of the ratio 1:2.

Figure 3.9 Models for Electrolyte Conductivity

the two melts. Introducing molar volumes and mole fractions and extending the model to multi-component mixtures gives

$$\kappa_{mix,s} = \frac{\sum x_i \cdot v_i^{\phi}}{\sum \frac{x_i \cdot v_i^{\phi}}{\kappa_i}} \qquad (69)$$

Fellner states that this model can be shown to give a good description of systems that exhibit nearly ideal thermodynamic behaviour.

The parallel model, following the procedure for the series model, gives the following expression for the electrical conductivity $\kappa_{mix,p}$

$$\kappa_{mix,p} = \frac{\sum x_i \cdot \kappa_i \cdot v_i^{\phi}}{\sum x_i \cdot v_i^{\phi}} \qquad (70)$$

This model is a boundary model and the electrical conductivity is always less than that calculated.

The calculated data using all three of the models show good agreement with experimentally measured values for the electrical conductivity at various bath compositions used industrially. As shown in figure 3.10 the simple model shows very good agreement for binary cryolite melts at 1273 K with the exception of the Na_3AlF_6 - LiF system containing more than 5 wt% LiF. The experimental data for this system falls between the predicted values of the series and parallel models approximating to the former at low wt% LiF and to the latter at high wt% LiF.

Data calculated from the simple model for the tertiary system Na_3AlF_6 - Al_2O_3 - LiF is shown in figure 3.11. In this system Al_2O_3 decreases the conductivity while LiF increases it. This then provides a good test for the suitability of the simple model to predict conductivity data. The data shows good agreement with measurements by Matiasovsky et al[72].

The electrical conductivity of molten aluminium is such that the resistance of the metal pad may be neglected or assumed constant and included in the overall resistance of the cathode.

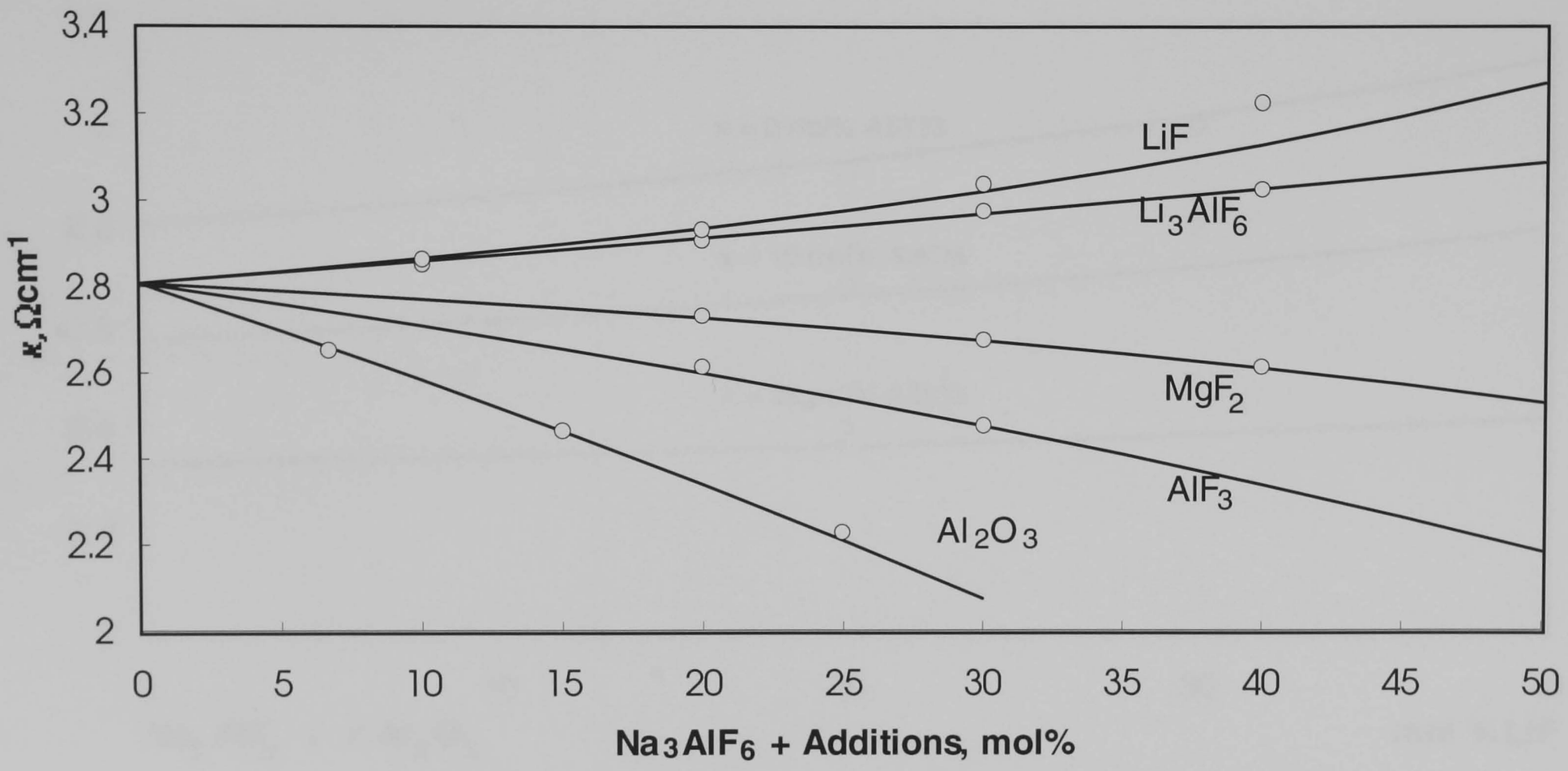

Figure 3.10 Results of Fellners Simple Model for Binary Systems

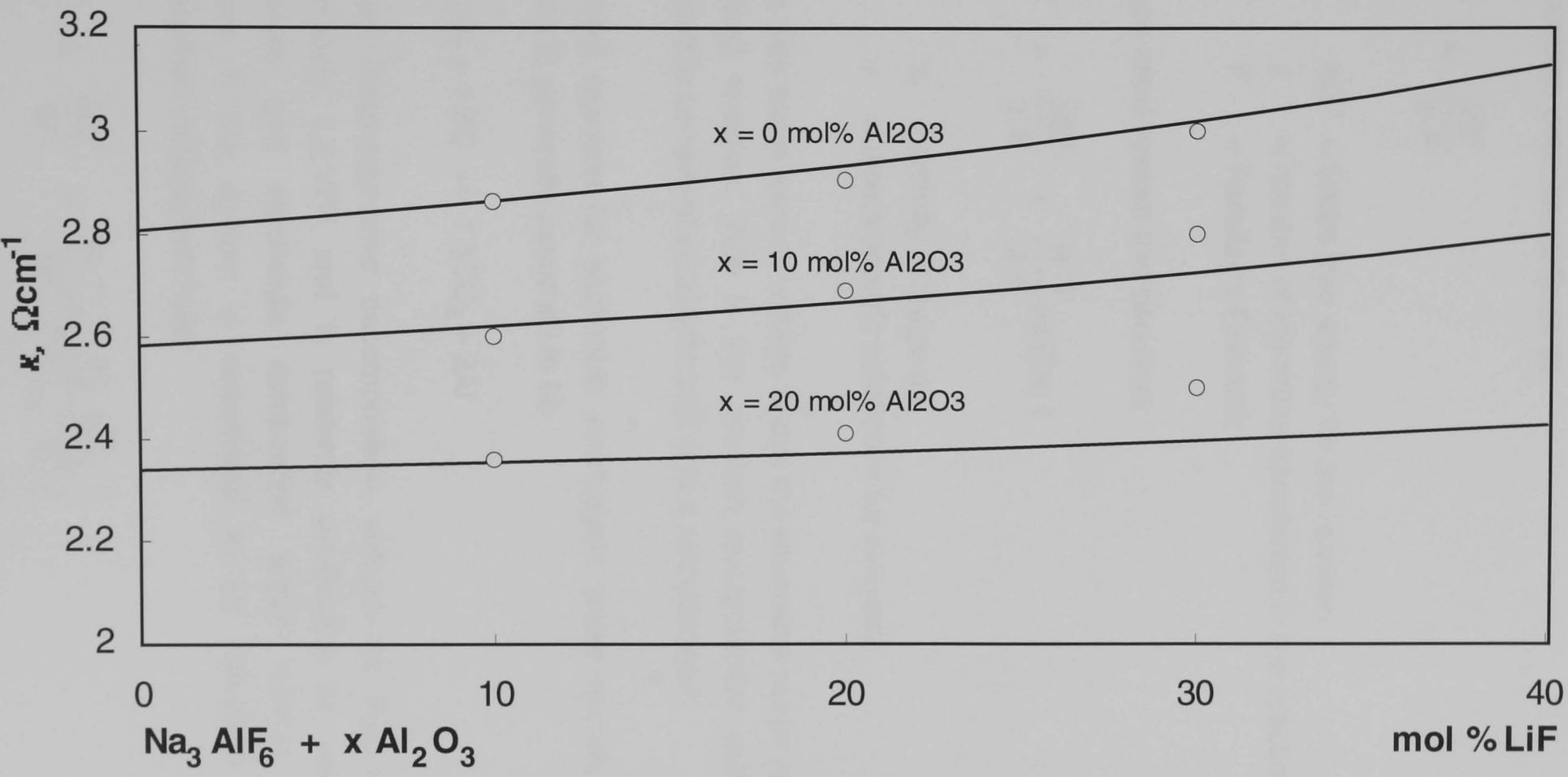

Figure 3.11 Results of Fellners Simple Model of Tertiary System

3.7.2 Reversible decomposition potential and electrode overpotential

For an overall cell reaction there is a thermodynamically reversible decomposition potential defined as

$$E^{\phi} = \frac{\Delta G^{\phi}}{z \cdot F} \qquad (71)$$

where ΔG^{ϕ} = Gibbs free energy for the reaction
z = number of electrons transferred in the reaction
F = Faraday's Constant

For a non ideal system this becomes

$$E^{\phi} = \frac{\Delta G^{\phi}}{z \cdot F} + \frac{R \cdot T}{z \cdot F} \ln\left(\prod a_i^{v}\right) \qquad (72)$$

where a_i = activity of reagent i
v = stoichiometric coefficient for reagent i

There is also some excess voltage above the reversible range required for the overall reaction. This is the reaction overpotential and may be considered to consist of an anodic part and a cathodic part.

The overall reaction for aluminium electrolysis under normal operating conditions is generally assumed to be

$$Al_2O_3 + 1.5C \rightarrow 1.5CO_2 + 2Al \qquad [4]$$

The ideal thermodynamic decomposition voltage for this reaction is approximately 1.2 V[73] and is relatively unaffected by variations in temperature and electrolyte compostion within normal operating conditions. If the system is considered to be non-ideal then the decomposition voltage becomes

$$E^{\phi} = \frac{\Delta G^{\phi}}{6F} + \frac{R \cdot T}{6F} \ln\left(\frac{a_{Al}^{2} \cdot a_{CO_2}^{1.5}}{a_{Al_2O_3} \cdot a_{C}^{1.5}}\right) \qquad (73)$$

Haupin[74] assumes the activities of all reactants and products, except alumina, to be unity. This is valid if these components may be assumed to exist in their standard states, that is that the aluminium and carbon are essentially pure condensed phases and that nearly pure carbon dioxide contacts the anode at approximately 1 atm pressure. Alumina in solution will have unit activity only at saturation and Haupin uses the following relationship for alumina activity

$$a_{Al_2O_3} = \left(\frac{C_{Al_2O_3}}{C_{sat}} \right)^{2.77} \qquad (74)$$

where $C_{Al_2O_3}$ = alumina concentration wt%
C_{sat} = saturation concentration of alumina wt%

This relationship is derived from work by Dewing[75] on alumina activity in pure cryolite at 1300 K.

Under normal electrolysis and non-equilibrium conditions, the overall cell reaction voltage is higher than the reversible decomposition potential. This is because excess voltage above the reversible value is required for the reaction to proceed at practical rates. The voltage in excess of the reversible decomposition potential is the cell overpotential.

The total overpotential across the cell consists of an overpotential at each electrode and investigations of cell potential generally consider the cathodic and anodic overpotentials separately. In the aluminium reduction cell, the overpotential is primarily affected by alumina concentration, anode carbon characteristics, current density and temperature.

Haupin[30] considers the overpotential at an electrode to be composed of two parts. These are a surface or reaction overpotential, η_s, and a concentration overpotential, η_c. The total overpotential at the electrode, η_t, is then

$$\eta_t = \eta_c + \eta_s \qquad (75)$$

Under different circumstances the concentration and reaction overpotentials have greatly different values and the reaction can become concentration or surface limited

3.7.3 Cathodic overpotential

Many investigators have measured cathodic overpotential and found it fitted a Tafel relationship over the range of commercial interest. Laboratory measurements by Thonstad and Rolseth[76], for electrolytes of industrial interest without stirring, gave Tafel plots

$$\eta = \alpha + \beta \log i \qquad (76)$$

where η = electrode overpotential V
i = electrode current density for reaction A cm^{-2}
α, β= Tafel coefficients

with coefficient α ranging from 0.19 to 0.21 and β ranging from 0.23 to 0.25. Stirring lowered the overpotential by 40-50% which Haupin[30] takes to indicate a concentration overvoltage. Thonstad and Rolseth found the cathodic overpotential in industrial cells to be between the values for unstirred and vigorously stirred laboratory cells at about 0.1 V. Alcoa data for industrial cells[77] resulted in the following empirical relationship valid for current densities above 0.1 A cm^{-2}.

$$\eta_{ct} = \frac{R \cdot T \cdot (1.375 - 0.125 \cdot CR)}{1.5 \cdot F} \ln\left(\frac{i_c}{0.257}\right) \qquad (77)$$

where η_{ct} = total overpotential at the cathode
CR = cryolite ratio, mole ratio NaF/AlF3
i_c = cathodic current density

References

1 Richard, M. C., *"Use of a Mathematical Cell Model to Determine Cell Parameter Design Changes for Production Maximization"*, AIME Light Metals, 1975, pp95

2 Sulmont, B. and Hudault, G., *"Application of a Thermoelectric Model to the Investigation of Reduction Cell Thermal Equilibrium"*, AIME Light Metals, 1978, pp73

3 Blake, S. R., *"A Model for the Variation of Alumina Concentration in Industrial Hall-Héroult Cells"*, MSc Thesis, Department of Chemical Engineering, University of Newcastle upon Tyne, June 1983

4 Ek, A. and Fladmark, G. E., *"Simulation of Thermal, Electric and Chemical Behaviour of an Aluminum Cell on a Digital Computer"*, AIME Light Metals, 1973, pp85

5 Hashimoto, T. and Ikeuchi, H., *"Computer Simulation of Dynamic Behaviour of an Aluminum Reduction Cell"*, AIME Light Metals, 1980, pp273

6 Thonstad, J., Nordmo, F. and Paulsen, J. B., *"Dissolution of Alumina in Molten Cryolite"*, Metallurgical Transactions, vol 3, February 1972, pp403-407

7 Gerlach, J., Hennig, U. and Kern, K., *"The Dissolution of Aluminium Oxide in Cryolite Melts"*, AIME Light Metals, vol 1, 1974, pp49-61

8 Thonstad, J., *"The 4th Int. Course on Process Metallurgy of Aluminium"*, Trondheim, 1985

9 Winkhaus, G., *"On the Dissolution Rate of Alumina in Cryolite Melts"*, 99th AIME Annual Meeting, Denver,1970, Paper A70-25

10 Maeda, H., Matsui, S., and Era, A., *"Measurement of Dissolution Rate of Alumina in Cryolite Melt"*, AIME Light Metals, 1985 pp763-780

[11] Asbjørnsen, O. A., Andersen, J. A., *"Kinetics and Transport Processes in the Dissolution of Aluminium Oxide in Cryolite Melts"*, AIME Light Metals 1977, pp137-152

[12] Kachanovskaya, I. S., Osivik, V. I. and Kukhotkina, T. N., *"Phase Transformations and Alumina Dissolution in Cryolite"*, Tsvetnye Metally, No 12, 1971, pp10-23

[13] Jain, R. K. et al, *"Interaction of Aluminas with Aluminium Smelting Electrolytes"*, AIME Light Metals, 1983, pp609

[14] Thonstad, J., Johansen, P., and Kristensen, E. W., *"Some Properties of Alumina Sludge"*, AIME Light Metals, 1980, pp227-241

[15] Hove, S.J. and Kvande, H., *"Centre-Break Alumina Feeding and Sludge Control of Prebaked Cells"*, AIME Light Metals, 1982, pp513

[16] Keller, R., *"Alumina Dissolution and Sludge Formation"*, AIME Light Metals, 1984, pp513

[17] Less, L. N., *"The Crusting Behaviour of Smelter Aluminas"*, AIME Light Metals, 1976, pp315

[18] Thonstad, J., Rønning, S. and Entner, P., *"Formation of Bottom Crusts in Aluminium Pots. A Laboratory Study"*, AIME Light Metals, 1982, pp485

[19] Bagshaw, A. N., Kuschel, G., Taylor, M. P., Tricklebank, S. B., and Welch, B. J., *"Effect of Operating Conditions on the Dissolution of Primary and Secondary (Reacted) Alumina Powders in Electrolytes"*, AIME Light Metals, 1985, pp649-660

[20] Entner, P, Scmidt-Hatting, W., Mitrovic, Z., Gruber, U., Rufer, D. and Fjørnes, *"Investigation of the Dynamic Behaviour of Aluminum Pots"*, AIME Light Metals, 1984, pp701

[21] Haupin, W. E., *"Mathematical Model of Fluoride Evolution from Hall-Héroult Cells"*, The 4th Int. Course on Process Metallurgy of Aluminium, Trondheim, 1985

[22] Sidorov, L.N., Kolosov, E.N. and Shol'ts, V.B., Russian Journal of Physical Chemistry, 42, pp1382-1386, 1968

[23] Grjotheim, K., Kvande, H. and Motzfeldt, K., *"Vapor-Liquid Equilibria in the System NaF-AlF_3-Al_2O_3"*, AIME Light Metals, 1975, pp125-137

[24] Newitt, Dombrowski and Knellman, Trans. Inst. Chem. Engr., vol 32, 1954, p244

[25] Azbel, D.S. and Lee, S.L., *"Two-Phase Momentum Heat Transfer Chemistry"*, Process Eng. Syst., vol 1, p159, 1978

[26] Grjotheim, K., Haupin, W.E and Welch, B. J., *"Current Efficiency -- Relating Fundamental Studies to Practise"*, AIME Light Metals, 1985, pp679

[27] Frovlova, E.B., Dobrokhotov, V.B. and Tsyplakov, A.M., Trudy V.A.M.I, 89, vol 36, 1971

[28] Waddington, J. and Pearson, T. G., *"Electrode Reactions in the Aluminium Reduction Cell"*, Discussions, Faraday Society, 1947, vol 1, pp307-320

[29] Vetyukov M. M. et al, Isv. Vyssh. Uchebn. Zaved., Tsvetn. Metall., 1978, p62

[30] Haupin, W. E., *"The 4th Int. Course on Process Metallurgy of Aluminium"*, Trondheim, 1985

[31] Qiu, Z. and Fan, L., *"The Rate Determining Step of Metal Loss in Cryolite-Alumina Melts"*, AIME Light Metals, 1984, pp789

[32] Poole, R.T., Etheridge, C., *"Aluminium Reduction Cell Variables and Operations in Relation to Current Efficiency"*, AIME Light Metals, 1975, pp163-183

[33] Wittner, H., *"Working Methods for High-Current Efficiency and Flexible Amperage"*, AIME Light Metals, 1975, pp139-150

[34] Wittner, H. and Giulini, Gebr., *"How to run a Smelter with Current Efficiency higher than 90%-Scientific and Practical Basis"*, AIME Light Metals, 1977, pp153-161

[35] Bratland, D., José del Campo, J. and Cho, K., *"Current Efficiency Measurements in Laboratory Aluminium Cells. Influence of Bath Volume, Anode Size and Anode Quality"*, AIME Light Metals, 1981, pp281-308

[36] Berge, B., Grjotheim, K., Krohn, C., Naeumann, R. and Tørklep, K., *"The Influence of Operating Parameters on the Current Efficiency in the Aluminium Reduction Cells"*, AIME Light Metals, vol 1, 1976, pp23

[37] Robl, R. F., Haupin, W. E., and Sharma, D., *"Estimation of Current Efficiency by a Mathematical Model Including Hydrodynamics Parameters"*, AIME Light Metals, vol 1, 1977, p185

[38] Evans, J.W., Zundelevich, Y. and Sharma, D., Met. Trans, vol 12B, 1981

[39] Levich, V.G, *"Physicochemical Hydrodynamics"*, Prentice Hall, New Jersey, 1962, pp690-698

[40] Lillebuen, B., Ytterdahl, S. A., Huglen, R., and Paulsen, K. A., *"Current Efficiency and Back Reaction in Aluminium Electrolysis"*, Electrochimica Acta, vol 25, No, 2, February 1980, p131

[41] Lillebuen, B., and Mellerud, Th., *"Current Efficiency and Alumina Concentration"*, AIME Light Metals, 1985, p637

[42] Aarebrot, E. et al, Metall. vol 32, no 41, 1978

[43] Bratland, D., Grjotheim, K., Krohn, C. and Motzfeldt, K., Journal of Metals, vol 19, 1967, pp13

[44] Vetyukov, M. M. et al, Physical Chem. and Electrochem. of Molten Salts and Slags, Kiev, 1969, pp367

[45] Gjerstad et al, Symposium on Industrial Electrode Processes with Gas Evolution, Electrochem. Soc., 1966

[46] Belyaev et al, Izv, Vyssh. Ucheb. Zav., Tsvetn. Met., vol 4, no 3, 1961, p67

[47] Grjotheim K. et al, Can. Met. Quart., vol 11, 1972, p295

[48] Firsanova et al, Izx. Vyssh. Ucheb. Zav., Tsvetn. Met., vol 5, no 3, 1962, p52

[49] Bersimenko et al, Tsvet. Met., vol 46, no 3, 1973, p30

[50] Szekér, Acta Tech. Acad. Sci. Hung., vol 10, 1955, p91

[51] Abramov et al, *"Theoretical Principles of the Electrometallurgy of Aluminium"*, Moscow, 1953

[52] Schmitt, H., *"Extractive Metallurgy of Aluminium"*, vol2, Intersci. Pub., New York, 1963, p169

[53] Thonstad, J. et al, Proceedings, 3rd Czech. Aluminium Symposium, Banská Bystrica, 1976, p88

[54] Poole, R. T. and Etheridge, C., *"Aluminium Reduction Cell Variables and Operations in Relation to Current Efficiency"*, AIME Light Metals, 1977, pp163

[55] Rolseth, S. and Thonstad, J., *"On the Mechanism of the Reoxidation Reaction in Aluminum Electrolysis"*, AIME Light Metals, 1981, pp289

[56] Vasiliadis, C. G., *"Mass Transfer Studies related to Aluminium Electrolysis"*, MSc Dissertation, Oct 1981, University of Newcastle upon Tyne

[57] Arita, Y., Urata., N. and Ikeuchi, H., *"Estimation of Frozen Bath Shape in an Aluminum Reduction Cell by Computer Simulation"*, AIME Light Metals, 1978, pp59

[58] Sulmont, B. and Hudault, G., *"Application of a Thermoelectric Model to the Investigation of Reduction Cell Thermal Equilibrium"*, AIME Light Metals, 1978, pp73

[59] Peacey, J. G. and Medlin, G. W., *"Cell Sidewall Studies at Noranda Aluminum"*, AIME Light Metals, 1979, pp475

[60] Haupin, W. E., *"Calculating Thickness of Containing Walls Frozen from Melt"*, AIME Light Metals, 1971, pp188

[61] Thonstad, J. and Rolseth, S., *"Equilibrium between Bath and Side Ledge in Aluminium Cells. Basic Principles"*, AIME Light Metals, 1983, pp415

[62] Paulsen, K.A., Huglen, R., Andersen, J.A., Lillebuen, B., and Ytterdahl, S.A., *"Variation of Side Lining Temperature, Anode Position and Current/Voltage Load in Aluminium Reduction Cells"*, AIME Light Metals, 1980, pp325-339

[63] Bennet and Meyers, *"Momentum, Heat and Mass Transfer"*, McGraw-Hill, 1962

[64] Filimonov, S. S., Kryukova, M. G. and Teplov, S. V., Thermal Physics of High Temperatures, vol 2, no 6, 1964, pp901

[65] Solheim, A. and Thonstad, J., *"Heat Transfer Coefficients between Bath and Side Ledge in Aluminum Cells. Model Experiments"*, AIME Light Metals, 1983, pp425

[66] Welch, B.J., *"Energy Balance-Transient Thermal Effects During Cell Operation"*, The 4th Int. Course on Process Metallurgy of Aluminium, Trondheim, 1985

[67] Haupin, W.E., *"A Scanning Reference Electrode for Voltage Contours in Aluminum Smelting Cells"*, Journal of Metals, Oct., 1971

[68] Bruggeman, D.A., Ann. Physik, vol 24, 1935, p632

[69] Sides, P.J. and Tobias, C.W., J. Electrochem. Soc., vol 129, 1982, p2715

[70] Choudhary, G., *"Electrical Conductivity for Aluminum Cell Electrolyte between 950°–1025°C by Regression Equation"*, J. Electrochem. Soc., vol 120, 1973, pp381-383

[71] Fellner, P., Grjotheim, K. and Kvande, K., *"Model Calculations of Cryolite Melts"*, AIME Light Metals, 1984, pp805

[72] Matiašovsky, K., Danek, V. and Malinovský, M., *"Effect of LiF and Li_3AlF_6 on the Electrical Conductivity of Cryolite-Alumina Melts"*, J. Electrochem. Soc., 116, 1969, pp1381-1383

[73] Lewis, R. A., *"Technical Fundamentals of the Aluminum Reduction Cell Process"*, Reduction Division Technical Manual I, Kaiser Aluminum Internal Publication, 1973

[74] Haupin, W.E., *"Overvoltages Determined by Nonlinear Regression Analysis of Cell Volts vs. Current Density"*, AIME Light Metals, 1980m pp183-190

[75] Dewing, E.W., *"Liquidus Curves for Aluminum Cell Electrolyte v. Representation by Regression Equations"*, J. Electrochem. Soc., 117, 1970, pp780-781

[76] Thonstad, J. and Rolseth, S., Proceedings of 3rd ICSOBA Conference, Nice, 1973, p657

[77] Haupin, W.E. and Frank, W.B., *"Comprehensive Treatise of Electrochemistry"*, eds. Bockris, Conway, Yeager and White, Plenum Publishing Corp., New York, 1981, p308

4.0 Development of a Dynamic Model

A conceptual model of the aluminium reduction process is shown in figure 4.1. The interconnections between the functional blocks represent the flow of mass, energy and information. Each block represents a set of equations describing the relationships between the inputs and outputs of that block. These relationships take the form of differential and algebraic expressions derived from analysis of published work, plant data and mathematical modelling techniques.

4.1 Reactor Modelling

Electrochemical cells can be analysed in the same way as any chemical reactor. The equations describing the process fall largely into two types: balance equations (materials and energy) and rate equations (reaction rate, heat and mass transfer etc). A general mass balance would be written

Rate of accumulation = Rate in - Rate out + Rate of reaction

For a stirred tank reactor with a number of streams entering and leaving the vessel this can be written

$$V\sum_{j=1}^{m}\frac{dC_j}{dt} = \sum_{k=1}^{n}\sum_{j=1}^{m}Q_k C^f_{k,j} - \sum_{l=1}^{p}\sum_{j=1}^{m}Q_l C_j + \sum_{j=1}^{m}R_j - \sum_{j=1}^{m}C_j\frac{dV}{dt} \quad (1)$$

where
- V = volume of the reaction mixture
- C_j = concentration of species j in the vessel
- Q_k = flow rate of stream k into the vessel
- $C^f_{k,j}$ = concentration of species j in feed stream k
- Q_l = flow rate of stream l out of vessel
- R_j = rate of reaction for species j

The mass balance for an electrochemical cell differs primarily in that there are both chemical and electrochemical reactions to be considered. The reaction term in equation (1) therefore becomes

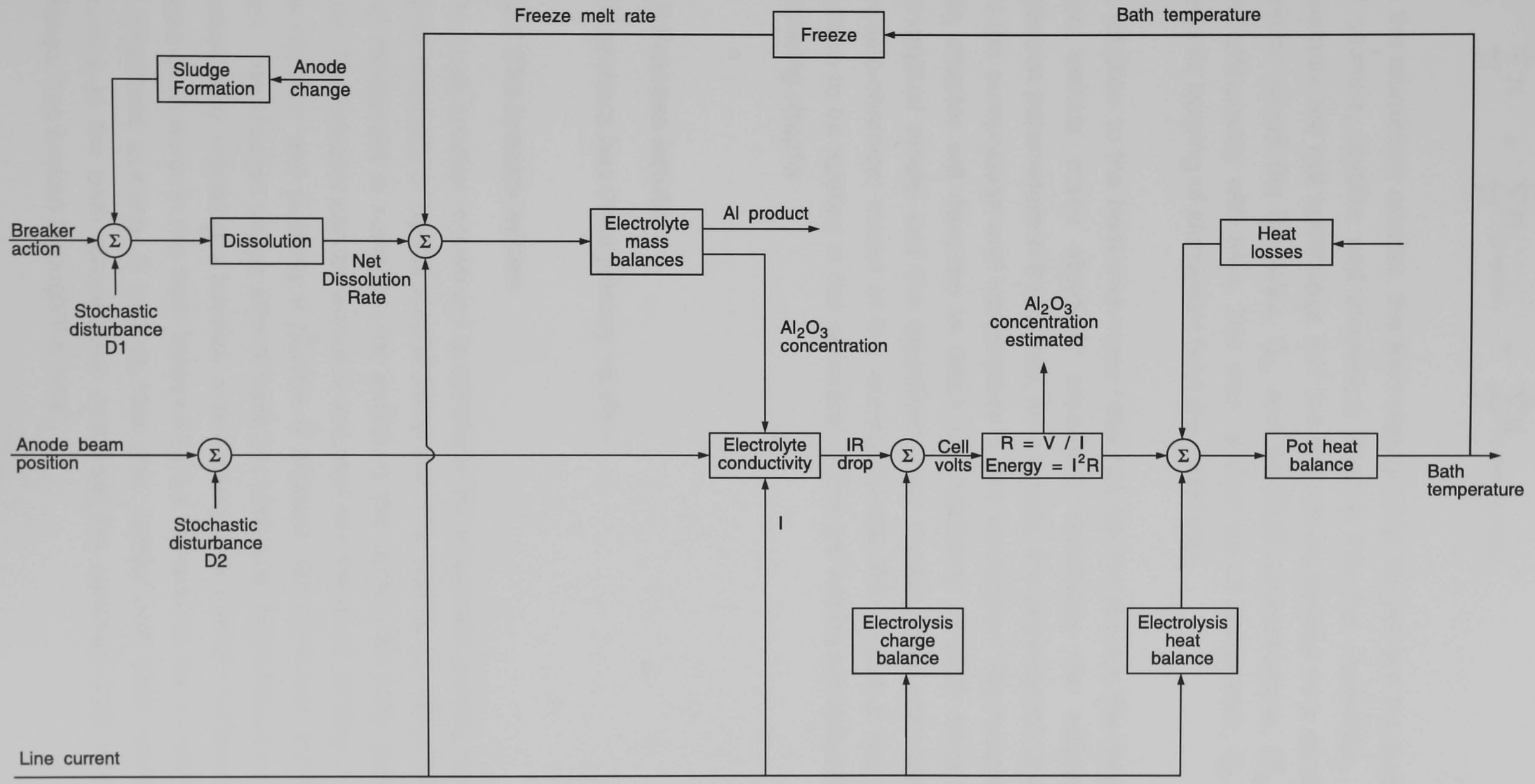

Figure 4.1 Conceptual Model of the Aluminium Reduction Cell

$$\sum_{j=1}^{m} R_j = \sum_{j=1}^{m} R_{j\,(chemical)} + \sum_{j=1}^{m} R_{j\,(electrochemical)} \qquad (2)$$

In the aluminium smelter, the feed streams into the cell are the feed rates of alumina, cryolite and aluminium fluoride into the electrolyte. These flowrates are not continuous and the cell can be treated as a semi batch reactor where the flowrates, Q_k, and the feed concentrations, $C^f_{k,j}$, vary discontinuously with time. The main stream out of the reactor, Q_l, is the periodic tapping of aluminium from the metal pad.

In addition to the heat and mass balances for the reactor, the model will also include many algebraic equations describing the relationships between parameters in the model, for example, the dependence of density on the composition and temperature of the electrolyte. The remainder of this chapter will describe in detail the modelling of each block in the conceptual model and the equations used therein. This represents the physico-chemical model of the aluminium cell. The model of the control system to be applied in the operation of the cell will be considered in the following chapter.

4.2 Process Inputs

The process has three primary inputs:–

4.2.1 The breaker action

The crust breaker movement is controlled by pneumatic pumps, activated either manually or by the control computer. The pumps are either off or on and movement is controlled by switching the pumps for finite periods of time. The breaker can be raised or lowered into the crust, forcing a hole in the alumina and pushing a portion of alumina rich crust into the cryolite melt. The breaker action affects both the heat and mass balances in that immediately following a breaker action there is a sudden increase in the mass of alumina in the bath followed by an increase in the concentration of dissolved alumina. A loss of heat also results both from heating the alumina to the bath temperature and from the exposed bath where the breaker has broken through the crust.

4.2.2 Anode beam position

The anode beam position is controlled in the same way as the crust breaker by pneumatic pumps. Input is as a number of seconds activating the raise or lower pumps. The anode beam position governs the anode to cathode distance (ACD) and hence the voltage drop across the electrolyte. It also affects the mass balance as it is one of the parameters that affects the reoxidation of aluminium.

4.2.3 Line current

All cells in series draw the same current. Anode effects in other cells in a line can cause current fluctuations in individual cells. Current fluctuations are generally small and in this model the current will be assumed to be constant throughout the simulation. As well as determining the power input to the cell by the ohmic drop across the cell, the current determines the rate of the electrochemical reactions.

4.2.4 Anode change

The replacing of spent anodes is a manual operation that generally occurs at regular time intervals. Anodes may also be removed out of schedule if there is a problem such as spiking. The input is the duration of anode change. The changing of an anode represents a major disturbance to both the heat and mass balance in the cell.

4.2.5 Stochastic disturbances

Two stochastic disturbances are assumed to enter the system and represent a random variation in parameters in the model. The disturbance, D_1, represents the uncertainty in the amount of alumina fed into the electrolyte by the breaker action. D_2 represents the uncertainty in the anode beam position due to leakage from the air lines supplying the pneumatic motors etc. The stochastic disturbances are necessary in the model to fully test the control strategies to be implemented on the cell.

4.3 Alumina Dissolution

It has been shown in the previous chapter that the dissolution of alumina is dependent upon the method of feeding. This is due to the formation of agglomerates and sludge in the electrolyte. Laboratory experiments have differentiated between two extremes of dissolution, that from finely dispersed particles of alumina and that from alumina agglomerates and sludge. In an industrial cell dissolution will be by a combination of effects. This is reflected in the models used by Blake[1] and Entner[2] in which alumina is assumed to exist as dissolved ions, a suspension of small particles and sludge. The models differ in that Blake assumes a sequential mechanism from sludge to suspension to solution whilst Entner assumes a parallel mechanism from sludge to solution and suspension to solution. Blake assumes a proportion of alumina to enter each state on addition to the electrolyte whilst Entner assumes a settling of suspended alumina to sludge.

The sequential model for dissolution must assume the stripping of alumina from sludge into suspension by the movement of electrolyte across the surface of the sludge. This is more applicable to sludge at the side walls than to large agglomerates floating on the metal pad and is therefore a more realistic model for side break cells in which large amounts of sludge are present at the sidewalls than in half break and point feed cells.

A model for the settling of alumina in the cell will produce an alumina concentration distribution but will increase the number of calculations required for solution. The accuracy of the model will depend upon the number of zones used and the assumptions for the settling of alumina. This in turn will depend upon the geometry and hydrodynamics of individual cells. If a uniform distribution of alumina is assumed then this model approximates to that used by Blake.

In this work, alumina will be assumed to exist in three states in the electrolyte and these will be termed solution, suspension and sludge. In solution alumina will be assumed to exist as Al^{3+} and O^{2-} ions. In practise dissolved alumina is thought to exist as Al-O-F complexes. It is the individual ions that are of interest in the mass balance, however, since it is the oxide ion that is oxidised and reacts with the carbon anode to form CO_2 gas. Measurement of the concentration of alumina in the electrolyte

detects the presence of the oxygen atom by precipitation of alumina and so empirical relationships do not depend upon the form that dissolved alumina takes.

In line with experimental results[3] alumina in suspension will be assumed to exist as alumina particles and small agglomerates suspended in the electrolyte. Sludge will refer to larger agglomerates and alumina deposits on and around the aluminium, not the bottom crusts and deposits sometimes found under the metal pad.

The assumption that a proportion of alumina added to the cell goes directly into solution used in Ek's model[4] is only valid when the rate of dissolution immediately after addition is very great. This will be the case when the alumina concentration at addition is well below the saturation concentration of the electrolyte and the driving force for dissolution is great. If the concentration is close to saturation this assumption will no longer be valid. This situation can occur if the cell is overfed, perhaps due to an inadequate control system. As the primary purpose of this work is to investigate control strategies, it is desirable to be able to simulate this condition. For this reason, all alumina added to the cell will be assumed to enter only as suspended particles or sludge.

There is general agreement that the rate of dissolution can be described by a first order model at least at higher concentrations of alumina. The first order model will approximate to the zeroth order model where the saturation concentration is much greater than the actual concentration. The first order model is therefore more generally applicable and shall be used in this work. The rate of dissolution is then given by equation (3)

$$r = k_0 \cdot \exp\left(\frac{E}{RT_0} \cdot \left(1 - \frac{T_0}{T}\right)\right) \cdot (c^* - c) \qquad \left[g\ cm^{-2}\ min^{-1}\right] \qquad (3)$$

where r = rate of dissolution of alumina g cm^{-2} s^{-1}
A = contact area for dissolution cm^2
k_0 = reaction rate constant cm s^{-1}
E = activation energy kcal $mole^{-1}$
R = universal gas constant kcal $mole^{-1}$ K^{-1}
T_0 = reference temperature °K

T = reaction temperature °K
c^* = saturation concentration of alumina in melt g cm^{-3}
c = concentration of alumina in melt g cm^{-3}

Values for the parameters in the above equation have been determined by a number of sources and have been summarised by Asbjørnsen[5]. The data from Kachanovskaya will be used in the simulation, the values of the parameters being $k_0 = 0.00124$ cm s^{-1}, $T_0 = 1383$ °K and $E = 18.153$ kcal mol^{-1}. For simplicity, alumina dissolving from both sludge and suspension will be assumed to obey the same rate expressions with the same values for kinetic parameters. The dissolution rates will be different due to differing areas of contact between the electrolyte and the alumina as sludge and in suspension

The individual dissolution rates will therefore be

$$r_{diss(suspn)} = A_{suspn}. K. (c^* - c) \quad (4)$$

$$r_{diss(sludge)} = A_{sludge} . K. (c^* - c) \quad (5)$$

where

$$K = k_0 \cdot \exp\left(\frac{E}{RT_0} \cdot \left(1 - \frac{T_0}{T}\right)\right) \quad (6)$$

suspn refers to alumina in suspension
sludge refers to alumina as sludge

The contact area for alumina in suspension will be less than the specific area of the alumina as measured in a typical analysis due to the presence of alumina/bath agglomerates. Sludge will tend to form piles on the bottom of the cell and the contact area will be further reduced. The contact areas will be based upon the specific area for the particular alumina used but will be fitted to produce the desired dissolution curve. This will allow the simulation of the effects of different types of alumina and different cell geometries allowing the formation of different sized agglomerates.

Alumina fed to the bath contains an amount of Na_2O which reacts with AlF_3 in the electrolyte

$$3Na_2O(soln) + 2AlF_3(soln) \rightarrow 6NaF(soln) + Al_2O_3(soln) \qquad [1]$$

Although the proportion is small, typically 0.5% Na_2O by weight, over a period of time it has a noticeable effect on the weight ratio NaF/AlF_3 in the electrolyte. For simplicity, all alumina in suspension and sludge will be assumed to contain Na_2O in the same proportion as the alumina feed. The dissolution rate of Na_2O into solution will be assumed to be proportional to that of alumina and given by

$$r_{Na2Odiss} = \%Na_2O.\ (\ r_{diss(suspn)} + r_{diss(sludge)}\ ) \qquad (7)$$

where $r_{Na2Odiss}$ = net dissolution rate of Na_2O into solution
$\%Na_2O$ = wt% Na_2O present in alumina fed to the cell

In many cases the alumina is also blended with material captured in the exhaust scrubbers. This 'catch' consists predominately of $NaAlF_4$ from particulate fluorides and AlF_3 from the chemisorbtion of gaseous fluorides onto Al_2O_3. It may therefore be considered to be a mixture of NaF and AlF_3 and the dissolution rates will be determined in the same way as that for Na_2O.

$$r_{AlF3diss} = \%AlF_3.\ (\ r_{diss(suspn)} + r_{diss(sludge)}\ ) \qquad (8)$$

$$r_{NaFdiss} = \%NaF.\ (\ r_{diss(suspn)} + r_{diss(sludge)}\ ) \qquad (9)$$

Again the actual amounts of each compound in the feed are small but significant with the total fluoride content of a blend being typically 0.5-1.0 wt%.

4.4 Electrolyte Mass Balance

The electrolyte mass balance block as shown in figure 4.1 may be divided into a number of separate processes. These are shown in figure 4.2.

In order to reduce the number of calculations required, and hence the simulation time, the bath will be considered to be a well mixed system. All species in the melt will be considered to be uniformly distributed

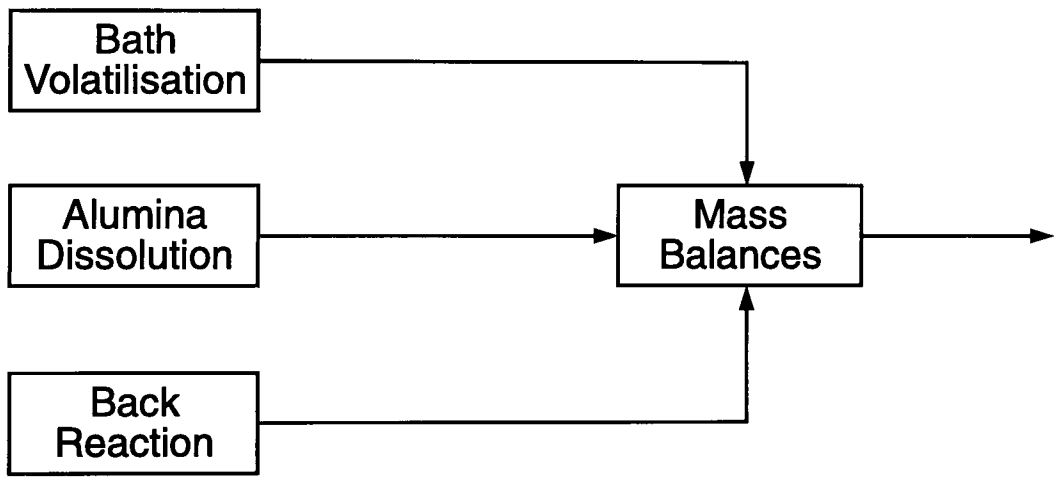

Figure 4.2 Electrolyte Mass Balance Processes

throughout the melt. As the electrolyte is constantly in motion due to electromagnetic stirring of the metal pad this is a reasonable assumption.

4.4.1 Bath volatilisation

Haupin's model for bath volatilisation[6] includes gaseous losses by chemical reaction and particulate losses by volatilisation and entrainment. The mechanisms for the first two losses have been widely investigated and the relationships appear to be reasonably accurate, with coefficients in that for gaseous fluoride evolution being fitted to Alcoa test data. The relationship for entrained electrolyte, however, is derived by difference from experimental data and the predictions of the other models. It therefore contains all the errors of measurement and the predictive error of the models, and, according to Haupin, will predict negative entrainments under certain conditions. As this would necessitate a discontinuity in the model and the amount of entrained electrolyte under normal conditions may be expected to be small, losses due to entrainment will not be included in this work.

The relationships derived by Haupin express the bath losses in terms of fluoride evolution as kg F/kg Al produced. For the complete dynamic mass balance on all species required here the relationships must be rearranged to express the rate of loss of individual electrolyte components through time.

4.4.2 Gaseous emissions

The model for gaseous emissions only includes losses due to the hydrolysis of bath to HF. The reaction responsible for these losses is given by Haupin as

$$^1/_3AlF_3 + {}^1/_2H_2O \rightarrow HF + {}^1/_6Al_2O_3 \qquad [2]$$

If the water for this reaction is assumed to be an addition to the electrolyte then this will cause an increase of oxide ions in the bath and a decrease of fluoride ions.

The rate of fluoride evolution is given by Haupin in kg Fluoride per metric ton aluminium produced

$$F_G = \frac{2310000}{\%CE} - \frac{955000}{P_b} \cdot R_b \cdot \left[\exp\left(7.553 - \frac{8444}{T} \right) \right] \cdot$$

$$\left[\frac{\%H_2O \text{ in } Al_2O_3}{37.44} + \frac{\%H \text{ in anodes}}{21.5} \right]^{1/2} \cdot$$

$$\exp\left(0.44199 - 3.1733R_b + 0.78127R_b^2\right) \cdot \left[\frac{C_{Al_2O_3}}{C^{sat}_{Al_2O_3}} \right]^{-0.462} \qquad (10)$$

where F_G = gaseous fluoride evolved per metric ton aluminium produced kg F/ tonne Al

%CE = current efficiency as percentage

R_b = weight ratio NaF/AlF_3

P_b = barometric pressure kPa

$C_{Al_2O_3}$ = concentration of alumina in bath wt%

$C^{sat}_{Al_2O_3}$ = saturation concentration of alumina wt%

The production rate of aluminium is given by

$$r_{Al} = \frac{\%CE}{100} \cdot \frac{I}{3 \cdot F} \qquad \text{moles Al } s^{-1}$$

$$= \frac{\%CE}{100} \cdot \frac{I}{3 \cdot F} \cdot \frac{27}{1 \times 10^6}$$

$$= \frac{\%CE \cdot I \cdot 9}{F \cdot 1 \times 10^8} \qquad \text{tonne Al } s^{-1} \qquad (11)$$

where r_{Al} = rate of aluminium production

%CE = current efficiency %

I = total current for electrolysis A

F = Faradays constant C mol^{-1}

The rate of evolution of gaseous fluoride is then given

$$\frac{dM_{F(g)}}{dt} = F_G \cdot r_{Al}$$

$$= \frac{\%CE}{100} \cdot \frac{I}{3 \cdot F} \cdot \frac{27}{1 \times 10^6} \cdot \left(\frac{2310000}{\%CE} - \frac{955000}{P_b} \cdot R_b \cdot \left[\exp\left(7.553 - \frac{8444}{T} \right) \right] \cdot \right.$$

$$\left[\frac{\%H_2O \text{ in } Al_2O_3}{37.44} + \frac{\%H \text{ in anodes}}{21..5} \right]^{1/2} \cdot$$

$$\left. \exp\left(0.44199 - 3.1733R_b + 0.78127R_b^2\right) \cdot \left[\frac{C_{Al_2O_3}}{C_{Al_2O_3}^{sat}} \right]^{-0.462} \right) \qquad (12)$$

The rate of gaseous fluoride evolution is the rate of reaction [2]. By stoichiometry the rate of addition of oxide ions to the electrolyte by this reaction is

$$\frac{dM_{O(g)}}{dt} = \frac{1}{2} \cdot \frac{dM_{F(g)}}{dt} \cdot \frac{W_O}{W_F} \qquad g\ O\ s\text{-}1 \qquad (13)$$

where $\frac{dM_{O(g)}}{dt}$ = rate of addition of oxide to bath by gaseous evolution of fluoride

W_O = atomic weight of oxygen = 16 g mol^{-1}

W_F = atomic weight of fluorine = 19 g mol^{-1}

4.4.3 Particulate emissions by volatilisation

As with gaseous emissions, Haupin derives a relationship for the evolution of particulate emissions in terms of kg fluoride per tonne aluminium. Using the information in his model the rate of volatilisation of electrolyte may be determined.

Vapour over electrolyte has been demonstrated to be composed of $NaAlF_4$ in equilibrium with its dimer, $Na_2Al_2F_8$. Assuming that the pot gases are saturated with these molecules at their vapour pressures, the mole fractions of the monomer and dimer in the gas are

$$x_m = \frac{p_m}{P_b} \qquad (14)$$

$$x_d = \frac{p_d}{P_b} \qquad (15)$$

where m,d refer to the monomer and dimer respectively

x = mole fraction of species in pot gases

p = vapour pressure of species

P_b = barometric pressure above electrolyte

The maximum rate of evolution of pot gases is the rate of production of gases by electrolysis at the anode. If the gases evolved in a cell are assumed to be CO_2 under normal operation and CF_4 during anode effect then the rate of evolution is given

$$r_{pot\ gas} = \frac{I}{4 \cdot F} \quad \text{mol s}^{-1} \qquad (16)$$

and the rates of volatilisation

$$r_m = x_m \cdot r_{pot\ gas} = \frac{I}{4 \cdot F} \cdot \frac{p_m}{P_b} \quad \text{mol NaAlF}_4\ \text{s}^{-1} \qquad (17)$$

and

$$r_d = x_d \cdot r_{pot\ gas} = \frac{I}{4 \cdot F} \cdot \frac{p_d}{P_b} \quad \text{mol Na}_2\text{Al}_2\text{F}_8\ \text{s}^{-1} \qquad (18)$$

where r_m and r_d are the rates of volatilisation of monomer and dimer respectively. The total rate of material volatilised from the electrolyte expressed as $NaAlF_4$ is then

$$\frac{dM_{vol}}{dt} = (r_m + 2 \cdot r_d) \cdot W_{NaAlF_4}$$

$$= \frac{I}{4 \cdot F} \cdot \frac{(p_m + 2 \cdot p_d)}{P_b} \cdot W_{NaAlF_4} \quad \text{g s}^{-1} \qquad (19)$$

where W_{NaAlF_4} = molecular wt of $NaAlF_4$ = 126 g mol^{-1}

The vapour pressure of molten cryolite with additives has been extensively studied and there is good agreement among recent investigators. The data has been combined by Haupin to produce the following formula which will be used in this work

$$P_v = \exp\left(B - \frac{A}{T}\right) \quad \text{kPa} \tag{20}$$

where

$$A = 7101.6 + 3069.7 \cdot \text{Ratio} + 635.77 \cdot \text{Ratio}^2 + 51.22 \cdot (\%\text{LiF}) - 24.638 \cdot \text{Ratio} \cdot (\%\text{LiF}) + \frac{764.5 \cdot (\%Al_2O_3)}{\left[1 + 3.2029 \cdot (\%Al_2O_3)\right]} + 13.2 \cdot (\%CaF_2)$$

$$B = 7.0184 + 0.6844 \cdot \text{Ratio} - 0.08464 \cdot \text{Ratio}^3 + 0.01085 \cdot (\%\text{LiF}) - 0.005489 \cdot \text{Ratio} \cdot (\%\text{LiF}) + \frac{1.1385 \cdot (\%Al_2O_3)}{\left[1 + 3.2029 \cdot (\%Al_2O_3)\right]} + 0.0068 \cdot (\%CaF_2)$$

where % = wt% of species in electrolyte
P_v = vapour pressure above electrolyte

The total vapour pressure above the electrolyte is also the sum of the partial pressures of the monomer and dimer.

$$P_v = p_m + p_d \tag{21}$$

The equilibrium constant for dimerization has been correlated from mass spectrographic measurements[7] and is given by Haupin as

$$K_d = \frac{p_d}{p_m^2} = \exp\left(\frac{-21414}{T} + 15.6\right) \tag{22}$$

where K_d = equilibrium constant
T = temperature °K

combining equations (21) and (22) and rearranging to eliminate p_d gives

$$p_m = \frac{\left[-1 + (1+4\cdot K_d\cdot P_v)^{0.5}\right]}{2\cdot K_d} \qquad (23)$$

introducing equations (21) and (23) into (19) and rearranging gives

$$\frac{dM_{vol}}{dt} = \frac{I}{4\cdot F}\cdot\frac{\left(2\cdot P_v - \left[-1+(1+4\cdot K_d\cdot P_v)^{0.5}\right]\right)}{2\cdot K_d\cdot P_b}\cdot W_{NaAlF_4} \text{ g s}^{-1} \qquad (24)$$

and in terms of oxide ions, sodium fluoride and aluminium ions

$$\frac{dMO_G}{dt} = \frac{1}{2}\cdot\frac{dMF_{G,net}}{dt}\cdot\frac{W_O}{W_F} \text{ g O s}^{-1} \qquad (25)$$

$$\frac{dMNaF_{vol}}{dt} = \frac{dMF_{vol}}{dt}\cdot\frac{W_{NaF}}{W_{NaAlF_4}} \text{ g NaF s}^{-1} \qquad (26)$$

$$\frac{dMAl^{3+}_{vol}}{dt} = \frac{dMF_{vol}}{dt}\cdot\frac{W_{Al}}{W_{NaAlF_4}} \text{ g Al s}^{-1} \qquad (27)$$

where $\frac{dMO_G}{dt}$ = rate of addition of O^{2-} ions to electrolyte by the evolution of HF gas g s^{-1}

$\frac{dMNaF_{vol}}{dt}$ = rate of volatilisation of NaF g s^{-1}

$\frac{dMAl^{3+}_{vol}}{dt}$ = rate of volatilisation of Al^{3+} ions g s^{-1}

The pot gases from all cells are collected by an exhaust system and passed into a baghouse where particulate fluorides are filtered and gaseous fluorides are chemisorbed onto alumina. The product, termed fines, is added to the alumina fed to the cells.

4.4.4 Aluminium dissolution and back reaction

All the models proposed for the rate of the back reaction of aluminium require the estimation of a number of parameters. In general, these parameters will differ from cell to cell and the ability to tune the model to the real cell will depend upon the number of parameters that must be estimated and the complexity of the model. The complexity of the model also determines the speed of calculation in dynamic simulation.

The models of Robl[8] and Evans[9] may be capable of estimating the rate of reaction in different sections of the cell but the difficulty in estimating the parameters required reduces the accuracy under dynamic conditions. The complexity of these models also makes them unsuitable for dynamic simulation.

The assumption that the bulk of the electrolyte is well mixed leads to a uniform distribution of all species. Under these conditions the mixed rate models for the back reaction of aluminium proposed by Haupin and Robl reduce to the dissolution rate controlled model of Lillebuen[10]. This model has shown reasonable agreement with industrial cells when used for the calculation of steady state current efficiencies and shall be used in this work.

The loss of current efficiency in the cell is assumed to be by the reaction

$$Al + 1.5CO_2 \rightarrow 0.5Al_2O_3 + 1.5CO \qquad [3]$$

which is assumed to occur instantaneously between dissolved species. The rate of reaction is therefore controlled by the dissolution rates of the reactants into the electrolyte. These rates are given by Lillebuen when the concentration of CO_2 in the bulk is assumed to be zero

$$\begin{aligned} r_{Aldiss} &= A_{Al} \cdot k_{Al} \cdot \left(C^*_{Al} - C_{Al}\right) \\ r_{CO_2diss} &= A_{CO_2} \cdot k_{CO_2} \cdot \left(1 + \frac{k_{Al} \cdot C_{Al}}{k_{CO_2} \cdot C^*_{CO_2}}\right) \cdot C^*_{CO_2} \end{aligned} \qquad (28)$$

where r = rate of dissolution of species

A = interfacial area of species and electrolyte
k = dissolution rate constant
C = concentration of species
C^* = saturation concentration of species
suffix Al refers to aluminium
CO_2 refers to carbon dioxide

These rate equations have been used by Lillebuen to calculate steady state current efficiencies by equating the rates of dissolution of each species to the rate of reaction. The current efficiency has then been calculated from the rate of dissolution of aluminium and it has been implied that this is the rate controlling step. In the dynamic situation the assumption that the concentration of dissolved carbon dioxide, C_{CO_2}, is zero means that all CO_2 that dissolves in the melt must be consumed by the reaction. The rate of the back reaction is therefore controlled by the rate of dissolution of CO_2 only. From the stoichiometry of reaction [3] the rate of reaction of aluminium dissolved in the electrolyte is therefore

$$r_{Al} = {}^2/_3 \cdot r_{CO_2 diss} \qquad \text{mol Al s}^{-1} \qquad (29)$$

It is still necessary to calculate the rate of dissolution of aluminium for the mass balance on aluminium in the electrolyte.

The models presented for the dissolution of aluminium based upon the hydrodynamics of the system (Robl, Evans) are complex and require the estimation of a large number of unknown quantities. The advantage of these models is offset by the lack of any data relating parameters in the equation to operating conditions.

Of the models based upon dimensionless parameters only that of Vasiliadis is for a similar physical system to the aluminium cell. Although this relationship does not include a complex hydrodynamic model it does include the effect of gas bubbles at the anode and all the parameters required are obtainable from literature or by direct measurement. Furthermore the dissolution rate is directly related to parameters known to effect the current efficiency of a cell. For these reasons Vasiliadis' model for the rate of dissolution of aluminium will be used in this work. The dissolution rate constant for aluminium in the electrolyte is

$$k_{Al} = 2.147\times10^{-11}\left(\frac{i\cdot T}{\ell}\right)^{1.42}\cdot\left(1+313.3V^{2.5}\right)\cdot\left(\frac{\mu_{Al}}{\rho_{Al}}\right)^{0.33}\cdot D_{Al}^{0.67} \qquad (30)$$

where
- k_{Al} = dissolution rate constant m s^{-1}
- i = anodic current density A m^{-2}
- T = electrolyte temperature K
- ℓ = anode to cathode distance m
- V = max velocities in the metal pad m s^{-1}
- μ = viscosity of electrolyte Ns m^{-2}
- ρ = density of electrolyte kg m^{-3}
- D_{Al} = diffusivity of aluminium into electrolyte m^2 s^{-1}

The dissolution rate constant for carbon dioxide has been proposed by Haupin as

$$k_{CO_2} = \frac{D_{CO_2}}{\delta_{CO_2}}\cdot\frac{1.703-0.7630\cdot\ln Re_{CO_2}}{1-0.6272\cdot\ln Re_{CO_2}}\cdot Re_{CO_2}^{0.5}\cdot Sc^{0.5} \qquad (31)$$

where
- D_{CO_2} = diffusivity of carbon dioxide in electrolyte
- δ_{CO_2} = carbon dioxide bubble diameter
- Re_{CO_2} = Reynolds number for carbon dioxide boundary layer $= \dfrac{V_e\cdot\rho_e\cdot\delta_{CO_2}}{\mu_e}$
- Sc = Schmidt number for carbon dioxide in electrolyte $= \dfrac{\mu_e}{\rho_e\cdot D_{CO_2}}$
- V_e = velocity of the electrolyte
- ρ_e = density of electrolyte
- μ_e = viscosity of electrolyte

Haupin does not, however, state how this relationship was determined and so no comment may be made upon its validity. There is as yet no data relating bubble diameters to operating conditions or the geometry of the cell. As the current efficiency is determined from the dissolution rate of carbon dioxide these relationships must be known in order to simulate the effect of the parameters. Until such data is available Haupin's relationship has limited use in dynamic simulation.

Lillebuen proposed that the dissolution rate constants for aluminium and carbon dioxide were equal based upon the assumption that the interfacial area for carbon dioxide dissolution is ten times that for aluminium and the ratio of $k_{CO_2} \cdot A_{CO_2}$ to $k_{Al} \cdot A_{Al}$ is 0.1. Vasiliadis, however, found an average value of this ratio to be 0.06 and hence $k_{Al} / k_{CO_2} = 0.6$.

The interfacial area for carbon dioxide dissolution has since been related to the concentration of alumina in the melt but unfortunately to no other parameters such as temperature. Using Haupin's relationship however

$$A_{CO_2} = \frac{(0.02723 + 1.003Wt - 0.3208Wt^2 - 0.05874Wt^3 + 0.03268Wt^4 + 0.00181Wt^5)}{(1 - 0.4715Wt + 0.06247Wt^2)} \cdot I_O \quad cm^2 \quad (32)$$

where A_{CO_2} = interfacial area of CO_2 gas / electrolyte
Wt = wt% of alumina in solution
I_O = current associated with the oxide reaction
Valid between 1 and 8 wt% alumina

it can be seen that the ratio of areas will vary with alumina concentration and anode current as the aluminium pad area remains approximately constant. The ratio of mass transfer coefficients will therefore depend upon the average operating conditions. In this work, due to the lack of carbon dioxide bubble data, the dissolution rate constant for carbon dioxide will be determined

$$k_{CO_2} = f \cdot k_{Al} \quad (33)$$

where f is a fittable constant that may be adjusted to account for the average operating conditions in the cell.

4.4.5 Current efficiency during anode effect

All the mathematical models in literature have dealt specifically with loss of current efficiency under normal operating conditions where the reaction is assumed to be between aluminium and carbon dioxide. During anode effect, however, carbon dioxide is no longer produced at the anode and since there is assumed to be no accumulation of carbon dioxide in the cell

this reaction is no longer possible. If this is the only mechanism for current efficiency losses then during anode effect an efficiency of 100% would be obtained. General operating experience on central point feeding cells has indicated high current efficiency at low alumina concentrations ie close to anode effect although this could be due solely to the reduction in bubble surface area at low alumina concentrations as shown by Haupin's relationship and not the presence of an alternative reaction. The current efficiency during anode effect in industrial cells cannot be determined by gas analysis and the Pearson and Waddington equation because the gas contains species other than CO and CO_2.[11]

Assumption that loss of current efficiency is only due to a reaction with CO_2 introduces a discontinuity at anode effect. The presence of a fluorocarbon bubble adhering to the anode will prevent aluminium in the melt from physically reaching the surface and so, if the current efficiency is not to be 100%, an alternative reaction must account for this loss. In this work, the anode gas produced during anode effect is assumed to be purely CF_4. The back reaction for aluminium during anode effect will be assumed to occur between dissolved aluminium and CF_4 and it will be treated in the same way as that during normal operating conditions with the reaction being

$$Al(soln) + {}^3/_4CF_4(soln) \rightarrow AlF_3(soln) + {}^3/_4C(soln) \qquad [4]$$

and occurring between dissolved species. Carbon particles are found in the electrolytes of industrial cells where they burn on the surface of the bath although these could come from break down of the anode itself.

The rate of dissolution of CF_4 into the melt is then given

$$r_{CF_4diss} = A_{CF_4} \cdot k_{CF_4} \cdot \left(1 + \frac{k_{Al} \cdot C_{Al}}{k_{CF_4} \cdot C^*_{CF_4}}\right) \cdot C^*_{CF_4} \qquad (34)$$

and by stoichiometry the rate of consumption of dissolved aluminium by reaction [4] is

$$r_{Al} = {}^4/_3 \cdot r_{CF_4diss} \qquad (35)$$

Due to the lack of data available for the dissolution of CF_4 into molten electrolyte the dissolution rate constant and the saturation concentration of CF_4 will be taken to be the same as the values calculated for CO_2 dissolution. As fluorocarbons cause dewetting of the anode surface and coalesce to form a single large bubble, the interfacial area between electrolyte and CF_4 gas will be approximately equal to the surface area of the anode covered by the gas. Defining a fractional coverage of the anode surface by CF_4 as ϕ gives the interfacial area for CF_4 dissolution as

$$A_{CF_4} = \phi \cdot A_{Anode} \qquad (36)$$

where A_{Anode} is the effective area of the anodes for electrolysis.

In the build up to anode effect both oxygen and fluoride ions are oxidised and during this period aluminium will be consumed by both the above reactions. The net rate of consumption of dissolved aluminium is then

$$r_{back} = r_{Al1} + r_{Al2} = {}^{2}/_{3} \cdot r_{CO2diss} + {}^{4}/_{3} \cdot r_{CF4diss} \quad \text{mol Al s}^{-1} \qquad (37)$$

4.4.6 Current efficiency losses at the cathode

Current efficiency is also lost by the co-deposition of undesired metal ions eg sodium at the cathode. This decreases the partial current density associated with the reduction of aluminium ions and hence the rate of reaction below the theoretical maximum. Some measure of this effect can be determined from the purity of the aluminium produced. Crudely, the purity of the aluminium will be inversely proportional to the amount of co-deposition. Under normal conditions in a particular cell the concentration of sodium in the aluminium pad will remain approximately constant and it will be assumed that the current efficiency of the reduction reaction of aluminium is constant. This effect will, in any case, be far outweighed by the current efficiency losses already discussed above.

By definition the current efficiency of an electrochemical reaction

$$J^{n-} + ne \rightarrow J \qquad (38)$$

at an electrode is

$$CE_j = \frac{i_j}{i_t} \tag{39}$$

where CE_j = current efficiency for reaction of species j

i_j = current associated with the electrolysis of j

i_t = total current through the electrode = Σi_j

The rate of reduction of aluminium at the cathode will therefore be

$$r_{Al} = \frac{i_{Al}}{z_{Al} \cdot F} = CE_{Al} \cdot \frac{I}{z_{Al} \cdot F} \tag{40}$$

where I = total current flowing through the cell

CE_{Al} = cathodic current efficiency for the reduction of Al

4.4.7 Overall current efficiency

The overall current efficiency is defined as the ratio of the actual rate of production of aluminium to the theoretical rate and differs from that determined by the Pearson Waddington equation in that it includes effects other than chemical reaction of aluminium at the anode. Here, the current efficiency losses are assumed to be due to back reaction and cathodic losses. The net rate of aluminium production is therefore

rate of production at cathode - rate of back reaction

$$= r_{Al} - r_{back} = CE_{Al} \cdot r_t - r_{back} \tag{41}$$

The overall current efficiency of the cell is then given

$$CE = \frac{CE_{Al} \cdot r_t - r_{back}}{r_t} = CE_{Al} - \frac{r_{back}}{r_t} \tag{42}$$

where the theoretical rate of production, r_t, is determined from Faraday's law and the total current through the cell

$$r_t = \frac{I}{z_{Al} \cdot F} = \frac{I}{3F} \tag{43}$$

4.4.8 Mass balances

In order to fully describe the system a mass balance must be performed for each species present in the electrolyte and overall for the molten bath and metal pad. As the bath is assumed to be well mixed the differential equations need only to be derived with respect to time and not space. In this block it is also necessary to calculate the concentrations of species in the electrolyte. In this work the electrolyte is assumed to consist of alumina, sodium fluoride, aluminium fluoride, calcium fluoride and aluminium. For simplicity all species are assumed to dissociate into simple ions.

The general form for a mass balance on species j is then

Accumulation of species j	=	Mass of j added to system	–	Mass of j removed from system	–	Mass of j consumed by reaction

where the reactions may be electrochemical or chemical. For a system with a number of streams entering and leaving this may be expressed

$$\frac{dM_j}{dt} = \sum_{k=1}^{m} Q_k \cdot C_{k,j}^{f} - \sum_{l=1}^{n} Q_l \cdot C_j - R_j \qquad (44)$$

where M_j = mass of species j in the system
C_j = concentration of species j in the system
Q_k = flow rate of stream k into the system
= concentration of species j in feed stream k
Q_l = flow rate of stream l out of system
R_j = net rate of reactions for species j

The mass balances for individual species in the aluminium reduction cell are developed in the following sections.

4.4.9 Material in suspension and as sludge

The alumina fed to a cell is not pure but contains significant quantities of Na_2O, NaF and AlF_3 the latter two compounds being added to the feed by blending the alumina with material captured in the baghouse. The actual quantities are small compared with the mass of alumina, typically less

than 2.0 wt% total, but have a marked effect upon the operation of the cell and therefore must be included. For simplicity the rates of dissolution of each compound are considered to be proportional to the rate of dissolution of alumina. It is therefore assumed that all sludge and suspension has the same chemical composition as the feed and the mass balances will be performed as on a homogenous material.

The mass balances on material in suspension and as sludge are

In: material added as a feed by the crust breakers
material added by action of changing an anode

Out: material dissolved into the electrolyte

In this work alumina added to the electrolyte is assumed to become sludge or suspension by a constant proportionality factor. The mass balances may be expressed mathematically

$$\frac{dM_{suspn}}{dt} = (1-S_f)\cdot\left[\frac{dM_{feed}}{dt} - \frac{dM_{ac}}{dt} - r_{diss(suspn)}\right] \qquad (45)$$

$$\frac{dM_{sludge}}{dt} = S_f\cdot\left[\frac{dM_{feed}}{dt} - \frac{dM_{ac}}{dt} - r_{diss(sludge)}\right] \qquad (46)$$

where S_f = fraction of feed that becomes sludge

$\frac{dM_{feed}}{dt}$ = rate of addition by crust breakers

$\frac{dM_{ac}}{dt}$ = rate of addition due to anode change

Alumina additions by the crust breakers and anode change are not continuous and it will be assumed that any alumina introduced to the electrolyte will instantly enter the sludge and suspension states. The addition rates may therefore be represented by a series of impulses with varying period and height. The period represents the frequency of operation of the crust breakers or anode change and will be set by the control system. The height represents the amount added to the cell and is subject to a random proportionality factor to simulate the uncertainty

between the actual mass added and the intended mass. The mean and variance of the amount of alumina added to the cell may be measured by sampling a working cell. The random variable may then be generated from a distribution function based upon these variables. An example of the form the rates of addition might take is shown in figure 4.3.

4.4.10 Al^{3+} ions in solution

In: By dissolution of Al_2O_3 from sludge and suspension
= 2 × molar rate of dissolution Al_2O_3 × atomic weight Al
By dissolution of AlF_3 from sludge and suspension
= molar rate of dissolution AlF_3 × atomic weight Al
By addition of bagged AlF_3 to maintain ratio
= molar rate of addition AlF_3 × atomic weight Al

Out: By volatilisation of bath as $NaAlF_4$
Rate of freezing of Al^{3+} ions into frozen sidewalls
Rate of freezing of Al^{3+} ions onto cold anode

Electrolysis: – Rate of reduction at cathode

Reaction: + Rate of back reaction

expressed mathematically this becomes

$$\frac{dMAl^{3+}}{dt} = \left[2\cdot\left(r_{diss(sludge)} + r_{diss(suspn)}\right) + r_{AlF_3diss} + \frac{dM_{bag}}{dt}\right]\cdot W_{Al} - \frac{dMAl^{3+}_{vol}}{dt} - \frac{dMAl^{3+}_{f}}{dt} - \frac{dMAl^{3+}_{ac}}{dt} - CE_{Al}\cdot\frac{I}{z_{Al}\cdot F}\cdot W_{Al} + r_{back} \quad (47)$$

where $\frac{dM_{bag}}{dt}$ = molar rate of addition of bagged AlF_3

$\frac{dMAl^{3+}_{f}}{dt}$ = rate of transfer of Al^{3+} ions into frozen sidewalls, +ve for freezing

$\frac{dMAl^{3+}_{ac}}{dt}$ = rate of transfer of Al^{3+} ions into frozen layer on cold anode, +ve for freezing

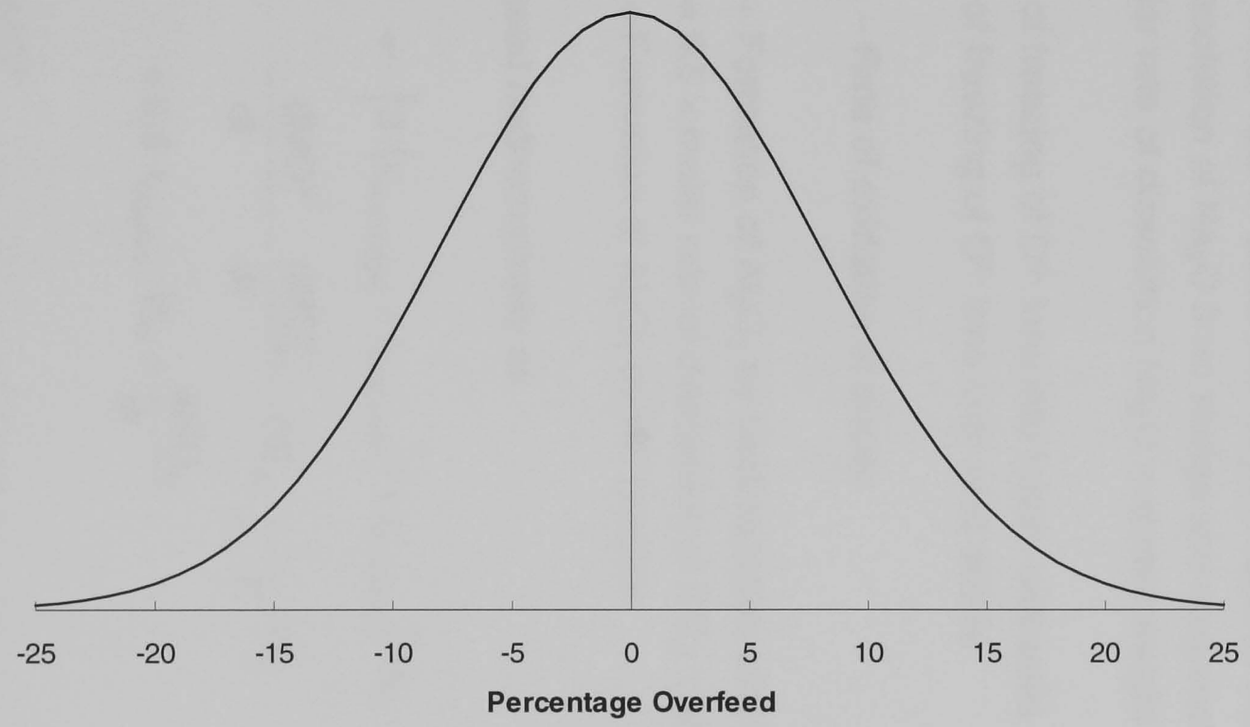

Figure 4.3 Random Variation on Mass of Alumina Fed to a Cell

W_{Al} = atomic weight of aluminium = 27 g mol^{-1}

z_{Al} = charge transferred in reduction of Al = 3

4.4.11 O^{2-} ions in solution

In: By dissolution of Al_2O_3 from sludge and suspension
= 3 × molar rate of dissolution Al_2O_3 × atomic weight O
By dissolution of Na_2O from sludge and suspension
= molar rate of dissolution Na_2O × atomic weight O

Out: Rate of freezing of O^{2-} ions into frozen sidewalls
Rate of freezing of O^{2-} ions onto cold anode

Electrolysis: – Rate of oxidation at anode

Reaction: + Formation of Al_2O_3 by back reaction with CO_2
= 0.5 × molar rate of dissolution of CO_2 × atomic weight O
+ Formation of Al_2O_3 by HF reaction

This is expressed mathematically as

$$\frac{dMO^{2-}}{dt} = \left[3\cdot\left(r_{diss(sludge)} + r_{diss(suspn)}\right) + r_{Na_2Odiss}\right]\cdot W_O - \frac{dMO_f^{2-}}{dt} - \frac{dMO_{ac}^{2-}}{dt} - CE_O\cdot\frac{I}{z_O\cdot F}\cdot W_O + 0.5\cdot r_{CO_2diss}\cdot W_O + \frac{dMO_G}{dt} \quad (48)$$

where $\frac{dMO_f^{2-}}{dt}$ = rate of transfer of O^{2-} ions into frozen sidewalls, +ve for freezing

$\frac{dMO_{ac}^{2-}}{dt}$ = rate of transfer of O^{2-} ions into frozen layer on cold anode, +ve for freezing

W_O = atomic weight O = 16 g mol^{-1}

4.4.12 Aluminium metal in electrolyte

Aluminium dissolves from the metal into the electrolyte where it can react with dissolved CO_2 or CF_4. The dissolved aluminium is assumed to be non ionic. The mass balance is then

In: Rate of dissolution of aluminium from metal pad

Reaction: Rate of back reaction of aluminium with CO_2 and CF_4

Mathematically this is

$$\frac{dMAl}{dt} = r_{Aldiss} - r_{back} \tag{49}$$

4.4.13 Aluminium in the metal pad

The metal produced in an aluminium cell contains a small percentage of impurities such as silicon and sodium. In this work the only impurity to be considered is sodium which is assumed to exist in the aluminium pad at a constant concentration. The actual amount is however, very small with the purity of aluminium produced being typically greater than 99.9%. The amount of sodium lost from the melt is therefore considered insignificant and will not be included in the mass balances. A mass balance on the aluminium in the metal pad will therefore constitute a mass balance on the whole of the metal pad.

The mass balance is

Out: Aluminium periodically tapped from the cell
Rate of dissolution of aluminium into the electrolyte

Electrolysis: + Rate of reduction of Al^{3+} at the cathode

Mathematically this is

$$\frac{dMAl_{pad}}{dt} = -\frac{dMAl_{tap}}{dt} - r_{Aldiss} + CE_{Al} \cdot \frac{I}{z_{Al} \cdot F} \cdot W_{Al} \tag{50}$$

where $\frac{dMAl_{tap}}{dt}$ = rate of metal tapped from the cell

4.4.14 Sodium fluoride

The sodium content of the cell is assumed to be independent of electrolysis although strictly a term should be included to account for loss of current efficiency at the cathode. The actual mass of sodium removed from the electrolyte by this means is very small however and will be considered negligible compared to other terms in the mass balance.

In this work all sodium in the electrolyte is assumed to be due to the presence of NaF. The concentration of individual sodium ions is not required because all the relationships for physical properties require the sodium content to be expressed as the weight ratio of NaF to AlF_3. The only other source of sodium ions is the addition of Na_2O as part of the alumina feed. This reacts with AlF_3 to form NaF

$$3Na_2O + 2AlF_3 \rightarrow 6NaF + Al_2O_3 \qquad [5]$$

At the operating temperature and composition of the cell this reaction will be fast and the rate determining step will be assumed to be the dissolution of Na_2O. Two moles of NaF will therefore be formed for every mole of Na_2O dissolved.

A mass balance on the NaF content of the electrolyte is

In: By dissolution of NaF from sludge and suspension

Out: Rate of freezing of NaF into frozen sidewalls
Rate of freezing of NaF onto cold anode
By volatilisation of bath as $NaAlF_4$

Reaction: + rate of reaction of Na_2O
= molar rate of dissolution $Na_2O \times 2 \times$ molecular weight NaF

$$\frac{dMNaF}{dt} = r_{NaFdiss} - \frac{dMNaF_f}{dt} - \frac{dMNaF_{ac}}{dt} - \frac{dMNaF_{vol}}{dt} + r_{Na_2Odiss} \cdot 2 \cdot W_{NaF} \quad (51)$$

where $\frac{dMNaF_f}{dt}$ = rate of transfer of NaF into frozen sidewalls, +ve for freezing

$\frac{dMNaF_{ac}}{dt}$ = rate of transfer of NaF into frozen layer on cold anode, +ve for freezing

$\frac{dMNaF_{vol}}{dt}$ = rate of volatilisation of NaF

W_{NaF} = molecular weight NaF = 42 g mol^{-1}

4.4.15 Calcium fluoride

As with sodium ions, the calcium ions in the electrolyte are assumed to be associated only with calcium fluoride. In practise the alumina fed to the cell contains a small percentage of CaO which reacts with AlF_3 in the melt to form CaF_2. The amount of CaO in the feed is typically a tenth of the amount of Na_2O and as such may be considered negligible. Similarly, the mass of calcium co-deposited at the cathode is a fraction of the mass of sodium and will also be assumed negligible. In this model the calcium fluoride content of the molten electrolyte will therefore only be affected by the rates of freezing at the sidewalls and on cold anodes.

Out: Rate of freezing of CaF_2 into sidewalls
Rate of freezing of CaF_2 onto cold anode

$$\frac{dMCaF_2}{dt} = -\frac{dMCaF_{2,f}}{dt} - \frac{dMCaF_{2,ac}}{dt} \quad (52)$$

where $\frac{dMCaF_{2,f}}{dt}$ = rate of transfer of CaF_2 into frozen sidewalls, +ve for freezing

$$\frac{dMCaF_{2,ac}}{dt} = \text{rate of transfer of } CaF_2 \text{ into frozen layer on cold anode}$$

4.4.16 Alumina in solution

Although alumina dissolved in the electrolyte has been assumed to dissociate into Al^{3+} and O^{2-} ions the equivalent mass of alumina is required since the industry uses the weight percent of alumina to describe the composition of a melt and most empirical relationships require the alumina concentration on a weight basis.

Since this work assumes that the only oxide containing species dissolved in the melt is alumina, (other compounds, eg Na_2O, react to form alumina) it follows that the mass of alumina is proportional to the mass of O^{2-} ions. From the chemical formula of alumina, Al_2O_3, it can be seen that each mole of oxide is equivalent to one third moles of alumina. The mass balance on alumina in solution is therefore

$$\frac{dM_{Al_2O_3}}{dt} = \frac{1}{3} \cdot \frac{dMO^{2-}}{dt} \cdot \frac{W_{Al_2O_3}}{W_O} \qquad (53)$$

where $\frac{dMAl_2O_3}{dt}$ = rate of change of mass of alumina in solution

$W_{Al_2O_3}$ = molecular weight of alumina = 102 g mol^{-1}

4.4.17 Aluminium fluoride

The mass of aluminium fluoride in the electrolyte must be determined as many of the empirical formulae require either the weight ratio of NaF to AlF_3 or the percentage excess of AlF_3 above the mass found in cryolite. As with alumina, the AlF_3 mass balance may be determined algebraically from the mass balances on individual ions.

This work assumes that cryolite is a mixture of NaF and AlF_3 in the mole ratio 3:1. Therefore, the only species in the electrolyte that contain the Al^{3+} ion are AlF_3 and Al_2O_3 with mole ratios 1 mole Al^{3+} per mole AlF_3 and 2

moles Al^{3+} per mole Al_2O_3 respectively. The Al^{3+} ions associated with alumina may be determined from the oxide content of the melt and any remaining Al^{3+} ions must therefore be associated with AlF_3. The aluminium fluoride mass balance is

$$\frac{dMAlF_3}{dt} = \left[\frac{dMAl^{3+}}{dt}\cdot\frac{1}{W_{Al}} - \frac{dM_{Al_2O_3}}{dt}\cdot\frac{2}{W_{Al_2O_3}}\right]\cdot W_{AlF_3} \qquad (54)$$

where W_{AlF3} = molecular weight of AlF_3 = 84 g mol^{-1}

4.4.18 Overall mass balance on electrolyte

The rate of change of the total mass of the bath is the summation of the rates of change of mass of the individual species that make up the electrolyte. That is

$$\frac{dMBath}{dt} = \frac{dMNaF}{dt} + \frac{dMAlF_3}{dt} + \frac{dMCaF_2}{dt} + \frac{dMAl_2O_3}{dt} + \frac{dMAl}{dt} \qquad (55)$$

This balance only considers species dissolved in the electrolyte, ie the liquid. The mass of bath is required to calculate concentrations, bath volume and for the heat balance.

4.5 Electrolyte Conductivity

Whilst the models proposed by Fellner appear to predict the conductivity of the electrolyte with reasonable accuracy, they rely upon data, such as the molar volume of each species, that is difficult to obtain for the varying conditions within the cell. The complexity of the models and thus the increased computation time required make the models unattractive. The empirical relationship developed by Choudhary is accurate for the conditions expected in an operational cell and is easy to calculate. The relationship has been modified by Roger Johnston at the Kaiser Aluminum Californian Research Center and is used at Anglesey Aluminium on a daily basis. The following relationship will be used in this work.

$$\rho = \frac{1}{1.06} \cdot \exp\left(\begin{array}{l} 2.0156 - 0.0207 \cdot \%Al_2O_3 - 0.005 \cdot \%CaF_2 \\ + 0.4349 \cdot R_b - \frac{2068.4}{T} \end{array} \right) \quad (56)$$

The resistance of the electrolyte can be calculated from the conductivity, the interelectrode gap and the area for current flow.

$$R = \frac{\ell}{A \cdot \rho} \quad (57)$$

The area for current flow through the electrolyte will be affected by the design of the electrochemical cell. A good approximation for the design of cell used at Anglesey Aluminium has been found to be the assumption of a two inch shadow around the block of anodes. The effective anode area is then

$$A_e = 2 \times \left(\frac{n}{2} \cdot x_a + \left(\frac{n}{2} - 1 \right) \cdot gap + 2.54 \right) \times \left(y_a + 5.5 \right) \quad (58)$$

where n = number of anodes
x_a = anode width
y_a = anode length
gap = gap between banks of anodes

This relationship assumes that all the anodes are drawing the same current. This is not the case however when an anode has been removed from the bath or a cold anode has been introduced to the bath and is insulated by a layer of frozen electrolyte. The heat balance across the anodes and the algorithms developed in a later section for the modelling of an anode change, calculate a fraction of the surface area of each anode that is effectively available for current flow. In this work, the effective anode area will be further modified by subtracting the area of each anode that is effectively insulated. The calculation of the effective anode area then becomes

$$A_e = 2 \times \left(\frac{n}{2} \cdot x_a + \left(\frac{n}{2} - 1 \right) \cdot gap + 2.54 \right) \times \left(y_a + 5.5 \right) - \sum_{j=1}^{n} \left(1 - f_j \right) \cdot x_a \cdot y_a \quad (59)$$

where f_j = fraction of anode able to conduct current

This modification maintains the two inch shadow around each anode.

4.6 Electrolysis Charge Balance: Reaction Modelling

Although electrode reactions vary in their complexity they can be represented simplistically by the diagram in figure 4.4 in which reactant A is transported from the bulk electrolyte to the electrode surface where it undergoes conversion via, perhaps, a number of reactive intermediates to product B. B is then transported back to the bulk.

The rate of reaction of A at the electrode is given by the Butler Volmer equation for the reversible reaction

$$A + ne \underset{\leftarrow i_-}{\overset{i_+ \rightarrow}{\rightleftharpoons}} B \qquad (60)$$

by the equation

$$i = i_0 \cdot \left(\underbrace{e^{-\alpha \frac{zF}{RT}\eta}}_{i_+} - \underbrace{e^{(1-\alpha)\frac{zF}{RT}\eta}}_{i_-} \right) \qquad (61)$$

where
- i = current density associated with the reaction
- i_o = exchange current density where $r_{for} = r_{rev} \equiv i_+ = i_-$
  - i_o is proportional to $zF[A]_s$
- η = overpotential at the electrode
- i_+ = current density associated with forward reaction
- i_- = current density associated with reverse reaction
- α = transfer coefficient
  - ≡ fraction of free energy of activation affecting i_-

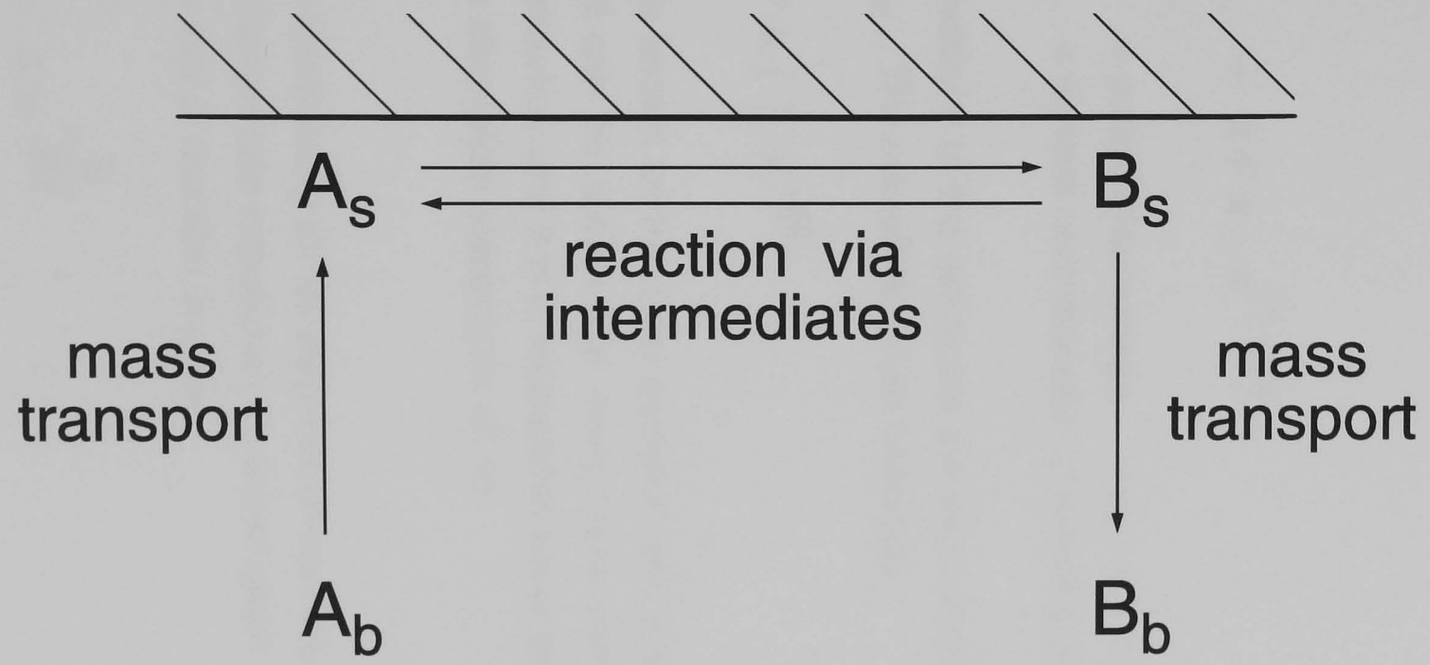

Figure 4.4 Schematic Representation of Reactions at an Electrode

The Butler Volmer equation can be rewritten for the individual rates

$$r_{for} = i_{+} = i_0 e^{-\alpha \frac{zF}{RT}\eta} = i_0 e^{-\alpha \frac{zF}{RT}\left(\phi_m - \phi_s - \phi_{ref} - \phi^0\right)}$$

$$= z \cdot F \cdot k_1 \cdot [A]_s \cdot e^{-\beta E} \qquad (62)$$

and

$$r_{rev} = i_{-} = z \cdot F \cdot k_{-1} \cdot e^{(1-\beta)E} \qquad (63)$$

where E = polarisation voltage $= \phi_m - \phi_s - \phi^0$

$[\,]_s$ = surface concentration of reacting species

Usually the conditions at the electrode are well removed from equilibrium and $i_{+ \text{ or } -} >> i_{- \text{ or } +}$. The overall rate then becomes

$$i = z \cdot F \cdot k \cdot [\,]_s \cdot e^{-\beta E} \qquad (64)$$

This equation is known as the Tafel equation and is shown schematically in figure 4.5. It can be shown that many more complex reactions also exhibit Tafel behaviour and it is a reasonable assumption that the primary reactions in the aluminium electrolysis do so.

Note

The Tafel relationship for an electrochemical reaction is analogous to the Arrhenius rate expression for a first order chemical reaction where the rate of reaction is given

$$r = A \cdot e^{-\frac{E}{RT}}$$

where *A* = *Arrhenius constant*

E = *Activation energy of reaction*

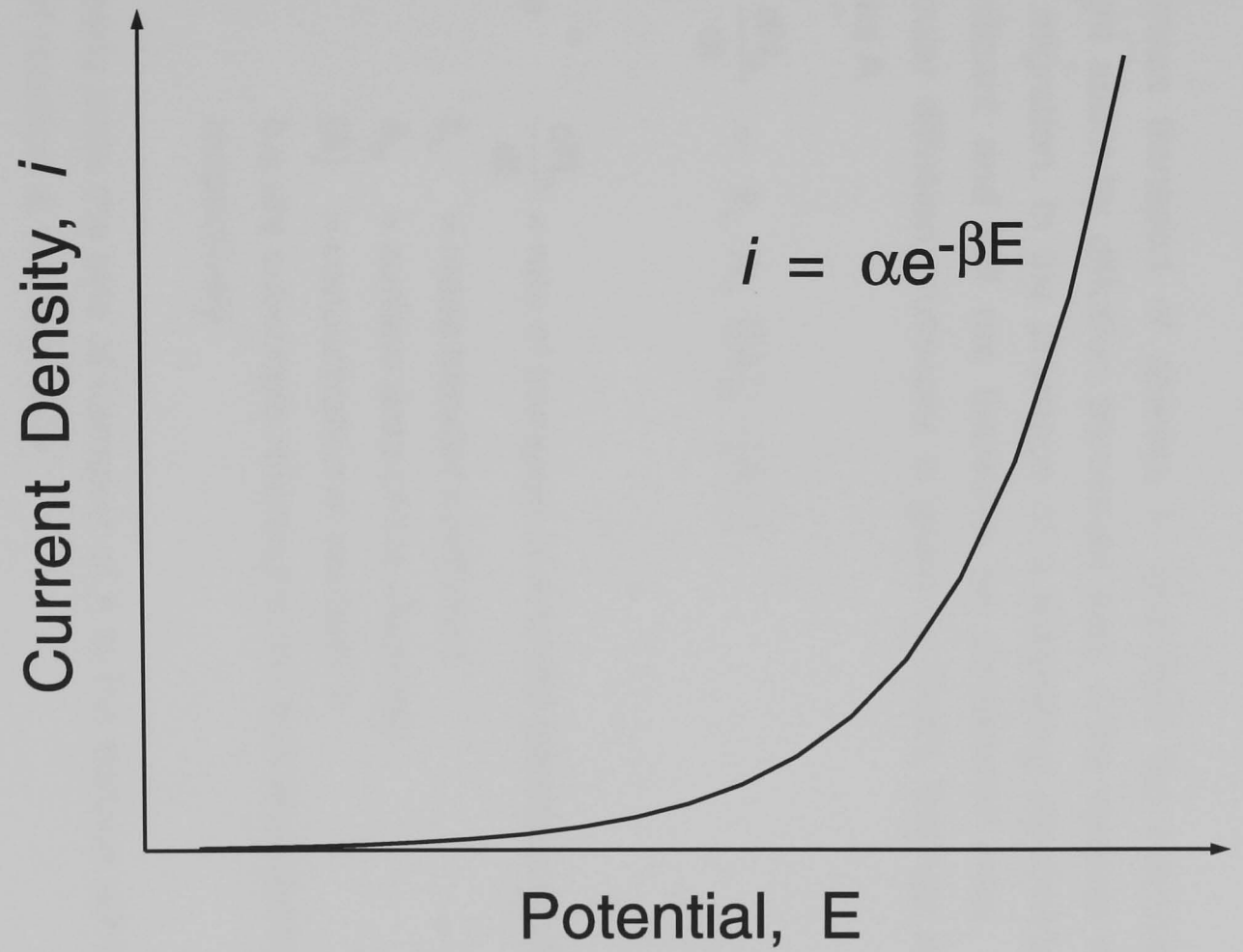

Figure 4.5 Schematic diagram of Tafel Derivation i+ >>i-

The rate of reaction of A is given by Faraday's law as

$$r_A = \frac{I}{z \cdot F} = \frac{A_e \cdot i_A}{z \cdot F} = A_e \cdot k \cdot [A]_s \cdot e^{-\beta E} \qquad (65)$$

where r_A = rate of electrolysis of species A
I = current for electrolysis
A_e = electrode surface area
i_A = partial current density associated with the reaction

The mass transport of species to and from the electrode surface is brought about by diffusion processes and, if the species is charged, by ionic migration. In the presence of a supporting electrolyte the latter is insignificant and will not therefore be considered here. Transport by molecular diffusion processes is given by Fick's first law of diffusion for species A

$$\frac{dN_A}{dt} = k_L \cdot A_e \cdot \left([A]_b - [A]_s\right) \qquad (66)$$

where $\frac{dN_A}{dt}$ = rate of transport of A to the electrode surface
k_L = mass transfer coefficient
A_e = surface area of the electrode
$[A]$ = concentration of reactant A
b,s are subscripts referring to the bulk and electrode surface respectively

At steady state the rate of transport of A to the surface will be equal to its rate of reaction at the electrode

$$r_A = \frac{dN_A}{dt} \qquad (67)$$

and, combining with Faraday's Law

$$r_A = A_e \cdot i_A = z \cdot F \cdot k_L \cdot A_e \cdot \left([A]_b - [A]_s\right) \qquad (68)$$

From (65) and (66) the following simultaneous equations can be obtained,

$$i_A = z\,F\,k_L\,([A]_b - [A]_s) \tag{69}$$

$$i_A = z\,F\,k\,[A]_s\,e^{-\beta E} \tag{70}$$

which taken together comprise the model for the reaction $A \rightarrow B$.

Rearranging (69) and (70) and eliminating $[A]_s$ gives

$$[A]_s = [A]_b - \frac{i_A}{z \cdot F \cdot k_L} = \frac{i_A}{z \cdot F \cdot k} e^{-\beta E} \tag{71}$$

and

$$i_A = \frac{[A]_b}{\frac{1}{z \cdot F \cdot k_L} + \frac{1}{z \cdot F \cdot k \cdot e^{-\beta E}}} \tag{72}$$

This expression models the reaction independent of a knowledge of surface concentrations at the electrode.

Although the model has been derived for the simple reaction

$$A + ze \rightarrow B \tag{6}$$

it applies to any reaction that exhibits Tafel type behaviour, and can be shown to be valid for many more complex reactions[12].

Much work has been done on measuring the polarisation voltage in aluminium reduction cells, although most of it has concentrated on determining the variation of voltage with alumina concentration prior to anode effect, with little consideration of the voltage rise during the anode effect itself. The primary electrochemical reaction at the anode during normal operation is the reduction of the oxide ions associated with the alumina dissolved in the electrolyte.

$$O^{2-} \rightarrow O + 2e \tag{7}$$

Most workers have fitted the experimental results to Tafel type behaviour although some have included a concentration overvoltage effect to accommodate the rise in voltage at low concentrations of alumina. Some of the relationships derived will be considered here and the parameters to be used in this work will be determined.

The annual International Course on Process Metallurgy of Aluminium at Trondheim considers the polarisation voltage in the cell in detail and the approach taken covers much of the research into the relationship between polarisation voltage and alumina concentration. It is this work that will form the basis for comparison with the model presented here.

In the Trondheim model, the overpotential at the anode is considered to be represented by two parts, the overpotential at the surface, η_{SA}, represented by a Tafel type relationship and a concentration overvoltage, η_{CA}.

$$\eta = \eta_{SA} + \eta_{CA} \tag{73}$$

where

$$\eta_{SA} = \frac{R \cdot T}{\alpha \cdot z \cdot F} \cdot \ln \frac{i}{i_o}$$

$$i_o = \gamma + \delta \cdot c_{b,Al_2O_3}$$

$$\alpha = \text{fn (porosity \& reactivity of carbon anode)}$$

$$\eta_{CA} = \frac{R \cdot T}{z \cdot F} \cdot \ln \frac{i_c}{i_c - i}$$

$$i_c = \left[5.5 + 0.018(T - 1323)\right] \cdot A^{-0.1} \cdot \left[c_{b,Al_2O_3}^{0.5} - 0.4\right]$$

$$\equiv \varepsilon \cdot \left(c_b^{0.5} - \mu\right) \text{ for a given temperature}$$

c_{b,Al_2O_3} = concentration of alumina in the electrolyte
A = anode area

For a given temperature the overpotential is then given by

$$\eta = A \cdot \ln \frac{i}{i_o} + B \cdot \ln \frac{i_c}{i_c - i} \tag{74}$$

Rewriting equation (74) in terms of the overpotential, $\eta = E - E^{\phi}$, gives

$$i = \frac{c_b}{\frac{1}{a \cdot e^{-b\eta}} + \frac{1}{z \cdot F \cdot k_L}} \qquad (75)$$

rearranging gives

$$\eta = \frac{1}{b} \cdot \ln \frac{1}{a} \cdot \left[\frac{z \cdot F \cdot k_L \cdot i}{z \cdot F \cdot k_L \cdot c_b - i} \right] \qquad (76)$$

denoting the limiting current, $z \cdot F \cdot k_L \cdot c_b$ by i_c and $z \cdot F \cdot k_L$ as i'_o gives

$$\begin{aligned} \eta &= \frac{1}{b} \cdot \ln \frac{1}{a} \cdot \left[\frac{i'_o \cdot i}{i_c - i} \right] \\ &= \frac{1}{b} \cdot \ln \frac{i'_o}{a} + \frac{1}{b} \cdot \ln i + \frac{1}{b} \cdot \ln \frac{1}{i_c - i} \\ &= \alpha + \beta \cdot \ln i + \beta \cdot \ln \frac{1}{i_c - i} \\ &= \beta \cdot \ln \frac{i}{\alpha' \cdot i_c} + \beta \cdot \ln \frac{i_c}{i_c - i} \quad \text{where } \alpha = -\beta \cdot \ln \alpha' \end{aligned} \qquad (77)$$

Comparison of equations (74) and (77) shows that although the two models are similar, they differ in several important respects and it is not possible to match the coefficients in the models and so determine the parameters required for this work.

The differences between the Trondheim model and the theoretical model are probably due to the derivation of the Trondheim model. The Trondheim model is highly empirical and has been derived over a number of years by amalgamating several empirical relationships as research has made them available. Whilst this approach can lead to good results over the specific range of parameters investigated, it may no longer be possible to relate the derived relationship directly to the underlying theory, as in this case, bringing the applicability of the relationship under a wider range of conditions into question. For this reason the theoretical relationship will be used in this work with the required Tafel coefficients and mass transfer coefficients being determined from the available empirical relationships for polarisation voltage.

4.6.1 Determination of Tafel constants and mass transfer coefficient

Tafel coefficients for a wide variety of carbon anodes with varying porosity have been determined by Zuca et al[13] and figure 4.6 shows the variation of overvoltage with current density for different carbon types at 965 °C. The Tafel plots determined by Zuca are also shown on the graph. The Tafel coefficients for the equation $\eta = a + b \log i$ and the range of current density over which Tafel behaviour was assumed are shown in table 4.1. The cryolite composition used was similar to that used in industrial cells with 5% alumina, 4% calcium fluoride and a cryolite ratio of 1.35.

The experimental data in figure 4.6 clearly shows the effect of mass transfer at higher current densities with the rise in potential as the reaction becomes mass transfer limited. It is evident from the graph that the range over which the Tafel coefficients are calculated includes some effect due to mass transfer and so the coefficients cannot be used directly in equation 72.

Assuming that anode effect is initiated when the oxide reaction becomes mass transfer limited then at this point the partial current density for the reaction will be given by

$$i = z \cdot F \cdot k_L \cdot c_b \qquad (78)$$

where c_b = the molar concentration of oxide ions in the electrolyte

Rearranging (78) gives

$$k_L = \frac{i}{z \cdot F \cdot c_b} \qquad (79)$$

It is known that in a typical cell at Anglesey Aluminium anode effect starts when the alumina concentration in the melt approaches 1.5 wt%. Assuming that a typical cell has the following operational parameters

Calcium fluoride	5 wt%
Weight ratio	1.25
Temperature	965 °C
Current density	0.7 A cm^{-2}

Anode Porosity %	Tafel intercept V	Tafel slope V/decade	Tafel range A cm^{-2}
spectral graphite 0	0.805	0.274	0.02-0.8
baked carbon 8.9	0.784	0.286	0.02-0.8
12.6	0.710	0.250	0.02-0.7
14.73	0.611	0.202	0.03-0.7

Table 4.1 Experimental Tafel Coefficients for Anodes of Varying Porosity

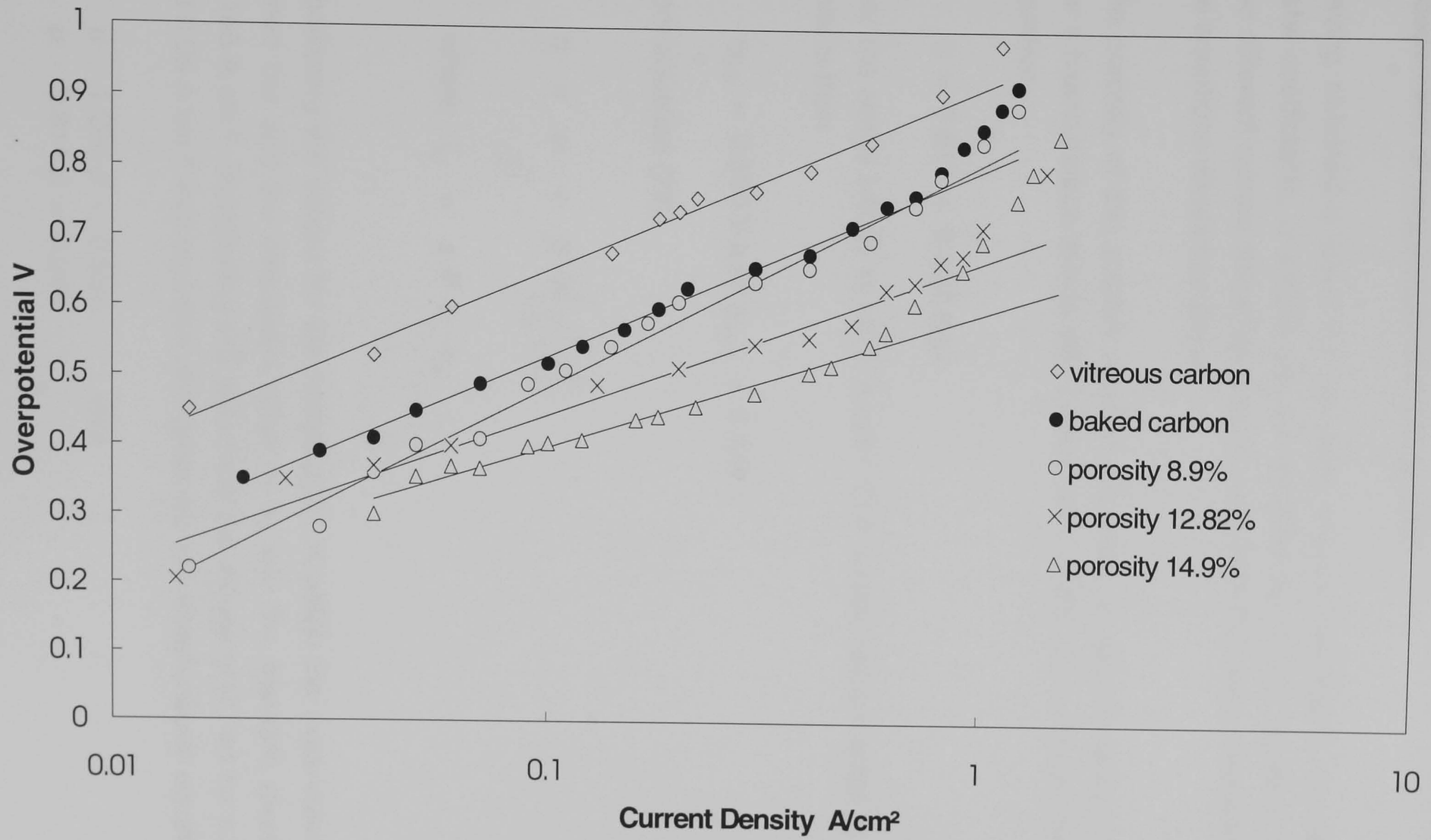

Figure 4.6 Overvoltages from Zuca

and that the oxide reaction is the only reaction occurring at the anode at this point, equation (79) gives the mass transfer coefficient for the reaction, k_L, as 3.9×10^{-3} cm s^{-1}. For simplicity, it will be assumed that k_L is independent of temperature and composition.

Having obtained a value for the mass transfer coefficient, the required Tafel coefficients, α and β, can be obtained by solving equation (77) at two different current densities, with the overpotential being calculated from the equations derived by Zuca.

The porosity of the anodes used at Anglesey is approximately 14.75%. For a baked carbon anode with porosity of 14.73%, Zuca derives the Tafel equation

$$\eta = 0.611 + 0.202 \log i \qquad (80)$$

over the range i=0.05 to i=0.5 A cm^{-2}. The anodic overpotential at these limits is then

$\eta_{0.5} = 0.550$ V and $\eta_{0.05} = 0.348$ V

From equation (77)

$$\eta = \alpha + \beta \cdot \ln\left(\frac{i}{i_c - i}\right) \qquad (81)$$

where $i_c = z \cdot F \cdot k_L \cdot c_b$

Substituting the values for the composition at which the experiment was carried out and the calculated value of k_L into the equation gives i_c = 2.3163 A cm^{-2}. Substituting this value and the values obtained for η at 0.5 and 0.05 A cm^{-2} into equation (80) gives the two simultaneous equations

$\alpha - 1.290\,\beta = 0.550$ and
$\alpha - 3.814\,\beta = 0.348$

Solving these gives $\alpha = 0.653$ and $\beta = 0.080$ and

$$\eta = 0.653 + 0.080 \cdot \ln\left(\frac{i}{752.7 \cdot c_b - i}\right) \qquad (82)$$

Equations (77) and (82) are plotted in figure 4.7 for an electrolyte composition of 5 wt% alumina, 4 wt% calcium fluoride, cryolite weight ratio of 1.35 and at 965 °C. The Tafel plot derived by Zuca for an anode porosity of 14.73%, equation (80), is also shown.

As would be expected, the equations (80) and (82) give very close results for the range of current density over which Tafel behaviour was assumed. As the current density increases, the rate of reaction becomes mass transfer controlled and the potential rises more rapidly.

There is a very great similarity between the shapes of equations (74) and (82) although the equation combining η_{SA} and η_{CA}, (74), produces an overpotential some 0.15 V less than that measured by Zuca. This could be due to the reference used in calculating the overpotential.

In addition to η_{SA} and η_{CA}, the Trondheim model also includes an empirical relationship for a cathodic overpotential derived by Alcoa.

$$\eta_{ct} = \frac{R \cdot T \cdot (1.375 - 0.125 \cdot CR)}{1.5 \cdot F} \ln\left(\frac{i_c}{0.257}\right) \qquad (83)$$

where η_{ct} = total overpotential at the cathode
CR = cryolite ratio, mole ratio NaF/AlF3
i_c = cathodic current density

The combined results of equations (74) and (83) are shown in figure 4.7 with the results from equation (82). The expression for the cathodic overpotential is only valid at cathodic current densities above 0.1 A cm^{-2}. Inclusion of the cathodic overpotential causes the two relationships to converge at higher current densities but results in a greater divergence in the Tafel region of the graphs. Information on the reference potential for the derivation of equation (83) was not available and it is possible that this could conflict with the reference used by Zuca or those used in the

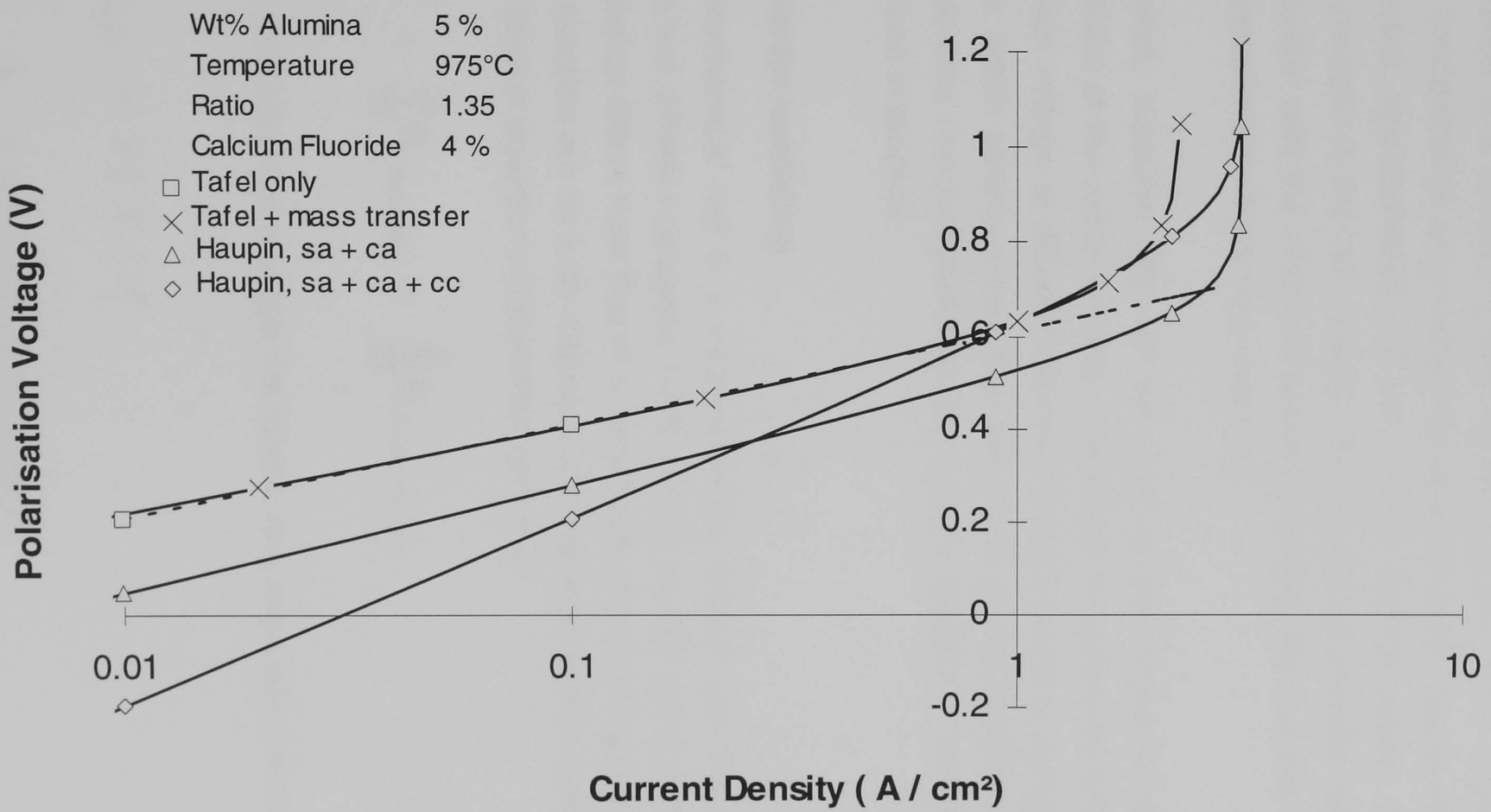

Figure 4.7 Overpotential vs Current Density

derivation of η_{SA} and η_{CA}, thus resulting in the discrepancy between the models.

Figure 4.8 shows the behaviour of the models to variation in alumina concentration at a constant anodic current density of 0.7 A cm^{-2}. As the alumina concentration approaches the point at which anode effect would be expected, approximately 1.5 wt% at this current density, there is a marked increase in the cell voltage. Only the model derived here exhibits this behaviour with the effect not occurring in the other models until much lower concentrations have been reached.

In this work, equation (82) will be used as the model for the anodic overpotential of the oxide reaction. The effect of current density upon the polarisation voltage at different alumina concentrations is plotted in figure 4.9. This graph clearly shows that the onset of anode effect occurs at higher alumina concentrations as the current density is increased as is experienced in practice.

4.6.2 Reactor modelling

An electrochemical cell is a heterogeneous reactor with the electrodes acting as two different catalysts, each forming its own set of products. The mass balance differs from that of a stirred tank chemical reactor in that the rates of reaction are for both chemical and electrochemical reactions. The reaction term in equation (1) therefore becomes

$$\sum_{j=1}^{m} R_j = \sum_{j=1}^{m} R_{j\,(chemical)} + \sum_{j=1}^{m} R_{j\,(electrochemical)} \qquad (84)$$

For a normal chemical reaction the kinetic rate expression would take the form

$$R_{j\,(chemical)} = k \cdot [\ ]^a \cdot [\ ]^b \qquad (85)$$

where k = rate constant for reaction
[ ] = concentrations of reactants
a,b = constants

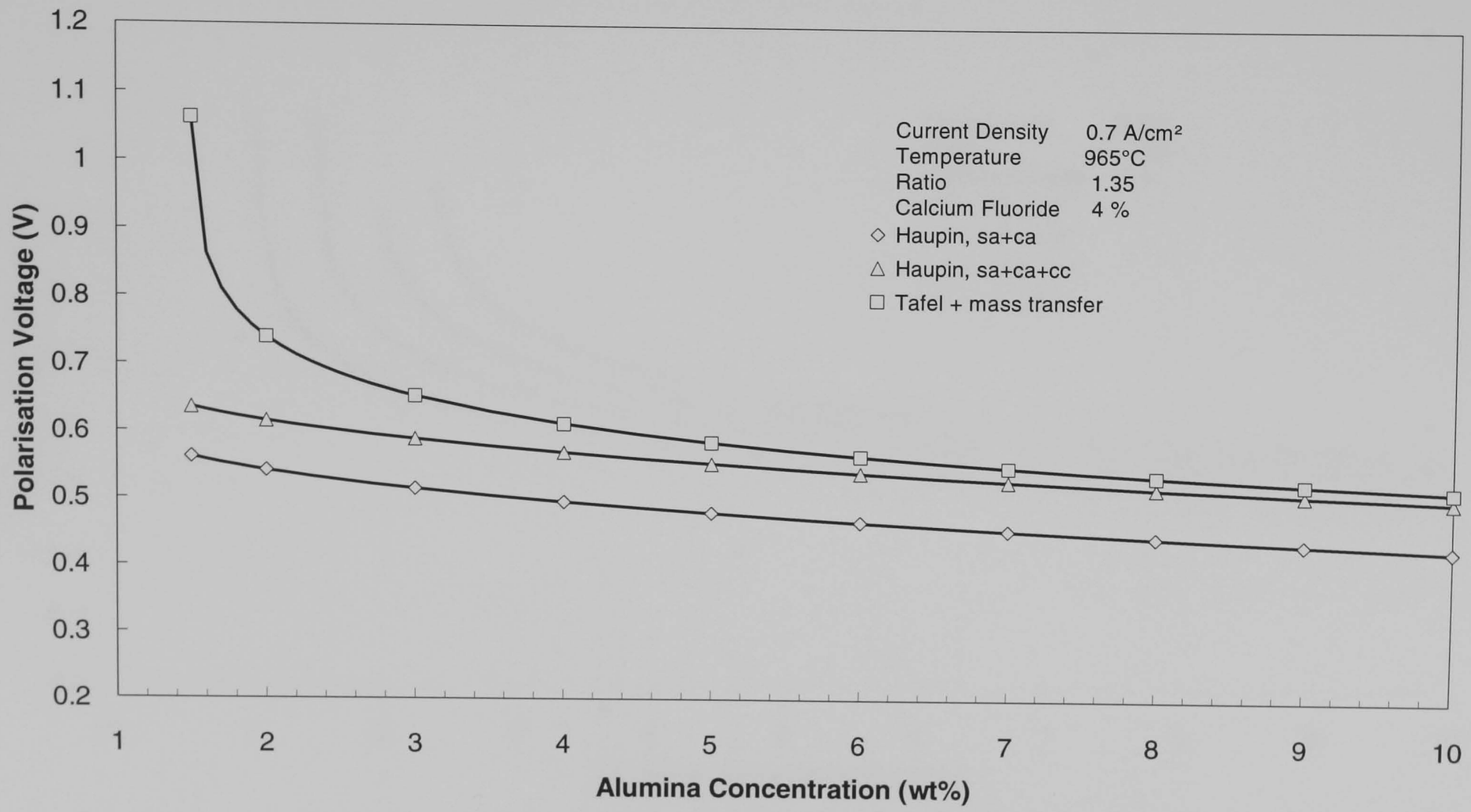

Figure 4.8 Overpotential vs Alumina Concentration

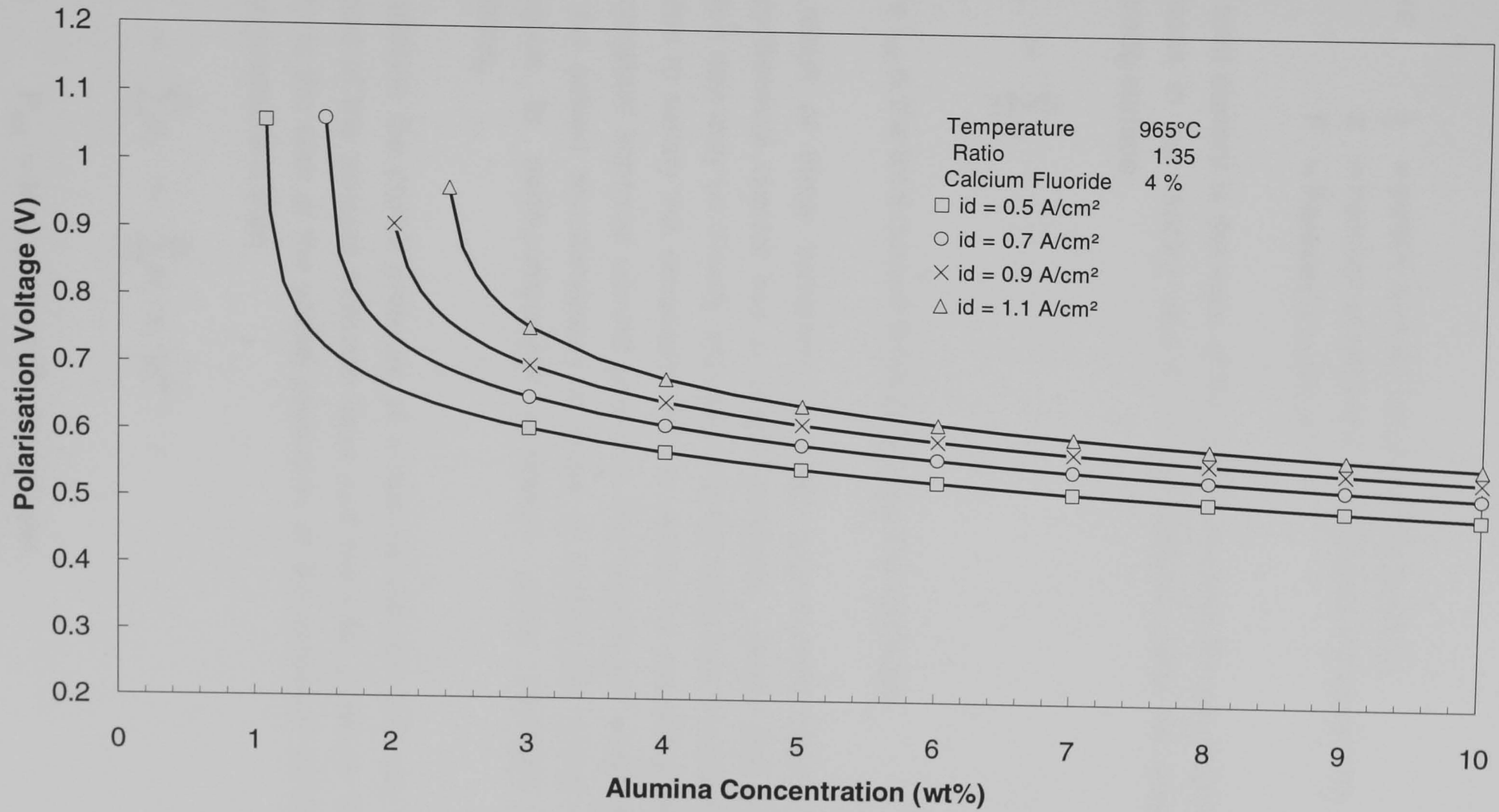

Figure 4.9 Overpotential by Mixed Model vs Alumina Concentration

but for an electrochemical reaction the corresponding equation is

$$R_{j\,(electrochemical)} = \frac{i_j}{z \cdot F} \qquad (86)$$

where i_j = partial current density of the reaction
z = number of electrons transferred in the reaction
F = Faraday's constant

The total current is the sum of the partial currents for all electrochemical reactions in the reactor and a current balance must be done on the electrode surface

$$i_{tot} = \sum_{j=1}^{m} i_j \qquad (87)$$

where i_{tot} is the total current flowing through the electrode.

The result of these balances on mass and current means that an electrochemical reactor has a unique property, namely that an overall reaction rate may be directly imposed and the individual reactions will take up rates to satisfy this constraint. This is utilised by operating the reactor at a constant imposed current and thus the current and mass balances must be solved simultaneously in order to model the system. This is analogous to multi-component distillation under constant boil up conditions.

In distillation the partial pressure of a species dictates the rate of mass transport of the species between trays and the total pressure within the column is the sum of the partial pressures of the individual species. The column pressure is then

$$P_{tot} = \sum_{j=1}^{m} p_j = \sum_{j=1}^{m} \alpha_j \cdot x_j \cdot p_j^{sat} \qquad (88)$$

where P_{tot} = total pressure in the column
p_j = partial pressure of species j
α_j = activity coefficient for species j

x_j = mole fraction of species j in the gas
p_j^{sat} = saturated vapour pressure of species j

The saturated vapour pressure of a component may be calculated from the Antoine equation which relates vapour pressure to temperature

$$p_j^{sat} = A \cdot \exp\left(-\frac{B}{C+T}\right) \tag{89}$$

where A, B and C are Antoine coefficients and T is the temperature of the gas. This is analogous to the Tafel equation relating current density to polarisation potential in the electrochemical system.

The total pressure is therefore given

$$P_{tot} = \sum \alpha_j \cdot x_j \cdot A_j \cdot \exp\left(-\frac{B_j}{C_j - T}\right) \tag{90}$$

Under constant boil up conditions a constant pressure is imposed upon the column and the pressure and mass balances must be solved simultaneously.

In the electrochemical reactor the partial current density for each species at an electrode may be related to activation (electrode potential) and mass transport by the polarisation curve. The equation for this curve has been derived in the previous section and the relationship for a reaction exhibiting Tafel behaviour is described by equation (72).

When a current is imposed on a cell, each electrode takes up an appropriate potential, even to the point of breaking down an apparently neutral substance (eg solvent) in order to achieve the imposed current. In the distillation analogy the temperature rises to maintain the required pressure. The electrode potential will be the same for all reactions taking place at the electrode surface. This can be calculated by simultaneously solving equations (72) and (87) for each electrode and species.

The solution of these simultaneous equations can become complex for multiple reactions but can be simplified for the aluminium reduction cell by making the following assumptions:

1. The only electrochemical reaction at the cathode is the reduction of aluminium.

2. During normal operation the only electrochemical reaction at the anode is the oxidation of oxide. The partial current for the oxide reaction is therefore the total current.

3. During the transition from normal operation to anode effect both oxygen and fluoride ions are oxidised at the anode. However, for anode effect to have initiated, the concentration of alumina in the electrolyte must have fallen to a low level and it will be assumed that the oxide reaction has become mass transfer limited. The equation for the partial current of the oxide reaction, I_o, then reduces to

$$i_o = z\,F\,k_L[O^{2-}]_b \qquad (91)$$

and can be easily calculated. The partial current for the anode effect reaction, the oxidation of fluoride ions, is then the remainder of the total current through the cell

$$i_F = i_{tot} - i_O \qquad (92)$$

and the polarisation voltage can then be easily calculated from equation (72).

4.6.3 Anode effect

Although there has been much research into the causes and conditions for the occurrence of anode effect, most of the experiments have been carried out in laboratory cells and have not attempted to quantify a model for the increase in voltage. A good summary of the laboratory research and the reaction model proposed to interpret the anode effect in laboratory cells under potentiodynamic conditions is given by Calandra et al[14].

As has been stated previously, the anode effect in an aluminium reduction cell results from a change in the electrochemical reactions occurring at the anode. During normal operation, electrolysis depletes the concentration of oxygen ions in the electrolyte until the concentration reaches a level where the reaction becomes mass transfer limited and the reaction is unable to proceed at the rate imposed by the current. As the cells are operated at a constant current alternative ions will be oxidised at the anode to maintain the overall rate of reaction. In the cryolite melt it is fluorine ions that are discharged.

The fluorine discharged reacts with the carbon anode to form various carbon fluorides, ie CF_4, C_2F_6 etc. Unlike the carbon dioxide formed under normal operating conditions, fluorine is very effective at preventing the wetting of the anode surface by the electrolyte. The fluorocarbon bubbles 'stick' to the anode surface and coalesce into an insulating gas film. This film spreads rapidly over the anode surface resulting in a high ohmic resistance across the anode-electrolyte interface.

The fluorocarbon gas film is tenacious, and whilst it covers the surface, normal anode reactions cannot be resumed, hence the requirement of mechanical agitation of the anodes in anode effect quenching routines.

A typical plot of voltage against current density for an electrochemical cell is shown in figure 4.10. As the current density increases beyond the limiting current density of the first reaction, a second reaction, eg the discharge of fluorine, will occur to achieve the imposed current. As the concentration of the species involved in the first reaction falls, so the limiting current density for the first reaction decreases.

The decomposition potential for the oxidation of fluorine ions is around 1.87 V compared with 1.2 V for the discharge of oxygen and the fluoride reaction has been assumed to exhibit Tafel behaviour. As the concentration of fluoride ions in the electrolyte is so great and anode effects are relatively infrequent and short lived, the fluorine ion concentration can be assumed constant and its effect upon the reaction can be ignored.

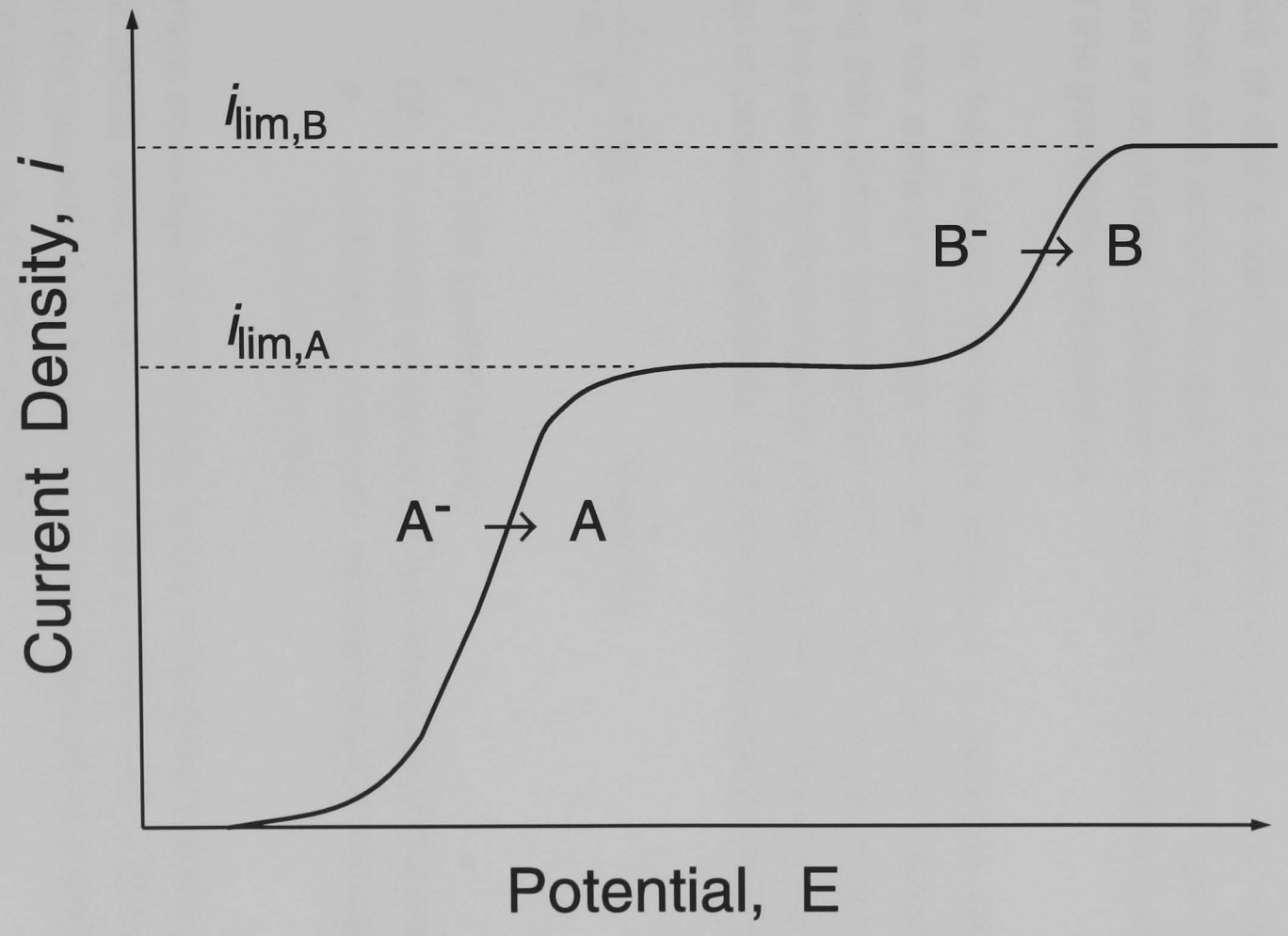

Figure 4.10 Current Density-Potential Curve for a Mixture of Two Compounds Oxidising at Different Potentials

The cell voltage during anode effect in the cells at Anglesey Aluminium is around 30 V, far in excess of the decomposition voltage associated with the discharge of fluorine. This is due to the insulating effect of the fluorocarbon gas film. As the gas film spreads across the anode, so less of the anode area is able to conduct the current into the electrolyte and the effective current density increases. An increase in current density increases the rate and polarization voltage for the fluoride reaction and so the film continue to grow until a point is reached where the ohmic resistance of film is less than the resistance due to the reaction. The current then arcs across the gas film and it is assumed that under these conditions a conductive gas plasma is formed. Electrolysis will then take place at the gas/electrolyte interface.

In order to fully model the anode effect, it is therefore necessary to calculate the surface coverage of the anodes by the fluorocarbon film. Assuming that carbon tetrafluoride, CF_4, is the only fluorocarbon formed and that the electrolytic discharge of fluorine is the rate limiting step in the formation of carbon tetraflouride, the rate of formation of the gas film is

$$\frac{i}{4 \cdot z_F \cdot F} \cdot CE_F \cdot \phi \qquad \text{moles s}^{-1} \qquad (93)$$

where i = cell current density
CE_F = current efficiency for the discharge of fluorine
ϕ = a fittable parameter representing the leakage of gas from the gas film

The surface coverage of the anode is the ratio of the bubble area to the effective anode area. Assuming that the bubble is of uniform thickness and that the gas will obey the ideal gas law, the rate of change of anode coverage during anode effect becomes

$$\frac{d\theta}{dt} = \frac{22400 \cdot T_b}{298 \cdot \ell} \frac{i}{4 \cdot z_F \cdot F} \cdot CE_F \cdot \phi \qquad (94)$$

where θ = surface coverage
T_b = electrolyte temperature
ℓ = bubble thickness

The partial current density for each reaction at the anode during anode effect then becomes

$$i_O = z_O \cdot F \cdot k_L \cdot [O^{2-}] \quad (95)$$

$$i_F = \frac{i}{1-\theta} - i_O \quad (96)$$

When the anode surface is completely covered, it will be assumed in this work that fluorine will be discharged at the bubble/electrolyte interface and that the voltage drop across the interface will be the sum of the voltage drop across the gas film and the polarization voltage associated with the fluorine reaction.

$$V = V_{film} + E_F \quad (97)$$

4.7 Cell Voltage, Energy Consumption and Cell Resistance

The cell voltage can be used to calculate the energy consumption of the cell by Ohm's law

$$Q_{cell} = I.V_{cell} \quad (98)$$

where Q_{cell} = power consumed by the cell W
I = current passed through the cell A
V_{cell} = electrical potential across the cell V

The cell voltage is not simply the sum of the electrode potentials but must include the ohmic drop across electrolyte and the cell structure. The total voltage drop across the cell is therefore

$$V_{cell} = E_{anode} + E_{cathode} + V_{electrolyte} + V_{structure} \quad (99)$$

where $E_{anode}, E_{cathode}$ = polarisation voltage at anode and cathode respectively
$V_{electrolyte}$ = voltage drop across the electrolyte
$V_{structure}$ = voltage drop across cell structure

The polarisation voltages and voltage drop across the electrolyte have been considered in detail above. The voltage drop across the cell structure is due to the resistance of the materials used in the cell construction and includes terms for the anodes and cathode, anode and cathode bus, anode riser and cathode flex. The resistance of each section was provided by Anglesey Aluminium and the data that will be used in this work is tabulated in table 4.2.

The voltage measured in practice is the cell voltage and includes all the above components. The cell resistance is calculated from this and can be used to infer conditions such as the alumina concentration in the electrolyte.

$$R_{cell} = \frac{V_{cell}}{I} \tag{100}$$

4.8 Heat Balance

Models to determine accurate temperature profiles and the heat flow within cells have been developed but the number of calculations required for solution make them unsuitable for simulation of a cells dynamic behaviour. A good approximation may be achieved by dividing the cell into a number of larger zones each of which is assumed to be well mixed and therefore at a uniform temperature. The schematic model of the cell and heat flows is shown in figure 4.11. The cell is divided into 8 coarse components: (A) the aluminium pad, (B) the molten electrolyte, (C) the anode, (D) the cathode, (E) the frozen ledge in the bath, (F) the frozen ledge in the metal, (G) the cell sidewalls and (H) the electrolyte crust.

In spite of thermal disturbances to the cell, the heat balance of the cell over a long period follows equation (101) for the steady state treatment.

$$Q_{res} = Q_R + Q_H + Q_{out} \tag{101}$$

where Q_{res} is the average power input to the cell, Q_R the net heat of reaction, Q_H the average heat required for the heating and dissolution of raw materials and Q_{out} the average total heat dispersed from the cell. However, for the simulation of the dynamic behaviour of a cell, the heat

Component	Resistance Ω
Anode rod clamp	1.044×10^{-5}
Anode stub	1.458×10^{-5}
Anode bus	4.1×10^{-7}
Anode riser	3.8×10^{-7}
Cathode flex	2.0×10^{-7}
Cathode bus	1.24×10^{-6}

Table 4.2 External Resistances

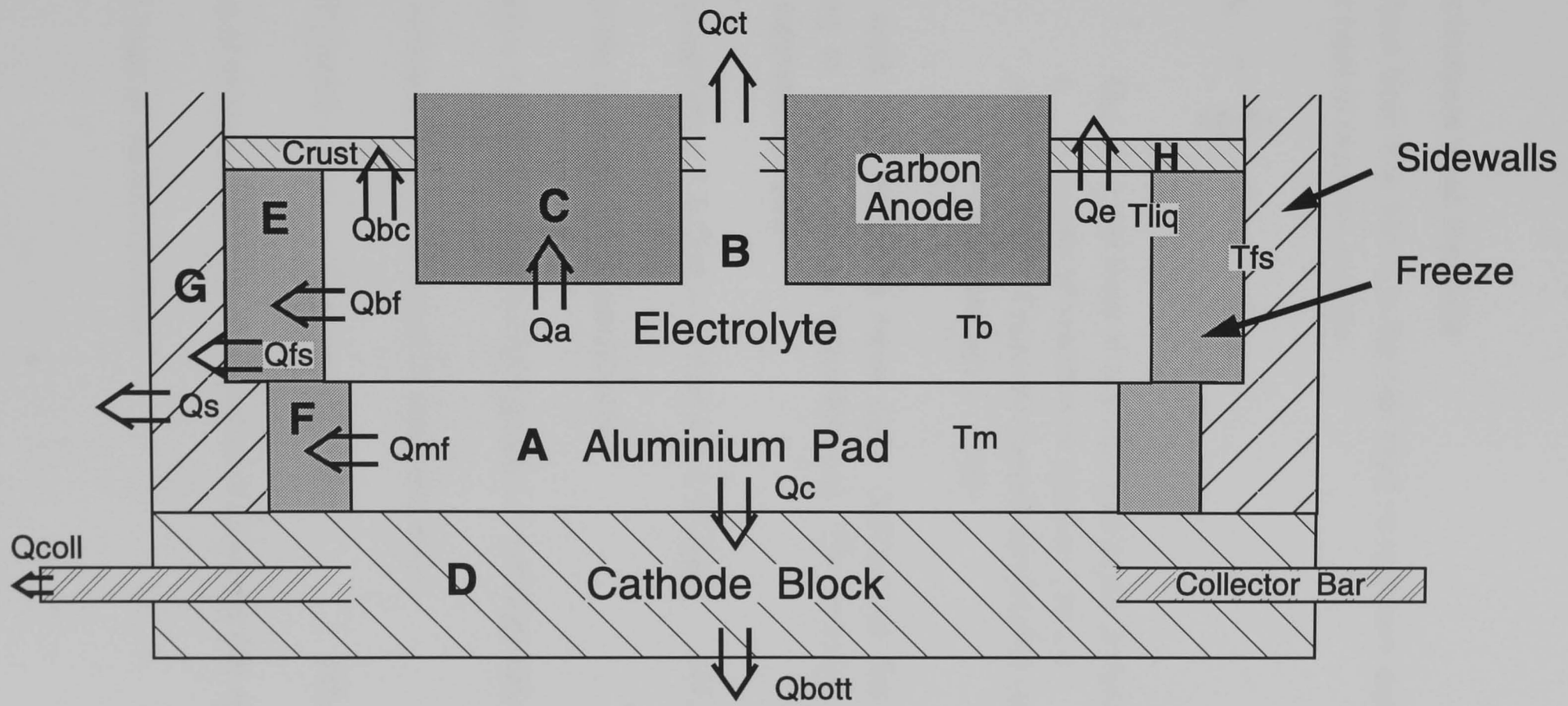

Figure 4.11 Schematic Diagram of Heat Flow in an Aluminium Cell

which changes momentarily must be considered. Its treatment is described precisely in the following sections.

4.9 Electrolysis Heat Balance

The output from this block is the net heat of reaction due to electrolysis. The net heat of reaction is given

$$Q_R = \sum_{i=1}^{n} r_i \cdot \Delta H_{R.T.i} \qquad (102)$$

where Q_R = net heat of reaction due to electrolysis W
r_i = rate of reaction of species i, mol s^{-1}
$\Delta H_{R,T,j}$ = heat of reaction based on species i at temperature T, J mol^{-1}

In this work four reactions have been defined as the main reactions occurring in the aluminium reduction cell. The primary reaction during normal operation is given

$$Al_2O_3(soln) + 1.5\ C(s) \rightarrow 2\ Al(l) + 1.5\ CO_2(g) \qquad \Delta H_1 \qquad [8]$$

Some of the aluminium is reoxidised by

$$Al(l) + 1.5\ CO_2(g) \rightarrow 0.5\ Al_2O_3(soln) + 1.5\ CO(g) \quad \Delta H_2 \qquad [9]$$

During anode effect the reaction is assumed to be

$$AlF_3(soln) + C(s) \rightarrow Al(l) + 0.75\ CF_4(g) \qquad \Delta H_3 \qquad [10]$$

and loss of current efficiency is assumed to occur by the reverse reaction.

The net heat of reaction is then

$$Q_R = \frac{1}{3}\cdot\frac{I_O}{z_O\cdot F}\cdot\Delta H_1 + \frac{1}{3}\cdot\frac{I_F}{z_F\cdot F}\cdot\Delta H_3$$

$$+\frac{2}{3}\cdot r_{CO_2diss}\cdot\Delta H_2 - \frac{4}{3}\cdot r_{CF_4diss}\cdot\Delta H_3 \qquad (103)$$

The enthalpy of reaction at any temperature may be determined from the heats of formation of the individual species involved in the reaction. Thus, for the reaction

$$aA + bB \rightarrow cC + dD$$

the heat of reaction is given

$$\Delta H_{R,T} = c\cdot H_T^f(C) + d\cdot H_T^f(D) - a\cdot H_T^f(A) - b\cdot H_T^f(B) \qquad (104)$$

where $H_T^f(i)$ is the heat of formation of species i at temperature T and can be determined from

$$H_T^f(i) = H_{T_\phi}^f(i) + \int_{T_\phi}^{T} Cp_i\cdot dT + \lambda_i \qquad (105)$$

where Cp_i = specific heat capacity of species i
T_ϕ = reference temperature K
λ_i = net latent heat for any changes in state of species i between T and T_ϕ

Over a narrow temperature range such as that encountered under standard operating conditions, the specific heat of a species may be assumed constant and this reduces to

$$H_T^f(i) = H_{Ta}^f(i) + Cp_i\cdot(T - T_a) \qquad (106)$$

where T_a is the average operating temperature and the heat of formation calculated at this temperature. For reaction [8] this gives

$$\Delta H_{1,T} = \left(1.5H^{f}_{Ta}(CO_2) + 2H^{f}_{Ta}(Al) - H^{f}_{Ta}(Al_2O_3) - 1.5H^{f}_{Ta}(C)\right)$$

$$-\left(1.5Cp_{CO_2} + 2Cp_{Al} - Cp_{Al_2O_3} - 1.5Cp_{C}\right)\cdot(T - T_a) \qquad (107)$$

The heats of reactions for [9] and [10] are similarly calculated.

4.10 Heat Losses

In this work heat losses from the cell are defined to be the heat transferred from the molten electrolyte and aluminium pad to the surrounding. In figure 4.11 the losses are shown as the heat transferred from the electrolyte to the anodes, Q_A, from the electrolyte to the frozen sidewalls, Q_{bf}, from the electrolyte to the crust, Q_{bc}, from the exposed bath to the cavity beneath the shields, Q_e, from electrolyte through the centre trench, Q_{ct}, from the metal pad to the cathode block, Q_C and from the molten pad to the frozen sidewalls, Q_{mf}. In this work it has been assumed that the resistance to heat transfer between metal pad and electrolyte is insignificant with the result that heat transfer between these zones is instantaneous and the temperatures of these zones are equal.

Heat may be lost from the cell by convection and, in the case of exposed bath, by radiation. Although the heat transfer coefficient for convection may be calculated from the Sieder-Tate equation for variations in physical properties and temperature this method is more suited for local heat transfer coefficients. As physical properties change little in the range of operating conditions and the velocity of the electrolyte and metal pad are largely affected by the anode configuration and cell design, a representative coefficient will be taken for each section and fixed for the duration of the simulation.

4.10.1 Heat transferred to the frozen sidewalls

The heat transferred to the frozen sidewalls from the electrolyte and metal pad is by convection only. In both cases the temperature at the ledge interface is assumed to be the liquidus temperature of the electrolyte. In the case of the metal ledge boundary this may be assumed due to the existence of a thin film of electrolyte between the metal pad and the frozen

ledge. This film circulates with the bulk of the electrolyte and will be assumed to have the same composition as the bulk electrolyte. The heat transferred to the ledge is then

$$Q_{bf} = h_{bf} A_{bf} (T_b - T_{liq}) \quad (108)$$

$$Q_{mf} = h_{mf} A_{mf} (T_b - T_{liq}) \quad (109)$$

where h = heat transfer coefficient
A = area for heat transfer
T_b = bulk temperature of electrolyte and metal pad
T_{liq} = liquidus temperature of the electrolyte
suffix
bf refers to bath/ledge interface
mf refers to metal pad/ledge interface

4.10.2 Heat transferred from metal pad to cathode block

The heat transferred to the cathode block is by convection from the bulk of the metal pad to the surface of the carbon cathode. The heat transferred from the metal pad is then

$$Q_C = h_{mc} A_{mc} (T_b - T_{Cs}) \quad (110)$$

where T_{Cs} = the temperature at the cathode surface
suffix mc refers to the cathode/metal pad boundary

The generation of Joule heat, due to the electrical resistance of the cathode block, and the inclusion of highly conductive metal collector bars within the cathode block require a heat balance be performed upon the cathode for the calculation of T_{Cs}. As the thermal dynamics of the cell are far quicker than those of the cathode, the cathode block will be divided into two unequal zones as shown in figure 4.12. This allows the surface temperature to react quickly to changes in the electrolyte temperature whilst maintaining the overall heat losses and reducing the number of calculations required in simulation. The heat balance for each zone is then

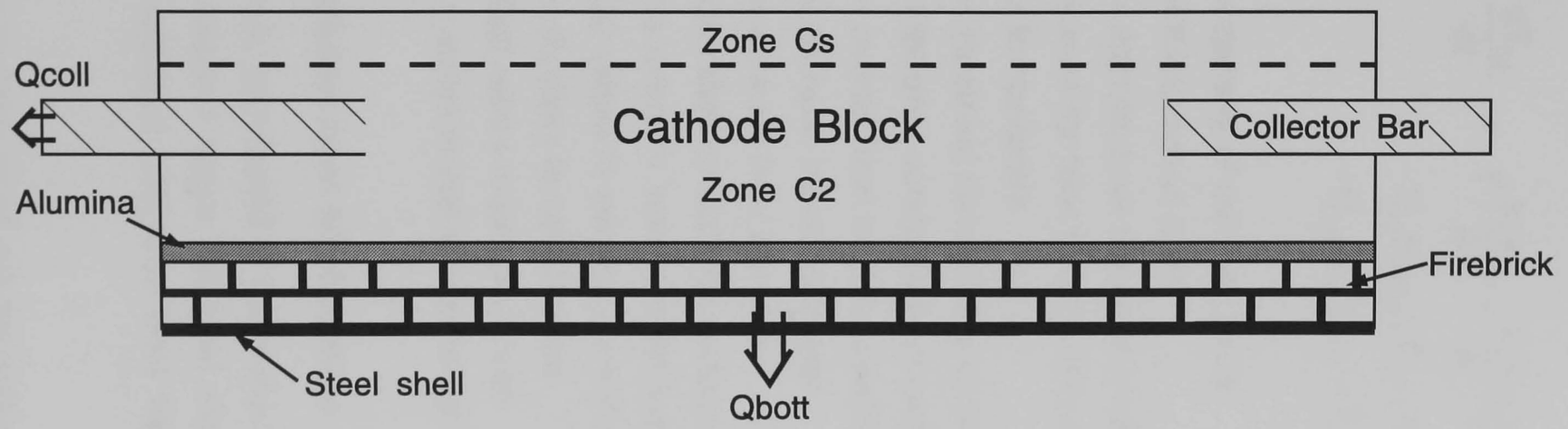

Figure 4.12 Heat balance across the cathode

$$\rho_c x_{Cs} Cp_c A_c \frac{dT_{Cs}}{dt} = I^2 \frac{k_c x_{Cs}}{A_c} + Q_C - U_{ca} P_c x_{Cs} (T_{Cs} - T_\infty) - \frac{\kappa_c x_{Cs}}{A_c} (T_{Cs} - T_{C2}) \quad (111)$$

$$\rho_c x_{C2} Cp_c A_c \frac{dT_{C2}}{dt} = I^2 \frac{k_c x_{C2}}{A_c} + \frac{\kappa_c x_{Cs}}{A_c} (T_{Cs} - T_{C2}) - U_{ca} P_c x_{C2} (T_{C2} - T_\infty) - U_{coll} A_{coll} (T_{C2} - T_\infty) - U_{bott} A_{bott} (T_{C2} - T_\infty) \quad (112)$$

where
- ρ_c = density of cathode block
- x = thickness of zone
- Cp_c = specific heat capacity of cathode block
- A_c = area for heat transfer through cathode block
- T = temperature
- k_c = electrical conductivity of cathode block
- κ_c = thermal conductivity of cathode block
- U = overall heat transfer coefficient
- P_c = cathode block perimeter
- A = area for heat transfer

Cs refers to cathode surface
ca refers to heat transfer from cathode to surroundings
C2 refers to second zone in cathode
coll refers to collector bar
bott refers to bottom of cell
∞ refers to cell surroundings

4.10.3 Heat transferred from electrolyte to cavity

In this work the heat transferred to the surface of the electrolyte has been defined in three distinct ways, as heat transferred to the crust, heat transferred from exposed bath and heat transferred through the centre trench.

For simplicity, the surface crust will be assumed to be always in contact with the electrolyte and will be treated in the same manner as the frozen sidewall. This necessitates that a mass balance also be performed upon the crust allowing freezing or melting into the electrolyte

$$Q_{bc} = h_{bc} A_{bc} \left(T_b - T_{liq} \right) \tag{113}$$

$$\frac{dM_{crust}}{dt} = \frac{Q_{bc} - U_{crust} A_{crust} \left(T_{liq} - T_{cav} \right)}{\left(\lambda_f + Cp_e \left(T_b - T_{liq} \right) \right)} \tag{114}$$

where λ_f = latent heat of fusion of electrolyte

Cp_e = specific heat capacity of electrolyte

suffix

bc refers to heat transfer from electrolyte to crust

cav refers to cavity beneath shields

For a centre break cell, heat transfer in the centre trench is alternately from exposed bath after breaker action and by convection to an insulating layer of alumina after a feed has been dumped onto the surface. As the alumina has good insulating properties and does not remain on the surface long enough to form a complete agglomeration with the electrolyte by capillary action there is little formation of a frozen layer as there is with the crust. The heat lost through the centre trench will then be by convection and radiation for exposed bath and predominately by convection and conduction for alumina cover. For simplicity, the heat transfer through the alumina cover will be assumed to be at steady state and represented by an overall heat transfer coefficient including the heat transfer coefficients at both surfaces and the thermal conductivity of the alumina layer. Therefore, for exposed bath

$$Q_{ct} = h_{ctc} A_{ct} \left(T_b - T_{cav} \right) + A_{ct} \varepsilon_{ct} \sigma \left(T_b^4 - T_{cav}^4 \right) \tag{115}$$

and for alumina cover

$$Q_{ct} = U_{ct} A_{ct} \left(T_b - T_{cav} \right) \tag{116}$$

where h_{ctc} = heat transfer coefficient from exposed bath in centre trench to cavity

ε_{ct} = emmissivity from exposed bath in centre trench to cavity

σ = Stefan Boltzmann constant

A_{ct} = area of centre trench

U_{ct} = overall heat transfer coefficient in trench for alumina cover

The overall heat transfer coefficient is given for steady state flow of heat through a composite wall as

$$\frac{1}{U} = \frac{1}{h_i} + \sum_{j=1}^{n} \frac{x_j}{k_j} \cdot \frac{A_i}{A_j} + \frac{1}{h_o} \cdot \frac{A_i}{A_o} \qquad (117)$$

where
- U = overall heat transfer coefficient based upon the inner surface area
- h = heat transfer coefficient at wall surface
- x = thickness of a layer
- k = thermal conductivity of a layer
- A = area for heat transfer
- suffix
  - i refers to inner surface
  - j refers to jth layer of composite wall
  - o refers to outer surface

The overall heat transfer coefficient across the alumina cover in the centre trench, where the area for heat transfer is assumed to be equal across each surface, is then

$$\frac{1}{U_{ct}} = \frac{1}{h_{bt}} + \frac{x_{ac}}{k_{ac}} + \frac{1}{h_{tc}} \qquad (118)$$

where suffix
- bt refers to heat transfer from bath to alumina
- ac refers to alumina cover
- tc refers to heat transfer from trench to cavity

Heat is also lost from exposed bath whilst the anode is removed from the cell when a spent anode is being replaced. The operation of anode removal lasts for several minutes and during this period the shield above the anode must also be removed. Heat transfer is therefore to the air surrounding the cell which may be at a significantly lower temperature

than the cavity beneath the shields. The heat transferred from the electrolyte will therefore be

$$Q_{ex} = h_{ex} \cdot A_{ex} \cdot (T_b - T_\infty) + A_{ex} \cdot \varepsilon \cdot \sigma_{ex} \cdot (T_b^4 - T_\infty^4) \qquad (119)$$

where the suffix *ex* refers to exposed bath.

4.10.4 Heat transferred from electrolyte to anodes

Heat losses to the anodes constitutes one of the major losses from the electrolyte. Heat is transferred from the electrolyte to the anode by convection and conducted away from anode/bath interface to the upper surface where it is dispersed. The replacement of a spent carbon anode in the cell with a new one at a temperature several hundreds of degrees Celsius below that of the cell constitutes a massive thermal disturbance. The initial effect is the formation of a frozen layer of electrolyte upon the anode surface which effectively insulates the anode and reduces the rate of heat loss from the bath. This layer initially grows, the latent heat of fusion being given up in heating the anode, until either the anode has reached a temperature such that the heat conducted away from the frozen surface is less than that transferred from the bath and the layer melts, or the frozen layer contacts the aluminium pad. In the latter case, the very low liquidus temperature of aluminium prevents further freezing and heat is conducted through the frozen layer and into the anode. The speed at which the anode is heated is thus increased and anodes are frequently 'set low' to take advantage of this effect. As the anode warms and starts to draw current, Joule heat is generated within the anode further warming it. The complex nature of this problem requires that a heat balance must be performed on each of the anodes and for this purpose each anode will be divided into a number of unequal zones as shown in figure 4.13. As with the cathode heat balance, the dynamics at the anode surfaces are considered to be most important and the zones in these regions are consequently the narrowest. Heat transfer is assumed to be uni-directional through the anode with no heat losses from the sides.

There are three methods of heat transfer from the electrolyte to an anode that must be considered. These are as follows:

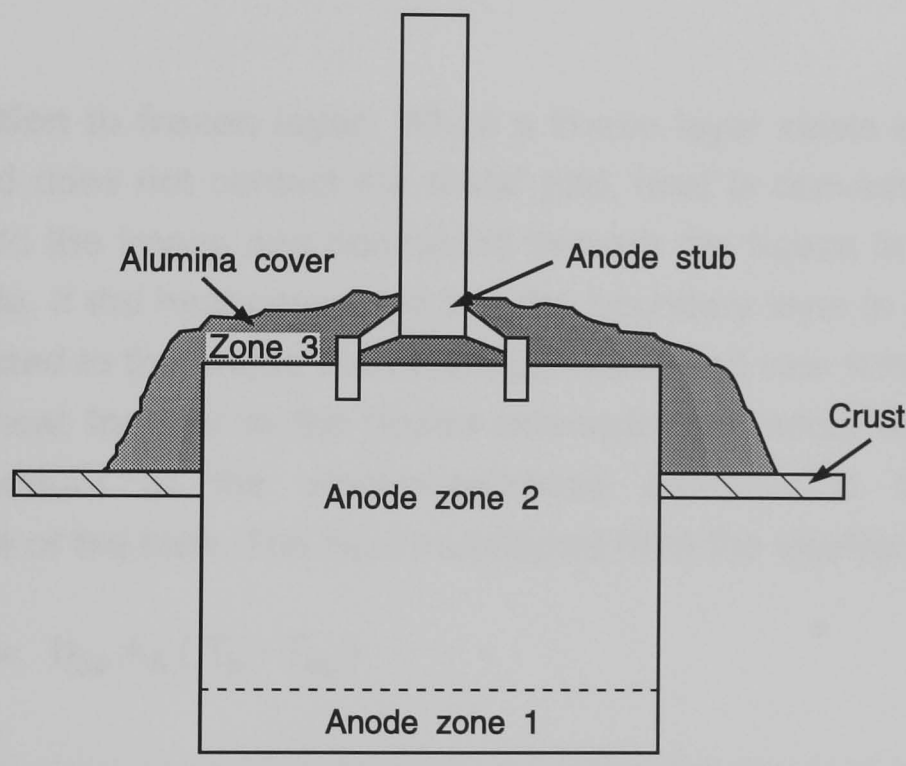

Figure 4.13 Heat balance across an anode

1) **Convection directly to the anode surface:** This is the case when there is no frozen layer on the anode surface. The heat transferred from the bath and into the anode is then given

$$Q_{Ai} = Q_{As} = h_{ba} A_A (T_b - T_{As}) \quad (120)$$

where Q_{Ai} = heat transferred from bath to anode i
Q_{As} = heat transferred into surface layer of anode
h_{ba} = heat transfer coefficient from electrolyte to anode surface
A_A = anode area
T_{As} = surface temperature of anode

2) **Convection to frozen layer:** When a frozen layer exists at the anode surface and does not contact the metal pad, heat is convected from the electrolyte to the freeze and conducted through the freeze to the surface of the anode. If the heat convected into the boundary layer is greater than that conducted to the anode then the layer melts and vice versa. As in the model for heat transfer to the frozen sidewalls this model assumes that the temperature at the electrolyte/freeze interface is the liquidus temperature of the bath. The heat transferred from the electrolyte is then

$$Q_{Ai} = h_{ba} A_A (T_b - T_{liq}) \quad (121)$$

and the heat conducted through the frozen layer into the anode surface is

$$Q_{As} = \frac{k_f}{x_{af}} A_A \left(T_{liq} - T_{As} \right) \quad (122)$$

where k_f = thermal conductivity of frozen electrolyte
x_{af} = thickness of frozen layer at the anode surface

Any difference between the heats into and out of the boundary layer results in freezing or melting of the layer. As with the heat balance upon the crust the rate of freezing can be determined by a performing a heat balance upon the boundary layer

$$\left(\lambda_f + Cp_e \cdot \left(T_b - T_{liq}\right)\right) \cdot \frac{dM_{af}}{dt} = Q_{As} - Q_{Ai} \qquad (123)$$

which gives the rate of change of thickness of the frozen layer

$$\frac{dx_{af}}{dt} = \frac{\left(Q_{As} - Q_{Ai}\right)}{A_A \cdot \rho_f \cdot \left(\lambda_f + Cp_e \cdot \left(T_b - T_{liq}\right)\right)} \qquad (124)$$

where $\frac{dM_{af}}{dt}$ = rate of freezing of frozen layer at anode surface kg s^{-1}

$\frac{dx_{af}}{dt}$ = rate of change of thickness of frozen layer on anode surface m s^{-1}

ρ_f = density of electrolyte at liquidus temperature kg m^{-3}

3) **Conduction through frozen layer:** The low liquidus temperature, about 660 °C, and high thermal conductivity of molten aluminium prevents a frozen layer of aluminium from forming on any anode freeze that contacts the metal pad. Growth of the frozen layer therefore ceases if the thickness exceeds the interelectrode gap. Heat transfer to the anode is then by conduction through the frozen layer:

$$Q_{Ai} = Q_{As} = \frac{k_f}{x_{af}} \cdot A_A \cdot \left(T_b - T_{As}\right) \qquad (125)$$

The rate of change in the temperature at the surface of the anodes is determined by performing a heat balance upon each anode similar to that performed upon the cathode. The anode is divided into three zones shown in figure 4.13 and the heat balance for each zone is

$$\rho_a x_{As} Cp_a A_A \frac{dT_{As}}{dt} = \frac{I_i^2 \cdot k_a \cdot x_{As}}{A_A} + Q_{As} - \frac{K_a \cdot x_{A2}}{A_A} \cdot \left(T_{As} - T_{A2}\right) \qquad (126)$$

$$\rho_a x_{A2} Cp_a A_A \frac{dT_{A2}}{dt} = \frac{I_i^2 \cdot k_a \cdot x_{A2}}{A_A} + \frac{K_a \cdot x_{A2}}{A_A} \cdot (T_{As} - T_{A2}) - \frac{K_{cov} \cdot x_{cov}}{A_A} \cdot (T_{A2} - T_{A3}) - U_{stub} \cdot A_{stub} \cdot (T_{A2} - T_{Cav}) \quad (127)$$

$$\rho_{cov} x_{cov} Cp_{cov} A_{cov} \frac{dT_{A3}}{dt} = \frac{K_{cov} \cdot x_{cov}}{A_A} \cdot (T_{A2} - T_{A3}) - h_{cov} \cdot A_{cov} \cdot (T_{A3} - T_{Cav}) - \varepsilon_{cov} \cdot A_{cov} \cdot \sigma \cdot (T_{A3}^4 - T_{cav}^4) \quad (128)$$

where I_i = current through anode i

ε_{cov} = emmissivity of alumina cover on top of anode

suffix

a refers to anode

As refers to anode surface

cav refers to cavity beneath shields

cov refers to alumina cover on top of anode

stub refers to anode stub

A2, A3 refer to zones 2 and 3 in anode model

The total rate of heat transferred from the electrolyte to the block of anodes is simply the sum of the individual rates. For n anodes this is

$$Q_A = \sum_{i=1}^{n} Q_{Ai} \quad (129)$$

The total heat lost from the cell is the sum of the individual components:

$$Q_{loss} = Q_A + Q_{bf} + Q_{mf} + Q_e + Q_{ct} + Q_C \quad (130)$$

4.11 Pot Heat Balance

As this work assumes that the resistance to heat transfer between the electrolyte and metal pad is negligible the two layers are considered as a single thermal mass. This combination will be referred to as the pot.

The overall heat balance on the pot is:

rate of accumulation of heat = rate of electrical heat generation due to ohmic drop across pot

- total heat of reaction

- enthalpy in materials leaving pot

- heat required to raise feed materials to temperature of pot

- heat of dissolution of materials added to the pot

- heat losses from the pot

The heat balance on the pot is taken relative to a reference temperature. If this datum is chosen to be the temperature of the electrolyte then all the terms for the enthalpy of materials leaving the pot become zero. These include the enthalpy in aluminium tapped from the cell and the enthalpy of the flue gases. The heat balance then becomes

$$M_{pot} \cdot Cp_{pot} \cdot \frac{dT_b}{dt} = Q_{Res} - Q_R - Q_{diss} - Q_{feed} - Q_{loss} \qquad (131)$$

where M_{pot} = total mass of electrolyte and metal pad

$= M_{bath} + M_{pad}$

Cp_{pot} = net specific heat capacity of electrolyte and metal pad

$$= \frac{M_{bath} \cdot Cp_{bath} + M_{pad} \cdot Cp_{Al}}{M_{bath} + M_{pad}}$$

Cp_{bath} = specific heat capacity of electrolyte

Cp_{Al} = specific heat capacity of molten aluminium

Q_{Res} = heat due to the voltage drop across the electrolyte

Q_R = net heat of electrochemical and chemical reactions

Q_{diss} = heat of dissolution of feed materials

Q_{feed} = heat required to raise feed materials to the temperature of the electrolyte

The heat due to the voltage drop across the electrolyte must be calculated from the cell voltage excluding the voltage drop across the cell structure.

$$V^0 = V_{cell} - V_{structure} \quad (132)$$

$$Q_{Res} = I \cdot V^0 \quad (133)$$

This is the only Joule heat that enters the electrolyte. The resistance of the cell structure causes heat to be generated within the structure itself, for example in the cathode block, and does not directly affect the molten electrolyte.

4.11.1 Heat of dissolution

All materials dissolved in the bath consume heat proportional to the amount of material added. The heats of dissolution for materials dissolved in molten cryolite are not well documented but an average value for alumina has been quoted by Thonstad[15] as 125 kJ mol^{-1}. This value will be used in this work as the heat of dissolution of the entire alumina feed, inclusive of the added fines and sodium oxide. The heat of dissolution is therefore given

$$Q_{diss} = H_{diss} \times (r_{diss(suspn)} + r_{diss(sludge)}) \quad (134)$$

where H_{diss} is the heat of dissolution of alumina.

The only other raw material added to the electrolyte in any quantity is aluminium fluoride. As this is added infrequently and in relatively small amounts compared to the alumina feed, 25 kg AlF_3 per day as to 90 kg Al_2O_3 every 70 minutes, the relative disturbance to the heat balance is very small. In this work, the aluminium fluoride is assumed to dissolve instantly and the heat of dissolution is assumed negligible.

4.11.2 Specific heat of feed materials

The feed materials added to the cell are much colder than the molten electrolyte at about 200°C and heat is required to raise them to the temperature of the melt, about 970°C. The amount of heat required to raise a substance from temperature T_1 to T_2 is given

$$H = \int_{T_1}^{T_2} Cp\, dT \qquad (135)$$

Although the specific heat capacity of feed materials may be assumed constant over the range of operating temperature, there is a significant variation between 200 and 970°C. Tables of heat content are, however, available for alumina and the heat required to raise the alumina feed from 200°C to temperature T may be found by interpolation

$$H_{Al_2O_3,T} = H_{927} + \frac{H_{1027} - H_{927}}{1027 - 927} \cdot (T - 927) - H_{200} \qquad (136)$$

using JANAF data[16] gives

$$H_{927} = 103.24 \text{ kJ mol}^{-1}$$
$$H_{1027} = 116.08 \text{ kJ mol}^{-1}$$
$$H_{200} = 16.41 \text{ kJ mol}^{-1}$$

and

$$H_{Al2O3,T} = 86.83 + 0.1284\ (T - 927) \qquad \text{kJ mol}^{-1} \qquad (137)$$

As alumina is the most significant component of the feed, this relationship will be used for the heat content of the entire feed inclusive of fines.

The heat loss due to addition of aluminium fluoride is much less significant and for simplicity, the specific heat capacity of this component will be assumed constant. The heat required to raise AlF_3 additions to the operating temperature, based upon data from Aylward and Findlay[17] is

$$H_{AlF3,\,T} = Cp_{AlF3}\ (T - 200) = 75 \cdot (T-200) \qquad (138)$$

4.12 Frozen Sidewalls

Models for the precise estimation of the frozen sidewall profile have been presented[18,19,20] but require the division of the cell into a number of triangular sections. A mass and heat balance must be performed across each section and the time required for these calculations makes these models unsuitable for dynamic simulation.

The profile of the frozen sidewalls is of prime importance in the study of the hydrodynamics of the cell. In this work, a simple hydrodynamic model is assumed and the detailed calculation of freeze profile is unnecessary. The frozen sidewall will be divided into two zones, that in contact with the molten electrolyte and that in contact with the molten aluminium. Two zones are required because of the difference in heat transfer coefficients in the electrolyte and aluminium pad.

In each zone the sidewalls are assumed to be of uniform thickness and the heat flow unidirectional.

The heat transferred from the molten bath to the freeze and from the cell outer wall to the surroundings is assumed to be purely by convection. Heat transferred through the freeze and composite wall is by conduction.

The heat flow through each section is therefore

$$q_b = h_b \cdot A_b \cdot (T_b - T_l) \tag{139}$$

$$q_f = \frac{k_f}{x_f} \cdot A_f \cdot (T_l - T_{fw}) \tag{140}$$

$$q_1 = \frac{k_1}{x_1} \cdot A_1 \cdot (T_{fw} - T_{w1}) \tag{141}$$

$$q_2 = \frac{k_2}{x_2} \cdot A_2 \cdot (T_{w1} - T_{w2}) \tag{142}$$

$$q_3 = \frac{k_s}{x_s} \cdot A_s \cdot (T_{w2} - T_s) \tag{143}$$

$$q_s = h_s \cdot A_s \cdot (T_s - T_a) \tag{144}$$

The primary area of interest is the heat flow into and out of the boundary layer at the surface of the frozen sidewall as this controls the melting and freezing of the frozen sidewalls. The resistance to heat transfer of the

freeze, composite sidewall and outer surface may be approximated to an overall heat transfer coefficient U, by

$$\frac{1}{U} = \left[\frac{x_f}{k_f \cdot A_f} + \frac{x_1}{k_1 \cdot A_1} + \frac{x_2}{k_2 \cdot A_2} + \frac{1}{h_s}\right] \cdot \frac{A_f}{A_s} \qquad (145)$$

where the heat transfer coefficient is based upon the internal area of the freeze. The equations for heat transfer across the boundary layer then become

$$\text{In} \quad q_b = h_b A_b (T_b - T_l) \qquad (146)$$

$$\text{Out} \quad q_f = U A_f (T_l - T_b) \qquad (147)$$

In addition to reducing the number of computations required, this approximation overcomes the problem of initialising the temperatures at each material interface.

If the boundary layer is assumed to be infinitely thin and at the liquidus temperature of the molten electrolyte then any accumulation of heat will cause melting of the sidewalls to the temperature of the bath. Performing a heat balance across the boundary layer gives

$$\frac{dm}{dt} \cdot \left[\lambda + Cp \cdot (T_b - T_l)\right] = q_b - q_f \qquad (148)$$

Change of state from solid to liquid + enthalpy of change in temperature — Heat in — Heat out

The rate of change of state of the frozen sidewalls is then given

$$\frac{dm}{dt} = \frac{q_b - q_f}{\lambda + Cp \cdot (T_b - T_l)} \qquad (149)$$

and the rate of change of the thickness of the freeze

$$\frac{dx_f}{dt} = \frac{q_b - q_f}{\rho_f \cdot A_f \cdot \left[\lambda + Cp \cdot (T_b - T_l)\right]} \qquad (150)$$

The cell wall in the metal pad region consists of a sloping carbon section and two layers of firebrick. As the cell ages the profile of the carbon section changes as shown in figure 4.14 with the slope in the metal pad area becoming less steep. In this model, the wall thickness in the metal pad area will be assumed to be of a uniform thickness as is more the case in an older cell. The assumptions made in general in this model do not favour the unpredictable behaviour of a cell that has been newly brought on line and the assumption of a freeze profile similar to that of an established cell is therefore justified.

The diffusion of species between the frozen ledge and the melt during freezing has been modelled by Hashimoto[21] and requires the estimation of a diffusion coefficient for each species and the velocity of solidification. A further constant, related to the diffusivity of the melt, must also be fitted and estimates by Hashimoto range between 0.1 and 0.00001 for commercial cells. The complexity of this model and the difficulty in obtaining meaningful values for these parameters make it unattractive. Chemical analysis of the composition of the frozen layer in spent cells at Anglesey suggest that the composition of the freeze remains approximately constant throughout the life of the cell, with weight ratios of 1.36 to 1.41 being obtained irrespective of the operating ratio in the bath. This allows a much simpler model to be developed for the migration of species between molten bath and frozen sidewall.

If the frozen sidewall is assumed to be of constant composition with a weight percent of alumina of A_f, calcium fluoride of C_f and a weight ratio of R_f then the mass of individual species transferred between the melt and the ledge during freezing can be obtained

$$\frac{dM_{A_f}}{dt} = \frac{A_f}{100} \cdot \frac{dM_f}{dt} \tag{151}$$

$$\frac{dM_{C_f}}{dt} = \frac{C_f}{100} \cdot \frac{dM_f}{dt} \tag{152}$$

$$\frac{dM_{AlF_{3,f}}}{dt} = \frac{(100 - A_f - C_f)}{100 \cdot (R_f - 1)} \cdot \frac{dM_f}{dt} \tag{153}$$

$$\frac{dM_{NaF,f}}{dt} = \frac{dM_f}{dt} - \frac{dM_{A_f}}{dt} - \frac{dM_{C_f}}{dt} - \frac{dM_{AlF_{3,f}}}{dt} \tag{154}$$

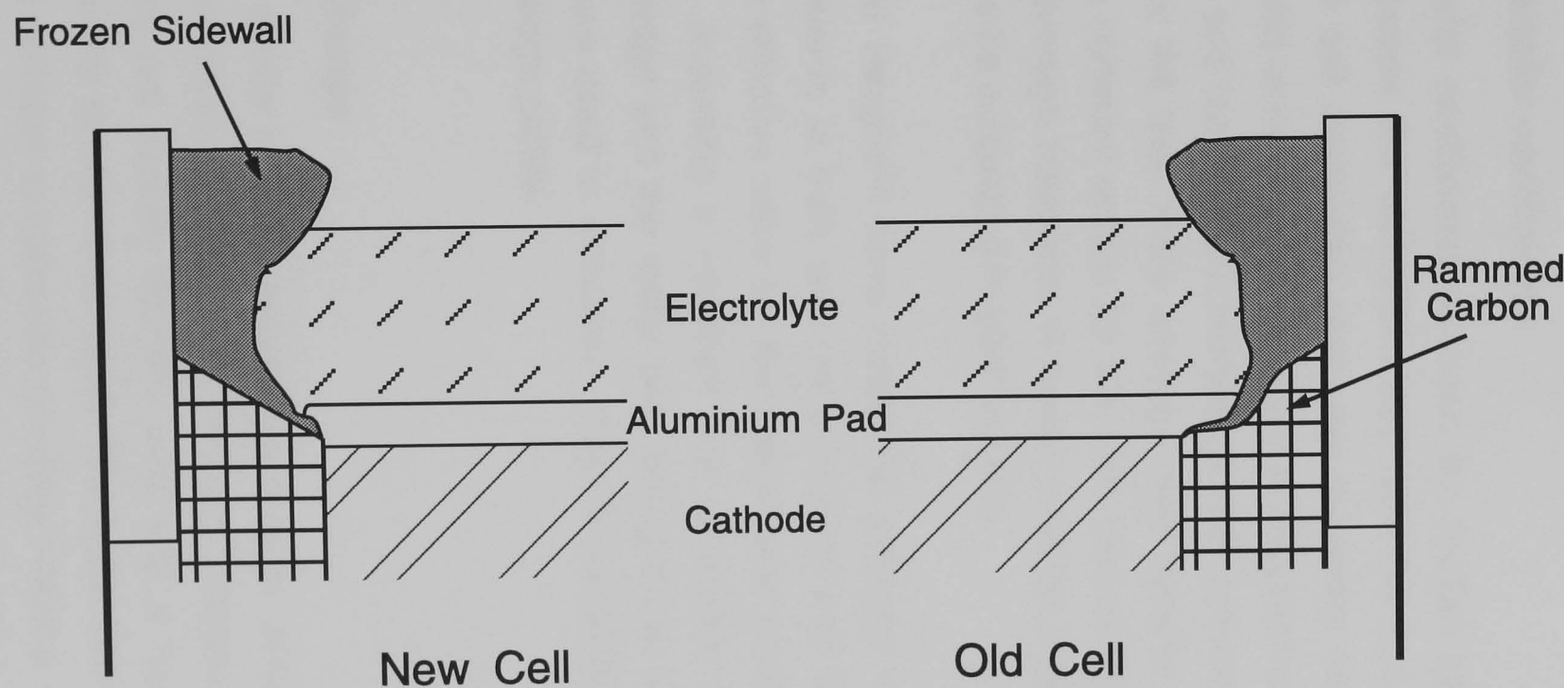

Figure 4.14 Cell Sidewall Profiles in Old and New Cells

where $\frac{dM_f}{dt}$ = rate of freezing of bath at sidewall

$\frac{dM_{i_f}}{dt}$ = rate of migration of species i between bath and ledge

4.12.1 Heat transfer coefficients

The heat transfer coefficients between the molten bath and the frozen ledge and between the aluminium pad and the frozen ledge will vary throughout the cell dependent upon the geometry and local conditions. The object of this work is not to calculate a detailed freeze profile and the hydrodynamic and temperature models already presented here would not be sufficient for the task. Here, average heat transfer coefficients will be assumed, with constant values for the bath and metal pad sections. This will allow an average thickness of freeze and the total heat lost through the sidewalls to be calculated in each section.

Both Arita and Haupin[22] have presented average values for the heat transfer coefficients in bath and metal regions and these are shown in table 4.3. The effective value for the metal zone presented by Haupin is calculated by assuming a constant film of molten electrolyte to exist between the ledge and the metal pad. Using these values as a starting point, the values used in simulation may be tuned for individual cells to give a stable ledge profile.

4.13 Anode Change

Changing an anode in a cell represents a large disturbance to both the heat and mass balances. During its removal, alumina from the crust and frozen sidewall are broken into the melt and a large area of bath is exposed while the anode is removed. The spent anode is replaced by a cold anode at ambient temperature causing freezing of the electrolyte on the anode surface which disrupts the current distribution through the bank of anodes.

source	bath	metal	effective
Haupin	3.7×10^{-2}	1.5×10^{-1}	1.1×10^{-1}
Arita	2.0×10^{-2}	4.0×10^{-2} (side break cell)	

Table 4.3 Heat Transfer Coefficients in Aluminium Reduction Cells

4.13.1 Heat losses

The heat lost from the electrolyte during an anode change and whilst the anode is warming may be divided into three stages.

1) Heat lost from exposed bath whilst the anode is removed from the cell
2) Heat transferred through a frozen layer of bath to the cold anode
3) Direct warming of the anode once the frozen layer has melted

1) When an anode is removed from the cell, a large area of bath is exposed while the new anode is manoeuvred into position. During this time, heat will be lost from the electrolyte by radiation and convection.

$$Q_{loss} = \text{heat lost due to forced convection} + \text{heat lost due to radiation}$$

$$= h_b \cdot A_{hole} \cdot (T_b - T_s) + \varepsilon \cdot \sigma \cdot A_{hole} \cdot (T_b^4 - T_s^4) \qquad (155)$$

where subscript b refers to bath
s refers to surrounding
hole refers to exposed area
A = area
T = temperature K
ε = emmissivity chosen to include view factor
σ = Stefan Boltzmann constant

The heat losses at this stage will last for the time it takes to replace an anode in the cell. At Anglesey, this takes approximately four minutes.

2) When a cold anode is lowered into the cell, the heat lost due to direct radiation and convection to the surroundings is immediately stopped. Heat is now lost by convection to the surface of the cold anode. This causes a layer of frozen electrolyte to form at the anode surface and the heat losses will be treated in the same way as for the frozen sidewalls.

$$Q_{loss} = h_b A_{Anode} (T_b - T_l) \qquad (156)$$

and the thickness of the frozen layer will be given by

$$\frac{dx_f}{dt} = \frac{q_{loss} - q_{anode}}{\rho_f \cdot A_{anode} \cdot \left[\lambda + Cp \cdot (T_b - T_l)\right]} \quad (157)$$

where q_{anode} = rate of heat transfer through the anode
ρ_f = density of frozen layer
T_b = Temperature of the electrolyte
T_l = Liquidus temperature
λ = Latent heat of fusion
Cp = Specific heat capacity of the electrolyte

When the thickness of the frozen layer becomes greater than the anode to cathode distance, the frozen surface will come into contact with the metal pad. The heat transfer coefficient in this section is much greater than that for the electrolyte and the heat transferred to the freeze will become

$$Q_{loss} = h_m A_{Anode} (T_b - T_l) \quad (158)$$

As the melting point of aluminium is much lower than that of the electrolyte, the frozen layer is unable to become thicker and the heat transferred from the aluminium pad will warm the anode much more rapidly than the heat transferred from the electrolyte. For this reason, new anodes are usually 'set low' for the first day so as to allow the anode surface to be closer to the metal pad thus increasing the rate at which the anode can attain normal operating temperature.

Unlike the sidewalls, which are assumed to remain at a reasonably steady state temperature, the anode is subject to a large increase in temperature as it warms both by heat conducted through the freeze from the electrolyte and by the passage of electrical current through the anode. The full heat balance detailed in section 4.10.8 must therefore be performed on the anode.

4.13.2 Resistance of anode block

Initially, the frozen layer of electrolyte on the surface of the cold anode prevents the flow of current through the anode. As the anode warms and the frozen layer melts the anode is able to draw current. In order to model this effect fully, it would be necessary to consider the current distribution

and resistance throughout the anode and freeze and this is beyond the scope of this work. The model may be simplified by assuming a profile for the surface coverage of the anode by an insulating layer. The resistance of the anode can be modelled as two resistances in series, R_1 relating to the resistance across the anode and R_2 relating to the resistance of the frozen layer and the lower conductivity of a cold anode. The total resistance of the anode is then

$$R_{anode} = R_1 + R_2 \tag{159}$$

Assuming that the resistivity of the frozen layer is much greater than that of the molten electrolyte in the same region gives

$$R_2 = \frac{\rho_l}{f \cdot A} \tag{160}$$

where ρ_l = effective resistance of frozen layer per unit area
A = Anode surface area
f = fraction of anode area unable to conduct current

The fraction of the anode surface area unable to conduct current can be related to time by an exponential function

$$f = a \cdot e^{bt} \tag{161}$$

where the pre exponential and exponential factors, a and b, are chosen to match the current distribution profile for a cold anode obtained on working cells.

The total resistance of a block of n anodes connected in parallel is given

$$\frac{1}{R_{block}} = \sum_{i=1}^{n} \frac{1}{R_i} \tag{162}$$

and the current drawn by the ith anode in the block

$$I_i = I_{tot} \cdot \frac{R_{block}}{R_i} \tag{163}$$

The total area for current flow through the cell is the sum of the effective areas through each anode

$$A_{Anodes} = \sum_{i=1}^{n} f_i \cdot A_i \qquad (164)$$

giving an overall current density for the cell of

$$i_{cell} = \frac{I_{tot}}{A_{Anodes}} \qquad (165)$$

In the cells at Anglesey Aluminium, it is known that a new anode in a cell takes approximately 32 hours to draw full current. A short program solving the heat and mass balances on an anode in a bath of constant temperature allows the values of a and b to be fitted to give the desired current profile. In this work, the values of $a=1.7\times10^{-4}$ and $b=6.69\times10^{-5}$ s^{-1} will be used, giving the profile shown in figure 4.15.

4.14 Phyico-Chemical Relationships

Many of the parameters in the model are determined from empirical relationships relating properties of the system to conditions within the cell. Empirical relationships for such properties as electrolyte density are continually being published as further research is carried out on aluminium smelting and this is an area of the model that may be subject to relatively frequent change as improved and more applicable relationships become available. Some of the relationships used in this model are summarised here.

4.14.1 Alumina solubility

The following relationship is taken from KACC Technical Manual[11] and will be used in this work.

$$C^*_{Al_2O_3} = 0.0557 \cdot T_b - 0.35 \cdot \%CaF_2 + 1.429 \cdot R_b - 45.644 \text{ wt\%} \qquad (166)$$

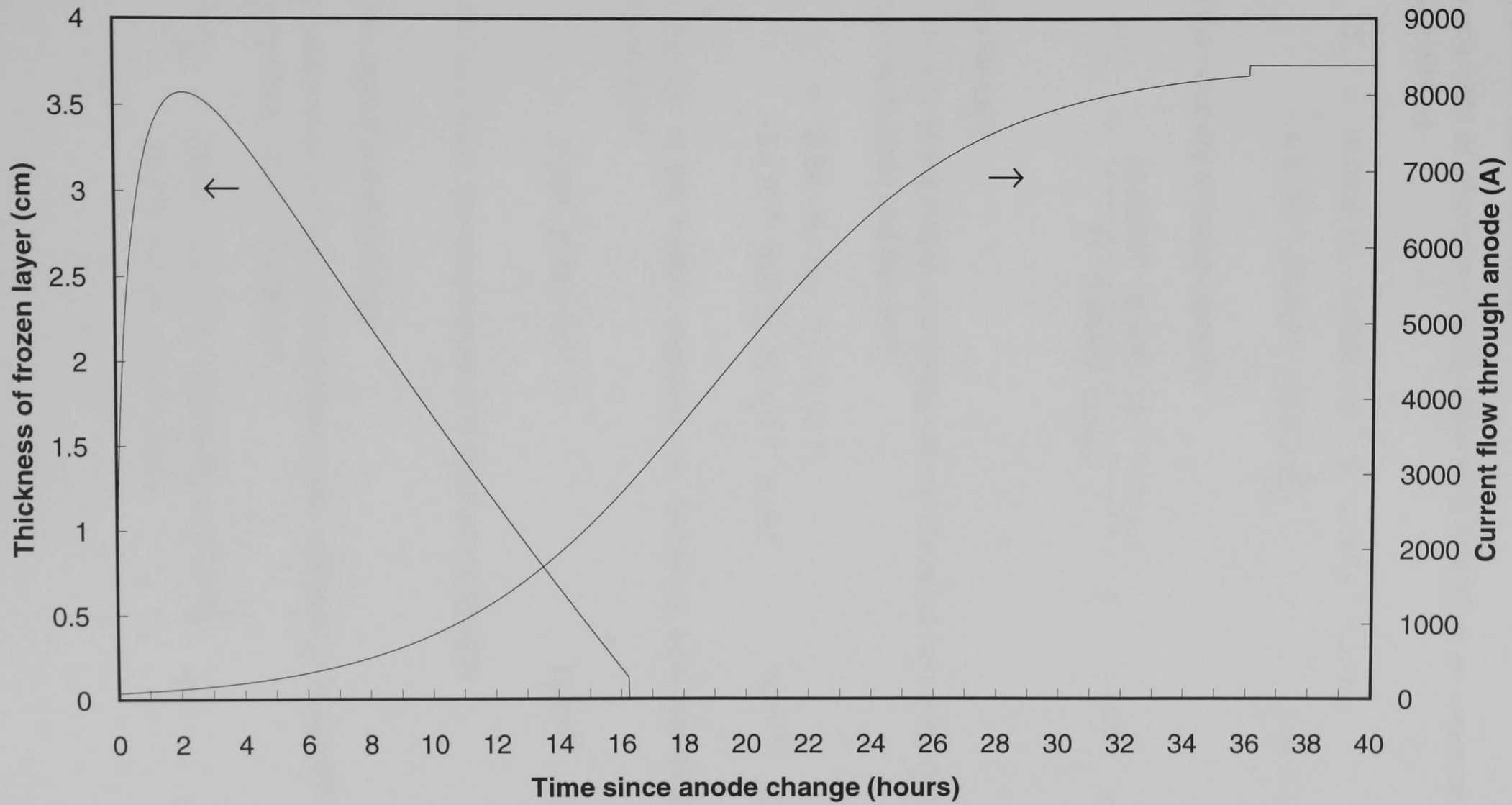

Figure 4.15 Current Drawn by a Cold Anode

4.14.2 Aluminium solubility

The solubility of aluminium in the electrolyte is quoted by Lillebuen and Mellerud[10] as

$$C^{*}_{Al} = (0.0268 \cdot R_b - 0.6755 + 10^{-3} \cdot T_b - 1.9 \times 10^{-3} \cdot \%CaF_2 - 4.3 \times 10^{-3} \cdot (\%Al_2O_3 - 12.5)) \cdot \frac{\rho_b}{100} \quad g\ cm^{-3} \quad (167)$$

and the solubility of carbon dioxide

$$C^{*}_{CO_2} = \frac{(0.03027 - 6.985 \times 10^{-4} \cdot \%Al_2O_3)}{(1 - 0.08989 \cdot \%Al_2O_3)} \cdot 10^{-3} \quad g\ cm^{-3} \quad (168)$$

4.14.3 Density

The density of the molten electrolyte will be calculated from a relationship derived by Kvande and Rørvik[23]

$$\rho_b = 2.64 - 8 \times 10^{-4} \cdot T_b + 0.18 \cdot R_b - 8 \times 10^{-3} \cdot \%Al_2O_3 + 5 \times 10^{-3} \cdot \%CaF_2 \quad kg\ m^{-3} \quad (169)$$

The density of the molten aluminium is calculated from the following relationship[11]

$$\rho_{Al} = 2.561 - 2.72 \times 10^{-4} \cdot T \quad kg\ m^{-3} \quad (170)$$

In both equations, the temperature is in degrees centigrade.

4.14.4 Liquidus temperature

The relationship for liquidus temperature was reported by Bullard[24] after work by Foster and Hollingshead.

$$T_{liq} = 733.6 + 392.5 \cdot R_b - 164.9 \cdot R_b^2 + 15.35 \cdot R_b^3 - 3.375 \cdot \%CaF_2 - 5.4 \cdot \%Al_2O_3 \quad ^{\circ}C \quad (171)$$

4.14.5 Viscosity of the electrolyte

A mathematical model for the viscosity of aluminium reduction cell electrolytes has been fitted to empirical data by Hertzberg et al[25]. The model will be used in this work.

$$\begin{aligned}\ln \mu_b = & \left(\frac{1-x}{100}\right)\cdot \ln \mu_{NaF} + x(d_y - x)\exp\left[-b_y(d_y - x)^2\right]\exp\left[-\frac{c_y y}{x+1}\right]\ln \mu_x \\ & + y(d_x - y)\exp\left[-b_x(d_x - y)^2\right]\exp\left[-c_x x\right]\ln \mu_y \\ & + \frac{x}{x^2+100}\exp\left[-e_1(25-x)^2\right]\exp\left[-e_2 y^2\right]\ln \mu_x \end{aligned} \qquad (172)$$

where

$$x = \frac{100 x_{AlF_3}}{x_{NaF} + x_{AlF_3}}$$

$$y = \text{wt\% } Al_2O_3$$

$$t = \frac{1}{T} - \frac{1}{273.14}$$

$$\ln \mu_{NaF} = 0.37758 - 3184t$$

$$\ln \mu_x = 0.001934 + 10.99t$$

$$\ln \mu_y = 0.01502 + 47.22t \qquad b_y = 8.515 \times 10^{-4}$$

$$\ln \mu_x = 1.188 + 5300t \qquad c_y = 0.6111$$

$$d_y = 37.89\exp(619.3t) \qquad b_x = 0.002657$$

$$d_x = 30.12\exp(-508.9t) \qquad e_1 = 0.05$$

$$c_x = 0.04051\exp(1948t) \qquad e_2 = 0.02253$$

Viscosity is predicted in m Pa s. Temperature is in degrees centigrade.

4.15 Summary

This chapter has described the formulation of the physico-chemical model of an aluminium cell that will predict how the cell will react to such actions as movement in the anode beam position and the breaking of the crust and addition of feed materials. The next chapter describes the modelling of the existing control system used at Anglesey Aluminium and discusses the implementation and simulation of alternative control strategies.

References

[1] Blake, S. R., *"A Model for the Variation of Alumina Concentration in Industrial Hall-Héroult Cells"*, MSc Thesis, Department of Chemical Engineering, University of Newcastle upon Tyne, June 1983

[2] Entner, P, Scmidt-Hatting, W., Mitrovic, Z., Gruber, U., Rufer, D. and Fjørnes, *"Investigation of the Dynamic Behaviour of Aluminum Pots"*, AIME Light Metals, 1984, pp701

[3] Johnston, A. R., *"Alumina Crusting and Dissolution in Molten Electrolyte"*, AIME Light Metals, 1981, pp373

[4] Ek, A. and Fladmark, G. E., *"Simulation of Thermal, Electric and Chemical Behaviour of an Aluminum Cell on a Digital Computer"*, AIME Light Metals, 1973, pp85

[5] Asbjørnsen, O. A., Andersen, J. A., *"Kinetics and Transport Processes in the Dissolution of Aluminium Oxide in Cryolite Melts"*, AIME Light Metals 1977, pp137-152

[6] Haupin, W. E., *"Mathematical Model of Fluoride Evolution from Hall-Héroult Cells"*, The 4th Int. Course on Process Metallurgy of Aluminium, Trondheim, 1985

[7] Sidorov, L.N., Kolosov, E.N. and Shol'ts, V.B., Russian Journal of Physical Chemistry, 42, pp1382-1386, 1968

[8] Robl, R. F., Haupin, W. E., and Sharma, D., *"Estimation of Current Efficiency by a Mathematical Model Including Hydrodynamics Parameters"*, AIME Light Metals, vol 1, 1977, p185

[9] Evans, J.W., Zundelevich, Y. and Sharma, D., Met. Trans, vol 12B, 1981

[10] Lillebuen, B., and Mellerud, Th., *"Current Efficiency and Alumina Concentration"*, AIME Light Metals, 1985, p637

[11] Lewis, R. A., *"Technical Fundamentals of the Aluminum Reduction Cell Process"*, Reduction Division Technical Manual I, Kaiser Aluminum Internal Publication, 1973

[12] Plimley, R. E, *"Process Modelling and Optimisation"*, Electrochemical Process Engineering Course, University of Newcastle upon Tyne, 1984

[13] Zuca, S., Herdlicka, C. and Terzi, M.,"On Porosity-Overvoltage Correlation for Carbon Anodes in Cryolite-Alumina Melts", *Electrochimica Acta*, vol 25, February 1980, pp211-216

[14] Calandra, A.J., Castellano, C.E., Ferro, C.M. and Cobo, O., *"Experimental and Theorectical Analysis of the Anode Effect in Industrial Cells"*, AIME Light Metals, 1982, pp345-358

[15] Thonstad, J., Nordmo, F. and Paulsen, J. B., *"Dissolution of Alumina in Molten Cryolite"*, Metallurgical Transactions, vol 3, February 1972, pp403-407

[16] JANAF Thermochemical Tables, NRDS, National Bureau of Standards 37

[17] Aylward, G. H. and Findlay T. J. V., SI Chemical Data, 2nd Edition, The Jacaranda Press, 1974

[18] Arita, Y., Urata., N. and Ikeuchi, H., *"Estimation of Frozen Bath Shape in an Aluminum Reduction Cell by Computer Simulation"*, AIME Light Metals, 1978, pp59

[19] Sulmont, B. and Hudault, G., *"Application of a Thermoelectric Model to the Investigation of Reduction Cell Thermal Equilibrium"*, AIME Light Metals, 1978, pp73

[20] Peacey, J. G. and Medlin, G. W., *"Cell Sidewall Studies at Noranda Aluminum"*, AIME Light Metals, 1979, pp475

[21] Hashimoto, T. and Ikeuchi, H., *"Computer Simulation of Dynamic Behaviour of an Aluminum Reduction Cell"*, AIME Light Metals, 1980, pp273

[22] Haupin, W. E., *"Calculating Thickness of Containing Walls Frozen from Melt"*, AIME Light Metals, 1971, pp188

[23] Kvande, H. and Rørvik, H., *"The Influence of Bath Density in Aluminium Electrolysis"*, AIME Light Metals, 1985, pp671-678

[24] Bullard, G., KACC Research Report, 2nd quarter, 1984

[25] Hertzberg, T., Tørklep, K. and Øye, H.A., *"Viscosity of Molten NaF-AlF_3-Al_2O_3-CaF_2 Mixtures"*, AIME Light Metals, 1980, pp159-170

5.0 The Control System

The overall control aim of an aluminium reduction cell is to maintain good current and energy efficiencies. The system is, however, highly complex and control involves the manipulation of several process variables at regular and irregular intervals.

There are three fundamental problems which the process presents to all process control systems. These are:

1. A multiplicity of relatively small but interdependent production units each of which must be individually controlled. Typically a potline may comprise over 100 reactors and a plant a number of potlines.

2. Lack of equipment to continuously and accurately add raw materials to and remove product from the process, although the process itself is continuous.

3. Lack of instrumentation and sensing devices to rapidly and accurately measure and control process variables.

These limitations have resulted in the reliance of the control system upon considerable manual intervention based upon the judgement of experienced cell operators. The use of digital computers and better mechanisation has, however, improved controllability of several but not all of the process variables.

The main tasks that must be performed in order to control the cell are as follows:-

1. Control of alumina feed rate for a desired anode effect frequency
2. Maintaining a desired operating voltage and temperature in the cell
3. Removal of liquid aluminium product
4. Maintaining a desired electrolyte composition
5. Maintaining a desired inter electrode gap
6. Maintaining an uniform current distribution
7. Regulating the thickness and shape of frozen sidewalls

The way in which these tasks are implemented constitutes the control strategy.

5.1 Alumina Concentration Control

The mass flow of materials into and out of the cell consists of the flow of solid raw materials to the cell and the flow of reaction products from the cell. Although the production of aluminium in the reduction zone is continuous the addition of the major raw material, alumina, is batchwise and it is this task that must take priority in the control scheme. If the level of alumina in the electrolyte rises to a high level, a sludge is deposited at the cathode causing poor operation of the cell. Ultimately, overfeeding may result in the density of the electrolyte exceeding that of the liquid aluminium and the two layers will invert with disastrous consequences. Alternatively, if the alumina concentration is allowed to fall below a critical level, anode effect occurs with the production of fluorinated carbon compounds at the anode accompanied by a large increase in cell voltage.

There is, at present, no means of accurately determining the concentration of alumina within the electrolyte on a continuous basis. The alumina feed rate must therefore be determined by inference from other parameters, notably voltage, and the calculated current efficiency of the cell.

5.2 Removal of Aluminium Product

The removal of aluminium product from the cell is also a batch operation with material being siphoned from the metal pad at regular intervals. The depth of the metal pad has an important effect upon the heat balance of the cell and upon the current efficiency by affecting the pad stability. More importantly though, the amount of aluminium removed gives an indication of the rate of production of aluminium in the cell and is used to calculate the overall current efficiency. This is used as a measure of the performance of the cell over a long period of time and is used in tuning other control variables.

The amount of metal removed from the cell is determined by the depth of the aluminium pad within the cell. Both the depth of pad and the amount of

metal tapped are generally measured by a crude dip stick method. The molten aluminium is siphoned off into a crucible. The amount tapped is measured by level in the crucible and is calculated to leave a desired level of metal pad depth in the cell. The recent introduction of electronic scales to weigh the crucible has improved the accuracy of the tapping operation and hence the calculated current efficiency but the control of metal pad depth is still very crude.

5.3 Electrolyte Composition

It is also necessary to maintain the composition of the bath by replacement of materials lost during anode effect and by bath volatilisation. The bath composition has a major effect upon the physical properties of the electrolyte and most importantly upon the electrolyte conductivity and current efficiency. With the exception of alumina and aluminium fluoride, the rate of change of concentration of particular species is small and does not take a high priority in the short term. The effect of aluminium fluoride concentration on the ratio NaF/AlF_3 is, however, more important and maintaining this ratio has a higher priority.

Again there is no method for the continuous monitoring of bath composition but it may be determined by analysis of bath samples taken weekly. Based upon this data over a period of time the average amount of material lost may be calculated. This is replaced by the addition of recovered exhaust materials to the alumina feed and by the addition of bags of aluminium fluoride to the melt at periodic intervals.

5.4 Anode to Cathode Distance

As well as controlling the ohmic drop across the electrolyte the anode to cathode distance affects the current efficiency and stability of the cell. Below a critical value the current efficiency falls off rapidly but above this level there appears to be little or no change with increasing interelectrode gap. Theoretically there is an optimum gap for any composition and temperature of electrolyte. There is no direct method of determining anode cathode distance although some control may be conferred upon it through overall cell voltage control.

The inter electrode gap may be altered by moving the anode bus bar relative to the cathode. This is done by pneumatic motors that may be activated either manually or automatically. The motors act upon the whole anode block, not individual anodes. Any anodes that are badly positioned relative to the block must therefore be reset manually.

5.5 Current Distribution

The maintainance of a uniform current distribution through the cell is desirable as it benefits the stability and hence the efficiency of the cell. In general, for a uniform distribution, the inter electrode gap for each individual anode should be equal. Due to the electrohydromagnetics of the cell and distortions in the cathode block, however, there tends to be a 'hump' in the middle of the metal pad. This requires that the anodes be set at different heights relative to the anode bus bar according to their relative position in the cell.

The current distribution through a cell may be measured manually by measuring the voltage drop across each anode stub. This is done each day and any anodes that are not pulling the expected current are marked down for resetting. As well as detecting poorly set anodes, this method can detect anodes that have short circuited to the cathode by 'spiking' or anodes that have burnt off from the stubs.

5.6 Voltage and Temperature Control

For a cell operating at a constant current the cell voltage determines the energy input and consequently temperature. Electrolyte conductivity is, however, affected by temperature and so to some extent, temperature affects cell voltage. Another effect of temperature is to alter the freeze profile and consequently cell voltage. These two parameters therefore show considerable interaction.

A low voltage drop across a cell is desirable in order to reduce the energy required to produce the aluminium. A reduced ACD may, however, have an adverse affect upon electrolysis by increasing the rate of back reduction and reducing the current efficiency. At times when the market

price of aluminium is high it is preferable to maximise the production rate over the energy required for production and vice versa.

Due to the highly corrosive nature of molten cryolite it is not possible to continuously measure the temperature of a cell. Instead, a sheathed thermocouple is used to measure the bath temperature daily and the overall appearance of the cell is noted. If the temperature is consistently high over a period of days and the cell 'appears' hot then the voltage set point may be lowered. This can be continued until the cell 'appears' to be operating satisfactorily. The temperature of the cell affects the current efficiency by increasing the solubility of aluminium in the electrolyte but more importantly it has a marked effect upon the frozen ledge profile.

5.6.1 Frozen sidewalls

The frozen sidewalls contain the molten electrolyte and aluminium and protect the cell walls from their corrosive effects. They also regulate the temperature of the cell by melting or freezing. A good freeze profile, however, is necessary for good current distribution and efficiency. If the freeze extends too far under the metal pad then the area for current flow is reduced. If the freeze becomes too narrow then the stability of the metal pad is reduced and ultimately the sidewalls become corroded.

The design of the cell structure and the materials used in its construction very much determine the shape of the frozen ledges, but the profile is also affected by the temperature and composition of the electrolyte. Although the freeze profiles cannot be measured easily they may be controlled by maintaining the electrolyte temperature and composition about the design conditions. The correctness of the operating temperature is, however, only reflected in the long term current and energy efficiency of the cell and it is this information which is used to alter the voltage set point.

5.7 Manual Control

The simplest method of control is to assign an operator to control a cell or group of cells. The operator manually adjusts the anode beam position to control the cell voltage and feeds alumina and other feed materials into the cell based upon observed conditions and control schedules. This type

of control relies greatly upon the judgement and commitment of the operator and for a reasonable level of control it would be necessary to have an operator assigned to only a small number of cells.

In most situations, some form of automatic control is preferable as it requires less manpower and will generally provide tighter and more consistent control.

5.8 Manual Control of Alumina Concentration

Alumina is fed manually by means of a mechanical crustbreaker. During this operation crust falls into the bath along with some of the loose alumina covering it. The alumina cover is subsequently replenished and a new crust formed. The batch weight is very poorly controlled by this method and the pot may be severely under or overfed. In order to ensure that alumina concentration does not exceed a critical value, feeding may be suspended to force periodic anode effects.

The termination of anode effect is not simply a matter of increasing the alumina concentration within the electrolyte. In order for this to be effective the carbon tetrafluoride gas bubbles which adhere to the anodes must be dispersed. This is achieved manually by raising and lowering the anodes and by the introduction of a 'green' stick (wet hazel rod) beneath the anodes. The bubbles from the burning stick cause enough turbulence in the cell to break up the CF_4 bubble. Streamers of aluminium are also thrown up from the metal pad momentarily shorting the cell so causing the electrolysis of fluoride to cease and the bubble to disperse.

5.9 Manual Control of Voltage

The cell voltage is the only parameter of an individual cell that may be monitored accurately, continuously and cheaply. With the exception of the voltage rise at anode effect which is controlled by the addition of alumina, other fluctuations are controlled by altering the inter electrode gap. Although anode movement may be activated manually by push buttons at the cell side the control of these fluctuations would require an operator dedicated to each cell. This an unfeasible task and manual voltage control

must concentrate upon achieving a long term average voltage by maintaining an approximately constant ACD. Movement of the anode bar is then only necessary when a setpoint change is required or during tapping when the metal pad level is falling rapidly.

5.10 Manual Control Strategy

Central to the manual control strategy is the "potline survey". This survey is conducted by the potline general foreman and involves the inspection of individual pots on the line on a shift to shift basis. The specific attributes inspected are:

flame colour
pot voltage and stability
carbon dusting in the bath
liquid levels.

All abnormalities are recorded and a severity factor ranging from 0.5-3.0 is assigned to the cell based upon the overall condition of the cell. Assignment of severity values is prescribed by the standard practice.

On completion of surveys upon all cells within the line, the individual cell severity values and abnormal characteristics are tallied and summarised. A complete record of the potline operating condition is thus available for applying compensatory corrective action on individual cells. Review of abnormal attributes and their previous history provides information for formulating cause removal corrective action.

5.11 Automatic Control

In the late 1950's automation of some of the more tedious and laborious hand operations on reduction cells began to take place. This initially consisted of the mechanisation of crust breakers on prebake cells and voltage control by means of mechanised anode movement controlled by pneumatic motors activated by operators from the floor. This was soon followed by analog electro-mechanical devices which broke crust, fed alumina and controlled cell voltage on some predetermined schedule set by potroom operating supervision. Automatic anode effect termination was

added as an additional task and the development of point feed cells allowed smaller amounts of alumina to be fed at more frequent intervals on a semi continuous basis.

Although automation had been applied to some aspects of process control other tasks such as removing metal from the cell, control of liquid levels and electrolyte composition remained unchanged. There was little improvement in instrumentation or sensing devices for increasing the amount of information immediately available about a cell's operating condition.

In the mid 1960's digital computers were first incorporated into pot line operation and process control. Although the environment is hostile to these devices due mainly to the strong magnetic fields and lack of cleanliness in the pot rooms this was overcome by the use of distributed systems.

5.12 Distributed Control

In a distributed system a control unit is dedicated to each part of the process with each unit linked back to a central computer for supervisory control of the overall process. The specialization of the units and their close proximity to that part of the process that they are controlling allows them to track process activities and make control decisions much faster and more accurately than a centralised system. As there is a high degree of independence between the control units, the failure of an individual unit need not prevent control of the process. The central computer now acts as system controller for the control units rather than the unit controller itself.

5.13 The CELTROL System

The distributed control system used by Anglesey Aluminium is shown in figure 5.1. The system consists of a microprocessor at each cell, a communications processor for each room, a supervisory computer for the plant and a backup/development computer. The microprocessor is known as CELTROL and provides potroom personnel with alumina addition,

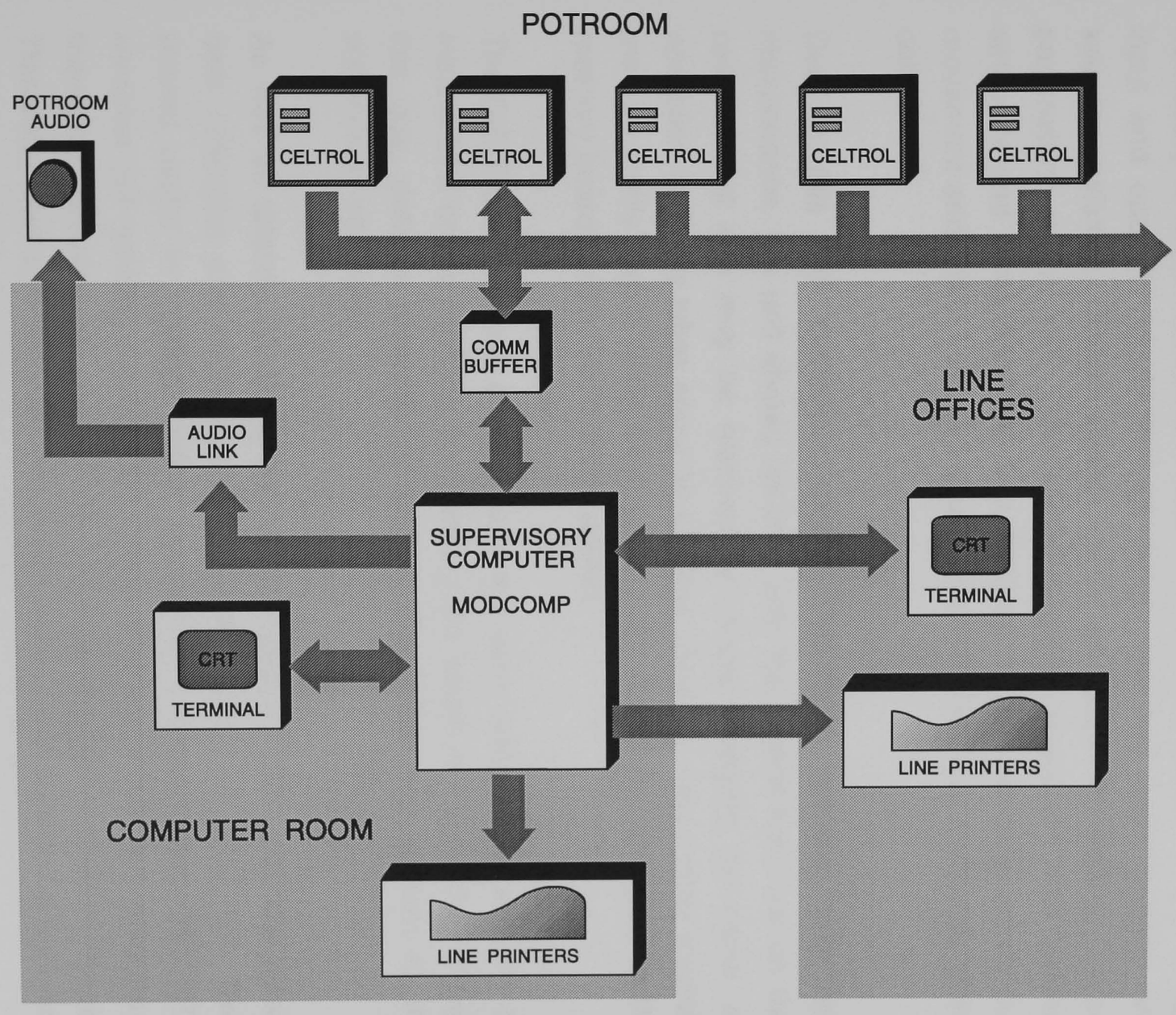

Figure 5.1 CELTROL Distributed Control System

voltage control, anode effect termination, stability control, line load control and information feedback.

5.13.1 The CELTROL unit: a microprocessor

Each CELTROL unit contains all the input/output functions and logic necessary to control a reduction cell. The hardware allows for cell voltage input and operator inputs through toggle switches, push buttons and selector switches. These switch inputs are used for altering control parameters at the cell, acknowledging alarm conditions and viewing setpoints and some historical data. Outputs to the cell allow anode bus movement and break and feed operations at the tap and duct ends of the cell.

Due to this self contained nature, CELTROL requires very little maintenance. If a unit should fail then only the control functions on that cell are lost and may be restored by simply changing the panel, an operation that only takes about 10 minutes. Similarly, new control routines may be easily tested upon small groups of cells simply by replacing the memory boards within the required panels.

The CELTROL units are connected to the room communication buffer by means of a communication bus running the length of the room. Through this bus, data is received or sent to the buffer and in turn to the supervisory computer.

As well as directly improving control to individual cells, the high speed data collection and information feed back facilities of CELTROL have proved useful in making further operational improvements. CELTROL samples cell resistance every 100 milliseconds and from the fluctuation in these values over 1 minute periods calculates the 'noise' level of the cell. This parameter with historical information provides indications of abnormal operating conditions in a cell.

5.13.2 The communications buffer

As well as providing communication between the CELTROL and the supervisory computer, the communications buffer reads the line amperage and voltage signals. The line amperage is received from measuring

equipment in the rectifier and is sampled by buffer software every 100 milliseconds. These values are digitally filtered and broadcast to each CELTROL every 500 milliseconds where it is used to calculate the cell resistance.

Location of the communications buffer in a more favourable environment than that of the CELTROL units makes failure rare. If a failure does occur, however, only the communication to that room of CELTROL's is lost. The CELTROL units continue to perform their control functions upon individual cells until the buffer is replaced.

5.13.3 The supervisory computer

The supervisory computer is a mini computer located in a central computer room at some distance from the pot lines and connected to each of the communication buffers by a standard RS-232 link. It has five main functions to perform:

1. detect and output alarm conditions on any cell
2. collect historical data for reports
3. allow line management to make control setpoint changes on any cell
4. perform line load control
5. make fine setpoint adjustments based upon historical data

Every thirty seconds the supervisory computer requests a status report from each cell. From this report it determines whether any alarm conditions exist and whether that condition should be output over the audio system. The information from this report is also recorded on magnetic disc and, if required, hard copy may be obtained on a printer.

Periodically the supervisory computer requests a memory dump from each CELTROL unit. This contains historical data about the cells operation over the period. This information may be compiled into reports on cell and plant operation and used to make decisions on operational changes. The supervisory computer itself has the ability to make routine decisions on setpoint changes by utilising the historical data on a cell's operation.

The supervisory computer is also connected to terminals in each of the line offices. Through these terminals, operators are able to view current

and historical operating data for the line and the facility is available to make control setpoint changes on individual cells. When not in use the terminals display any exceptional conditions that exist on the line allowing operators to know at a glance which cells require attention.

In case of failure of the supervisory computer only this monitoring ability is lost. The CELTROL units continue to function independently.

5.13.4 The development/backup computer

This is a second mini-computer that is identical to the supervisory computer and located in the computer room. It is used for program development and as a backup in case of failure of the supervisory computer.

Program development and testing is carried out on this computer so as not to interrupt or interfere with the supervisory computer's activities. When a program is ready for installation into the control system, it is passed between the two computers through a standard communications link.

The backup computer is also connected to the pot line communication lines and data storage facilities. This way in case of failure of the supervisory computer the backup can immediately take over all supervisory functions.

5.14 Automatic Control Strategies

Although digital computers are able to collect large amounts of data very quickly, the problems of lack of variety of information still remain. The power of a computer system lies in the ability to develop a control strategy based upon conditions that may be inferred from those variables that may be measured and the history of the cells operation. The computer can be programmed to take automatic action if appropriate or to alert operators that manual assistance is required.

Whilst a computer can be used to automate many of the tasks, a different strategy is required for each type of cell (half break or point feed) and the

different operating conditions e.g. anode effect, high alumina concentration and sick pot conditions. A specific program must be written to implement each of these control strategies. The current strategy applied for half break cells at Anglesey aluminium will be described in detail here.

5.15 Half Break Control Strategy

Anglesey's current half break automatic control strategy concentrates upon maintaining a desired anode effect frequency and average cell voltage. The temperature and condition of the cell are monitored daily by potroom staff and the voltage and alumina set points adjusted based upon the trends in these variables.

5.15.1 Automatic voltage control, AVC

The voltage drop across the aluminium cell is controlled by simple feedback control using proportional action. A control block diagram is shown in figure 5.2.

The voltage is sampled by the controller every 100 ms and the cell resistance calculated from this and the line current. This value is known as the 'raw' resistance and is subject to high frequency variation. The raw resistance is filtered through 1 and 3 minute digital filters to produce a smooth resistance. Voltage corrections are made proportional to the error of this value from a set point by movement of the anode beam. This beam is moved by pneumatic motors that are operated by solenoids activated by CELTROL. The voltage noise, leakage within the air pipes activating the pneumatic motors and the inertia of the anodes reduces the accuracy of the control such that small errors would cause unnecessary movement of the anodes. To prevent this, a dead band around the resistance set point is defined in which no anode movement is allowed to take place.

The operation of automatic voltage control is not always desirable, however. There are different routines within CELTROL to control the cell voltage under different operating conditions.

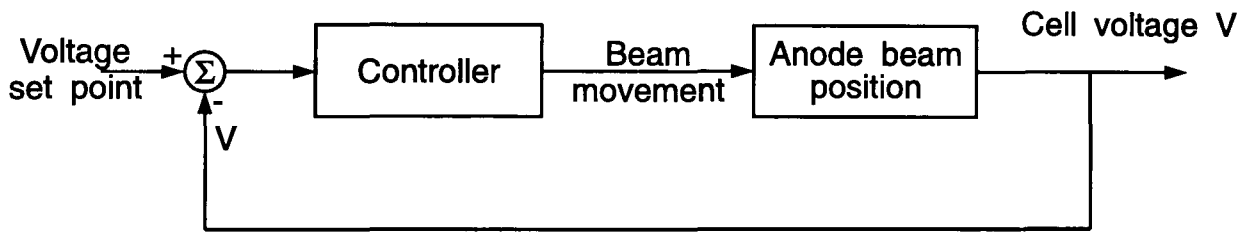

Figure 5.2 Voltage Control Block Diagram

5.15.2 Normal operation

Under normal operation the smooth resistance is compared with the set point every 3 minutes. If the absolute error is greater than the defined dead band, typically 1.2 μΩ, then the solenoid activation time is calculated

$$t_s = K_p \varepsilon + t_d \qquad (1)$$

where t_s = activation time for the solenoid
K_p = constant of proportionality
ε = absolute error
t_d = dead time of the airlines, pneumatic motors and solenoid.

The constant of proportionality is based upon an expected electrolyte conductivity and the rate of movement of the anodes by the motor. As movement is easier downwards than upwards, a different constant of proportionality is used in each case.

In order to prevent abnormal conditions, such as anode effect or low voltage, from causing the anodes to be removed from the electrolyte or driven into the cathode, limits are placed upon the resistance that may be controlled. These limits are expressed as a deviation from the target resistance and are typically ±1.6 μΩ. Outside these limits, normal voltage control, AVC, is not allowed and CELTROL may use an alternative routine or call for manual assistance.

5.15.3 Noisy cells

If the frequency or amplitude of the voltage noise exceeds predefined values then the fluctuating error in the smooth voltage may cause unnecessary movement of the anodes. This is overcome by increasing the dead band in which no control may take place and by activating a noise control routine.

It has been found that the stability of a cell is often increased by increasing the ACD and this is achieved by increasing the voltage set point. The noise control routine increases this set point temporarily and if successful, gradually reduces the increase until the set point is back to its original level.

5.15.4 Anode effect

At the onset of anode effect, the cell voltage rises due to the increase in polarisation potential and cannot be rectified by controlling ACD. Any attempt at control by the normal AVC routine would cause the anodes to be driven into the cathode. In order to prevent this, AVC is terminated if the cell voltage exceeds an upper limit. If the voltage continues to rise and exceeds 9V the cell is deemed to be in anode effect and an anode effect termination routine is activated. This routine incorporates both alumina feed and voltage control and is described in section 5.17.

5.15.5 Metal tap

The tapping of liquid metal from the cell lowers the pad depth so increasing the ACD and hence cell voltage. The rate of voltage increase is too great to be controlled by the normal AVC routine based upon a voltage filtered over 3 minutes and use of this routine would likely result in the cell voltage exceeding the upper limit of the controllable band.

The removal of metal from the cell is not directly detected by the controller and any routine for controlling the voltage during tapping must be activated by the operator. Use of normal AVC routines applied directly to the unfiltered resistance at 18 second intervals has been utilised with some success but often during the metal tapping operation the operator controls the voltage manually.

5.16 Alumina Concentration Control

Alumina is added to the electrolyte in batches of a fixed volume by breaking the surface crust and dumping alumina into the bath from a hopper suspended above the cell. The accuracy of this method is not great with typical errors of ±10-25% by weight expected for a single batch feed. It is not possible to accurately vary the amount of alumina fed and control is therefore concentrated upon the alumina feed rate.

There is no means of direct on line measurement of alumina concentration in the electrolyte and control aimed at maintaining concentration within a specified band. As anode effect is the only measurable reference point for

alumina concentration, control centres upon the control of anode effect frequency.

5.16.1 Normal operation

Under normal operation, the alumina is fed as a fixed batch weight at a regular time. The amount of alumina added to the cell and the feed time are designed such that the cell is purposely under fed so that anode effects will occur at intervals and an excessive amount of sludge is not allowed to build up at the cathode. The amount of alumina required for electrolysis for a particular feed time is calculated by:

$$M_f = \frac{CE}{100} \cdot \frac{1}{2} \cdot \frac{I}{z_{Al} \cdot F} \cdot W_{Al_2O_3} \cdot t_f \quad \text{kg} \qquad (2)$$

where M_f = alumina consumed by electrolysis kg
CE = current efficiency of the cell
I = cell current kA
t_f = fixed feed time s

The cell may be under fed by either increasing the feed time or decreasing the batch weight. Although this would theoretically give a regular and predictable anode effect frequency, the error in the batch fed and variations in current efficiency do not allow this in practice.

5.16.2 Search routine

The memory and rapid computational capabilities of digital computers allows monitoring of the change of ohmic resistance with time of individual cells. The trend of resistance with time and alumina content may therefore be used to control feeding of alumina. The search routine relies on the fact that, if all feeding on a cell is stopped, the cell voltage will rise as the alumina concentration in the bath falls. As anode effect is approached the voltage will rise sharply and this can be detected as a sharp rise in cell resistance. If this rise exceeds a specified value over a defined sampling period then the cell is deemed to be approaching anode effect and is fed.

Theoretically, this routine could be used to always detect the time at which a cell should be fed. Unfortunately, abnormal conditions in the cell may give rise to changes in cell voltage that can prematurely trigger feeding and cause serious overfeeding problems. For this reason, the strategy is subject to a number of restrictions that are designed to prevent this from happening.

Demand feed strategy is designed to enhance the fixed feed strategy by reducing the number of unscheduled anode effects in the under fed cell whilst ensuring that overfeeding does not become a problem. The basic feed time is retained and the Search routine activated only if the cell has not had an anode effect within the previous 12 hours.

Whilst the controller is searching for rate of change of voltage due to the decreasing alumina concentration there must be no movement of the anodes to mask these changes. AVC is therefore temporarily suspended whilst search is in progress.

Noise control and the metal tapping operation could also trigger feeding and for this reason Search is temporarily suspended should these conditions occur. As soon as the terminating condition is removed Search is able to restart.

5.16.3 Starve routine

The starve routine is included in this strategy to ensure that the alumina concentration and sludge content of the cell is unable to build up. This routine forces a scheduled anode effect by suspending all alumina feeding until anode effect has occurred and is only activated if the cell has not has experienced anode effect within the previous 9 hours.

The combined effects of the demand feed strategy and starve routines is to limit anode effect frequency whilst ensuring that the average alumina concentration remains at a reasonably low level. Low levels of alumina in centre fed prebaked cells, have been found by some researchers to be associated with good current efficiency [1] and occasional anode effects may be considered a better risk than the less controllable effects of too much sludge at the cathode.

5.17 Anode Effect Termination

As anode effect is not terminated simply by the addition of alumina to the cell the routine for anode effect termination consists of a sequence of operations that are performed until the cell voltage has returned to a normal operating level. This sequence uses aspects of both alumina concentration and voltage control.

The anode effect termination, AET, routine is activated if the cell voltage exceeds 9V. A typical AET routine is shown in figure 5.3. The routine consists of alternately raising and lowering the anodes in order to disperse the bubble layer, and the addition of alumina to increase the alumina concentration. These operations may be repeated a number of times, but if the failure location is reached then AET is deemed to have failed and manual assistance is required. The success of the AET routine results in an addition to the cell of double the standard feed weight of alumina.

5.18 Point Feeder Control Strategies

Point feeder cells are able to feed small quantities of alumina on a semi-continuous basis and are therefore, in theory, able to maintain the alumina concentration at a more constant level than a half break cell. The alumina control strategy for a point feed cell is basically the same as that for a half break cell with Search and Starve routines enhancing a fixed feed rate. The short feed times, however, require that these routines are subject to different rules to those in the half break routines.

The voltage control routine is the same as that used in a half break cell.

5.18.1 Search routine

The Search routine in a point feed cell is enabled if the cell has not had an anode effect within the previous 9 hours and the time is within a Search/Starve window. This window is designed to limit the search routine to the night shift (midnight to 8 am) in order to minimise manual disturbances to the feed routine.

	0	1	2	3	4	5	6	7	8	9
0	BRAK	LOWR	7.0	W006	JUMP	15	RAIS	5.0	DUMP	BRAK
1	LOWR	5.0	W006	LOP0	1 6	~RAIS	3.0	W005	RAIS	3.0
2	W006	BRAK	W005	DUMP	DUMP	DUMP	DUMP	----	----	----
3	----	----	----	----	----	----	----	----	~----	----
4	----	----	~----	----	----	----	----	W005	BRAK	W010
5	DUMP	DUMP	DUMP	DUMP						

Failure Location at: 15
Plus seconds up at: 2
Acc. Feed Point at: 50
AVC on at: 38

Feed loop start at: 38
Failure feed seq at: 0
Max feed allowed at: 34
Feed loop end at: 42

Sequence for Half Break Cell

	0	1	2	3	4	5	6	7	8	9
0	DUMP	BRAK	LOWR	2.0	DUMP	BRAK	JUMP	13	LOWR	2.0
1	DUMP	BRAK	W001	LOP0	1 8	JUMP	24	RAIS	3.0	DUMP
2	BRAK	LOWR	3.0	W001	LOP1	217	BRAK	DUMP	~RAIS	2.0
3	BRAK	DUMP	W002	RAIS	2.0	W002	RAIS	0.0	~W045	BRAK
4	DUMP	DUMP	~----	----	----	----	----	----	----	----
5	----	----	----	----						

Failure Location at: 28
Plus seconds up at: 2
Acc. Feed Point at: 50
AVC on at: 38

Feed loop start at: 38
Failure feed seq at: 0
Max feed allowed at: 34
Feed loop end at: 42

Sequence for Point Feed Cell

Nomenclature

BRAK	activate crust breaker, both ends
DUMP	activate alumina dump, both ends
LOWR n.n	lower anode bus for n.n seconds
RAIS n.n	raise anode bus for n.n seconds
JUMP nn	jump to location nn if anode effect terminated
Wnnn	pause nnn periods of 6 seconds = nnn $\times$ 6 seconds
LOPn xxyy	loop to position yy allowed xx times if AE not terminated eg LOP0 1 6 loops to 6. Loop is allowed only once
~	decision point

Figure 5.3 Anode Effect Termination Sequences

As point feed cells tend to operate at lower alumina concentrations than half break cells the gradient of the alumina resistance curve at the operating point is greater than for half break cells. The required rate of change in resistance to terminate Search is therefore greater in the point feed routine.

5.18.2 Starve routine

The only modifications to the Starve routine for point feed cells are the conditions required for activation. Starve will only occur if there has been no anode effect within the past 48 hours and the time is within the Search/Starve window.

5.19 Anode Effect Termination Routine

The basic form of Anode Effect Termination, AET, in a point feed cell is the same as that in a half breaker. A typical sequence for a point feed cell is shown in figure 5.3.

5.20 Alternative Strategies

The above strategy is that currently used at Anglesey and has been developed over many years. Clearly there are alternatives, both in use and under development. The alternative strategies reflect not just the different types of cell but also different control philosophies. The basic routines for feeding alumina and AVC are, however, much the same throughout the industry.

5.21 Alumina Concentration Control

There is some agreement[2,3,4,5,6,7] that the curve of current efficiency against alumina concentration passes through a minimum and a typical example is shown in figure 5.4. Current efficiency may be improved by working at either high or low alumina concentrations.

In the former strategy, the alumina levels must be maintained whilst avoiding excessive sludge formation at the cathode. In the latter,

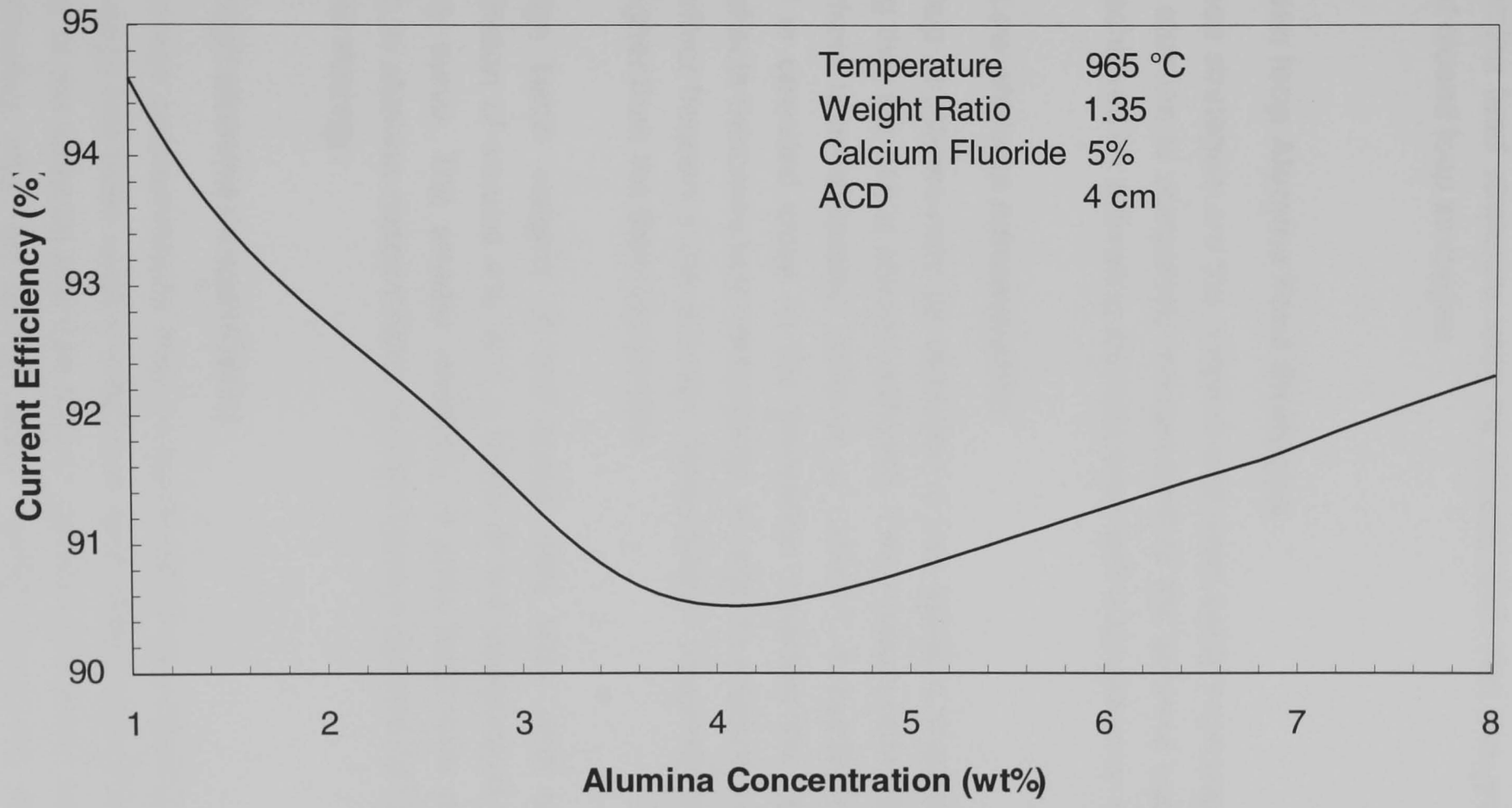

Figure 5.4 Cell Current Efficiency vs. Alumina Concentration

concentration must be kept as low as possible without causing too many anode effects. The particular strategy used depends upon the company's philosophy.

The alumina feed strategies may be broadly split into two groups, open loop and closed loop strategies.

5.22 Open loop Alumina Feed Strategies

Open loop strategies are the simplest and most easily implemented as the feed of alumina is completely independent of the alumina concentration. This is achieved by activating alumina feed with a simple timer device.

5.22.1 Low alumina concentration

Open loop strategies may be operated at low alumina concentrations by ensuring that the cell is always underfed. The problem with this approach is that there is an estimated variance of ±10-25% in batch weight fed. If the cell is operated close to the theoretical minimum the frequency of anode effects becomes less controllable. In order to achieve a reasonable anode effect frequency the average concentration frequently needs to be much higher than the theoretical value.

The large batch weights of half break cells often give an average concentration of around 4%, that is close to the minimum of the current efficiency curve. The smaller additions of point feed cells reduces the variation in alumina concentration but still cannot operate at the optimum using this strategy.

5.22.2 High alumina concentration

High average concentrations may be achieved by overfeeding of the cell. This strategy has been used in sidebreak cells where sludge settles along the edge of the cathode and can help to stabilise the metal pad. A period of overfeeding after an anode effect quickly increases the alumina concentration. This is maintained by a period of slight underfeeding followed by the forcing of an anode effect. This strategy is unsuitable in

centre break cells where the build up of sludge in the centre of the metal pad has a detrimental effect upon cell operation.

5.23 Closed Loop Alumina Feed Strategies

Closed loop feed strategies attempt to control the alumina concentration by inferring the concentration from cell resistance measurements. The strategies described here are under development at Anglesey and aim to operate the cells at low alumina concentrations.

5.23.1 Half break cells: adaptive feed strategy

This strategy uses a continuously varying (adaptive) feed time controlled by searching for anode effect before every feed. The search routine used is the same as that in Anglesey's current strategy. To prevent overfeeding of the cell by the termination of Search by conditions other than low alumina concentration, feeding is only allowed within a window based upon a base feed time.

The search routine is activated 40 minutes prior to the base feed time but feeding may not occur earlier than 20 minutes prior to base. If 25 minutes after the base feed time Search has not been successful then feeding occurs anyway. AVC is suspended during Search and for 5 minutes following a feed.

As a further safeguard against excessive overfeeding of the cell the Starve routine is activated in this strategy if the cell has not experienced anode effect within the previous 23 hours. This aims to produce an anode effect frequency of one anode effect per day.

5.23.2 Point feed cells: adaptive feed strategy

A combination of two strategies are used to control alumina feed and anode effects in point feed cells. These are an overfeed/underfeed strategy (O/U strategy) and the use of search and starve routines. The O/U strategy is designed to reduce the variance of alumina concentration by alternately over and underfeeding the cell depending upon voltage changes. The strategy has no means of determining the absolute value of

alumina and the search and starve routines are used to provide a reference point.

The target range for alumina concentration in this strategy is shown in figure 5.5. This is just off anode effect and the search routine is used to find the lowest alumina concentration without the cell having an anode effect. The O/U routine is then activated and takes over control of alumina feed to the cell. Provided that there are no mechanical faults or long interruptions to the control routines this strategy should eliminate anode effects. In practice, however, anode effects are forced periodically by use of the starve routine. This prevents overfeeding in the event of mechanical problems or failures in the control strategy.

5.23.3 Search routine

The search routine is the same as that described in section 5.18.1. Experience has found it advantageous to activate this routine every 9 hours. This helps to consume any extra feed the cell might receive such as during an anode change.

A number of operations disturb the cell and following these, the search routine is activated in order to find the appropriate alumina concentration for the O/U strategy. These Searches are not subject to the Search/Starve window restriction and will start 60 minutes after tapping or anode setting. On successful termination of Search, the cell receives a feed cycle at both ends. It will also trigger a change to overfeed and will suspend AVC for 30 minutes. This enables the voltage to stabilise and return to the level prior to the end of Search.

5.23.4 Overfeed/Underfeed strategy (O/U strategy)

The O/U strategy uses a rise in cell resistance to indicate a fall in alumina concentration i.e. underfeeding. Fall in cell resistance is correspondingly used to indicate a rise in concentration i.e. overfeeding. Since this strategy operates 24 hours a day it must be able to operate at the same time as the AVC routine. This requires that voltage changes must be detected before the AVC routine can move the bus to correct them. Voltage changes are therefore detected within the AVC 'dead band' and this band

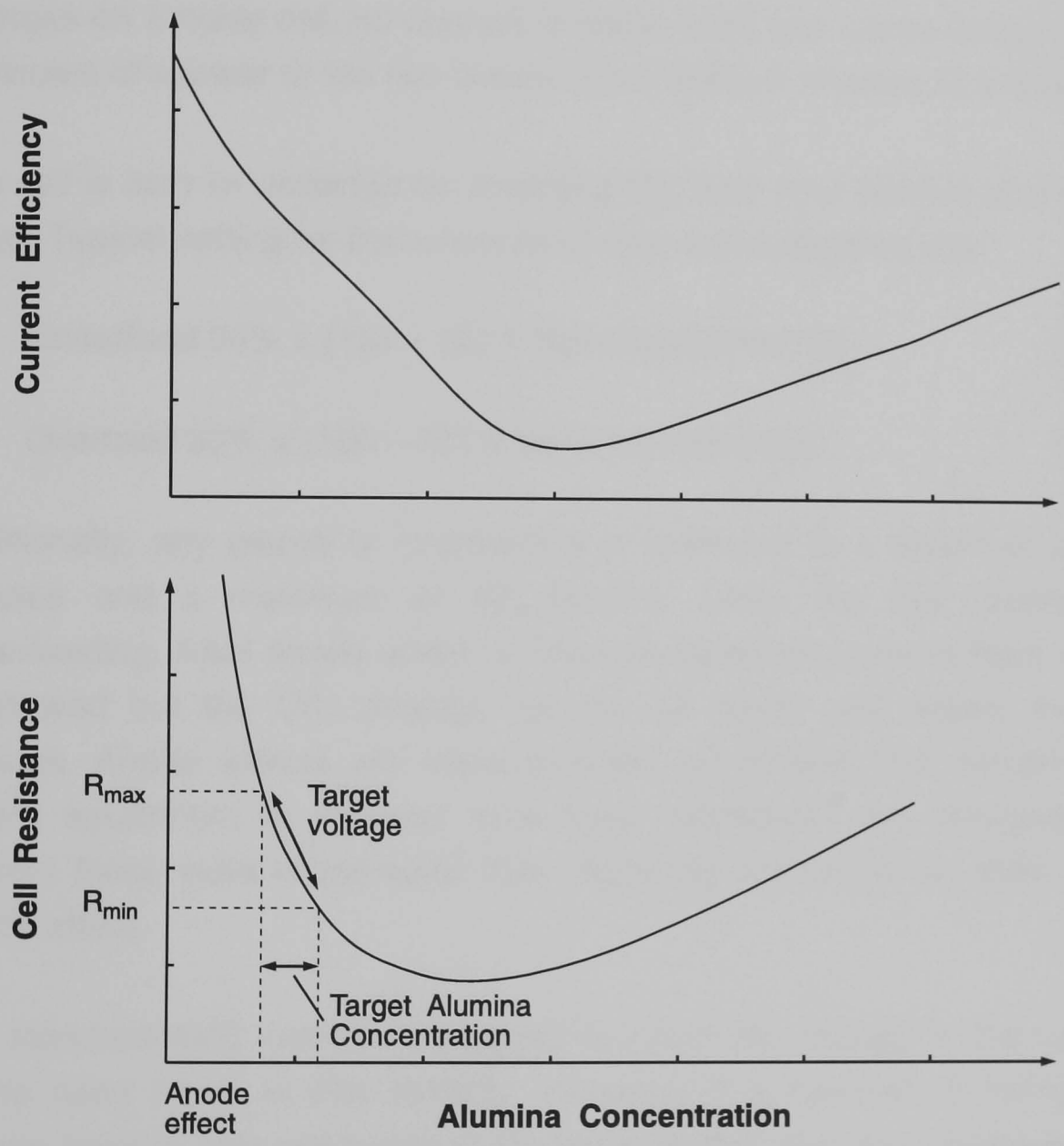

Figure 5.5 Target Voltage for Adaptive Feed Strategy for Point Feed Cells

is used as the limits for under and overfeeding. A typical voltage trace for the strategy is shown schematically in figure 5.6.

When cell voltage passes outside the dead band, AVC raises or lowers the bus to bring the voltage back inside the dead band. These movements are used to trigger over and underfeeding. Four consecutive raises changes the feed from over to underfeeding. Two consecutive lowers changes feed from under to overfeeding. In order to prevent frequent changes on a noisy cell, no change is made if the four raises occur within 9 minutes of a lower or the two lowers occur within 9 minutes of a raise.

The cell is over or underfed by changing the feed time relative to a base value. Typical setting for the amounts of over and underfeed are:

$$\text{Underfeed } 50\% = (100 + 50) \text{ X Base feed time}/100 \qquad (3)$$

$$\text{Overfeed } 30\% = (100 - 30) \text{ X Base feed time}/100 \qquad (4)$$

Additionally, any period of overfeeding is restricted to a minimum of 30 minutes and a maximum of 60 minutes, when the cell reverts to underfeeding. After anode effect or changes between types of feed, AVC is allowed but the O/U strategy ignores all raises and lowers for 12 minutes. Anode effects are often followed by several bus movements before equilibrium is reached and these restrictions are designed to prevent these extra movements from triggering underfeed too soon after anode effect.

The standard AVC routine is designed to return the voltage to the centre of the dead band. In this strategy, however, it is required to bring the voltage back to only just inside these limits so that over and underfeeding will control the voltage within the dead band. This is achieved by halving the value of K_p in equation (1) used in the standard AVC routine thus halving the bus movement called for by AVC.

5.23.5 Starve routine

The starve routine is used to prevent overfeeding due to mechanical problems or failure of the control strategy. The routine is identical to that described in section 5.18.2 and takes priority over search and

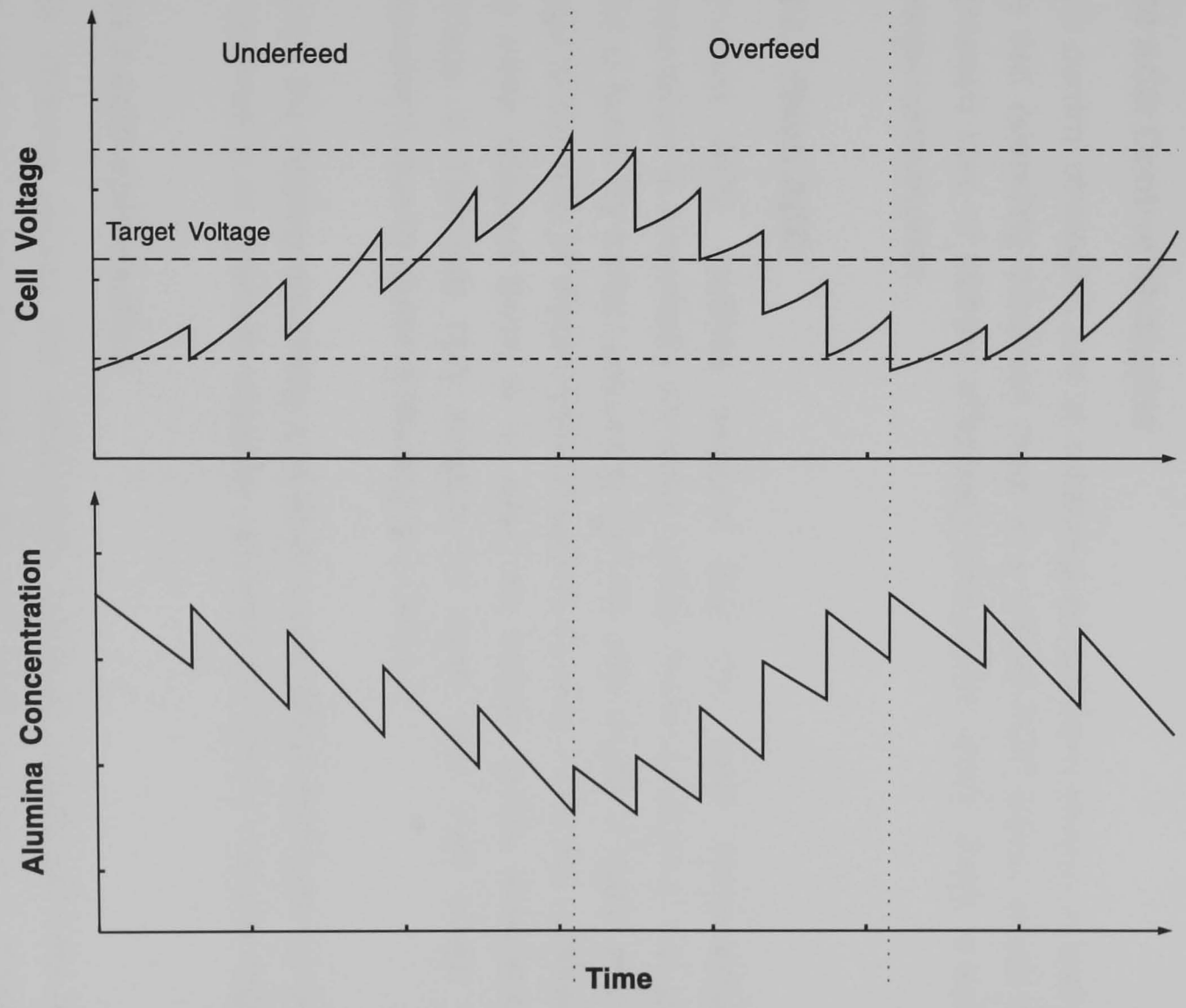

Figure 5.6 Typical Voltage Trace for Underfeed/Overfeed Control Strategy

overfeed/underfeed routines. This routine is activated if there has been no anode effect within the previous 48 hours. When the feed routines are working well, all anode effects will be due to Starve giving an average of 0.5 anode effects per pot day. Test cells have been run successfully with one anode effect every 10 days but this requires consistent alumina feed and good bath level control.

5.24 ACD Control Strategies

ACD control strategies aim at achieving an optimum energy efficiency. For any cell operating condition there is a critical ACD below which there is increased loss of current efficiency and above which there is increased energy consumption.

5.24.1 Fixed ACD

Constant ACD routines assume that the bath composition and temperature is essentially constant. Under these conditions, the optimum ACD is fixed. By further assuming that the rate of rise of metal pad level is equal to the rate of electrolysis of carbon anodes, once the optimum ACD has been attained there is no need for further anode movement. This strategy is therefore only suitable for point feed cells where voltage fluctuations due to alumina feeding are reduced.

During the tapping operation and after anode effect terminations, the ACD is returned to its optimum value by returning the cell to a target voltage.

5.24.2 ACD optimisation

This scheme utilises the relationship between anode-cathode distance and electrical noise generated by the cell. Electrical noise increases with decreasing ACD and becomes excessive when the point of voltage instability is reached. At this point current efficiency begins to be seriously decreased.

This strategy assumes that this is the point of optimum ACD and controls voltage just above the point of instability. Periodically, the anodes are lowered until noise becomes excessive and the voltage setpoint adjusted.

Voltage control is then by standard AVC routines. This method of control is not currently used at Anglesey Aluminium.

5.25 Summary

This chapter has discussed some control strategies than are used in industry and that can be investigated in simulation. The next chapter will discuss the programming of the aluminium cell model and the control systems and will compare the results of the simulation to experimental data in order to validate the model.

References

[1] Lewis, R. A., *"Technical Fundamentals of the Aluminum Reduction Cell Process"*, Reduction Division Technical Manual I, Kaiser Aluminum Internal Publication, 1973

[2] Gjerstad et al, Symposium on Industrial Electrode Processes with Gas Evolution, Electrochem. Soc., 1966

[3] Belyaev et al, Izv, Vyssh. Ucheb. Zav., Tsvetn. Met., vol 4, no 3, 1961, p67

[4] Grjotheim K. et al, Can. Met. Quart., vol 11, 1972, p295

[5] Firsanova et al, Izv. Vyssh. Ucheb. Zav., Tsvetn. Met., vol 5, no 3, 1962, p52

[6] Szekér, Acta Tech. Acad. Sci. Hung., vol 10, 1955, p91

[7] Bersimenko et al, Tsvet. Met., vol 46, no 3, 1973, p30

6.0 Dynamic Simulation of an Aluminium Reduction Cell

One of the main requirements of the simulation is that it should be able to be used both on-site at Anglesey Aluminium and at Newcastle University. With the advent of cheap powerful microcomputers this presents no problem and most of this work was carried out on a Compaq 32 bit IBM compatible personal computer. A wide range of programming languages are available for these machines and the choice of language is based upon the applications for which the simulation is intended.

6.1 Choice of Programming Language

The simulation is required to predict the dynamic behaviour of the cell over long periods of time. In order that this takes as short a run time as possible a compiled, rather than interpretative, language must be used.

The simulation of different control systems and types of cell requires that parts of the model be altered periodically. It is therefore desirable that the language used allows the program to be specified as a number of modules eg process model, control system, user interface etc. If changes are made to any module, only that module need be re-compiled not the whole program.

The program was originally written in a version of PASCAL that allowed a degree of modularisation. This was successful in simulation but attempts to produce a real time version with communication to the Anglesey Aluminium control computers, CELTROL through an industrial signal processor encountered problems due to the relative speeds of the simulation and communication.

A solution to this problem was the use of a language with multi-tasking capabilities that allows different routines in the programs to be given different priorities. Modula-2 was chosen as it is a language that has evolved from PASCAL and transition between the two was relatively simple. Further details of multi-tasking and real time simulation are given in chapter 7.

As well as providing multi tasking capabilities, Modula-2 has a number of other advantages over PASCAL. These are as follows:

1. **Increased Modularisation:** Modula-2 programs consist of a number of user defined and library modules that are linked together after the compilation stage. This has been utilised here to build up libraries of control and model routines. Different control strategies may be easily simulated by choosing the relevant routines from the library.

2. **Model Security:** Interfacing between individual program modules is by Definition modules. These contain information of the objects (eg Procedures, Variables) available from the program module. This allows objects to be used by a model builder without the necessity of source code being available.

3. **Debugging:** The use of small modules in developing large programs greatly reduces debugging and significantly improves software management. Each module can be individually tested and debugged and any faults in the program more easily tracked to a specific area.

4. **Portability:** The modular structure of the language greatly enhances the portability of programs between different machines. There are no predefined I/O statements, maths functions or string manipulation routines in the Modula-2 core. All such routines are imported from library files that may be produced specific to a particular machine.

6.2 Initialisation

The complexity of the overall process model does not allow for all of the variables to be initialised by steady state analysis. Initial conditions were therefore obtained by running the simulation with the approximate starting conditions and allowing the program to converge to a steady state. The process variables at this point were obtained as a memory dump from the program and provide the 'steady state' conditions of a 'standard' run. This is then used as the starting condition for subsequent simulations.

Once this start point has been achieved, memory dumps of the process variables represent the system at any point in time. The conditions at the

end of one simulation can therefore be used as the starting point of another simulation. In effect, the simulation can be continued without interruption.

This feature can be utilised to investigate the effects of changes in operational parameters relative to a standard run. An example of this is the simulation of the effects of changing to a different type of alumina. The memory dump of a standard run is used as the start up conditions but with the parameters pertaining to alumina type altered ie thermal conductivity, dissolution rate constants, specific heat capacity etc.

Separate memory dumps are produced for the control and model variables. In addition, the control variables may be initialised from complete or partial memory dumps. The complete version contains all historical data for the control system and allows the simulation to be continued from the point at which it was stopped. Use of the partial dump, however, allows for changes to be made in control parameters and simulates the resetting of a CELTROL device.

In addition to initialisation of the simulation from file, many of the operating conditions may be changed from a menu system in the program. This makes the software relatively easy to use by operators who have not been involved in the programming and is an important aspect of the program design if it is to be of use within the aluminium industry. Full details of the menu system developed are given in Appendix A.

6.3 Presentation of Results

The simulated conditions within the cell are continuously updated on screen as the simulation progresses. The screen format is designed to display those operating and control parameters that are normally available for a working cell. This allows the user to monitor the progress of the simulation and recognise situations that can occur in the working cells. The simulation allows for some operator settings, for example target voltage and metal tapping, to be changed interactively as conditions within the cell change. The output screen for the program is shown in appendix B.

The simulation results are also stored in ASCII format files on the computer disk. This produces vast quantities of data that must be processed. The best means of interpreting the data is graphically but the commercial spreadsheet programs available at the time of this work were unable to deal successfully with the amount of data produced. It was therefore necessary to produce a graphics package to do this. The program allows the user to produce graphs of combinations of parameters and includes facilities to 'zoom in' on areas of interests. Hard copy is provided on a Hewlett Packard plotter and full details of the package are given in appendix C.

6.4 Numerical Solution of Differential Equations

This simulation uses Euler's method for the solution of differential equations. This is a first order method and as such requires a much smaller integration time to achieve the same accuracy as a fourth order predictor method such as Runge Kutta.

Although the program is required to simulate cell operation over long periods of time the main CELTROL routines work on a one second interval and anode movement is calculated to one tenth of a second. In addition, anode effect termination sequences can effectively limit the duration of anode effect to one minute. An integration interval of around one second is therefore required to successfully simulate all aspects of cell operation.

With such a small integration interval, the accuracy afforded by Euler's method is perfectly adequate and has the advantage of being much simpler and quicker than a higher order method.

6.5 Simulation of Current Control System (CELTROL)

The CELTROL control algorithms are programmed in a derivative of FORTRAN and downloaded into the read-only memory (ROM) of the CELTROL computers. To simulate the operation of the aluminium cells the CELTROL algorithms must be converted into Modula-2 and linked into the physico-chemical model of the cell. As the behaviour of the cell cannot be separated from the effects of the operating system an accurate simulation

of the control algorithms must be produced to allow comparison of the simulation with measurements from the cell.

Initially the full control program for the operation of half break cells, including the starve and search routines, were programmed as a Modula-2 module exactly as they were implemented in Modcomp FORTRAN. This implementation of CELTROL was used as the 'standard' version for verifying and tuning the simulation.

6.6 Validation of the Simulation

A large number of unknown variables such as average heat transfer coefficients are unique for individual cells and are very difficult to determine. In order to validate the model, a 'standard' run will be defined with variables tuned to give the average conditions expected in operation of aluminium cells.

The complete set of initialisation variables used in the standard run are listed in appendix A and the results of a 170 hour simulation shown in figures 6.1 to 6.6. The simulation is for a mark IV half break cell operating at a target voltage of 4.39V with Anglesey Aluminium's search and starve routines activated. Alumina is fed at a rate of 90 kg on a base feed time of 67 minutes. The current through the cell is constant at 151 kA and the cell is configured for eighteen 53" anodes. A comparison of the average cell performance for the first half of 1986 with the simulated performance is shown in table 6.1.

The voltage trace for the simulation is shown in figures 6.1 and 6.2. This shows an anode effect frequency of 1.55 AEs per day with anode effects occurring at 7, 16, 35, 53.5, 64.5, 83, 101.5, 121, 139.5, 158 and 169 hours. Those occurring at 7, 35, 53.5, 83, 101.5, 121, 139.5 and 158 hours are due to the starve routine and successful searches have occurred at 28.3, 47.5, 77.2, 95.6 and 151.5 hours. The average voltage over the simulated period is 4.41 V the deviation from target voltage being due to anode effects. This voltage is that measured by CELTROL and is not directly comparable with the gross operating voltage which includes the voltage drop across the buswork between individual cells. This accounts for approximately 0.03V at 151 kA and gives the simulated gross

Parameter	Actual	Simulation
Energy Efficiency (DC kWh/kg)	14.8	14.6
Gross Voltage (V)	4.48	4.44
Current Efficiency (%)	90.1	90.5
Anode-Cathode Distance (cm)	4.85	4.68
Bath Temperature (°C)	969	971
Wt Ratio NaF/AlF_3	1.22	1.23

Table 6.1 Comparison of Simulated Performance and Actual Performance for a Half Break Cell in 1986

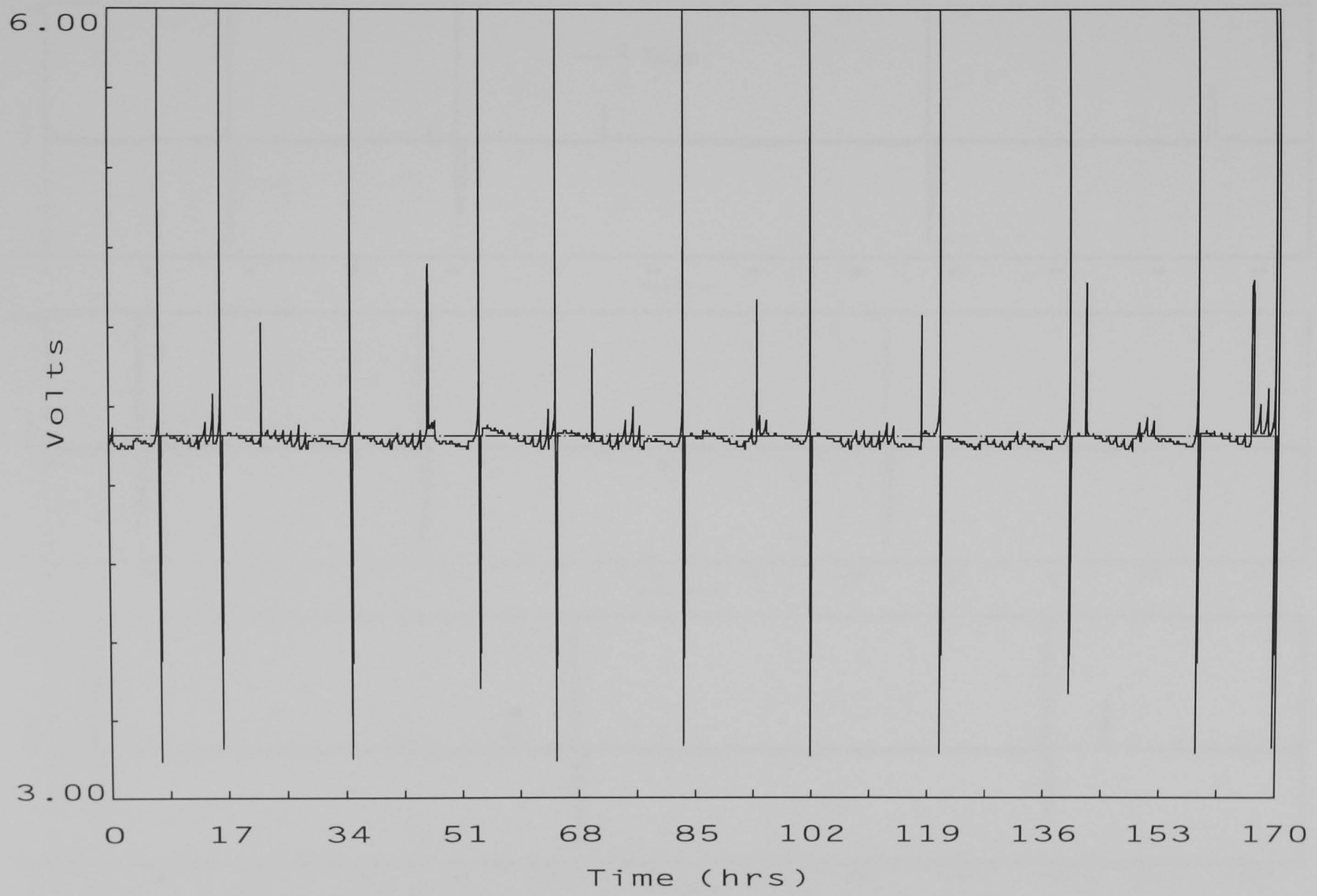

Figure 6.1 Simulated Voltage Profile for 151 kA Centre Break Cell

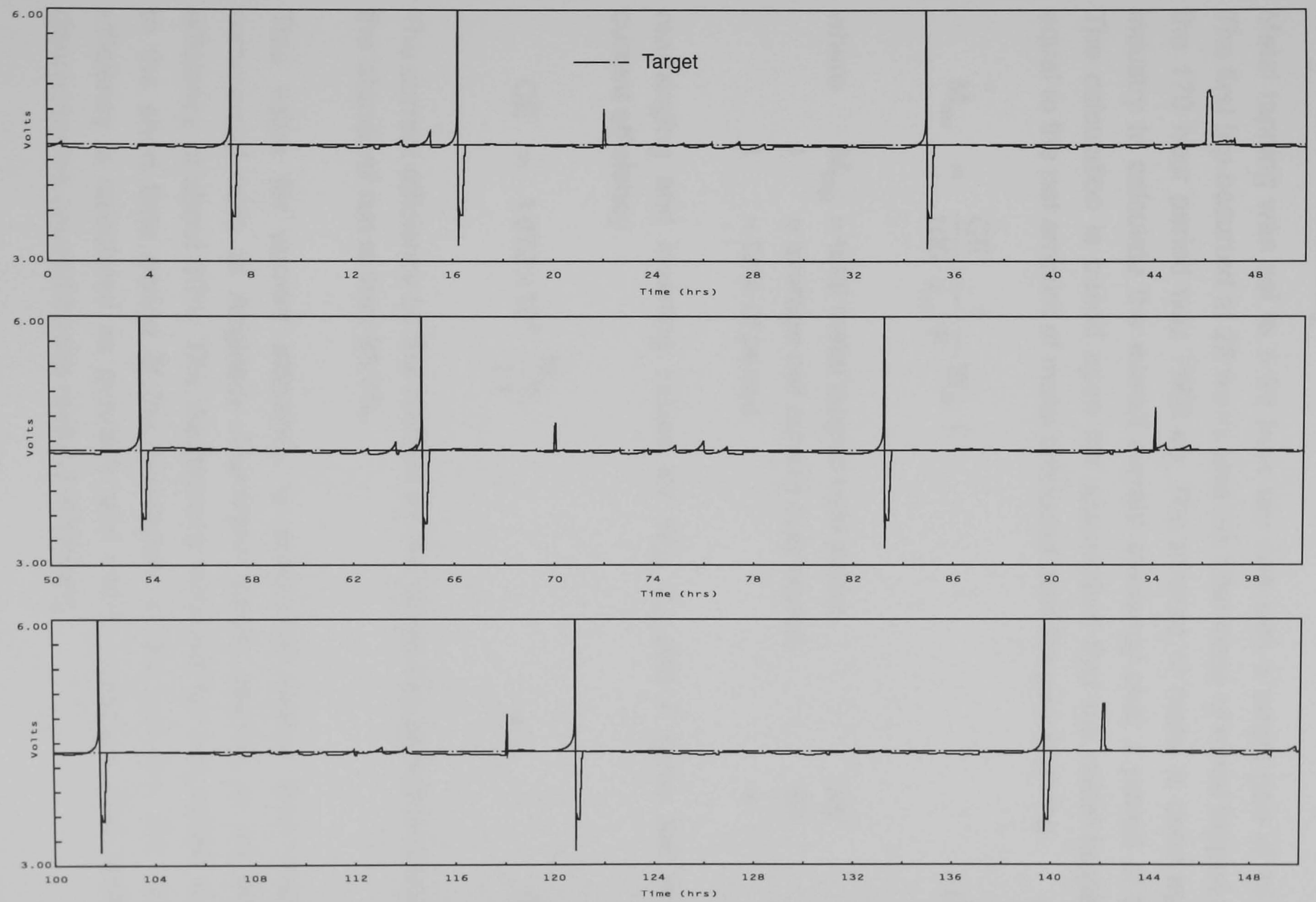

Figure 6.2 Simulated Voltage Profile for 151 kA Centre Break Cell

operating potential as 4.44V. This compares very favourably with the average value for the first half of 1986 of 4.48V[1].

6.6.1 Current efficiency

Metal tapping was set to a 24 hour tap rate with a target pad of 14 cm. The first tap occurred at 22 hours and the total mass of metal tapped over the 170 hour period was 7980 kg. The amount of metal is used by the industry to calculate the overall current efficiency over a period of time. The calculation is based upon the assumption that the metal tapped is equal to the net amount of metal produced over the period giving

$$M_{tap} = \frac{CE}{100} \cdot \frac{I}{z_{Al} \cdot F} \cdot W_{Al} \cdot t \qquad (1)$$

where M_{tap} = total metal tapped over period (kg)
I = average cell current over period (kA)
t = time of period (s)

rearranging and inserting values for W_{Al}, z_{Al} and F gives the overall current efficiency

$$CE = 1.072 \times 10^6 \cdot \frac{M_{tap}}{I \cdot t} \qquad (2)$$

The current efficiency by this method for the seven day period simulated in the 'standard' run is then 93.7%.

This value for current efficiency is somewhat higher than that for commercial cells at Anglesey Aluminium which operate at an overall efficiency of about 90%. The discrepancy between the two values is due to the short time period of the simulation. In the industry, the current efficiency is calculated as quarterly and yearly averages. This removes discrepancies caused by the method of tapping.

Although the aim of tapping is to return the pad depth to a target level the amount tapped is not directly proportional to the deviation from this set point. The schedule used for determining the metal tapped is shown in table 6.2

Deviation from target cm	Metal tapped kg
deviation at last tap < 0	0
>= 0	900
0	1140
1	1320
> 1	1500

Table 6.2 Aluminium Tapping Schedule at Anglesey Aluminium

The deviation from target pad is measured using a metal rod to a maximum accuracy of 0.1 cm. The value is then rounded to the nearest integer. Unless the metal pad at the time of tap is always at the target value, it follows that the pot will have periods when it is effectively over or under tapped. The frequency and duration of these periods will depend upon the actual current efficiency of the cell. The use of this method of calculation can therefore produce misleading results if the period in question is short.

An additional source of error is the use of depth, rather than volume, to determine the desired tap weight. Fluctuations in the thickness of the frozen sidewalls results in the depth corresponding to different volumes and can cause errors in the amount tapped. Over a long period of time these factors become negligible and the calculated current efficiency approaches the average current efficiency of the cell.

An alternative method of calculating the overall current efficiency of a cell is by taking the average of the instantaneous current efficiency over the period in question. This may be measured experimentally by gas analysis using the Pearson Waddington equation[2] but this method is not suitable for wide scale use on industrial cells. Additionally, the presence of gases other than carbon monoxide and carbon dioxide in the sample introduces errors in the calculation and for this reason it is not suitable during anode effects. The simulation, however, calculates the instantaneous current efficiency based upon the back reaction of aluminium in the melt and the results for the 'standard' run are shown graphically in figure 6.3. The average value for the 170 hour period is 90.4 % which compares favourably with the expected 90 %.

6.6.2 Energy efficiency

The energy efficiency of the cell is defined as the energy required to produce a kilogram of aluminium and is normally quoted in DC kWh per kg of aluminium. This is determined from the gross cell voltage and current efficiency by the relationship

$$\text{Energy Efficiency} = 298.1 \times \frac{\text{Gross Voltage (V)}}{\text{Current Efficiency (\%)}} \text{ DC kWh kg}^{-1} \quad (3)$$

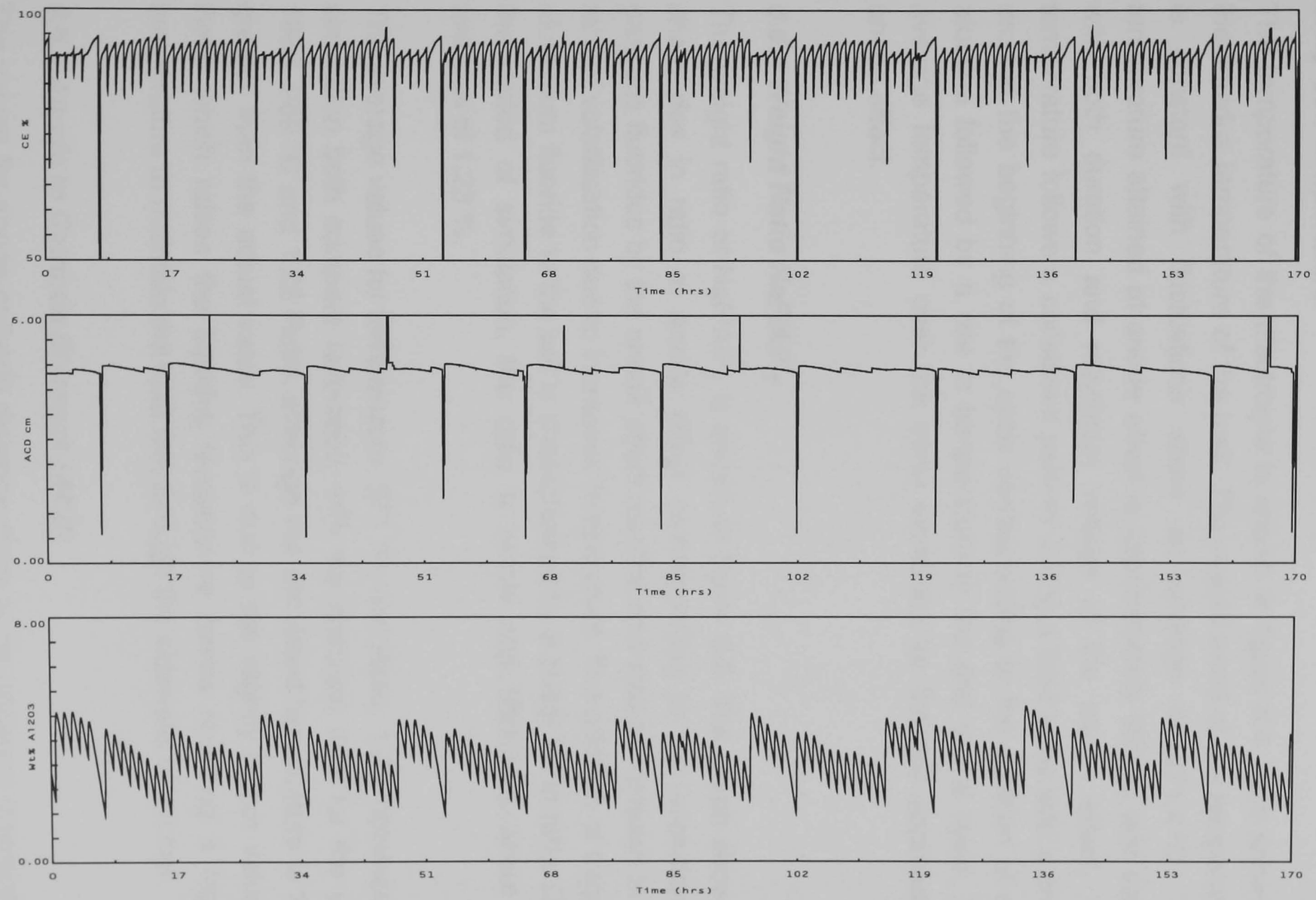

Figure 6.3 Simulated Current Efficiency, Concentration and ACD Profiles for 151 kA Centre Break Cell

The value for the simulation is therefore 14.6 DC kWh / kg which is close to the actual value for the mark IV cell of 14.8 DC kWh / kg.

6.6.3 Cell temperature

The temperature of the electrolyte is shown in figure 6.4. Also shown is the liquidus temperature of the melt. The overall trend of the temperature is constant with fluctuations about an average of 971.4 °C. The temperature attained at anode effect is approximately 990 °C and varies with both duration and maximum voltage of the anode effect. The temperature follows a consistent pattern during a feed cycle with a sharp drop at the beginning of the cycle corresponding to the addition of cold alumina followed by a rise in temperature to the end of the cycle. The average temperature over the cycle increases as the cell approaches anode effect.

6.6.4 Weight Ratio NaF/AlF_3

The weight ratio of NaF/AlF_3 is shown in figure 6.5. The graph shows a sharp rise in ratio at anode effect corresponding to the evolution of gaseous fluorides by the anode effect reaction and also an increase in the rate of volatilisation due to increased temperature. The addition of bagged aluminium fluoride to the cell is characterised by a sharp fall in ratio. Over the period of simulation, the ratio is stable and fluctuates about an average of 1.23 %.

The average values for temperature, 971 °C, and Ratio, 1.23, obtained by simulation both compare favourably with the historical data for the year 1986, 969 °C and 1.22 Ratio, although the simulated temperature is 2 °C greater than the actual value. This is due to the slightly higher value of Ratio which raises the liquidus temperature hence requiring a higher temperature to maintain the heat lost through the sidewalls of the cell.

6.6.5 Anode to Cathode Distance (ACD)

The values for anode-cathode distance show some apparent discrepancy with a value of 4.68 cm obtained by simulation compared to 4.85 cm for the actual value. Anode-Cathode distance is not measured directly on

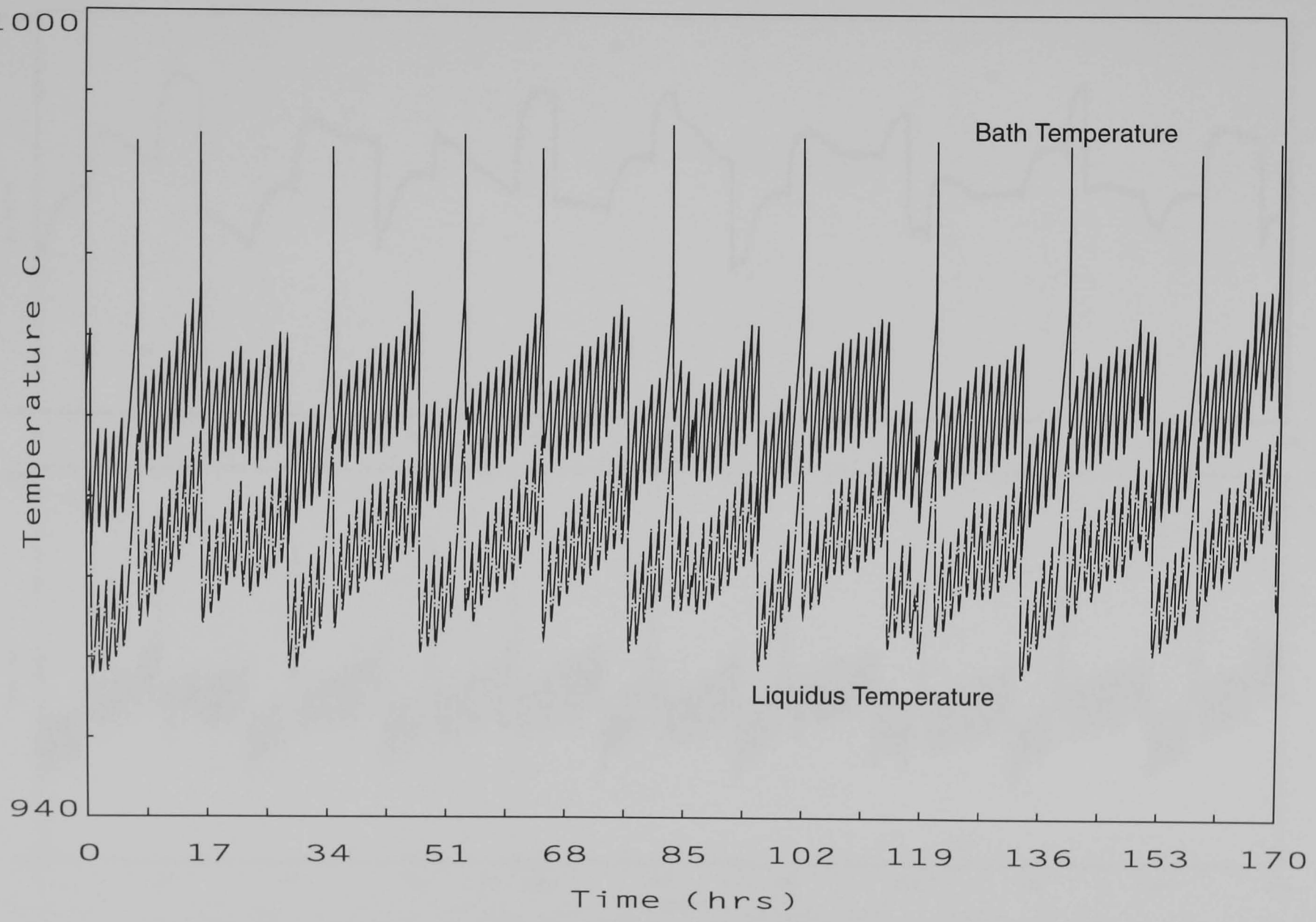

Figure 6.4 Simulated Temperature Profile for 151 kA Centre Break Cell

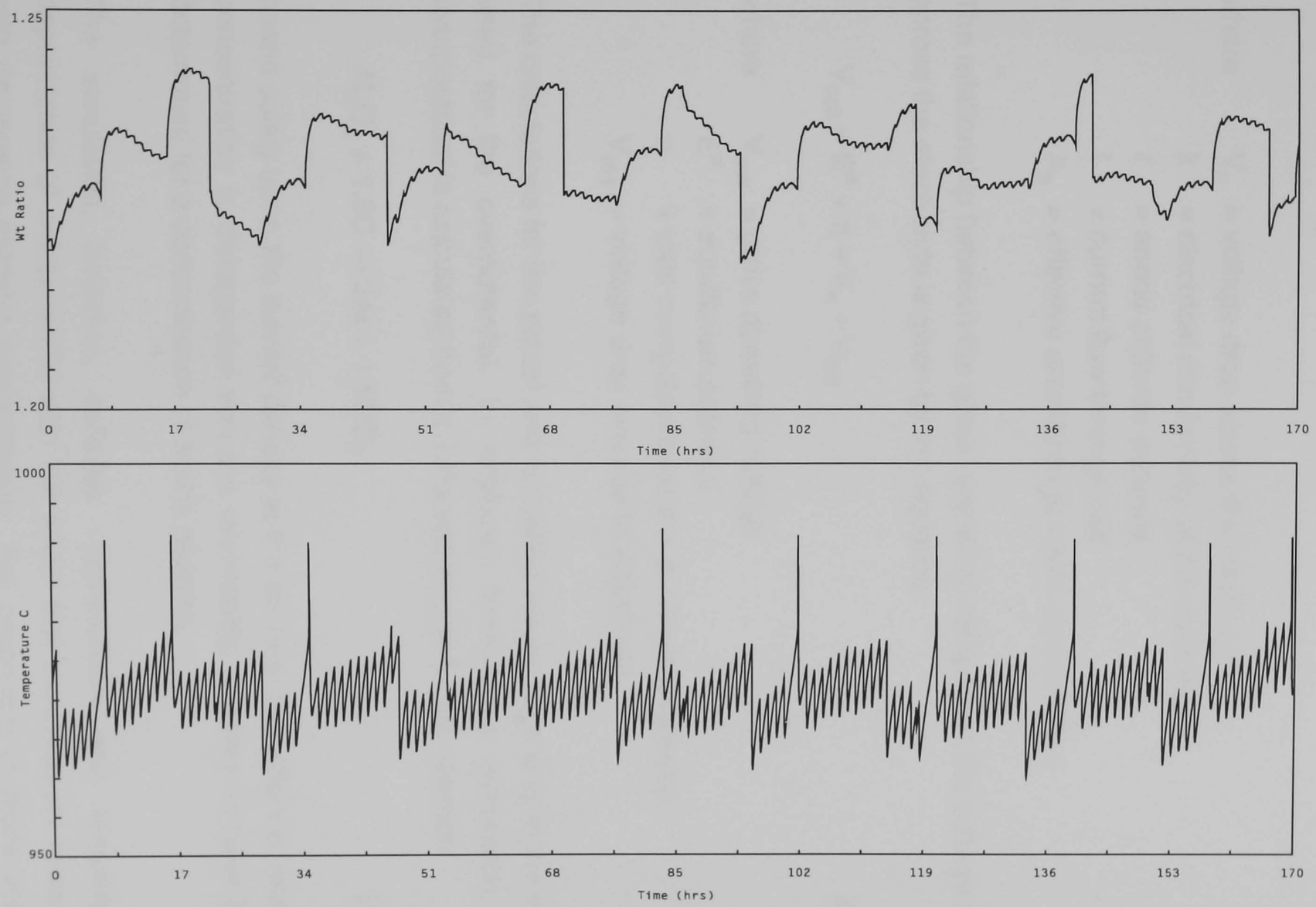

Figure 6.5 Simulated Ratio vsTemperature for 151 kA Centre Break Cell

commercial cells but is calculated from the voltage drop across the electrolyte by the relationship

$$V_e = I \cdot \frac{k \cdot \ell}{A_b} \qquad (4)$$

where V_e = voltage drop across the electrolyte
k = electrical conductivity of the electrolyte
ℓ = anode cathode distance
I = current flow through cell
A_b = effective area through which current flows

The relationship between the gross operating voltage and the voltage drop across the electrolyte is given by the equation

$$V_{cell} = E^{\circ} + \eta + V_e + V_{ext} \qquad (5)$$

where V_{cell} = gross operating voltage
E° = equilibrium potential
η = total overpotential at the anode and cathode
V_{ext} = voltage drop external to electrolyte

The calculations for the actual and simulated values differ only in the value used for the overpotential. In Anglesey Aluminium's calculation, the overpotential is calculated from a Tafel expression for the reaction

$$Al_2O_3 + 1.5C \rightarrow 2Al + 1.5CO_2 \qquad [1]$$

based solely upon the current density at the anodes. The effect of alumina concentration is disregarded and the relationship appears to have been determined for a concentration of 5 wt% alumina.

The simulation, however, includes concentration and temperature dependence of overpotential with the effect that overpotential increases with decreasing alumina concentration. The proportion of gross voltage attributable to the ohmic drop across the electrolyte is therefore decreased resulting in a smaller anode-cathode distance. Additionally, the value determined from simulation is the average over the period and includes

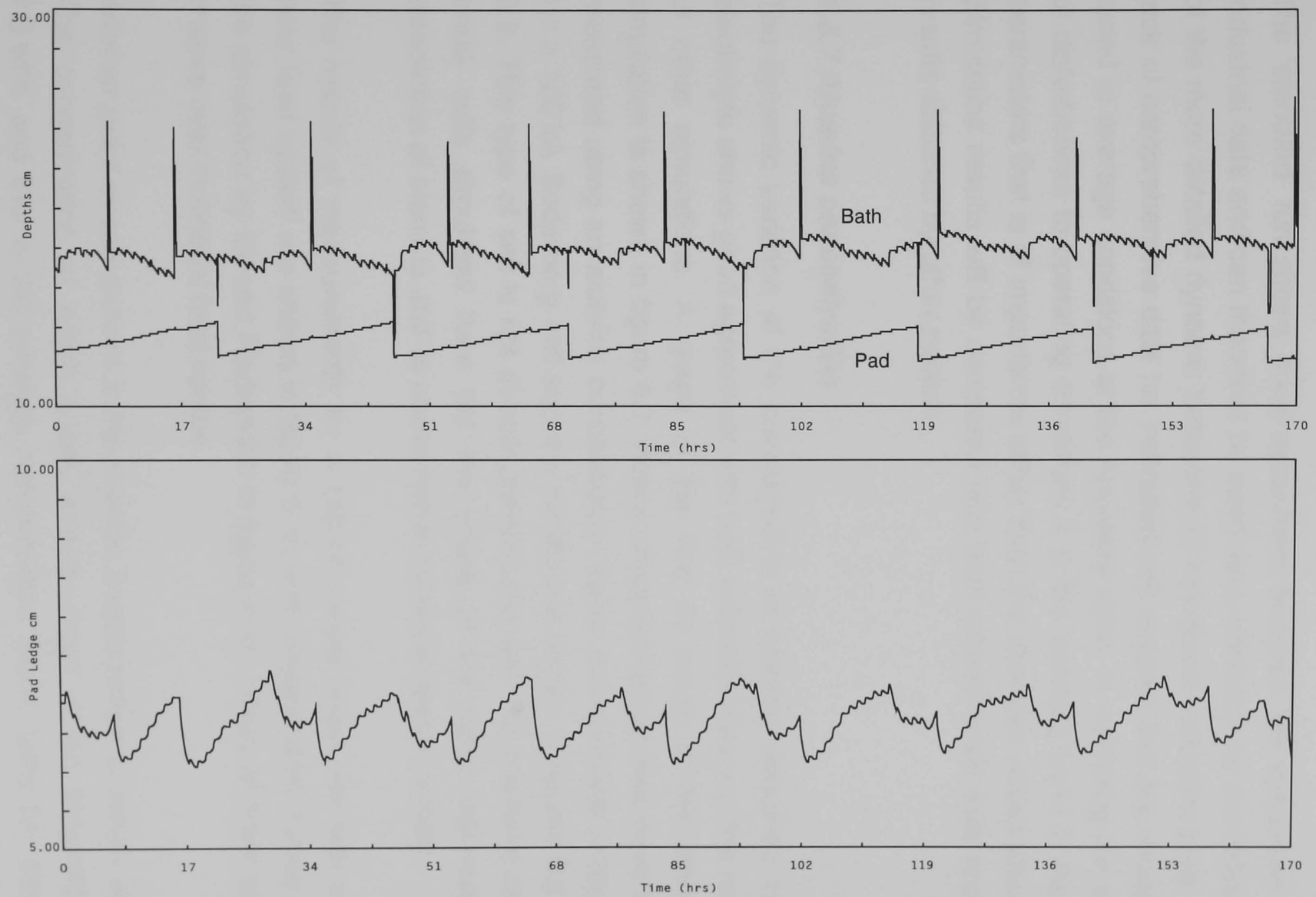

Figure 6.6 Simulated Bath and Pad Depths for 151 kA Centre Break Cell

the very low anode-cathode distances due to anode movement during anode effect termination.

6.6.6 Parameter trends

The 'standard' run shows good agreement between the simulation and industrial data and can therefore be used as a reference for the validation of the more detailed dynamic behaviour of aluminium reduction cells. The lack of comprehensive data for individual cell requires that the model be tuned to average conditions at the Anglesey plant. In validating the effect of disturbances to operating conditions it is the resulting trend in the cell parameters that is of importance rather than the absolute values attained. Simulation results will be compared with both experimental data and the results obtained by other models.

6.6.7 Alumina concentration

The dynamic variation of the concentration of alumina dissolved in the electrolyte shows good agreement with both industrial data and the results of other simulations. A graph of the first 24 hours of the standard simulation is shown in figure 6.7. Actual concentration profiles have been measured using an alumina concentration meter and chemical analysis[3] for a 100 kA Soderberg cell and the results are shown in figures 6.8 and 6.9. This type of cell is not directly comparable with the pre-bake centre break cells simulated here but the shape of the curve representing dissolution of alumina and its consumption by electrolysis is similar.

The results of measurements for a 150 kA centre break cell with a two hour feed cycle[4] are shown in figure 6.10 and concentration curves from the simulation by Ek and Fladmark[5] in figure 6.11. These all have similar shapes over individual feed cycles.

Another point of comparison is the alumina concentration at anode effect. The concentration at which anode effects occur in the simulation is 1.5 wt% and this is the average concentration found using the alumina concentration meter. Anode effects in figure 6.7 also occur between 1 and 2 % alumina. However, the concentrations measured in figure 6.8 are much lower at about 0.5 % whilst those simulated by Ek in figure 6.11 are higher at about 2.5 %.

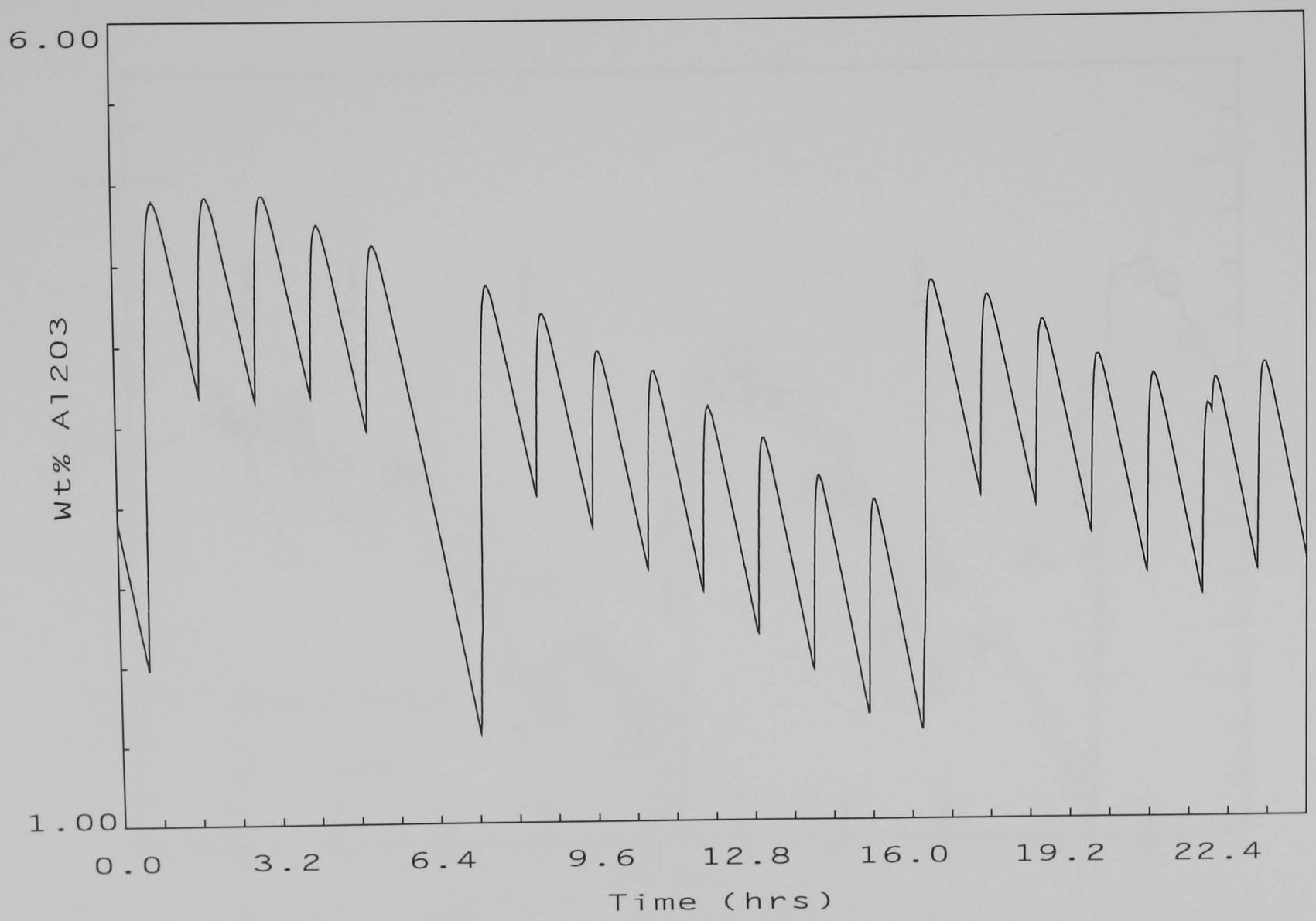

Figure 6.7 Alumina Concentration over First 24 Hours of the 'Standard' Run

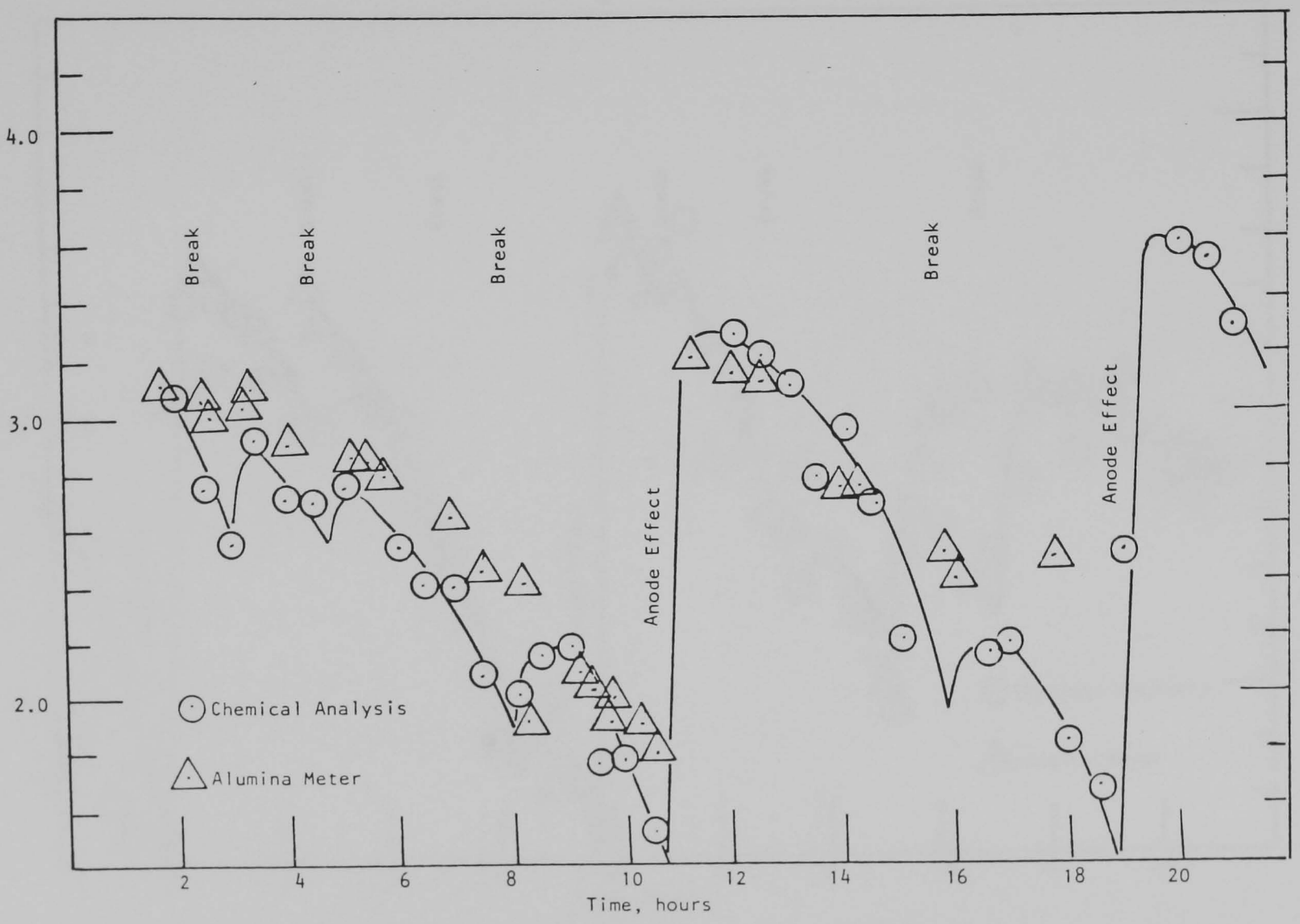

Figure 6.8 Measured Variation of Alumina Content in Reduction Cell Bath[3]

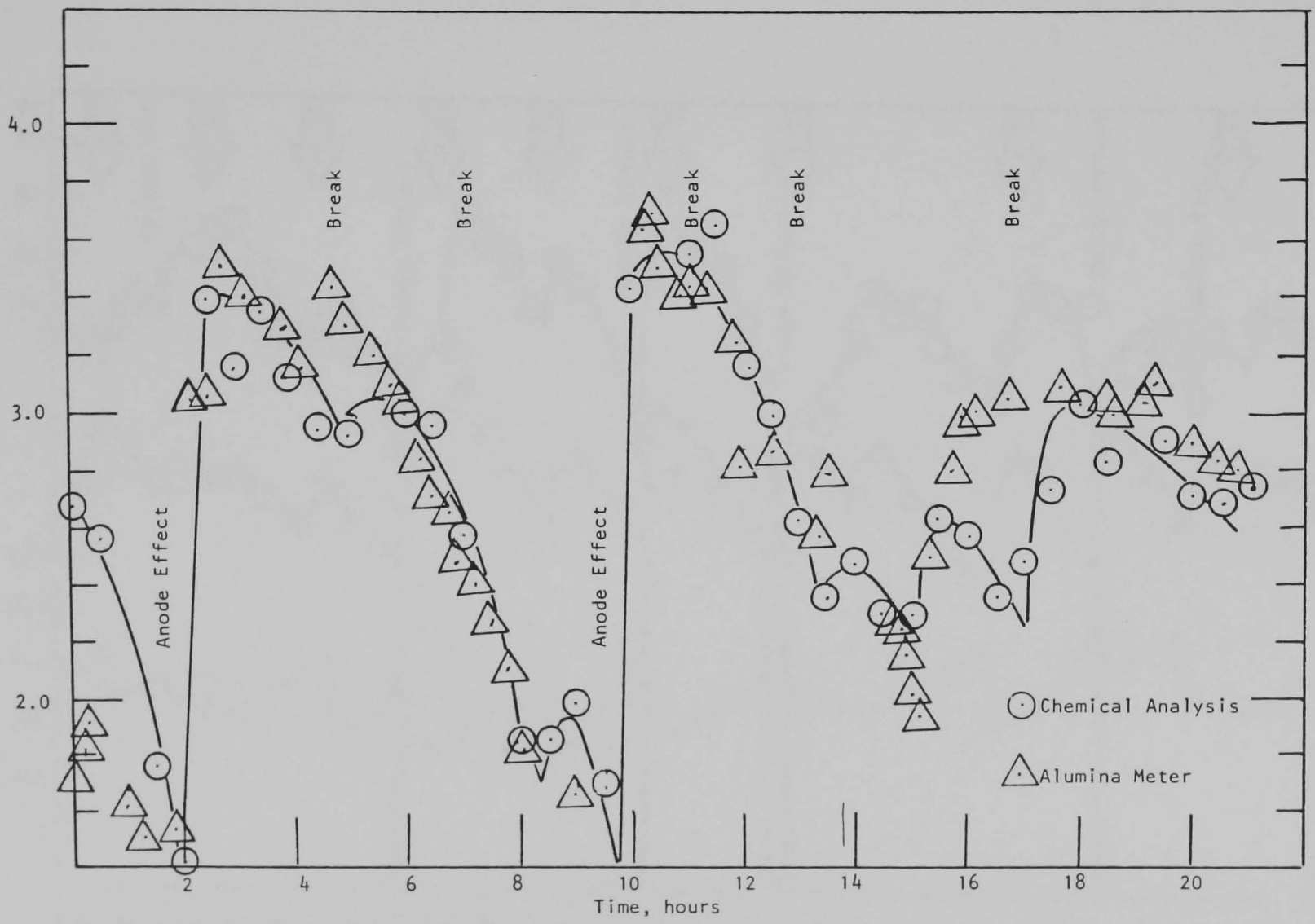

Figure 6.9 Measured Variation of Alumina Content in Reduction Cell Bath[3]

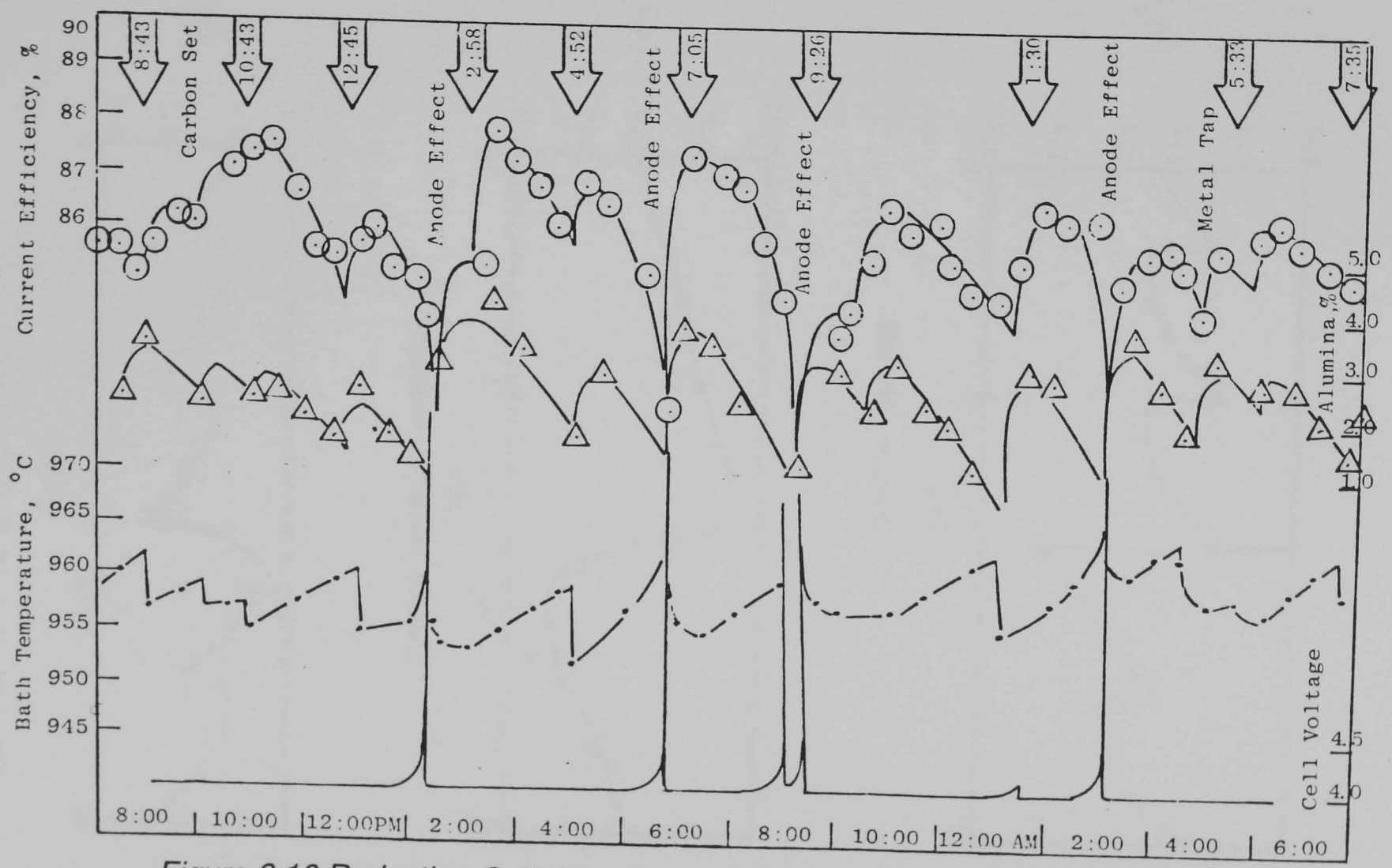

Figure 6.10 Reduction Cell Operation with Two-Hour Break/Feed Cycle[4]

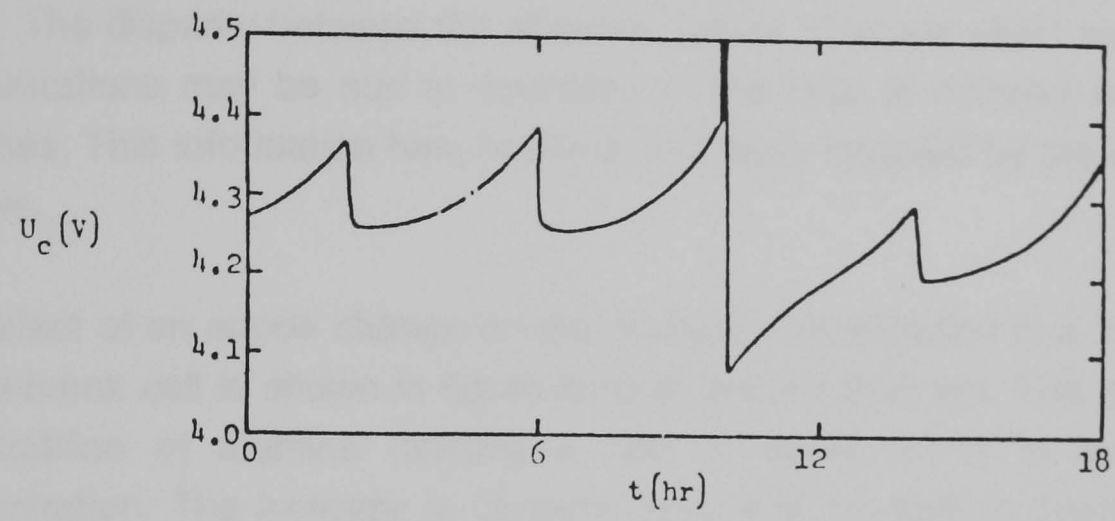

The cell voltage.

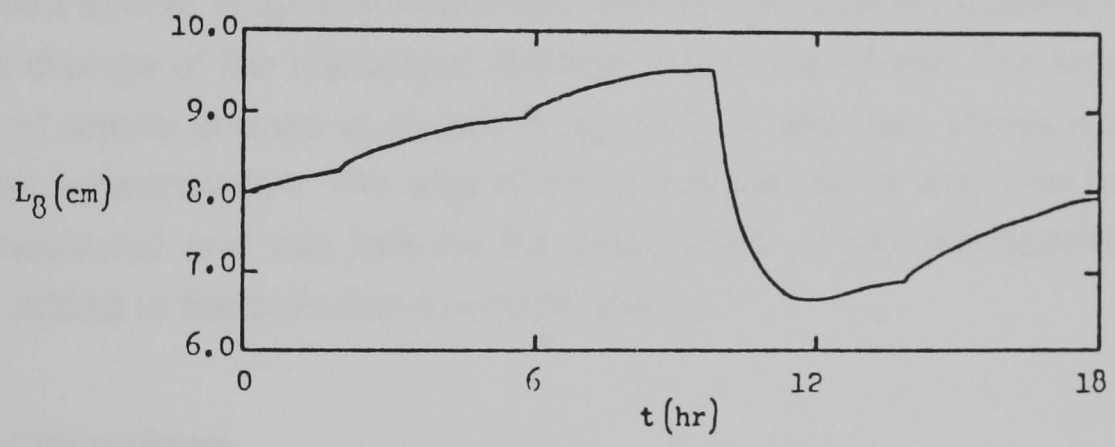

Thickness of upper freeze.

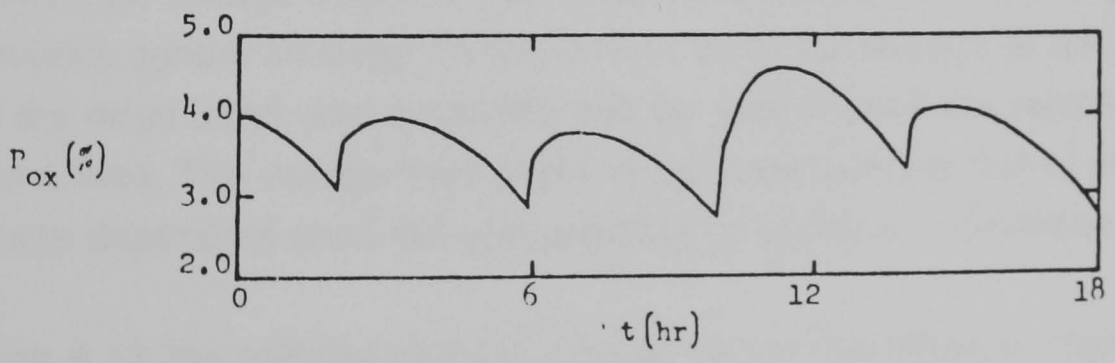

Consentration of Al_2O_3 in the bath

Figure 6.11 Simulation of Alumina Concentration, Freeze Thickness and Cell Voltage[5]

As anode effect occurs due to the current density at the anode exceeding the limiting current density for the reaction, the concentration at which anode effects occur will vary. This is reflected in the occasional triggering of an anode effect by the changing of an anode. Removal of an anode from the cell reduces the area for current flow and increases the anode current density. If the alumina concentration is low this may cause anode effect. The disparity between the absolute values of anode effect alumina concentrations may be due to operation of the cells at different current densities. This information has, however, not been supplied by the above authors.

The effect of an anode change on the alumina concentration in a 150 kA centre-break cell is shown in figure 6.10 at around 9:00 am. This shows the addition of alumina causing a rise of about 0.7 % in alumina concentration. The increase in alumina content of the bath is dependent upon the anode change operation and includes a highly random element as the crust and sidewalls are broken into the cell during the removal of the spent anode. Anglesey Aluminium estimate an alumina addition during anode change of the equivalent of about one dump of ore. The simulated effect of anode change is shown in figure 6.12 and also shows a rise in alumina concentration. The size of the simulated rise is only one tenth of that measured and this reflects the small mass of alumina specified as being added to the bath due to anode change.

6.6.8 Cell voltage

The dynamic behaviour of cell voltage also compares very well with that obtained from voltage traces of half break cells operating under Anglesey Aluminium's control strategy. During a feed cycle the voltage is controlled within the dead band until automatic voltage control (AVC) is switched off prior to a feed. The voltage then starts to increase with the rate of change of voltage dependent upon the concentration of alumina in the electrolyte.

In figure 6.13 the voltage change through an anode effect is compared with the results of a 3 minute voltage trace of cell 2A18. The cell was operating at a current of 152.3 kA and a base feed time of 68 minutes. The characters in the trace denote the following voltages:

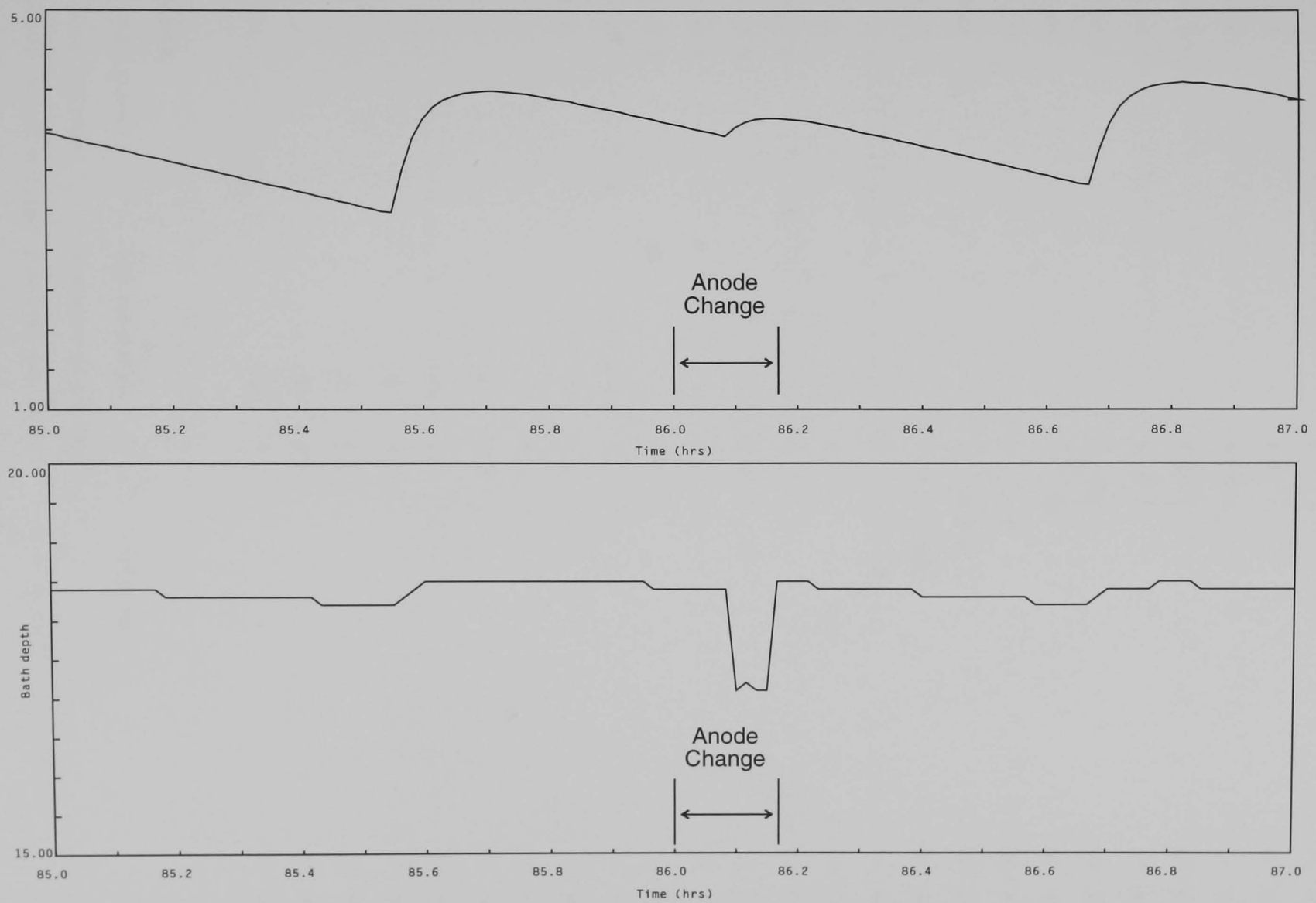

Figure 6.12 Simulated Effect of Anode Change upon Alumina Concentration

Day 0 0: 0

```
          4.02      4.12      4.22      4.32      4.42      4.52      4.62   TMR FED EVENTS
 0: 0 :....:....:....:....:....:....:....X.Z..:....:....:....:....:....:....  25  68
 0: 3                                :    X Z  :                              28  68
 0: 6                                :    TX SR:                              31  68
 0: 9                                :    T XZ :                              34  68
 0:12                                :    T  Z :                              37  68
 0:15                                :    T   ZR                              40  68
 0:18                                :    T    ZR                             43  68
 0:21                                :    T    : Z                            46  68 L
 0:24                                :    T    X S R                          49  68
 0:27                                :    T    :   SXR                        52  68 L
 0:30 :....:....:....:....:....:....:....T....:....:SRX.:....:....:....:....  55  68
 0:33                                :    T    :        S R              X   2  68  A
 0:36 X            S        R       :    T    :                             5  68  A
 0:39 X                              :    T R  :   S                         3  68
 0:42 X               Z              :    T    :                             6  68
 0:45 X               SR             :    T    :                             9  68 R
 0:48            X                   S R  T    :                            12  68 R
 0:51                                SR   T X  :                            15  68 R
 0:54                                 Z   T X  :                            18  68
 0:57                                Z:   T X  :                            21  68
 1: 0 :....:....:....:....:....:...SR....T.X..:....:....:....:....:....:....  24  68
 1: 3                                Z:   T X  :                            27  68
 1: 6                                Z:   T X  :                            30  68
 1: 9                                SR   T X  :                            33  68
 1:12                                SR   T X  :                            36  68
```

NOTATION

TMR Feed Timer FED Feed Time : Dead Band

T Target Voltage X Simulated Voltage

S Actual Smooth Voltage R Actual Raw Voltage Z Coincident Point (S R X)

EVENTS L Lower Anodes R Raise Anodes A Anode Effect

Figure 6.13 Comparison between Simulated and Actual Voltage Trace During Anode Effect in Cell 2A18

X simulated voltage
T target voltage 4.32 V
S actual smooth voltage (18 s filter)
R actual raw voltage (unfiltered)
Z common value for two or more voltages
¦ voltage dead band

There is good agreement between the rate of change of voltage prior to anode effect as well as in the duration of anode effect and the time taken for the voltage to return to target.

During anode effect termination, there are a number of rapid changes in cell voltage due to anode movement and noise. The large sampling time (3 minutes) of the trace can miss this effect and since the simulated and actual traces are not fully synchronised, this accounts for the larger discrepancy during the 36-45 minute period.

The voltage change during anode effect is shown in more detail in figure 6.14. The experimental data used here is from a 10 second scan for cell 1A3. The simulation again shows good agreement with the industrial data.

As is expected, the tapping operation causes an increase in cell voltage due to the lowering of the metal pad. In the simulation this is controlled by a CELTROL routine and results in a voltage peak of about 5 V. On site, this routine has been disabled and the voltage during tapping is controlled by the operator. The variation in voltage during the tapping operation can therefore increase or decrease as is shown in the resistance trace in figure 6.15.

6.6.9 Bath depth

The level of molten electrolyte in the cell is primarily affected by the temperature of the cell and by movement of the anodes. An increase in temperature in industrial cells generally results in an increase in bath depth due to melting of frozen electrolyte from the surface crust. The simulation predicts this trend as is shown in figures 6.16 and 6.17. The temperature in each of these runs is changed by introducing a step change in the target voltage. Figure 6.16 shows the continuation of run Al6c3 with a step change from 4.39 V to 4.29 V and figure 6.17 the effects of a further step change from 4.29 V to 4.49 V.

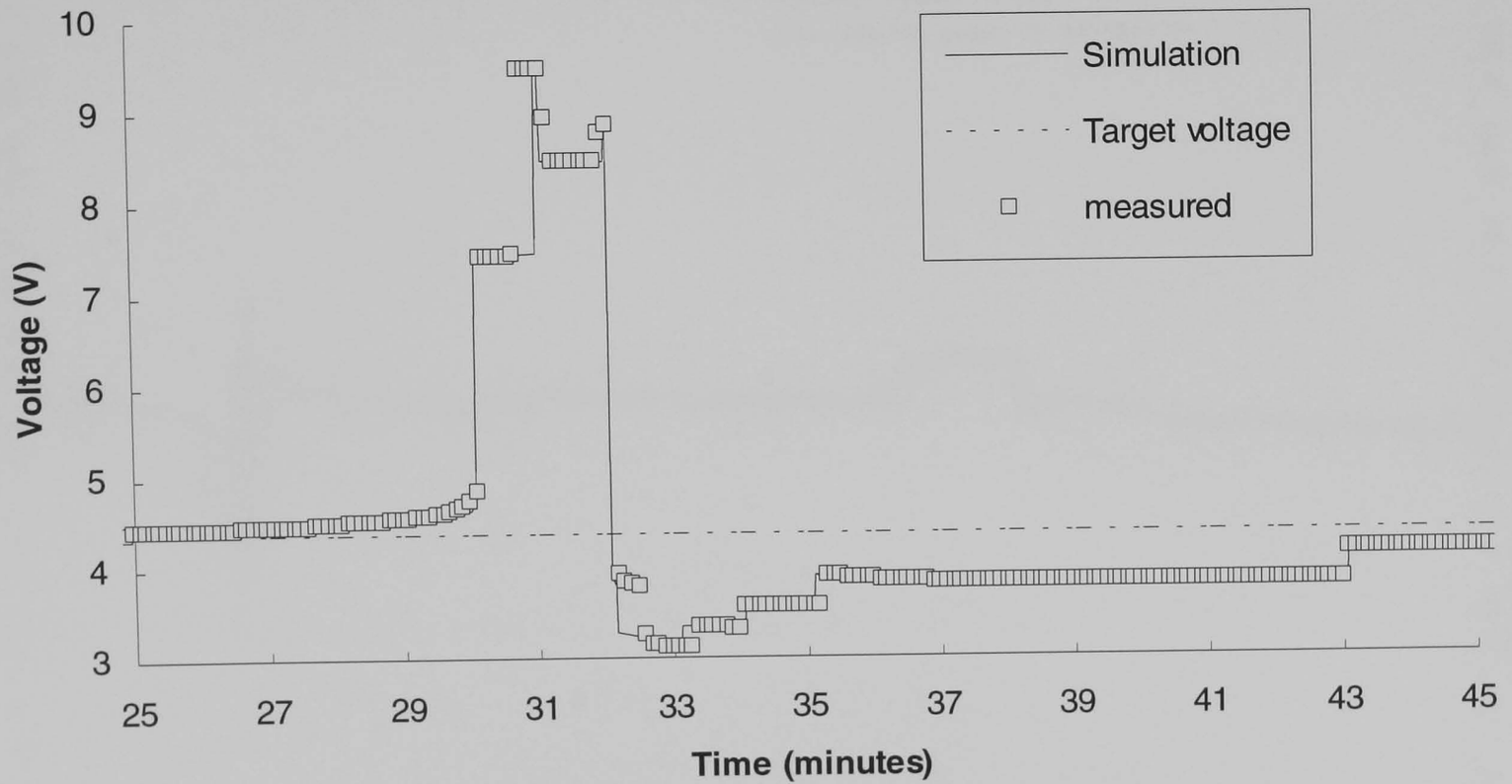

Figure 6.14 Voltage Trace of Anode Effect Predicted by Model

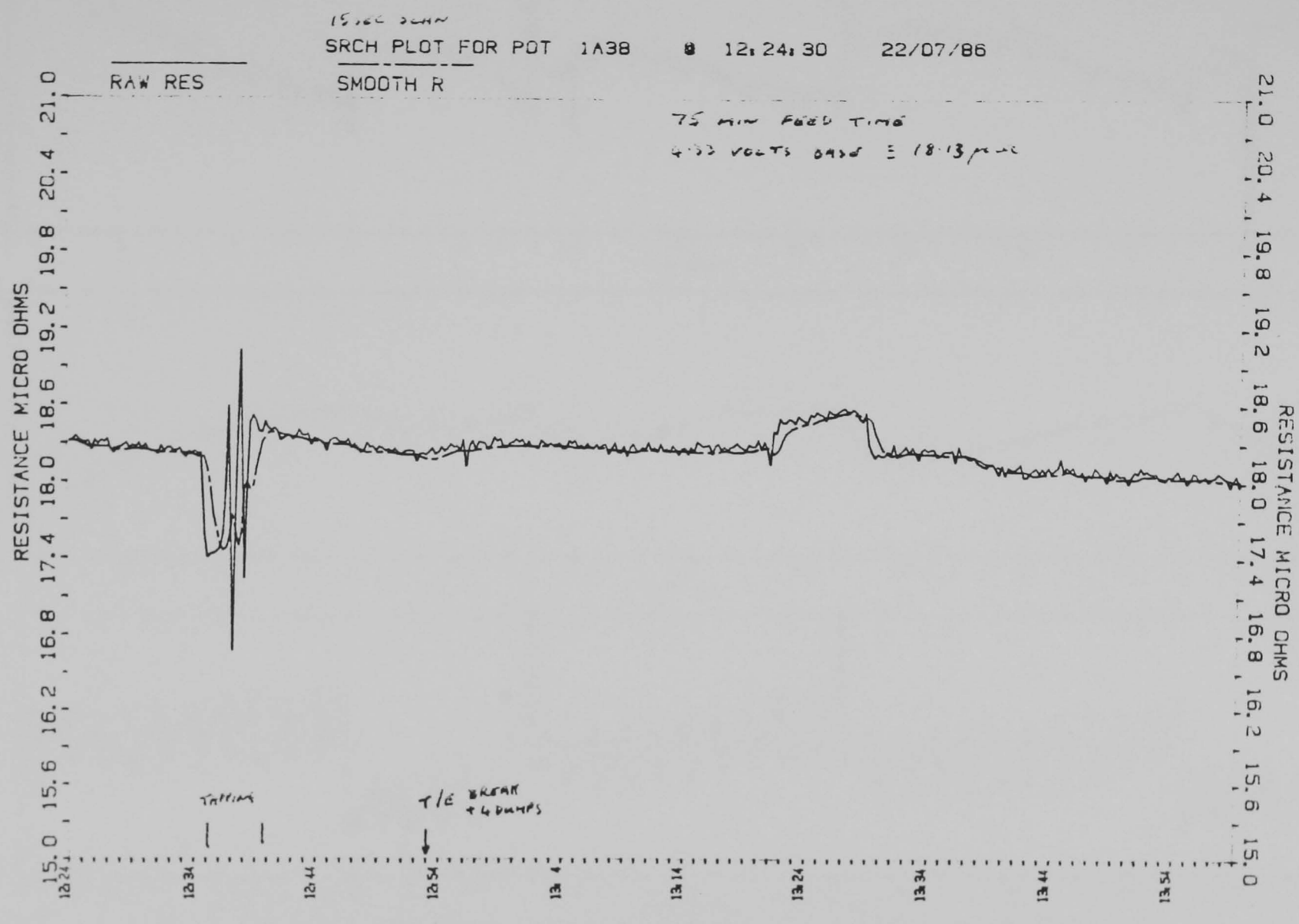

Figure 6.15 Resistance Trace during Tapping of Pot 1A38

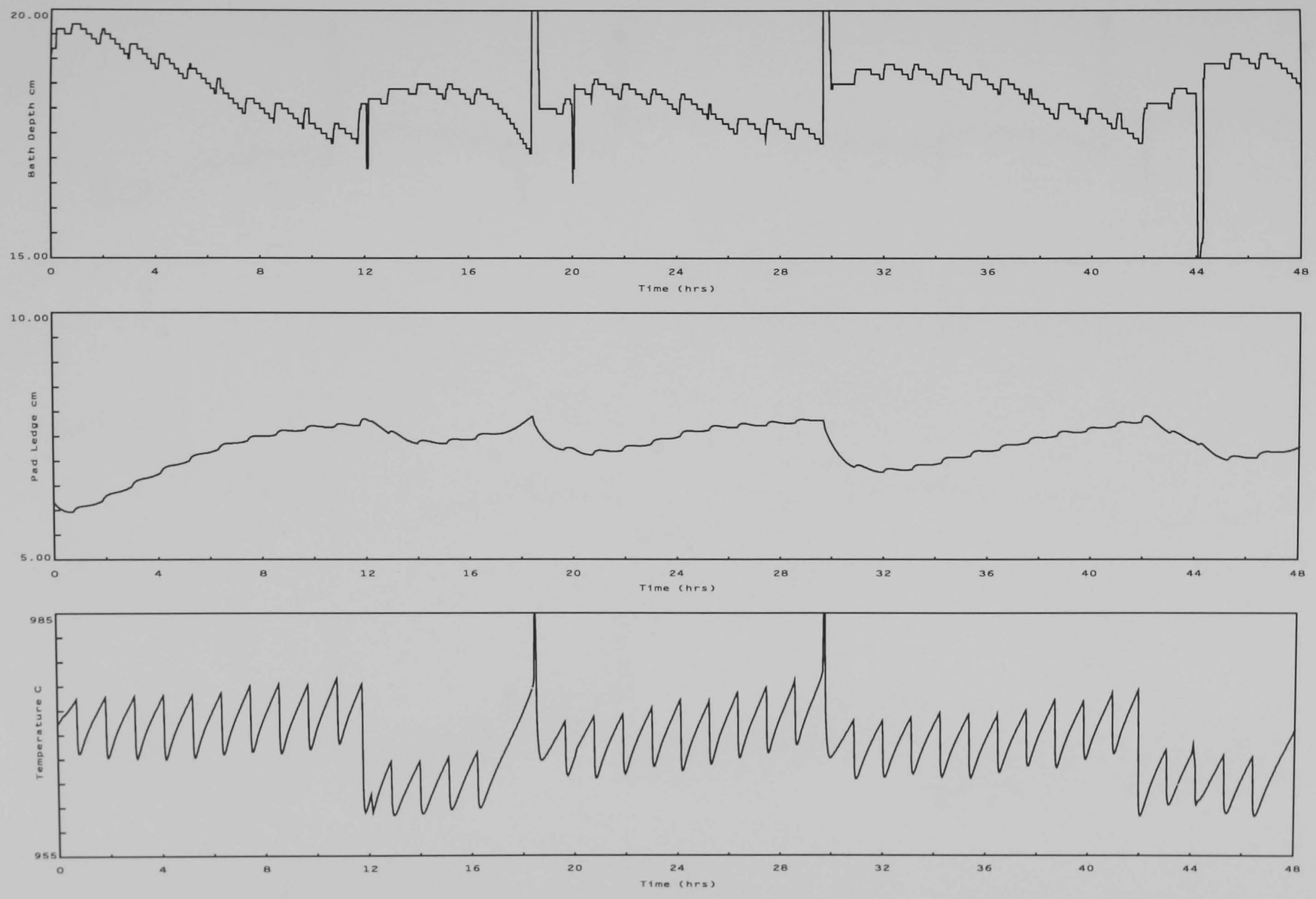

Figure 6.16 Change in Temperature and Bath Depth after a Simulated Decrease in the Target Voltage of 0.1V

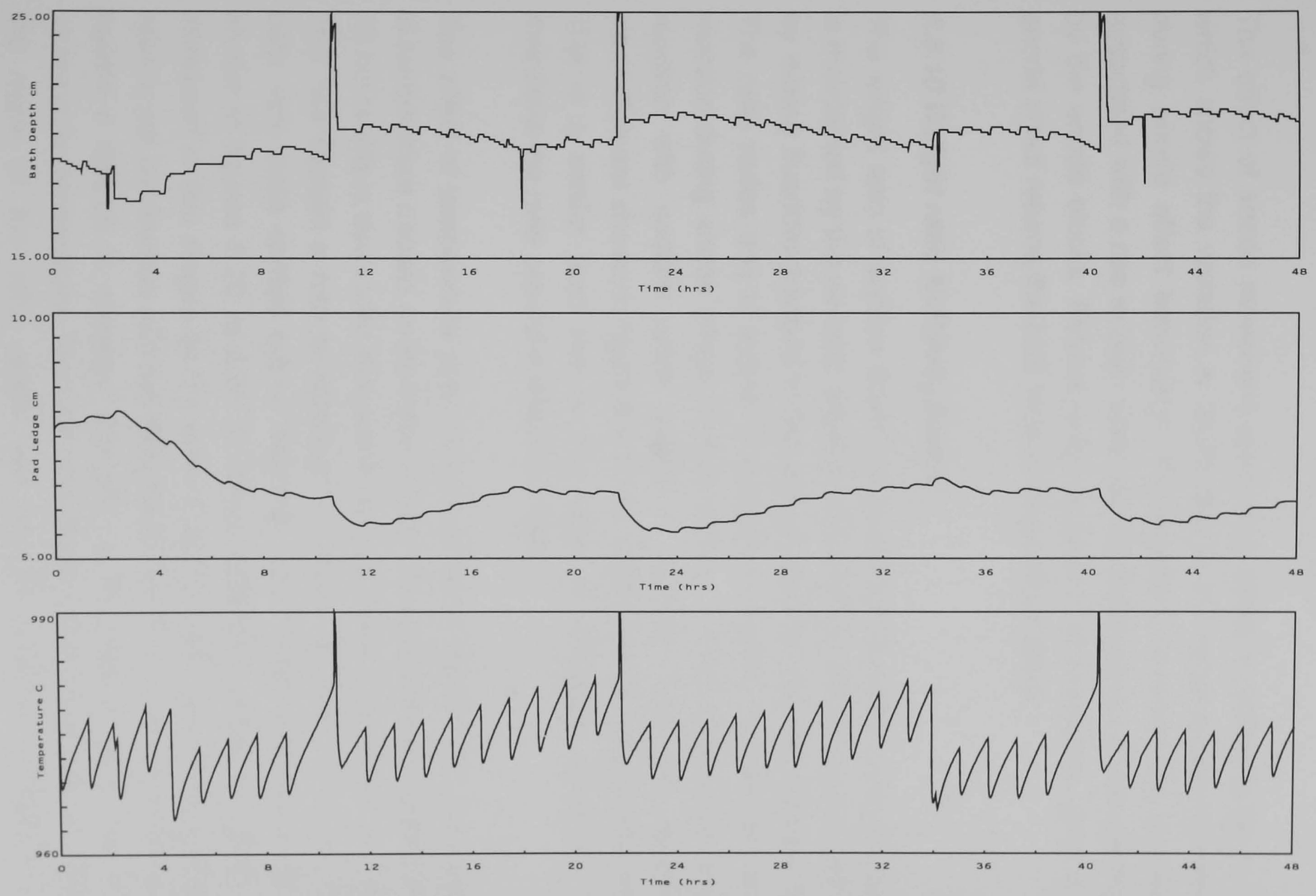

Figure 6.17 Change in Temperature and Bath Depth after a Simulated Increase in the Target Voltage of 0.2V

In the simulation of the step change in target voltage to 4.49 V the bath depth initially drops as the anodes are raised in the bath then increases as the ledges and crust melt into the electrolyte due to the overall rise in temperature associated with a voltage increase.

The effect of anode movement upon bath depth is shown in figure 6.18 which shows the variation in depth due to the large anode movements during anode effect termination. As expected, lowering the anodes is associated with a rise in bath depth due to displacement of the electrolyte by the anode blocks. Returning the anodes to their position prior to the anode effect returns the bath level to its previous depth.

6.6.10 Weight ratio NaF/AlF_3 (Ratio)

The weight ratio of sodium fluoride to aluminium fluoride in the electrolyte is maintained by the periodic addition of aluminium fluoride to the melt and by mixing fluorides trapped in the exhaust gases with the alumina feed. The ratio varies due to losses of aluminium fluoride by volatilisation, by reaction during anode effects to form carbon fluoride compounds and by reaction with sodium oxide added in alumina feed. The results of simulation are shown in figure 6.5 for an addition of 25 kg every 24 hours. This is a similar feed rate to that used at Anglesey Aluminium and maintains the ratio around a stable average.

The effect of temperature upon ratio is shown in figure 6.19. An increase in temperature causes an increase in ratio to a new average. Over the first 13 hours this is due to the increase in target voltage from 4.29 V to 4.49 V. This has caused a rate of increase of about 0.0023 hr^{-1}. The results of bath ratio tests carried out at Anglesey upon three industrial cells are shown in figures 6.20 to 6.22. In these tests the voltage set point was increased in two stages by 0.1 volts at each stage. The measurement of ratio is not continuous and the fluctuations in ratio of the sampling period makes it difficult to compare the rate of increase in ratio due to the increase in temperature. The rate of increase of ratio with time is given by the slope of the ratio graph and ranged between 0.0028 hr^{-1} and 0.0050 hr^{-1}. This compares favourably with the simulated value although the simulated value is at the lower end of the range. The reason for this is the lower temperature increase in the simulation in which the 0.2 V

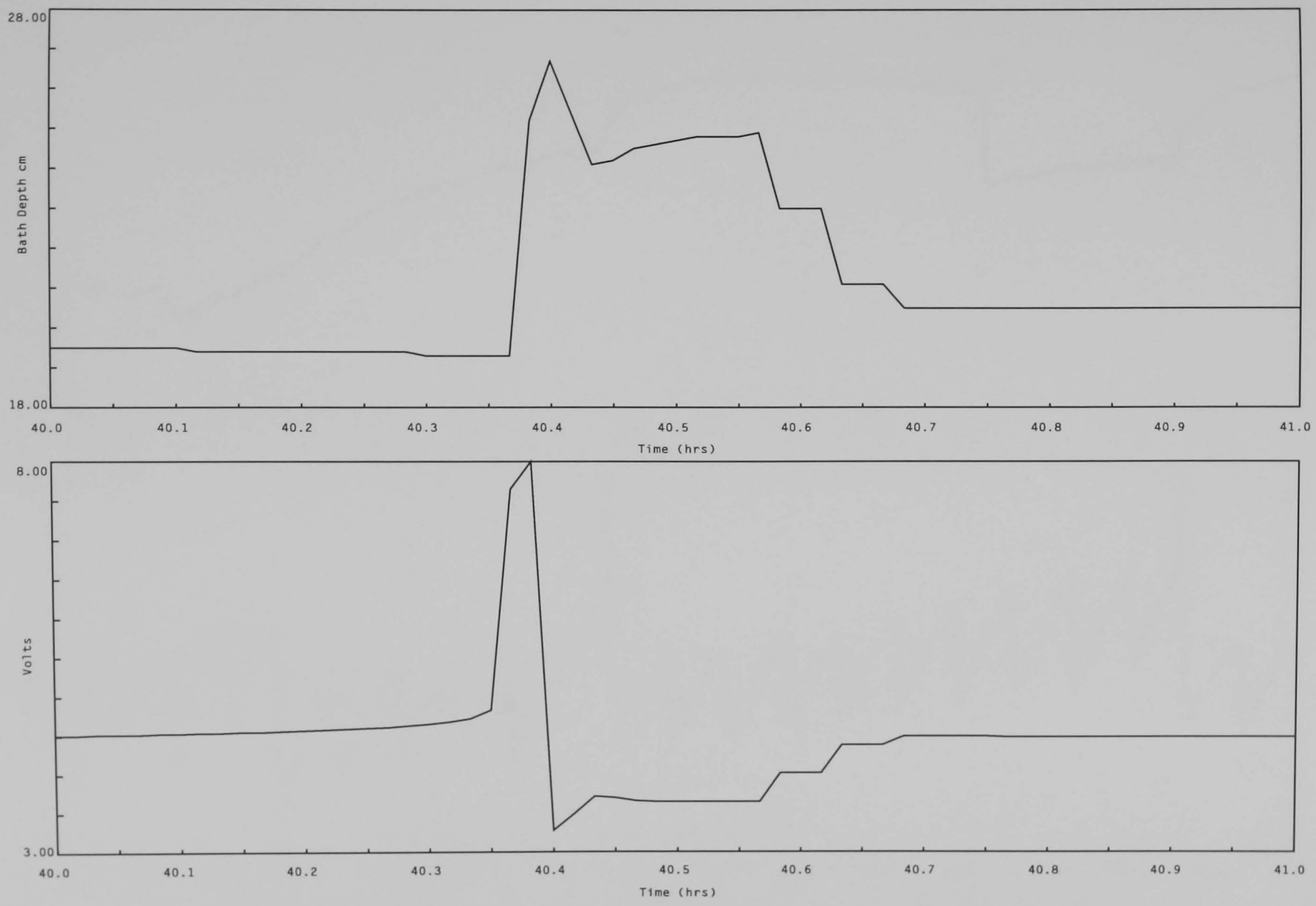

Figure 6.18 Simulated Effect of Anode Movement During Anode Effect Termination

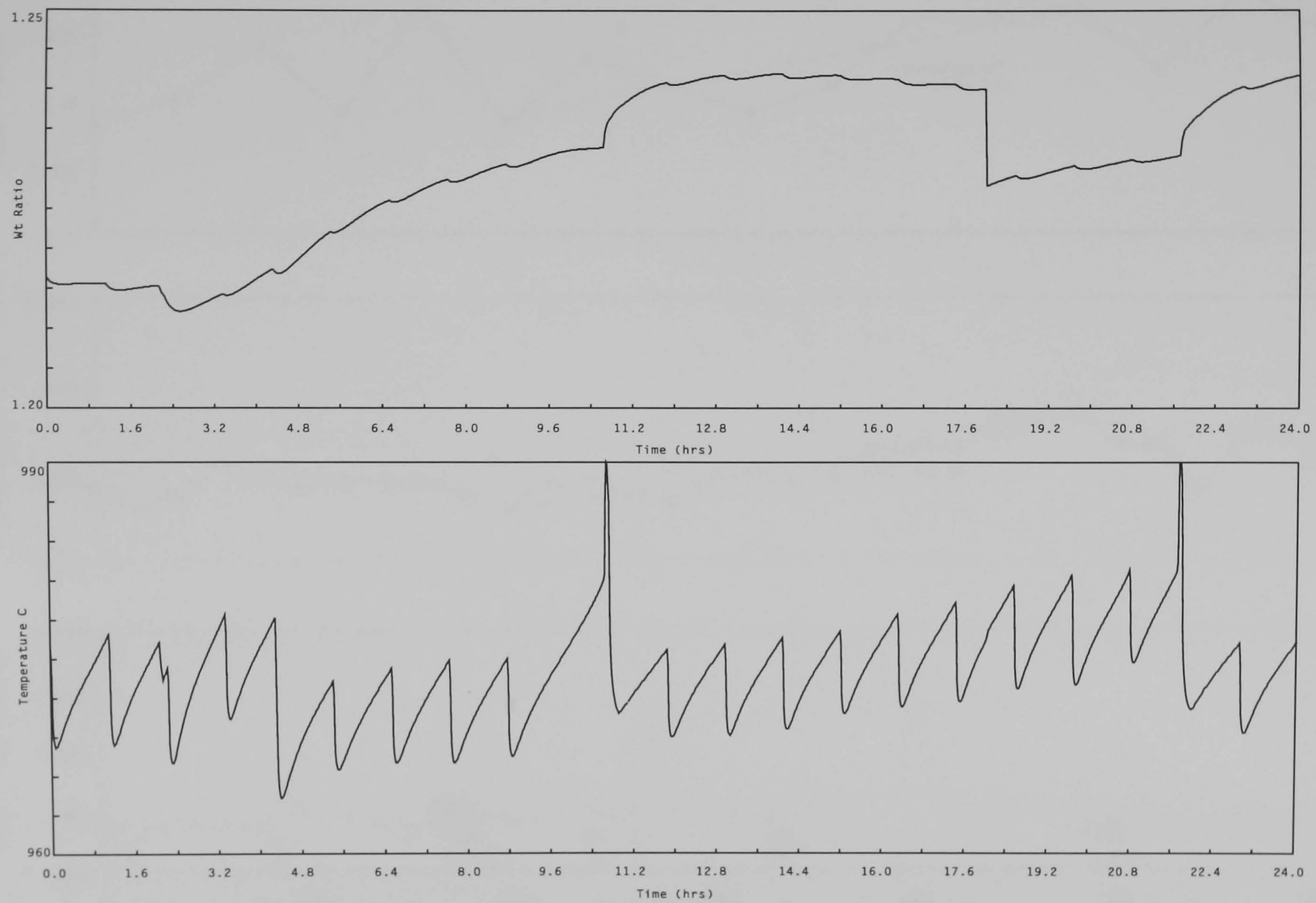

Figure 6.19 Simulated Dependence of Ratio upon Temperature

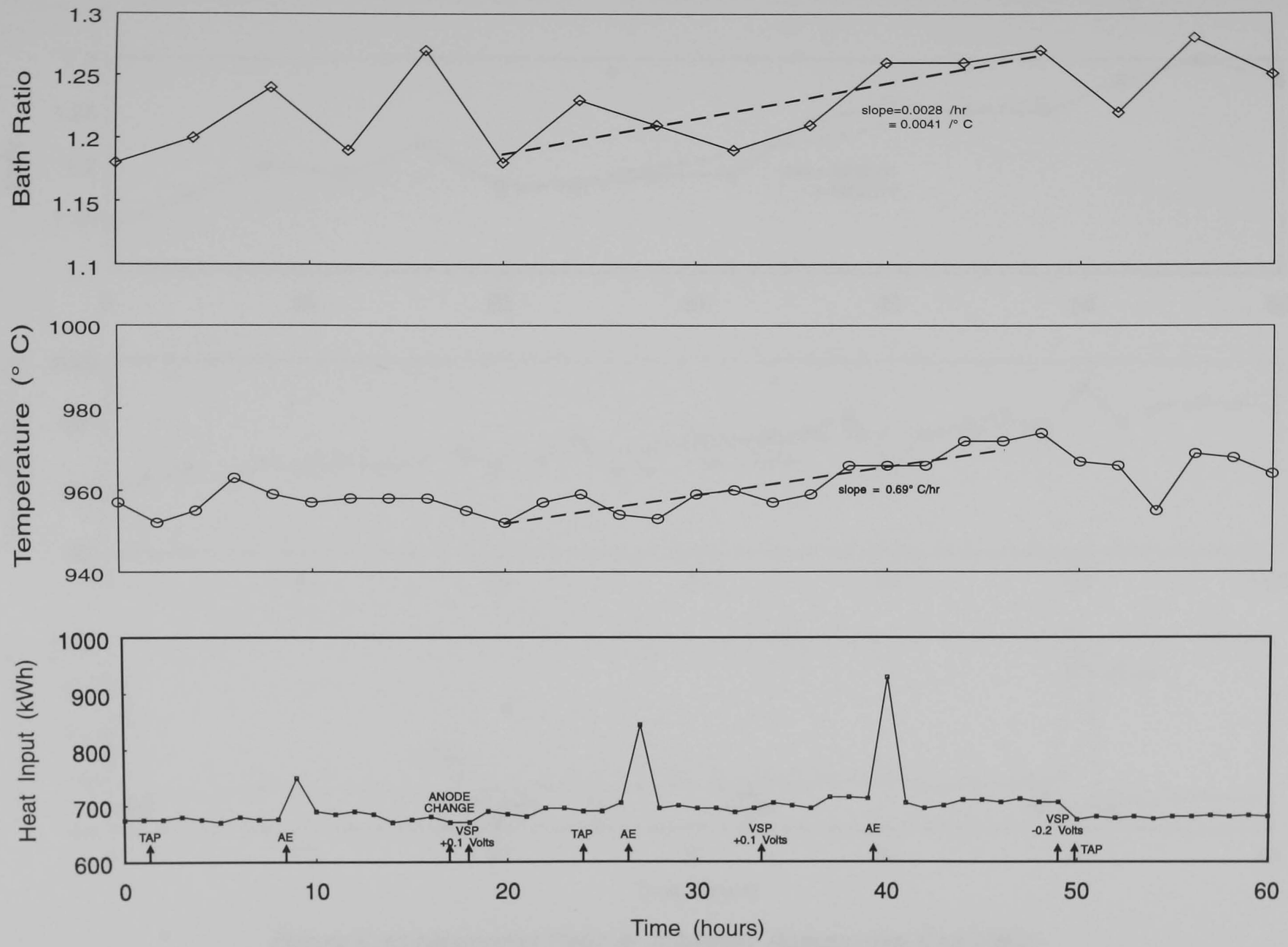

Figure 6.20 Measured Ratio in Anglesey Aluminiums Cell 1B61

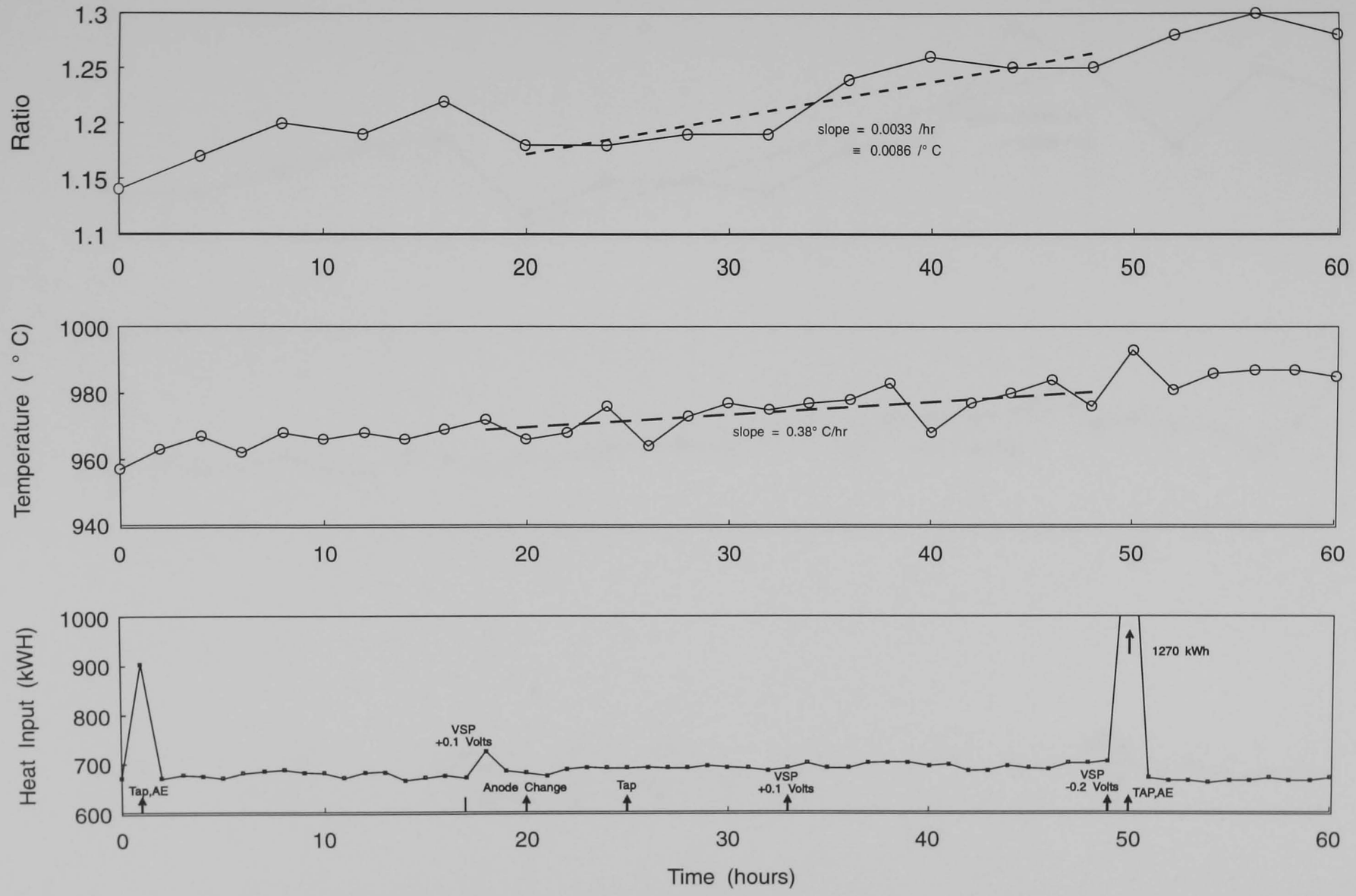

Figure 6.21 Measured Ratio in Anglesey Aluminiums Cell 1B62

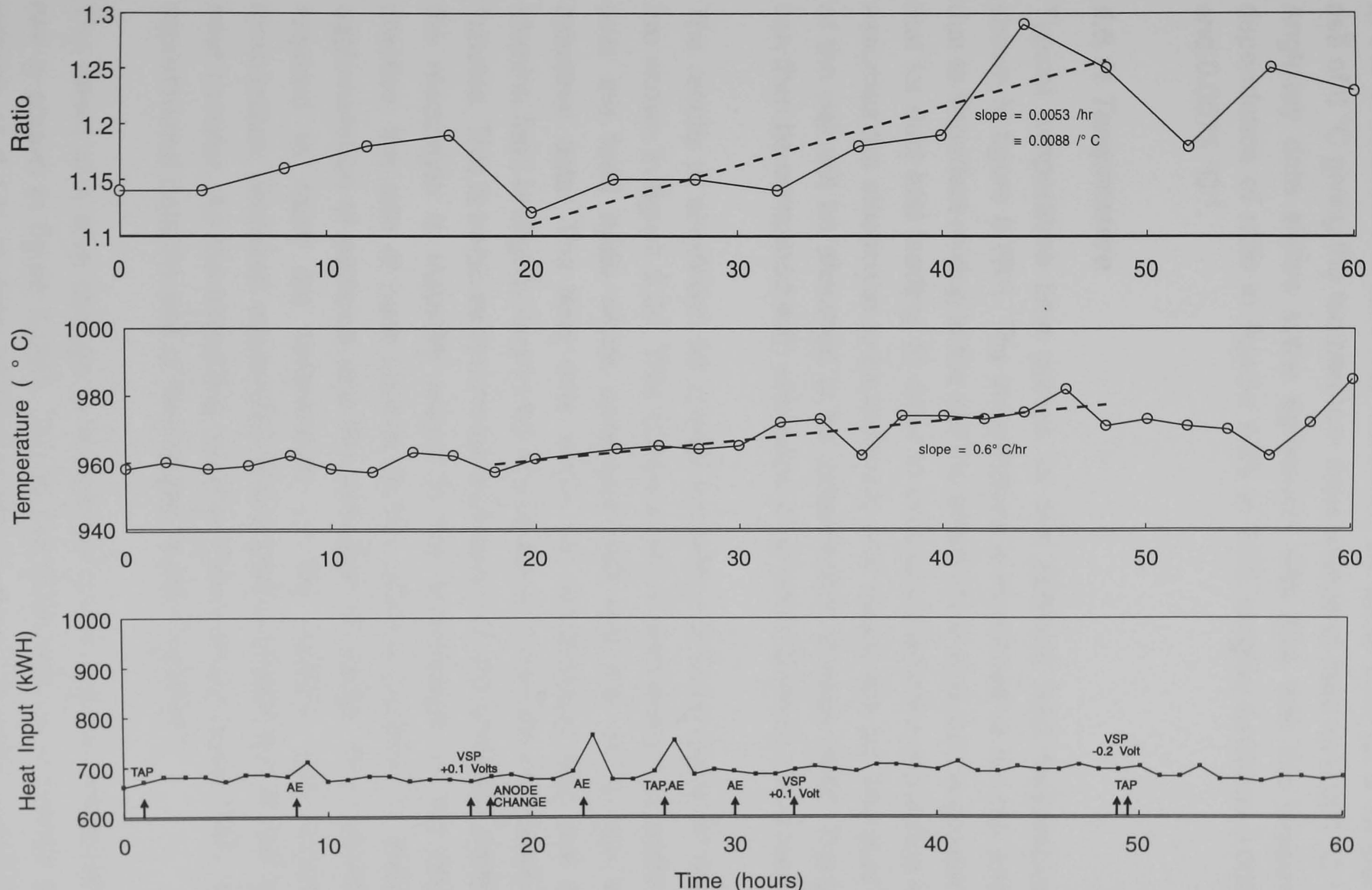

Figure 6.22 Measured Ratio in Anglesey Aluminiums Cell 1B63

increase is accompanied by a rise of 6 °C compared to a rise of about 15 °C in the experimental results.

In the simulation the ratio has increased by about 0.03 for a temperature rise of 6 °C giving the temperature dependence of ratio as 0.005 $°C^{-1}$. The Anglesey data shows some agreement with this, with the temperature dependence of ratio in figures 6.20 to 6.22 ranging between 0.005 $°C^{-1}$ and 0.0075 $°C^{-1}$.

6.6.11 Temperature

Typical temperature time curves for two different feed frequencies are shown in figure 6.23[6]. The temperature is measured at the tap end and due to imperfect mixing in the cell the effect of tap end feed is greater than that for duct end feeding. In order to compare this to the simulation which assumes the electrolyte to be thermally well mixed, the tap and duct ends of the cell will be assumed to be independent of each other. The graph can then be compared with simulation of about a 70 minute feed time.

The results of simulation for a feed frequency of 90 kg every 67 minutes are shown in figure 6.24. This shows a rise of temperature of some 8 °C over the feed cycle which compares well with the 11 °C rise in the industrial data. The time over which the temperature falls due to an alumina feed is slightly less in the simulation at 9 minutes compared to 15 minutes. This is because the model assumes that any chemical addition to the electrolyte is instantly raised to the temperature of the melt. In practise, the rate of heat transfer to the alumina particles is limited by agglomeration of particles and the formation of sludge. The overall heat required to raise the temperature of the alumina and hence the temperature decrease associated with a feed is unaffected by the rate of heat transfer. As the simulated cooling time is of the same order as the experimental data the use of this simpler model is justified.

The effect of a step change in voltage upon the average temperature in cell is shown in figure 6.25[6]. This is industrial data for a change in cell voltage of 0.1 V at time 20 hours with temperature being continuously measured at the tap end of the cell. The average temperature of the cell increases from 976 °C to 981 °C over a period of approximately 2 hours, giving a rate of temperature rise of 2.5 °C hr^{-1}. The results of simulation of

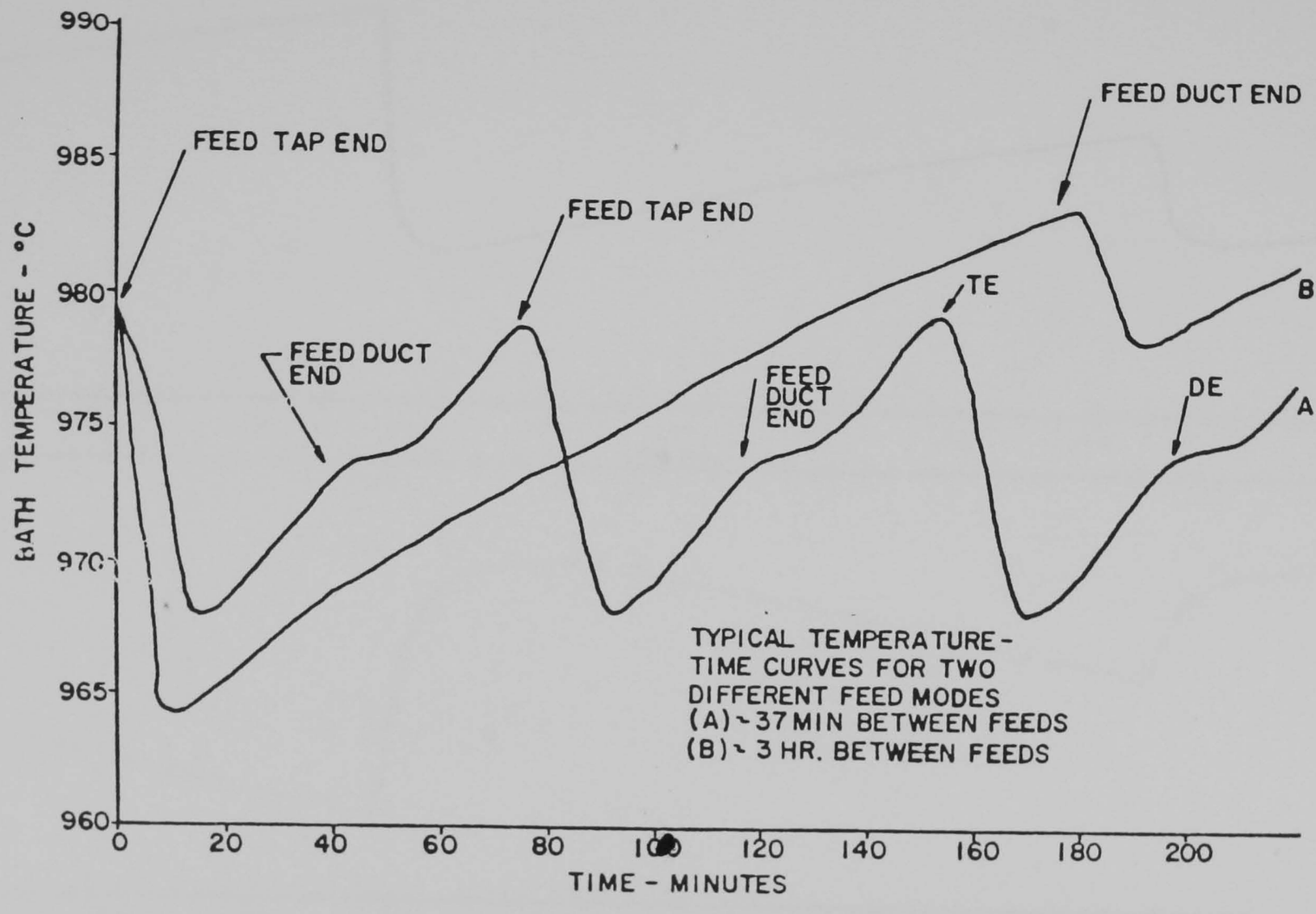

Figure 6.23 Typical Temperature-Time Curves for Two Different Feed Modes[6]

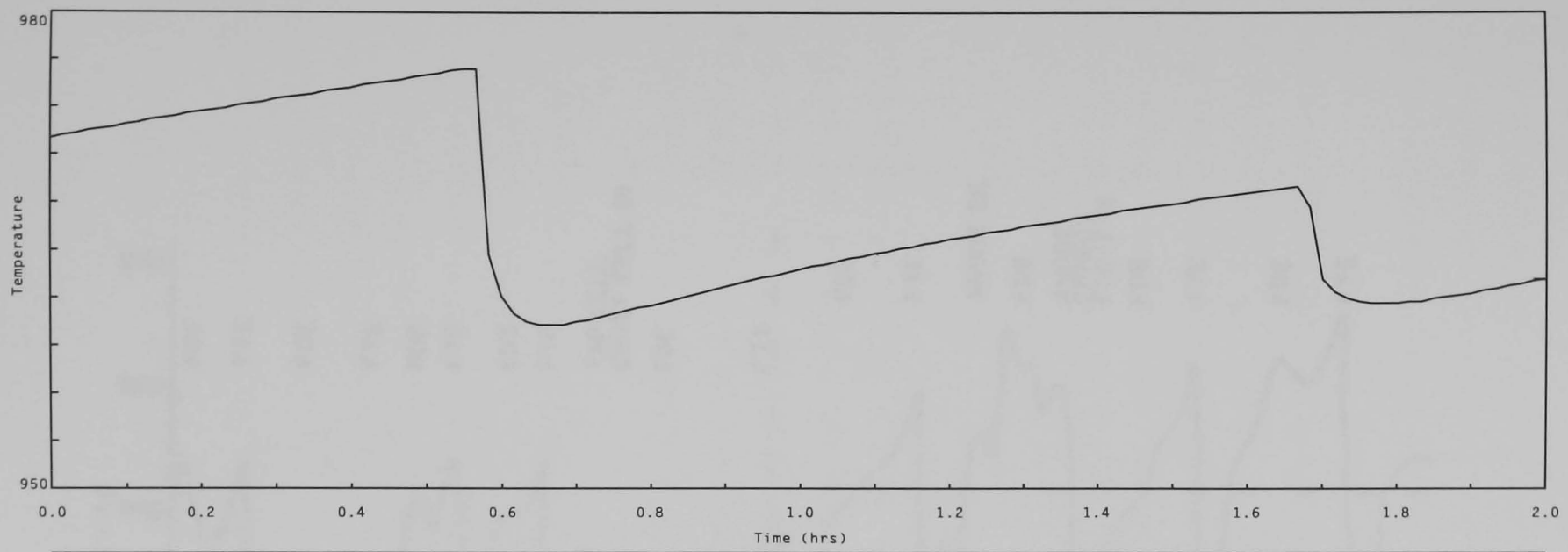

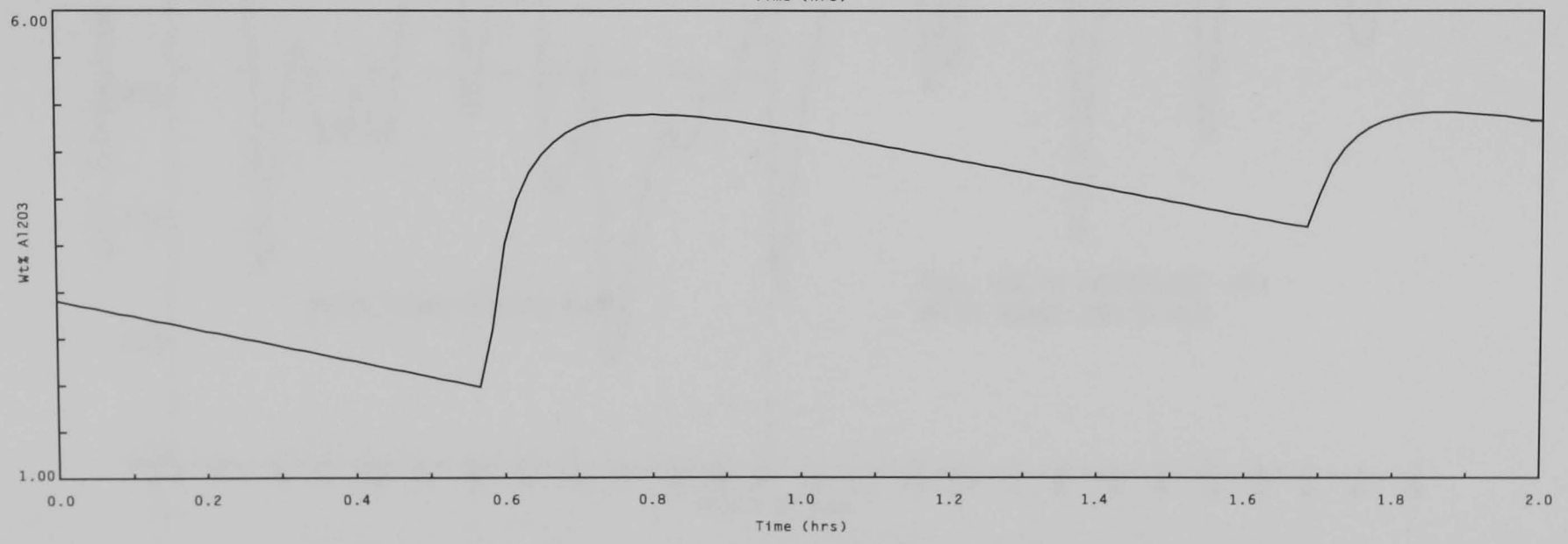

Figure 6.24 Simulated Temperature Profile over a 67 Minute Feed Cycle

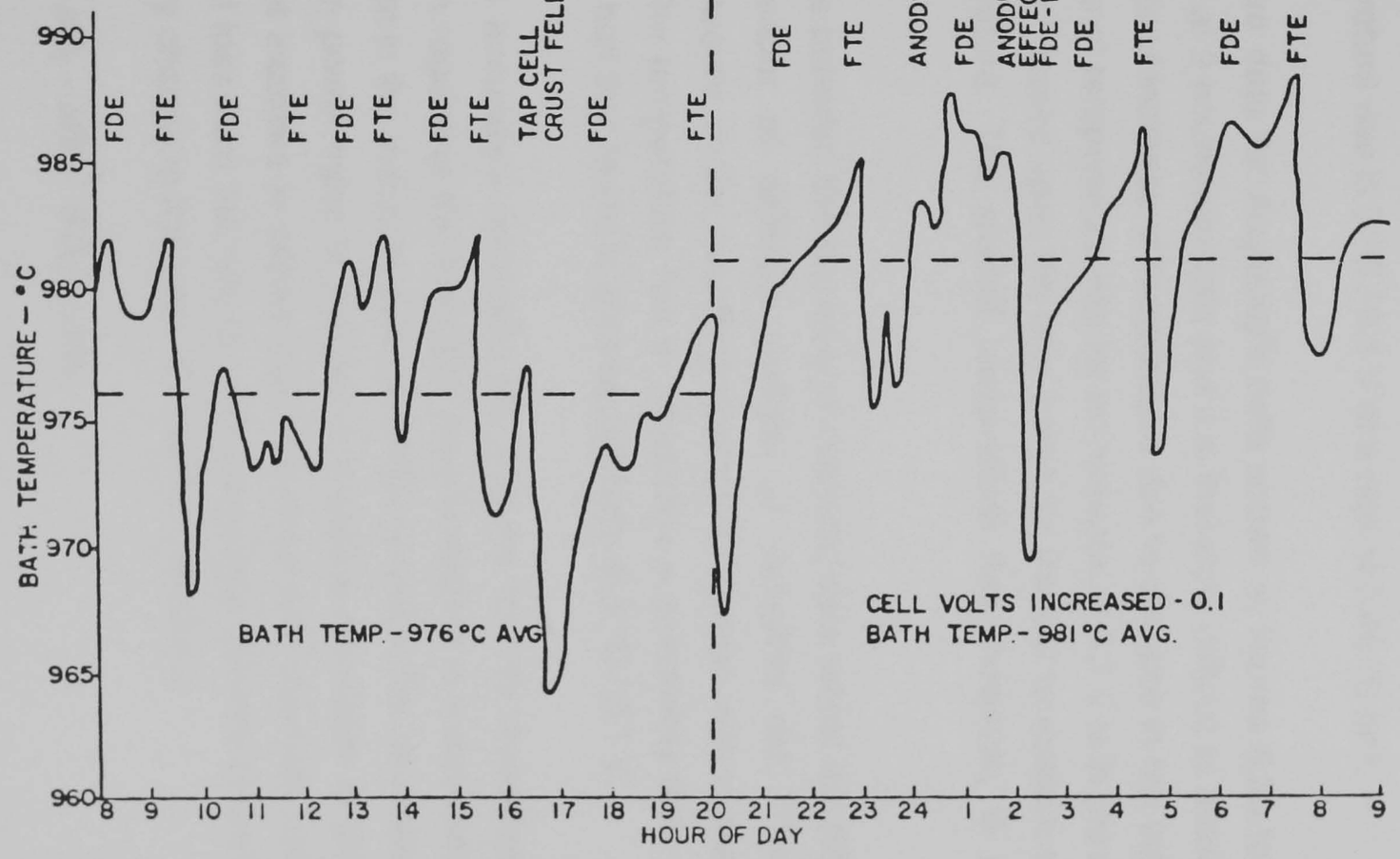

Figure 6.25 Average Temperature in an Industrial Cell After a 0.1V Increase in Operating Voltage[6]

a 0.2 V increase in target voltage upon the temperature and ratio of the electrolyte are shown in figure 6.19. It is difficult to judge the rate of increase of temperature from this graph due to the fluctuation throughout a feed cycle but the overall increase in average temperature is about 6 °C from 968 °C to 974 °C. The accompanying increase in ratio occurs over the first 13 hours of simulation which suggests that this is the length of time that the cell takes to reach its new average temperature. Based upon this, the temperature rise is 3 °C / 0.1 V at a rate of 0.46 °C hr^{-1}.

The temperature data for Anglesey's cells shown in figures 6.20 to 6.22 was measured at 2 hourly intervals and it is therefore difficult to determine an accurate rate of increase of temperature due to changes in cell voltage. The overall rate of temperature rise for an increase of 0.2 V is in the range 0.38-0.67 °C hr^{-1} based upon the time taken for the cell to achieve a new steady temperature. The overall temperature rise, however, is about 7.5 °C / 0.1 V.

The differences between the two sets of industrial data reflect the different dynamic behaviour of different designs of reduction cell. There is agreement, however, in the overall temperature increase with increase in cell voltage. The temperature rise in simulation is somewhat less, being approximately half that found in commercial cells at 3 °C / 0.1 V.

It is difficult to accurately determine the reasons for this discrepancy as the information regarding the industrial measurements is incomplete. The average current in the industrial cells is similar to that in the simulation and the increase in power input to the cell is therefore the same in the both cases. The net increase in power input however also depends upon the change in heat loss from the cell, the change in heat transfer to the frozen ledges and any change in the rates of chemical reactions.

$$\Delta Q_{I,net} = \Delta Q_I - \Delta Q_L - \Delta Q_{ht} - \Delta Q_R \qquad (6)$$

The temperature increase in the cell is then determined by dividing the net power input by the thermal mass of the cell

$$\frac{dT}{dt} = \frac{\Delta Q_{I,net}}{M_{bath} \cdot Cp_{bath} + M_{pad} \cdot Cp_{pad}} \qquad (7)$$

where M_{bath} = mass of electrolyte
Cp_{bath} = specific heat of electrolyte
M_{pad} = mass of aluminium pad
Cp_{pad} = specific heat capacity of aluminium pad

The main parameters affecting the temperature increase are therefore the volumes of aluminium and electrolyte in the cell and the composition of the electrolyte. These directly affect the thermal mass of the cell and contribute to the heat transfer and heat loss terms in the determination of the increase in net power input.

The heat transfer to the sidewalls is given by

$$Q_{bf} = h_{bf} A_{bf} (T_b - T_{liq}) \quad (8)$$

$$Q_{mf} = h_{mf} A_{mf} (T_b - T_{liq}) \quad (9)$$

where h = heat transfer coefficient
A = area for heat transfer
T_b = bulk temperature of electrolyte and metal pad
T_{liq} = liquidus temperature of the electrolyte
suffix
bf refers to bath/ledge interface
mf refers to metal pad/ledge interface

The area for heat transfer is directly related to the depth of the electrolyte and aluminium pad and hence the volume of these two sections. Both the heat transfer coefficient and liquidus temperature of the electrolyte are dependent upon the composition of the electrolyte. As these parameters are not available for the industrial cells it is impossible to determine the accuracy of the temperature rise predicted although it is to be expected that the Anglesey Aluminium cells are operated at a composition close to that used in the model. It is therefore likely that the heat transfer coefficients used in the model require some tuning with the simulated results being compared to additional industrial measurements where the above parameters have been recorded.

A contributing factor to this discrepancy is also the increase in current efficiency in the simulation causing a reduction in the heat input to the cell. In practise, an increase in temperature is usually accompanied by a reduction in current efficiency caused by an increase in the rate of the back reaction of aluminium to alumina and an associated increase in heat input. In the simulation the increase in the interelectrode gap to acheive the new target voltage appears to give a greater increase in current efficiency than the decrease accorded by the rise in temperature. This reduction in the rate of the back reaction reduces the heat output of the chemical reaction and hence the net heat input. It may be that the model for the dissolution of aluminium into the electrolyte has too great a dependency upon the interelectrode gap and not enough upon the temperature and this should be investigated further.

A continuous record of electrolyte temperature during anode effect in a commercial cell is shown in figure 6.26[6]. This shows an anode effect lasting about 4 minutes. The normal increase in bath temperature accelerated markedly about six minutes prior to anode effect. During anode effect, the temperature increased rapidly reaching 1020 °C before the anode effect was terminated. The temperature returned to the value prior to anode effect in about 10 minutes due to the addition of alumina feed.

The simulated variation of temperature during anode effect is shown in figure 6.27. This shows good agreement with the data in figure 6.26 with a marked increase in the rate of temperature rise about five minutes prior to anode effect and the return to the pre-anode effect temperature about 10 minutes after the anode effect termination sequence has been activated. The maximum temperature achieved in the simulation is 30 °C less at 990 °C associated with a maximum voltage during the anode effect of 27 V. Unfortunately, no information is given for the maximum voltage achieved in the commercial cell, although this is typically in the range 25-40 V and it is reasonable to assume that the higher temperature is due to a larger anode effect voltage.

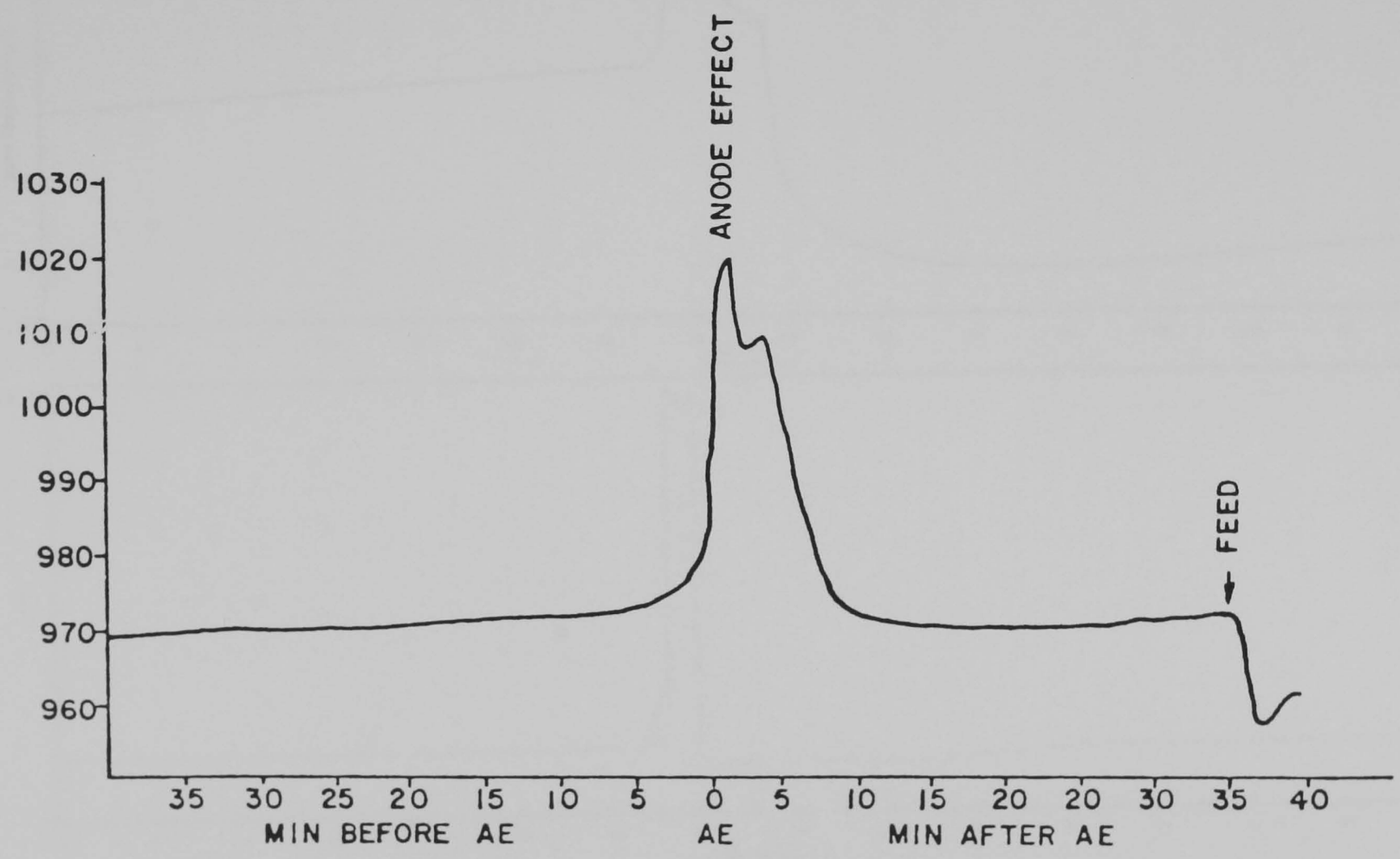

Figure 6.26 Temperature in an Industrial Cell During Anode Effect[6]

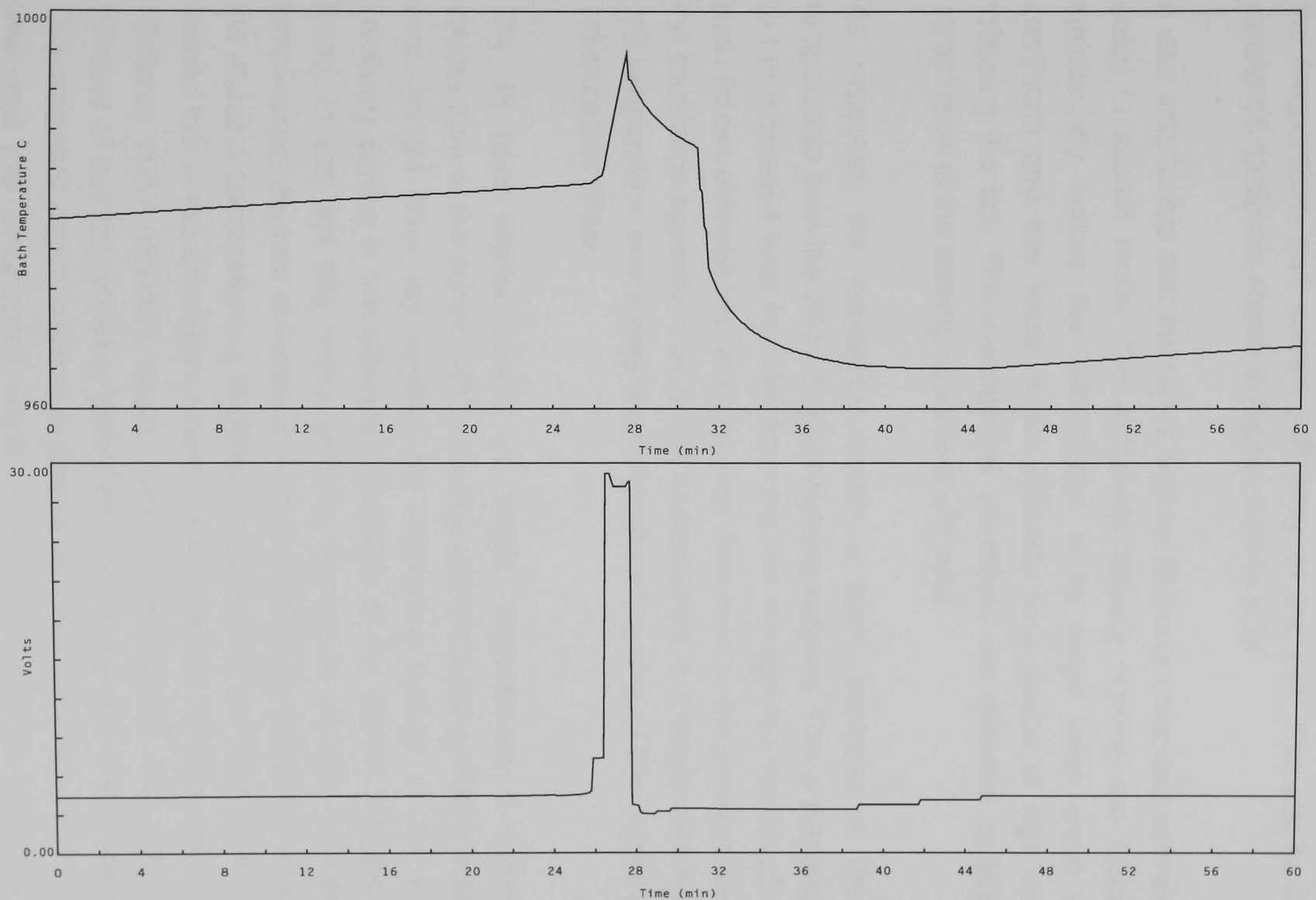

Figure 6.27 Simulated Temperature Profile During Anode Effect

6.7 Plant Trials

Since this work was completed at Newcastle University, the simulation has been in use at Anglesey Aluminium to investigate the cell operation. An early study considered the effect of changing the metal tap interval upon the temperature and current efficiency of the cell. The results of the simulation study are shown in figures 6.28 to 6.30.

It was unfortunate that the tap at around 50 hours coincided with the cell being in search mode. The automatic tapping routines are unable to successfully restore the cell voltage to its target value under these conditions and this leads to an artificially long period of high voltage following the tap. The average cell conditions are distorted by this, but comparison of the tapping regimes is still valid.

As expected, the simulation shows a slight decrease in the cell temperature from the 24 to 32 hour tapping regimes. This is primarily due to the increased heat transfer from the cell through the increased metal pad / frozen sidewall interface. As was discussed in the previous section, the simulation appears to be a little unresponsive to changes affecting the cell temperature and it may be that improved tuning of the model would enhance this effect.

The 48 hour regime shows no further improvement in either the temperature or the current efficiency, the efficiency being slightly improved over the 24 hour tap regime. An interesting feature of the current efficiency curves is the difference in shape of the curves between feed times, In the first fifty hours, prior to the period of high voltage and temperature, the rate of increase of current efficiency increases rapidly as the alumina composition is depleted at the end of the feed cycle. In the second half of the simulation, where the temperature is higher, the current efficiency curve shows a much more rounded profile, with the rate of increase of current efficiency tailing off towards the end of the feed cycle. This smoother profile leads to a greater average efficiency over the feed time and the unexpected result of increased current efficiency with increasing temperature. This is due to the strong dependence in the model of the aluminium dissolution on the interelectrode gap. In should be noted that in the second half of this simulation the acd is unreasonably large and as such may not be truly indicative of the performance of the

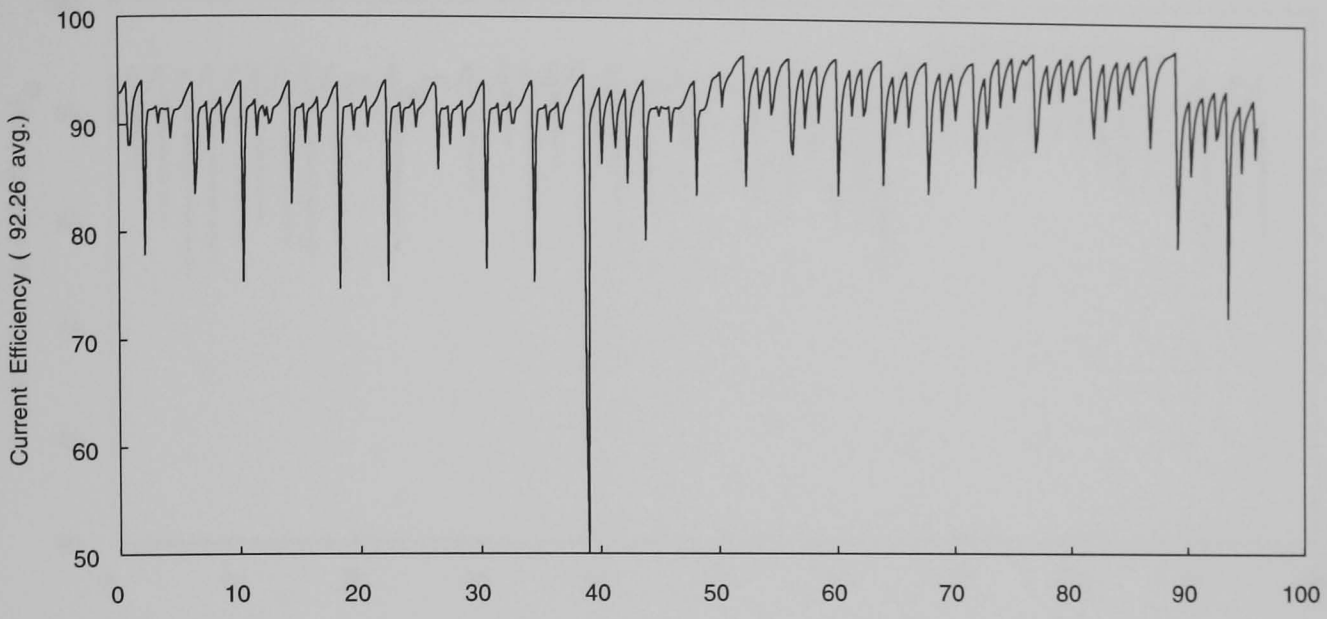

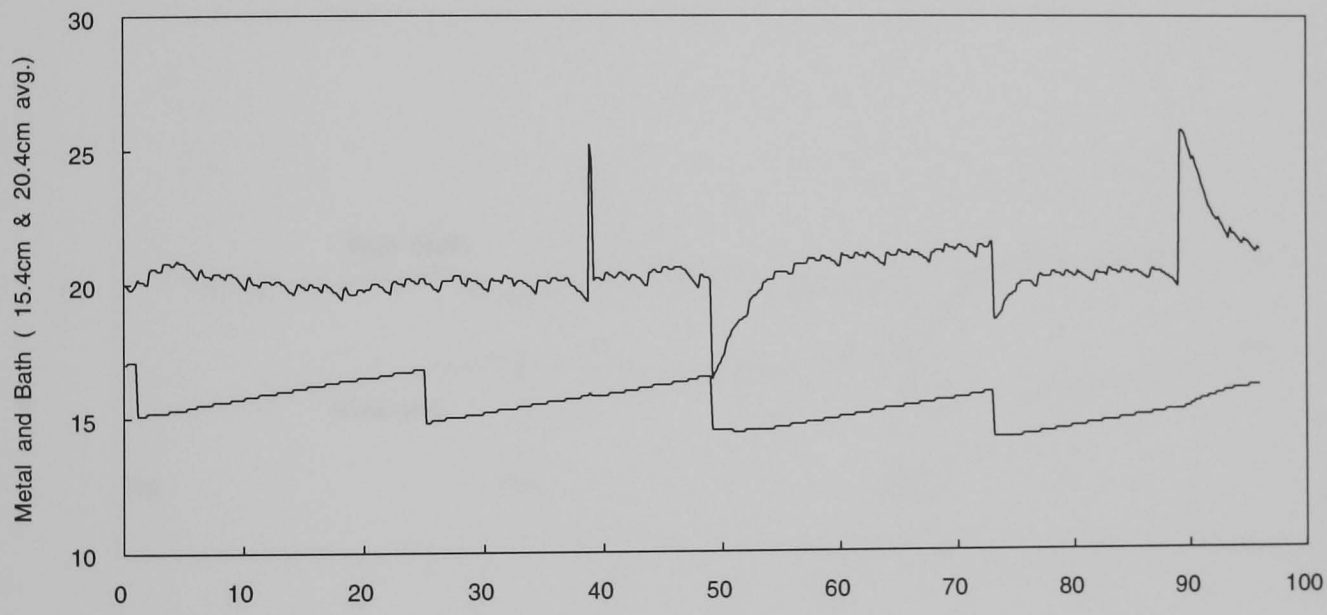

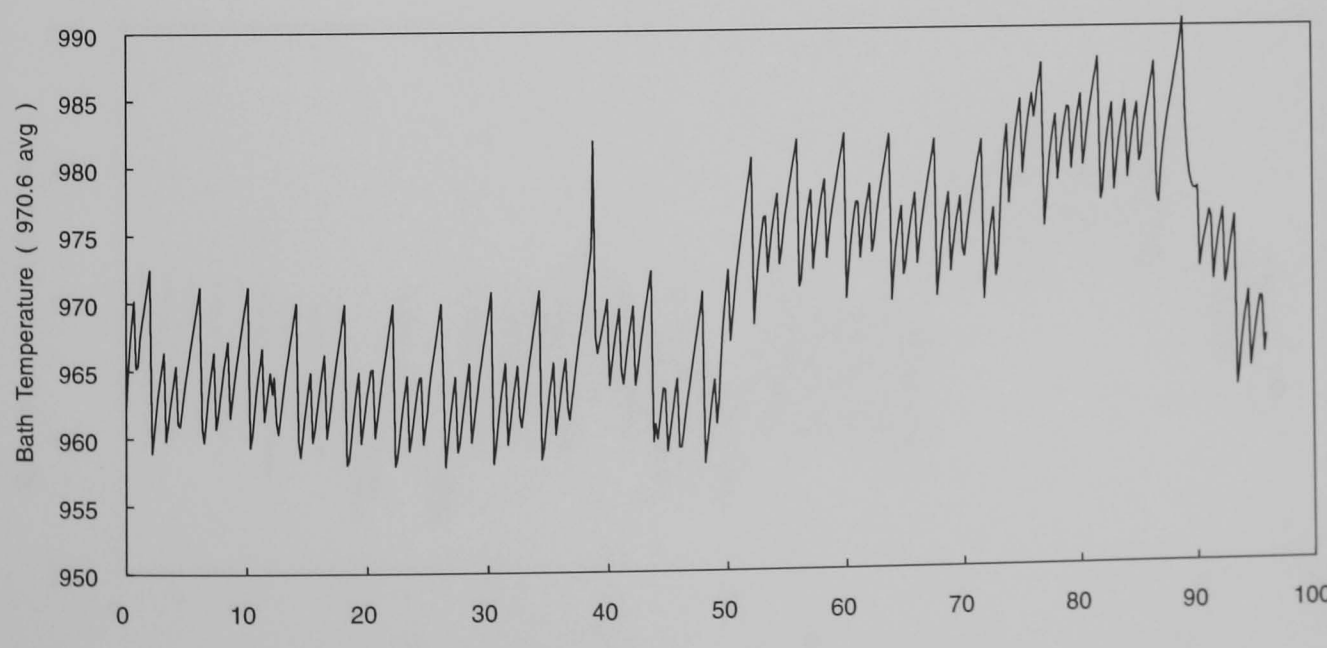

Figure 6.28 Simulated Results of 24 Hour Tapping Schedule

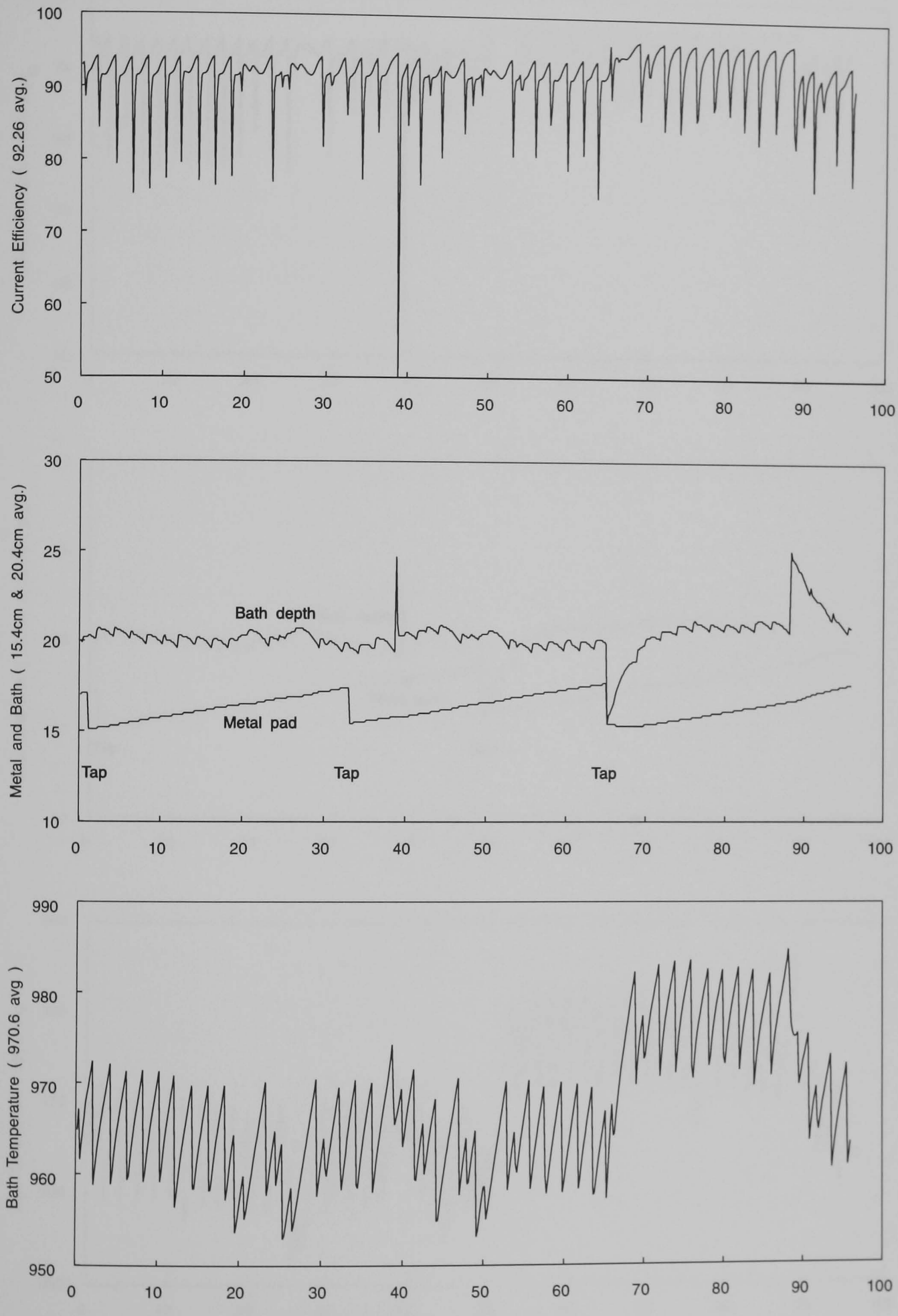

Figure 6.29 Simulated Results of 32 Hour Tapping Schedule

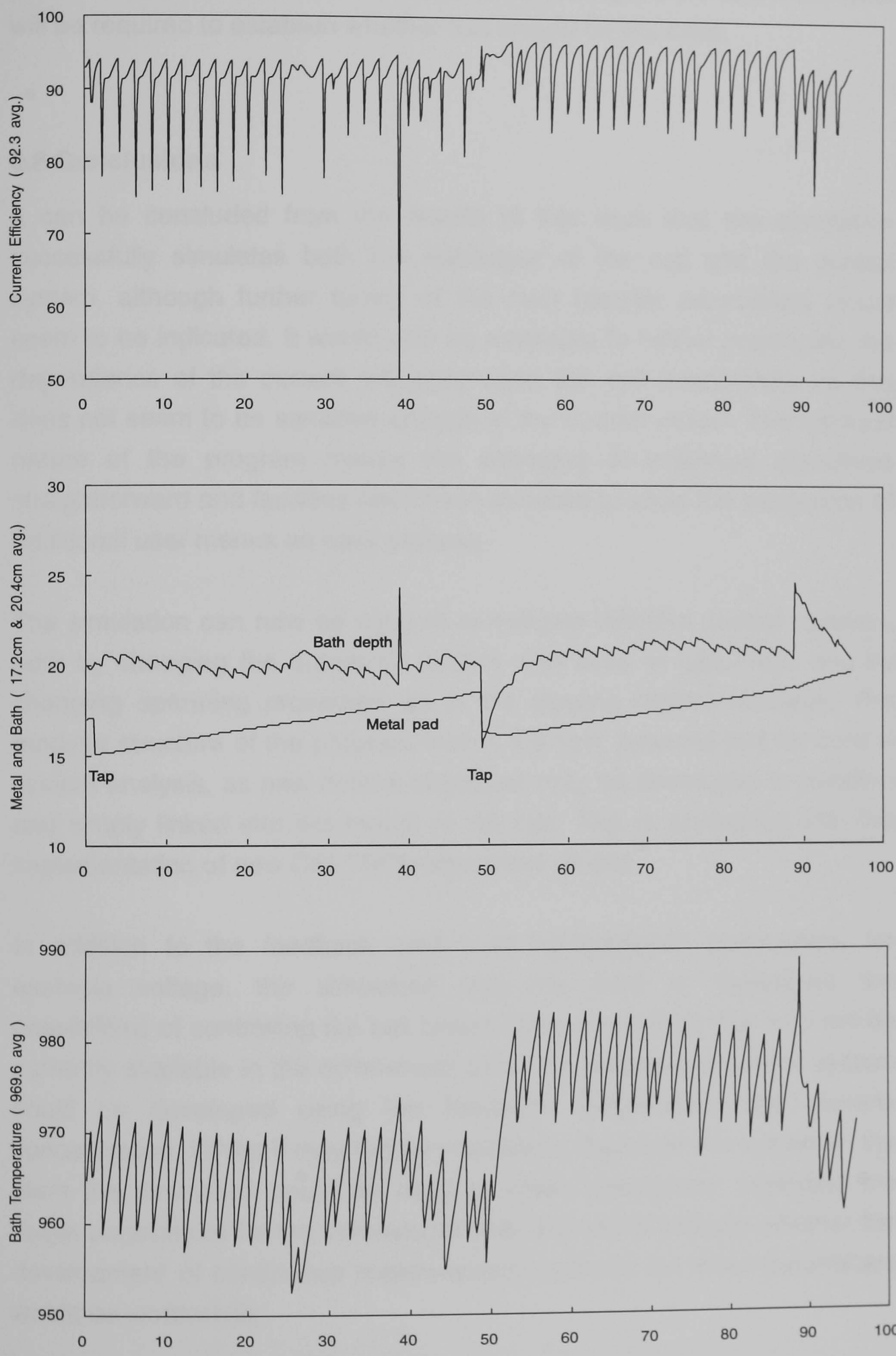

Figure 6.30 Simulated Results of 48 Hour Tapping Schedule

model. This is however, further evidence that the current efficiency in the model may be biased towards acd rather than temperature and more work will be required to establish whether this should be the case.

6.8 Conclusions

It can be concluded from the results of this work that the simulation successfully simulates both the behaviour of the cell and the control system, although further tuning of the heat transfer parameters would seem to be indicated. It would also be advisable to further investigate the dependence of the current efficiency upon the cell temperature as this does not seem to be sensitive enough in the current model. The modular nature of the program makes the changing of individual algorithms straightforward and facilities have been included to allow the integration of additional user menus an easy process.

The simulation can now be used to investigate different control systems, both by changing the automatic control algorithms in CELTROL and by changing operating procedure as in the tapping regime example. The modular structure of the program makes it a very powerful tool for control system analysis, as new control strategies may be developed in isolation and simply linked into the model of the cell. This is analogous with the implementation of new CELTROL algorithms on site.

In addition to the feedback control of 'conventional' parameters, for example voltage, the simualtion may be used to investigate the possibilities of controlling the cell based upon information that may not be currently available in the commercial cells. For example, a control system could be developed using the feedback temperature and alumina concentration. Whilst it may not be possible to duplicate this system in the plant the simulation could be used to obtain information regarding the target parameters for the commercial cells and could indicate whether the development of continuous measurement methods for these parameters would be worthwhile.

	al6c3	al6c4	al6c5	al6c6	al6c7
Current (kA)	151.0	151.0	151.0	151.0	151.0
Cell Voltage (V)	4.40	4.30	4.50	4.41	4.41
Target Volts (V)	4.39	4.29	4.49	4.39	4.39
Bath Depth (cm)	17.95	18.68	20.49	18.94	19.26
Pad Depth (cm)	13.26	12.89	12.72	14.18	11.86
Pad Ledge (cm)	6.64	7.45	6.24	6.72	6.63
Current Efficiency (%)	90.46	89.73	91.22	90.44	90.48
ACD (cm)	4.67	4.36	5.00	4.68	4.69
Alumina Conc. (wt%)	3.38	3.51	3.10	3.29	3.20
Bath Temp °C	970.5	968.6	974.2	971.4	972.5
Liquidus Temp °C	959.6	958.6	962.6	960.7	961.4
Wt Ratio	1.231	1.221	1.240	1.234	1.237

Table 6.3 Average Parameters From Five 170 Hour Simulations of a Half Break Cell

References

[1] Anglesey Aluminium Internal Memorandum

[2] Waddington, J. and Pearson, T. G., *"Electrode Reactions in the Aluminium Reduction Cell",* Discussions, Faraday Society, 1947, vol 1, pp307-320

[3] Tabereaux, A.T. and Richards, N.E., *"An Improved Alumina Concentration Meter"*, AIME Light Metals, 1983, pp495-506

[4] Wilson, C.A and Tabereaux, A.T., *"Alumina Control in Center-Break Cells"*, AIME Light Metals, 1983, pp479-493

[5] Ek, A. and Fladmark, G. E., *"Simulation of Thermal, Electric and Chemical Behaviour of an Aluminum Cell on a Digital Computer"*, AIME Light Metals, 1973, pp85

[6] Dow, D.W. and Goodnow, W.H., *"Influence of Operating Variables on Reduction Cell Bath Temperature"*, AIME Light Metals, 1972, pp3-20

7.0 Recommendations For Further Work

7.1 Inferential Control

An area of work worthy of investigation with the model is real time control of the aluminium cells using the model to predict parameters in the cell that cannot be measured or are not available on a continuous basis, for example, the alumina concentration. By connecting a real time version of the simulation in parallel with the cell as shown in figure 7.1 the simulation could output the required control signals based upon continuous results of simulation. This would allow the optimal control strategy to be developed continuously for any particular cell.

The model would continually correct its predicted parameters based upon any available data from the cell, eg voltage, tap time, length of anode change, periodic temperatures and electrolyte composition.

The first stage in this work was to develop a real time version of the simulation that was controlled by a CELTROL panel. This was then connected in parallel with a working cell with the aim being the comparison of available experimental data against the predicted parameters. This open loop system would allow the tuning of the model to the particular cell aid in the validation of the model.

7.2 Development of the Real Time Simulation (RTS)

In the development of a Real Time Simulation three areas have to be addressed:

1. A real time kernel
2. Data logging interface
3. Data storage / Operator interface

1. In order for the model to be used successfully for real time control, the simulation must run several times faster than real time. In order to co-ordinate the model and the logging of experimental data for comparison a real time kernel must be developed. The kernel has a number of functions as shown in figure 7.2.

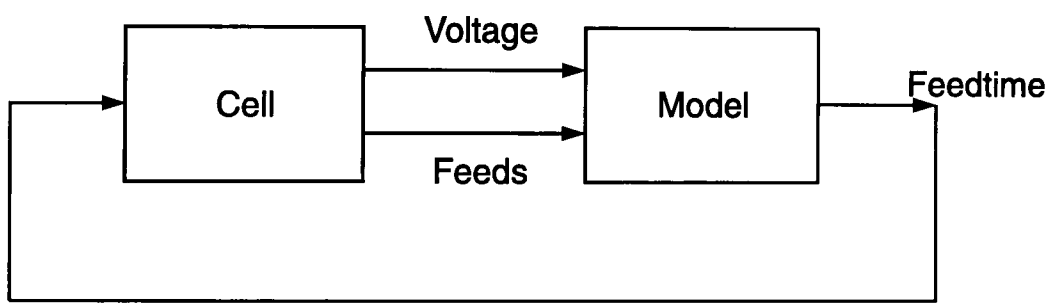

Figure 7.1 Real Time Simulation in Parallel with Working Cell

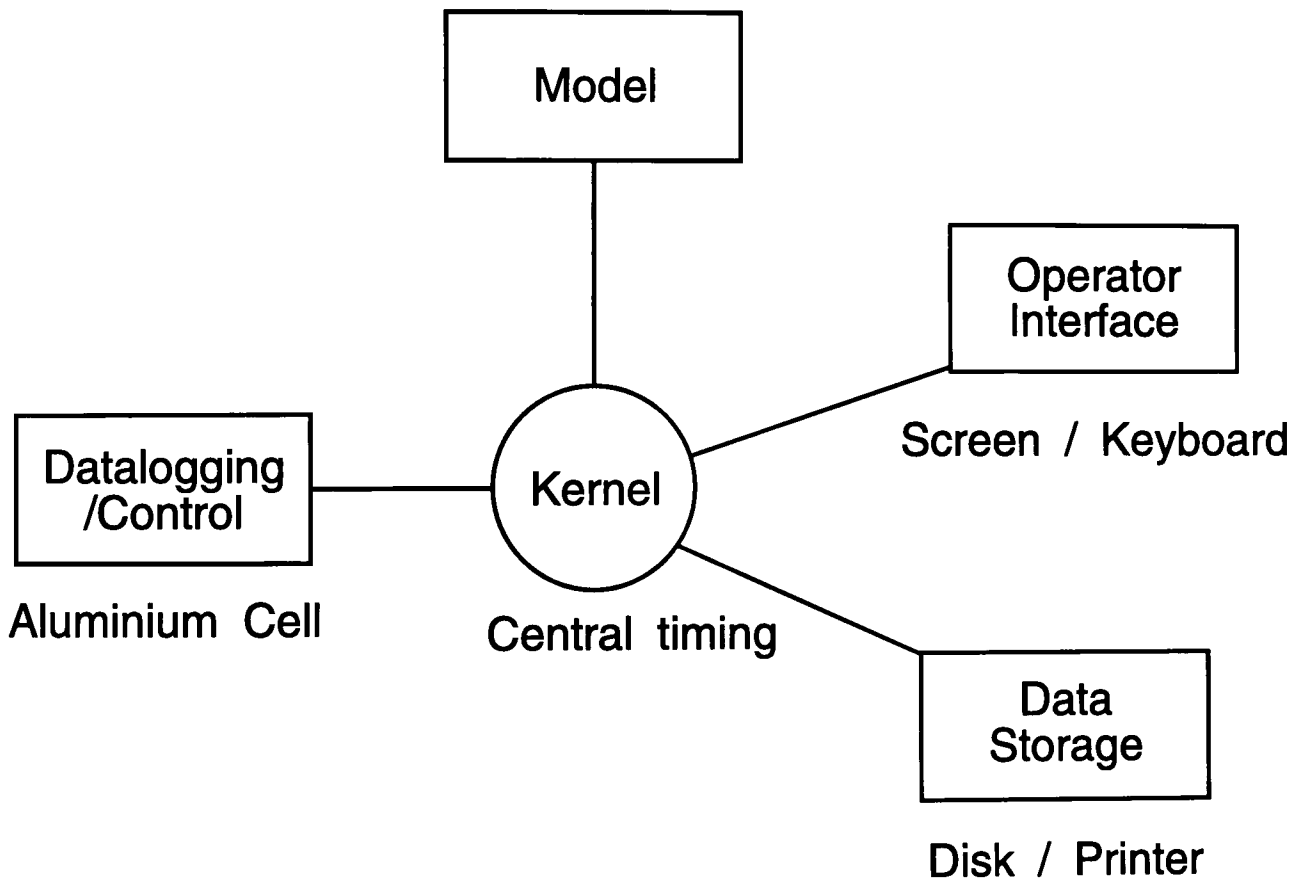

Figure 7.2 Use of Model in Real Time Control

The real time kernel must schedule the events depending upon a pre-set timing and priority. In the simulation the order priority of the tasks is

1) Data logging / Control The control system operates on a 0.1s interval. If a control signal, eg the raising of an anode, is missed then there will be poor agreement between the model and reality. Data logging takes a small amount of run time and therefore can be made a high priority, without being detrimental to the running of the model.

2) Model For good agreement between the model and reality the process must be simulated at a frequent interval. Additionally, it will be necessary to run the model a number of times adjusting various parameters until the results agree with the logged data. The simulation of the process must therefore have a high priority and must also be fast. It may not be necessary however to solve the equations faster than the base interval for the control signals. The noise in the measured data, eg Voltage, prohibits the use of raw data logged at the same interval as the control signals and a filtered signal should be used. It would be sufficient to compare the 'results' at intervals of say 30s, so long as all the control actions are known.

3) Data Storage Data storage to a permanent medium is a comparatively slow process and longer intervals between data sets are generally required. There is no need for the data to be stored all at once but instead it can be buffered and stored during periods when the simulation is in an idle state.

4) Operator Interface The facility must exist for an operator to communicate with the model without interrupting the running of the simulation. This will allow the model to receive information regarding the process that is not available through instrumentation and allows the operator to change the display and storage parameters. This task has a low priority as it must not be allowed to interrupt the simulation or the data logging.

A very simple real time kernel can consist of a timing loop that calls each of the tasks in turn, where the time taken for each task is known. If the lower priority tasks are known to take longer than the interval required for

the higher priority tasks then the higher priority tasks may also be called by the lower priority tasks. For example, if there are three tasks, DATALOGGING, MODEL and STORAGE with descending priorities then the kernel could be written

```
        Call STORAGE
        Timer loop

STORAGE:  Call MODEL
          ..
          ..
          Call DATALOGGING
          ..
          Call MODEL
          ..
          ..
          Call DATALOGGING

MODEL:    ...
          Call DATALOGGING
          ...
          Call DATALOGGING
          ...

DATALOGGING: ...
```

where the ellipsis represents the required code for each task.

This method is cumbersome and requires a great deal of tuning of the timing loops to ensure that all tasks are complete within the required intervals. It does not, however, require any multitasking capabilities and is applicable to most machines and languages.

This approach was originally tried in order to validate the response of the model to the control actions of the CELTROL computer. The program was written in PASCAL and connected to the CELTROL panel via a TCS signal processor.

The CELTROL panel outputs digital signals for the control of the raising and lowering of the crust breakers, the operation of the feed dump and the raising and lowering of the anodes. It inputs an analog signal of the cell voltage in the range 0 to 30 V. The CELTROL IO signals are represented schematically in figure 7.3.

The simulation was connected via the TCS signal processor to the CELTROL panel. Communication between then signal processor and the computer was via the RS232 serial port. This is shown schematically in figure 7.4.

The simulation outputs the simulated cell voltage to the CELTROL panel which returned the control signals for the simulation. Initial trials with an isolated CELTROL panel were successful with the simulation responding correctly to the signals from the panel to raise/lower anodes and feed the cell. The next stage was to connect the simulation in parallel with a working cell so that the simulation would receive the same control signals as the cell in order that the results from the simulation might be compared with the data from the cell. This configuration is shown in figure 7.5.

In this case the CELTROL computer operated upon the actual cell voltage. It was also necessary for the simulation to use the actual line current that was being supplied to the cell. This was obtained as an analog signal through the TCS signal processor.

This experiment was unsuccessful because of the communication link between the computer and the TCS processor. The use of an RS232 link to the signal processor did not allow a reliable means of handshaking between the devices at the speed required and it was necessary to communicate at a low baud rate of 1200 baud. At these speeds however, the simulation was unable to run sufficiently fast to complete the data logging and model solving tasks in the required intervals. The failure to communicate properly with the signal processor caused the computer to hang and it was impossible to get any useful data from this trial, using a very simple real time kernel.

A more sophisticated real time kernel can be written using languages that allow concurrency, that is allow multiple tasks to be run simultaneously.

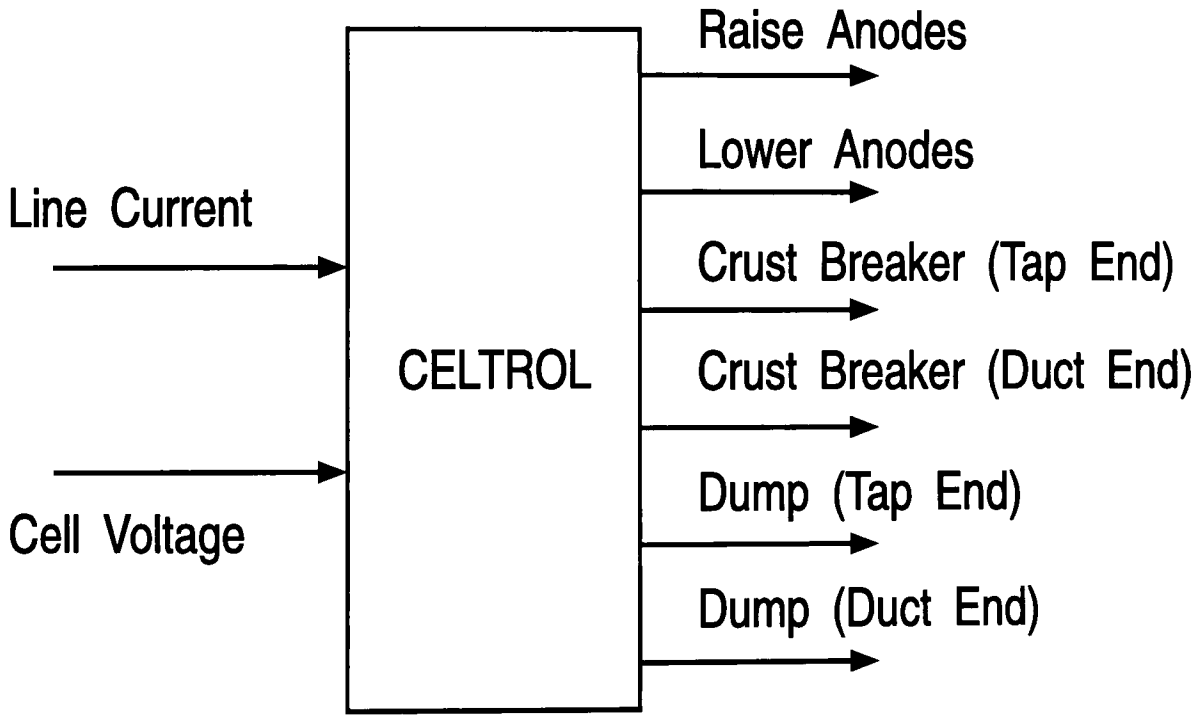

Figure 7.3 CELTROL Analog/Digital Inputs and Outputs

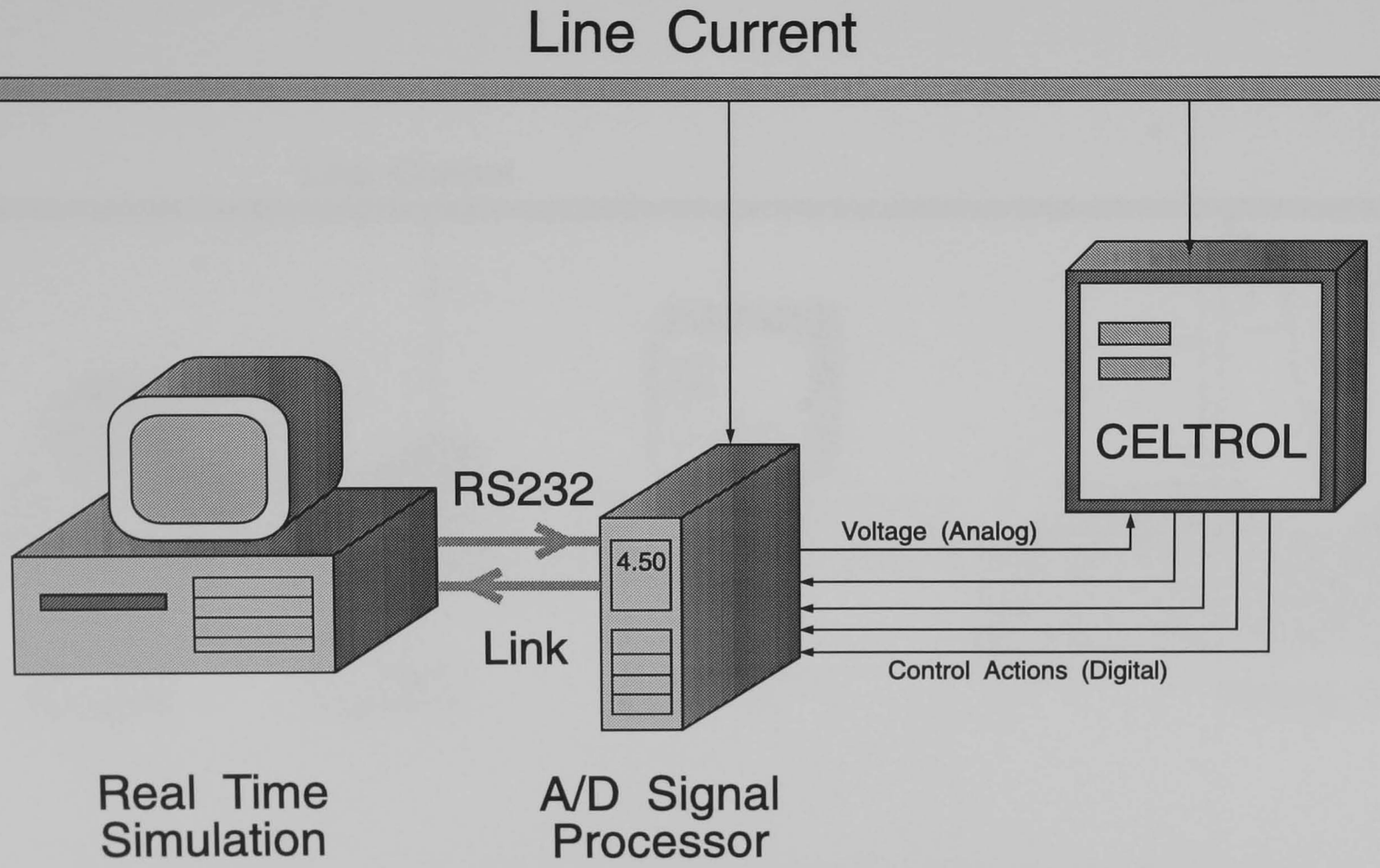

Figure 7.4 RS232 Link Between Simulation and CELTROL

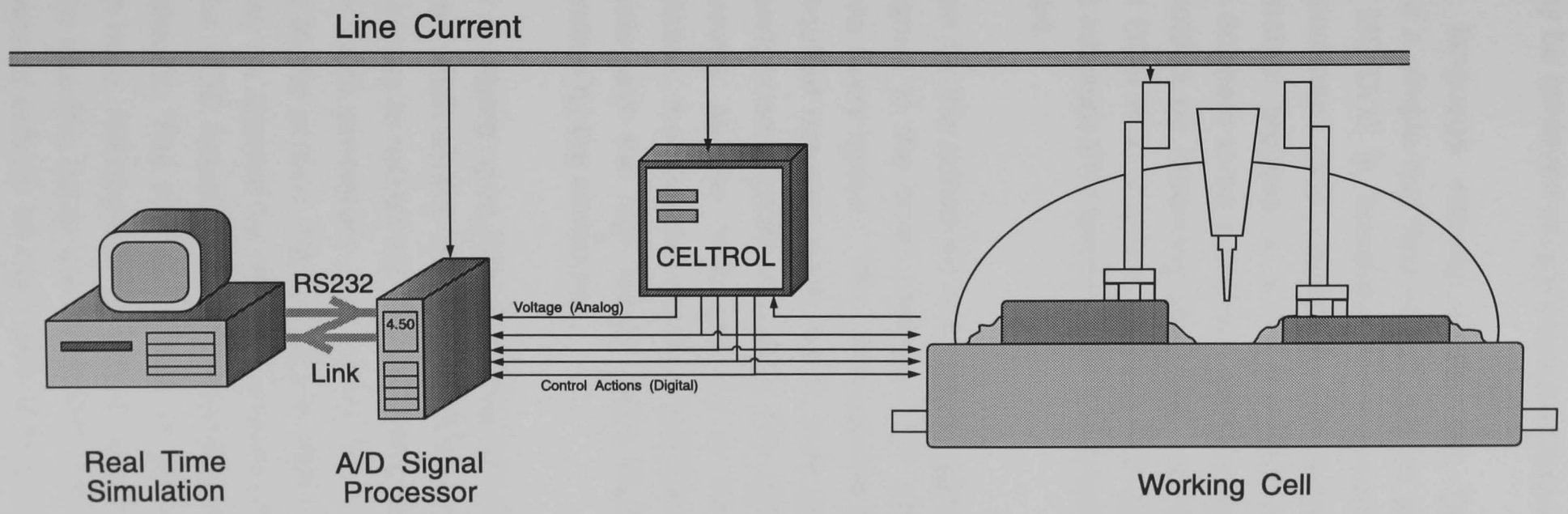

Figure 7.5 Simulation Connected to Working Cell

True concurrency can only be achieved by using hardware that allows several tasks to be processed simultaneously, although pseudo-concurrency may be achieved simply through software.

The Modula-2 language running under MS DOS allows pseudo concurrency and a simple real time kernel may be written to manage the required tasks. MS DOS is, however, non-re-entrant. That is, if DOS is processing a command and control is transferred out of the DOS command to another process, it is not possible to return to the DOS command. This appears to be a problem when writing a real time kernel but may be avoided by observing the basic principle of avoiding task switching whilst DOS is in a critical section. This can be determined by calling the DOS interrupt 21H function 34H which indicates if DOS should not be interrupted.

The flow diagram for the scheduler is shown in figure 7.6. The scheduler should be assigned to the timer interrupt DOS interrupt 1CH which is called 1024 times every second. The timers should be set to the number of timer ticks required between each call to each process and the timer tests must be performed in order of priority. The lowest priority task may be run continuously as the main process to be interrupted. In the aluminium simulation, the operator interface and data storage may be run as the main tasks with the high priority tasks of data logging and the model being handled by the scheduler.

A disadvantage of relying upon DOS not being in a critical period is that it reduces the times when control may be transferred between processes. It is therefore necessary to reduce the number and frequency of critical DOS calls. The main DOS processes that cannot be re-entered are the IO routines, writing to the screen, input from the keyboard and data storage on disk. This may be avoided by directly accessing the relevant hardware without using the DOS functions. This does however make the program very machine specific. The modular nature of Modula-2 can be used to great advantage here. Although the low level routines such as screen I/O must be machine specific, these can be stored in modules with the same names and means of use on all machines. It then becomes very easy to transfer a program between machines by simply recompiling the software with the relevant modules.

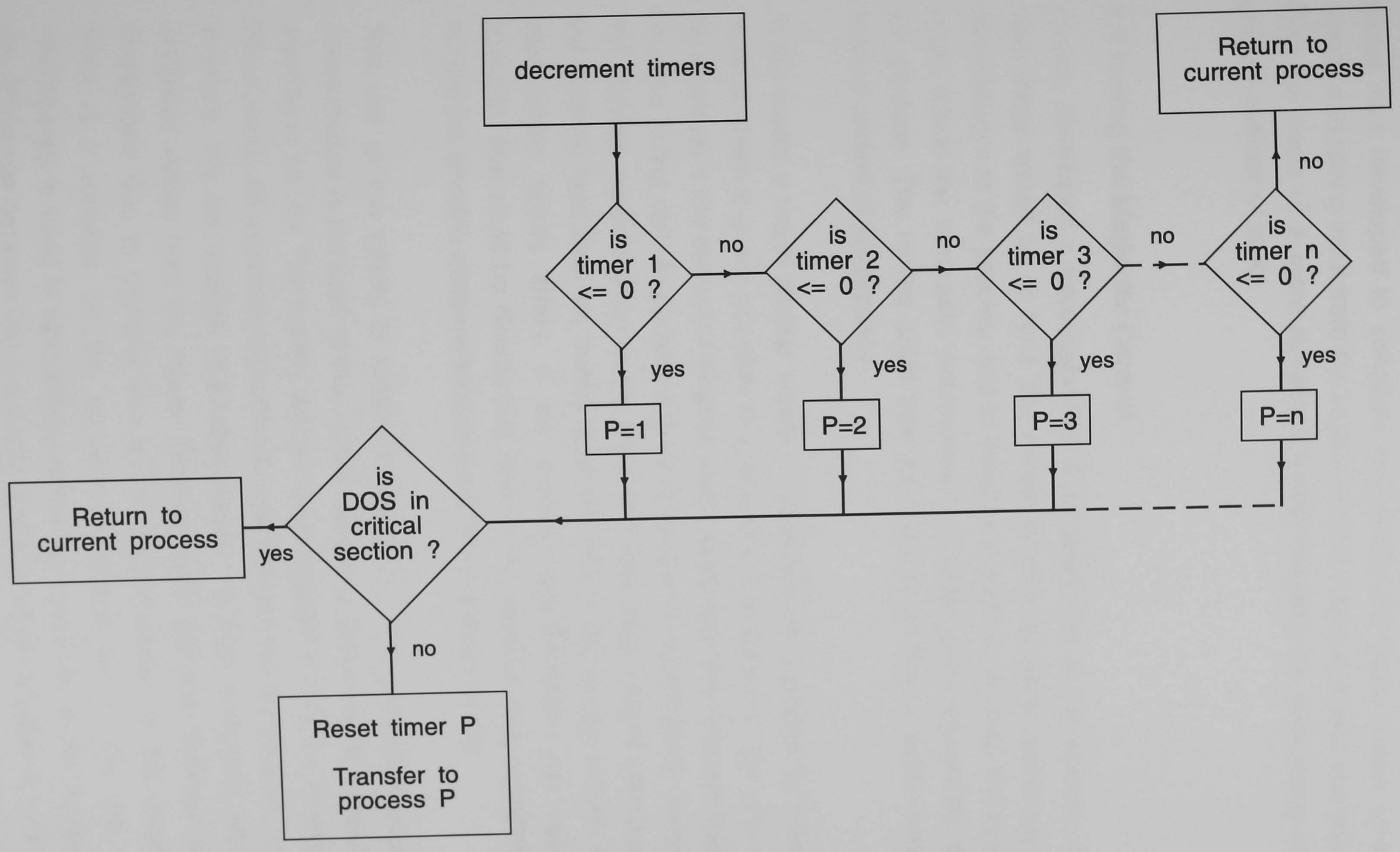

Figure 7.6 Flow Diagram for DOS Task Scheduler

Time did not allow for any more than preliminary work to be carried out on a real time simulation of the aluminium smelter. An elementary real time kernel was developed to schedule two simple I/O tasks writing to the screen and taking input from the keyboard. This was successful and would form the basis of a more advanced kernel allowing the scheduling of a greater number of tasks.

7.3 Tuning the Model for Control

Having developed a successful real time simulation of the process, the next stage would be to tune the model to give accurate responses to disturbances to the process and to develop a method by which the model could adjust the stochastic parameters to achieve good agreement with the process. The model could then be used to provide a much greater level of control of the process.

In the model a much greater variety of variables are available for control, most of which it is not possible to measure continuously on the process. An example is the control of alumina feed based upon the concentration of alumina in the cell. At present it is not possible to continuously measure the alumina concentration in the melt and feed back control methods to the alumina feed time are based upon the rate of rise of cell voltage as it approaches anode effect. If the alumina concentration was known, however, this could be directly fed back to the alumina feed algorithm to control the alumina concentration at much more precise levels.

This use of the model is shown in figure 7.7. The simulated alumina concentration is fed back to the control system to determine the amount of alumina to be fed. The control signal is then passed to both the model and the process. All available measurable parameters from the process, in this example, the cell voltage and temperature, are then compared with the predicted values from the model. Discrepancies will arise between these parameters due to uncertainties in the control action. In this example, there is a variation on the amount of alumina fed to the cell. This discrepancy is used to alter effects of the control action in the model until the difference between the measured and predicted variables is within the required tolerance. The simulation is then continued and this procedure is repeated at the next integration interval.

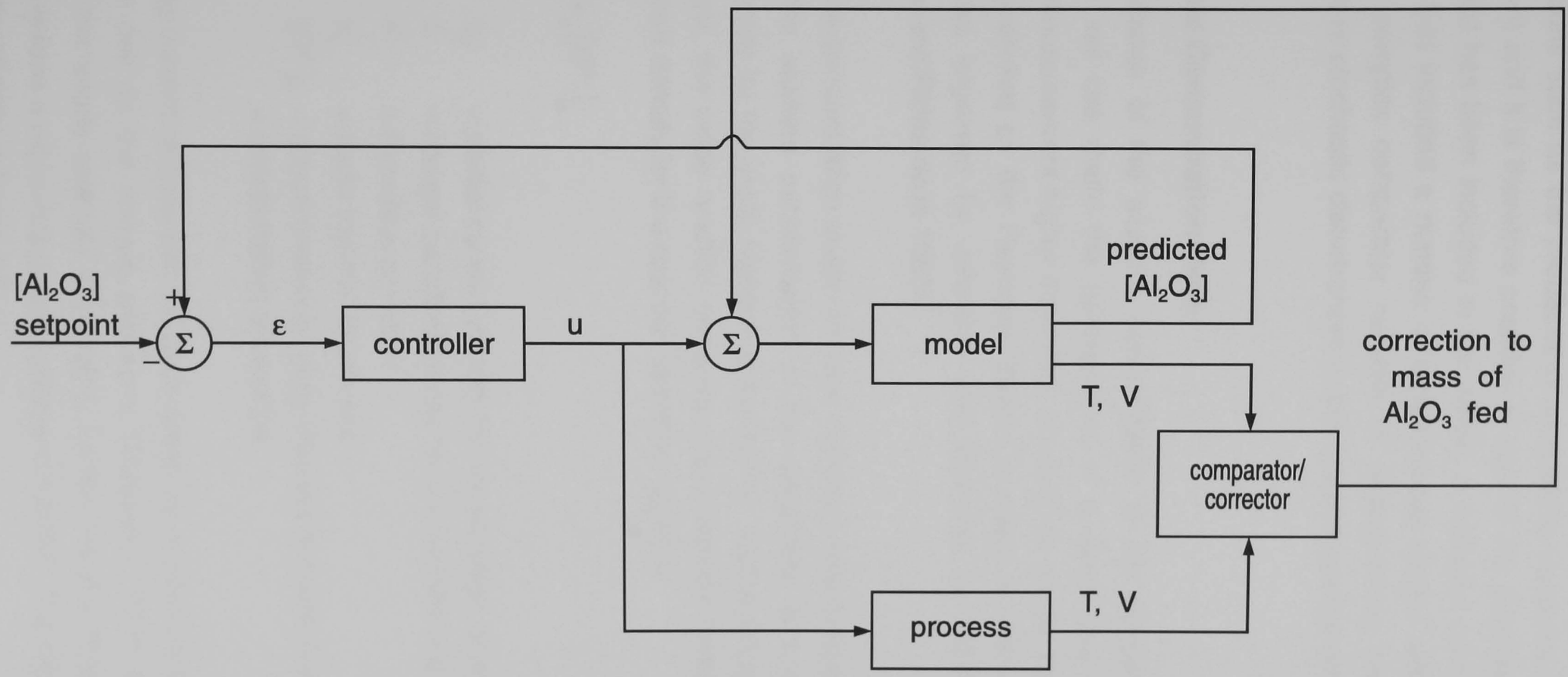

Figure 7.7 Inferential Control

The complexity of the control system in the model is not limited to practical considerations such as the problems of monitoring variables in a hostile environment and it is therefore possible to control the process upon any variable that has been included in the model. A complex control system, however, that included a number of simultaneous control actions would require a complex comparator capable of distinguishing between the effects due to stochastic disturbances to the different control actions.

7.4 Alumina Concentration Meter

The importance of the alumina concentration in the operation of the aluminium cell has made the development of a direct and continuous means of measurement highly desirable. An alumina concentration meter was first patented by the Reynolds Metal Company in 1969[1] and the method was improved by Johnston and Richards in 1974[2] and by Tabereaux and Richards in 1983[3].

The alumina concentration meter employs the electrochemical relationship between the alumina concentration in the electrolyte and the limiting current density for the oxide reaction at the anode. As the cell approaches anode effect, the oxide reaction becomes mass transfer limited and the partial current density for the reaction becomes equal to

$$i_O = z F k_L \left[O^{2-}\right]_b \qquad (1)$$

where i_O = partial current density for the oxidation of oxygen
z = charge transfer number for the reaction = 2
F = Faradays constant
k_L = Mass transfer coefficient
$[O^{2-}]_b$ = concentration of oxide ions in the electrolyte
≡ concentration of alumina

The limiting current density can be determined by monitoring the voltage across the cell as the current density is increased. When the current density at the anode reaches the limiting current density for the oxygen containing anions a rapid increase in voltage will occur. This relationship is shown schematically in figure 7.8.

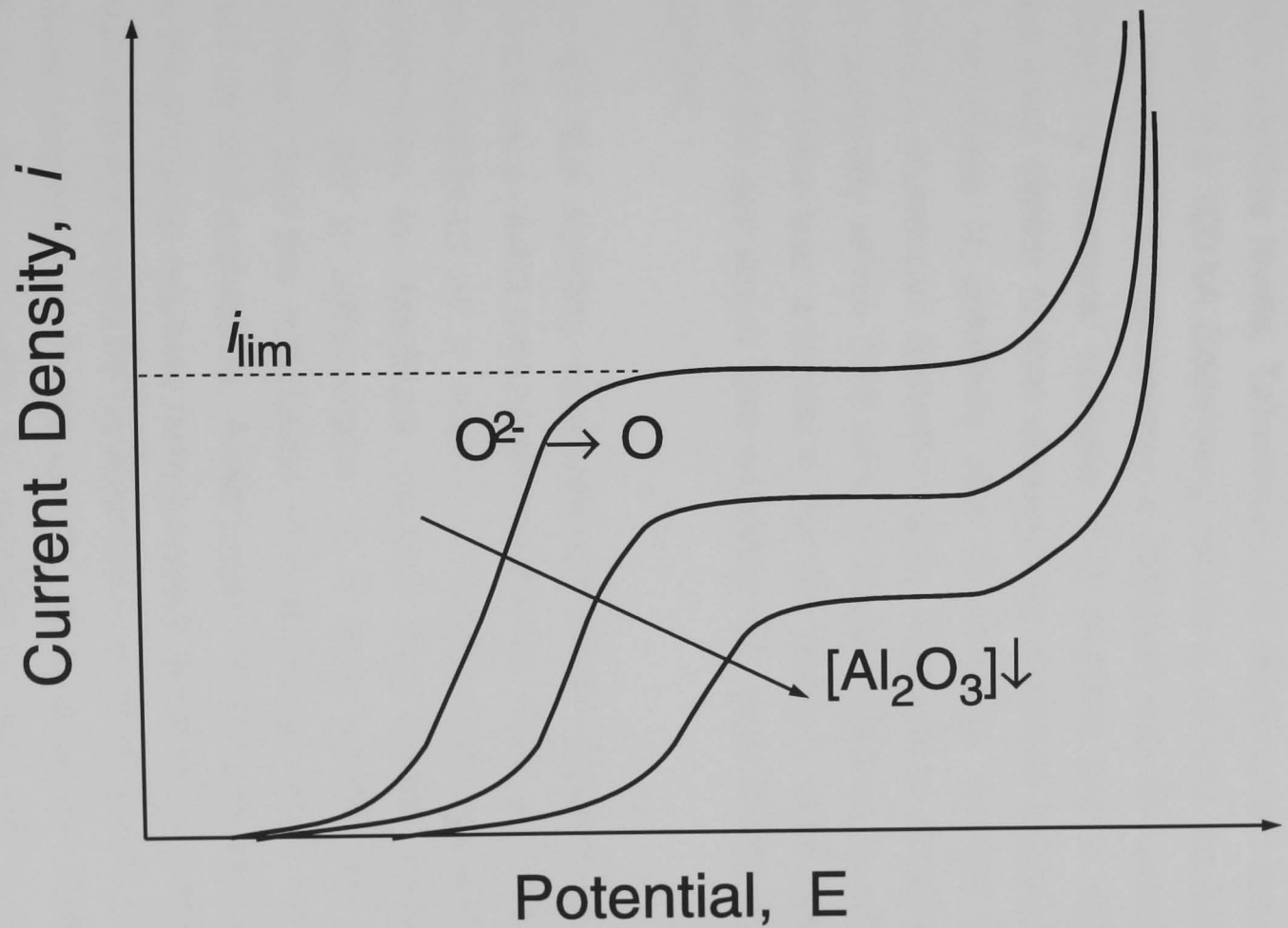

Figure 7.8 Relationship Between Limiting Current Density and Alumina Concentration

The alumina concentration meter comprises a probe, that inserts into the molten electrolyte, and a voltage-current programmer that measures the voltage drop across the probe for a programmed series of imposed current steps. The probe is shown in figure 7.9 and consists of graphite anode and cathode separated with a boron nitride insulator encased in a steel sheath.

After calibration in the laboratory, using synthesised bath and a range of specific alumina levels, Tabereaux and Richards immersed the probe in the bath of a 100 kA Soderberg cell for a 42 hour period and compared the concentration measurements obtained with the probe against those obtained by chemical analysis. The alumina profile obtained with the probe were similar to that obtained by chemical analysis indicating that this technique is generally able to correctly monitor the variation of alumina in aluminium reduction cells. The values obtained by the meter were generally within 0.25 wt% of those obtained by chemical analysis although there was a tendency for the meter to read high after alternate feeds to the cell which was probably due to localised conditions around the probe.

Although the alumina concentration meter appears to be reasonably accurate as a direct measurement device, it has a number of drawbacks when considered as a means of continuously measuring the alumina concentration for feedback control. The hostile environment of the reduction cell is unfavourable to a long service life of this type of instrument and the installation of a probe for every cell in a pot room would be cost prohibitive. Additionally, Tabereaux and Richards indicate that the probe tip required fairly frequent resurfacing to obtain reproducible results and this would be undesirable in a working cell. Finally, the effects of local conditions upon the results obtained by the meter would require that more than one probe be installed in each cell to provide a reliable indication of the general conditions in the cell and this would again be cost prohibitive.

In order to utilise this technique for the direct measurement of alumina concentration it will be necessary to devise a much simpler probe that can be manufactured and installed cheaply and easily within the cell. The approach taken was to incorporate the measurement anode within the

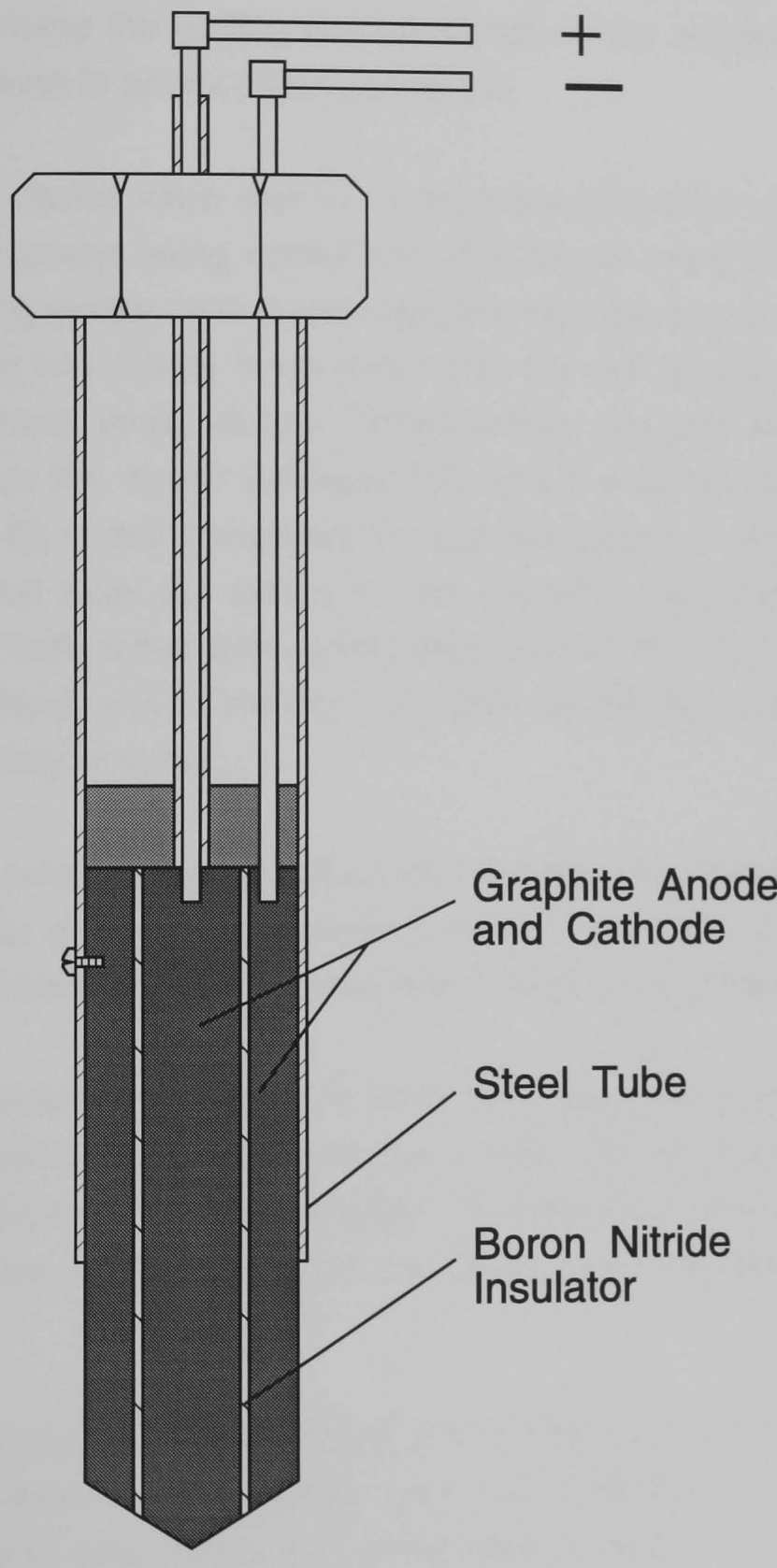

Figure 7.9 Electrolyte Probe for Reynolds Alumina Concentration Meter

prebake carbon anodes used in cell as shown in figure 7.10. The measurement probe consists of a rod of carbon drilled from the anode and then insulated from the main anode by solid cryolite. A potential control device is connected across the carbon rod and the cell cathode and this is used to determine the limiting current density at the anode by forcing the carbon rod alone to anode effect conditions.

Trials of this device were started at Anglesey Aluminium in a half break cell, with the probe being drilled from the anode using the existing drill used for taking quality control core samples from the anode. The core was approximately two inches in diameter with the drill leaving a hole with a diameter around three inches. Unfortunately, the drill was in a fixed position above the anode conveyor belt and it was not possible to fit a long enough bit to drill completely through the anode. In order to obtain a continuous rod from the anode it was therefore necessary to drill the sample from both sides with careful alignment of the drill. This task was extremely difficult and in the time available for the trial only a single rod was successfully obtained.

The rod was inserted back in the anode, and the gap between the rod and the anode was packed with crushed cryolite. The anode was then loaded into the cell normally and the connections made to the potentiostat device.

Although installation appeared to have been successful, the trial did not yield any satisfactory results and the anode was removed early due to poor performance. It was impossible to determine whether the anode failure was due to the insertion of the probe or simply due to the anode itself.

Although this trial was unsuccessful, it is recommended that this research be pursued further. This design for an in-situ alumina concentration meter has a number of advantages over other types of probe:

1. The probe is relatively easy and cheap to manufacture, allowing it to be installed in multiple positions within the cell. This could allow a better estimate of the true bulk concentration than that obtained from a single measurement. The manufacture of the device could be simplified by using a drill designed for the task. It may also be

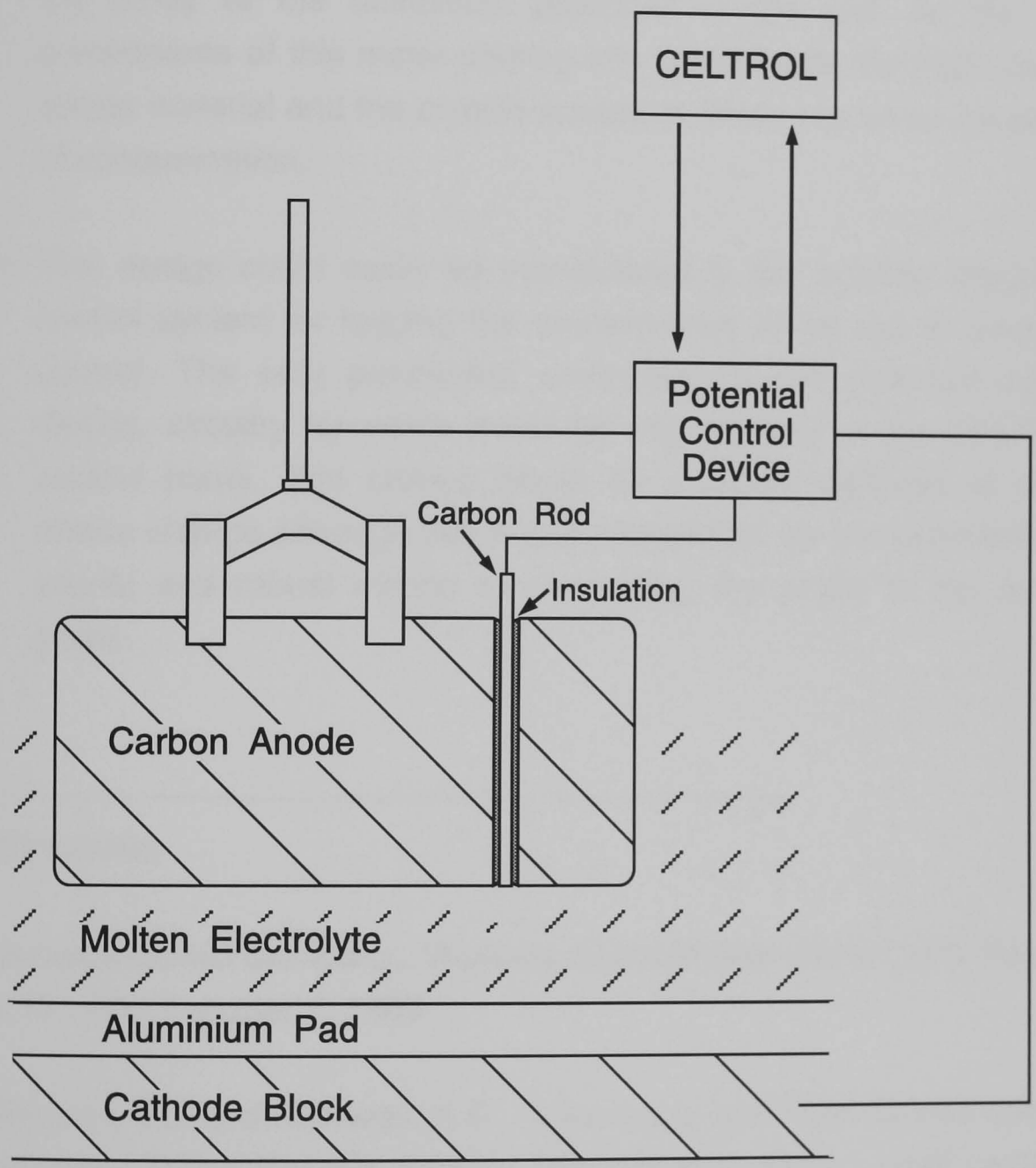

Figure 7.10 In Situ Alumina Concentration Meter

possible to improve the insulation between the probe and the anode by using molten rather than solid cryolite.

2. Due to the highly corrosive nature of the electrolyte, probes containing metal components tend to be dissolved into the bath. Although this can introduce only small amounts of impurities into the system, continuous usage is likely to have a significant effect upon the purity of the aluminium produced in the cell. As the only components of this meter coming into contact with the bath are the anode material and the cryolite insulation, there can be no possibility of contamination.

3. This design could easily be incorporated in the existing distributed control system for logging the concentration or for use in feedback control. The only permanent component is the potential control device, circuitry for which could be incorporated in the CELTROL control panel. The probes would be routinely replaced at every anode change although this would necessitate the development of a simple and robust means of connecting the probe to the control panel.

References

[1] Reynolds Metals Company, *"Alumina Concentration Meter"*, U.S. Patent 3,471,390, October 7, 1969

[2] Johnston, T.J. and Richards, N.E., *"Laboratory and Field Studies with an Improved Direct Reading Alumina Concentration Meter"*, AIME Light Metals, vol 1, 1974, pp94

[3] Tabereaux, A.T. and Richards, N.E., *"An Improved Alumina Concentration Meter"*, AIME Light Metals, 1983, p495-506

Appendix A Initialisation of the Simulation Program

A.1 Initialisation Files

The aluminium reduction cell simulation program, ALSIM, is initialised from two ASCII text initialisation files, one containing the initialisation parameters for the cell model and the other containing the initialisation parameters for the control system, CELTROL. The file used to initialise the model parameters in the simulation of the 'standard' run used in this work is listed below.

At the end of every simulation, the program dumps the model and control parameters to disk in ASCII format. These 'end' files can then be used as the initialisation files for subsequent simulations.

(*This is the end file of a 170 hr run with model 6c. It will be used as
(*an initialisation file for further runs on that model.
DATA
(* Model Version
SIXC
(* Cell type
HALF
(* current A
1.5100E+005
(* random number seed absolute variance on feed ± 20%
 3 2.0000E-001
(* mass of feed g/dump
  2.3000E+004
(* mass of bagged AlF3 added g
  2.5000E+004
(* pad depth bath depth acd cm
 1.2783E+001 1.7027E+001 4.6014E+000
(* ratio wt% alumina wt% CaF_2
 1.2211E+000 2.9064E+000 5.3509E+000
(* Temperatures C
(* bath surrounding cavity crust
 9.7203E+002 2.5000E+001 2.0000E+002 4.0104E+002
(* Anode dimensions cm

18 8.0000E+001 1.3460E+002 4.0000E+001 2.2500E+001 5.0000E+000
1.5600E+000

(* External pot dimensions cm

8.8800E+002 4.0000E+002 4.7800E+001

(* Cathode dimensions cm

8.1000E+002 3.2200E+002 3.8000E+001

(* shell wall thicknesses cm

1.2000E+001 2.2000E+001

(* freeze thicknesses and alumina cover cm

1.2375E+001 6.9079E+000 7.0103E+000 5.0000E+000

(* htc bath, pad, shell, exposed bath W m^{-2} K^{-1}

6.0000E-002 1.0000E-001 2.0000E-003 1.0000E-002

(* htc cavity break padS crust anode W m^{-2} K^{-1}

1.0000E-003 1.0000E-002 1.5000E-001 6.0000E-002 8.0000E-002

(* Thermal conductivity k_{shell} k_{freeze} $k_{alumina}$ W m^{-1} K^{-1}

3.1000E-001 1.0000E-002 4.0000E-003

(* Thermal conductivity k_{bath} k_{crust} k_{anode} $k_{cathode}$ W m^{-1} K^{-1}

2.0000E-002 8.0000E-003 4.4000E-002 8.0000E-002

(* Specific heat capacity cp_{al} cp_{bath} $cp_{alumina}$ J g^{-1}

1.0800E+000 1.6570E+000 2.0000E+000

(* Specific heat capacity cp_{anode} $cp_{cathode}$ cp_{ledge} J g^{-1}

1.5450E+000 1.5450E+000 1.6570E+000

(* Enthalpy of alumina at 473, 1200, 1300 K

1.6400E+004 1.0300E+005 1.1600E+005 1.3000E+002

(* Heats of reaction main reaction, back reaction, anode effect reaction

9.9600E+005 -3.5900E+005 8.0800E+005

(* Alumina heat of dissolution, latent heat of fusion

1.2500E+005 5.5300E+002

(* External Resistances

(* Anode bus, riser+flex Ohms

4.1000E-007 3.8000E-007

(* rod+clamp, stub to anode Ohms/anode

1.0440E-005 1.4580E-005

(* cathode, cathode flex, cathode bus Ohms

2.3000E-006 2.0000E-007 1.2400E-006

(* resistivity of anode

4.0000E-003 6.9000E-003

(* initial masses

(* alumina in suspn, sludge added by anode change aluminium in solution

6.5510E-003 1.6442E+001 2.2000E+004 1.2924E+003

(* dissolution rate parameters k0 temp0

1.2450E-003 1.3830E+003

(* specific areas for alumina in sludge and suspension

7.5000E+001 1.5000E+002

(* sludge factor

5.0000E-001

(* Tafel coefficients for oxide reaction ao bo and anode effect af bf aev

4.7250E-004 6.9500E-005 2.5500E+000 3.0000E+001 5.0000E+000

(* Anode effect bubble parameters thickness,leakage,conductivity

6.1000E-001 1.0000E+000 2.0300E-002

(* Aluminium dissolution parameters kl padvel0 cm/s kco2diss/kaldiss

3.9030E-003 1.3500E+001 1.0000E+000

(* cathodic current efficiency

1.0000E+000

(* beam speed, (up/down)

2.6000E-001 4.0000E-001

(* taprate g/s

5.0000E+003

(* composition of ledge ratio, wt% alumina, wt% CaF2

1.4000E+000 4.0000E+000 4.0000E+000

(* density al2o3, ledge, cathode, alumina

4.0000E+000 2.5000E+000 1.6000E+000 1.0000E+000

(* emmissivity bath, alumina, crust

7.5000E-001 3.0000E-001 5.0000E-001

(* wt% Na_2O AlF_3 NaF in alumina

4.0000E-001 1.0000E+000 2.1000E-001

(* Atmospheric pressure N/m2

1.0133E+005

(* % water in alumina, %H in anodes

2.5000E+000 9.3000E-002

(* anode stub htc and area

7.5000E-003 3.1400E+002

(* collector bars htc and area

6.5000E-003 2.1550E+003

(* htc cathode side and bottom
6.1400E-005 7.0000E-005

(* temperature of cathode layers
9.7271E+002 9.9825E+002
(* last anode changed
7
(* temperature of cold anode
2.0000E+002
(* number of anode slices
2
(* thicknesses of anode layers
1.0000E+000 3.9000E+001
(* factors a, b for fraction of maximum current drawn f=a*exp(bt)
1.7000E-004 6.6900E-005
(* anode #1 f, fraction of current drawn xf thickness of freeze on anode
1.0000E+000 0.0000E+000
(* Temperatures in anode zones Tf, T1, T2, TTop
9.6574E+002 9.5433E+002 9.4292E+002 3.9230E+002
(* anode #2f, xf
1.0000E+000 0.0000E+000
(* Tf, T1, T2, TTop
9.6574E+002 9.5433E+002 9.4292E+002 3.9230E+002
(* anode #3 f, xf
1.0000E+000 0.0000E+000
(* Tf, T1, T2, TTop
9.6574E+002 9.5433E+002 9.4292E+002 3.9230E+002
(* anode #4 f, xf
1.0000E+000 0.0000E+000
(* Tf, T1, T2, TTop
9.6574E+002 9.5433E+002 9.4292E+002 3.9230E+002
(* anode #5 f, xf
1.0000E+000 0.0000E+000
(* Tf, T1, T2, TTop
9.6574E+002 9.5433E+002 9.4292E+002 3.9230E+002
(* anode #6 f, xf
1.0000E+000 0.0000E+000
(* Tf, T1, T2, TTop

9.6571E+002 9.5426E+002 9.4280E+002 3.9225E+002
(* anode #7 f, xf
1.8224E-003 4.6010E+000
(* Tf, T1, T2, TTop
5.6439E+002 5.4695E+002 5.2978E+002 2.9026E+002
(* anode #8 f, xf
1.0000E+000 0.0000E+000
(* Tf, T1, T2, TTop
9.6574E+002 9.5433E+002 9.4292E+002 3.9230E+002
(* anode #9 f, xf
1.0000E+000 0.0000E+000
(* Tf, T1, T2, TTop
9.6574E+002 9.5433E+002 9.4292E+002 3.9230E+002
(* anode #10 f, xf
1.0000E+000 0.0000E+000
(* Tf, T1, T2, TTop
9.6574E+002 9.5433E+002 9.4292E+002 3.9230E+002
(* anode #11 f, xf
1.0000E+000 0.0000E+000
(* Tf, T1, T2, TTop
9.6574E+002 9.5433E+002 9.4292E+002 3.9230E+002
(* anode #12 f, xf
1.0000E+000 0.0000E+000
(* Tf, T1, T2, TTop
9.6574E+002 9.5433E+002 9.4292E+002 3.9230E+002
(* anode #13 f, xf
1.0000E+000 0.0000E+000
(* Tf, T1, T2, TTop
9.6574E+002 9.5433E+002 9.4292E+002 3.9230E+002
(* anode #14 f, xf
1.0000E+000 0.0000E+000
(* Tf, T1, T2, TTop
9.6574E+002 9.5433E+002 9.4292E+002 3.9230E+002
(* anode #15 f, x
1.0000E+000 0.0000E+000 f
(* Tf, T1, T2, TTop
9.6574E+002 9.5433E+002 9.4292E+002 3.9230E+002
(* anode #16 f, xf

```
 1.0000E+000  0.0000E+000
(* Tf, T1, T2, TTop
 9.6574E+002  9.5433E+002  9.4292E+002  3.9230E+002
(* anode #17 f, xf
 1.0000E+000  0.0000E+000
(* Tf, T1, T2, TTop
 9.6574E+002  9.5433E+002  9.4292E+002  3.9230E+002
(* anode #18 f, xf
 1.0000E+000  0.0000E+000
(* Tf, T1, T2, TTop
 9.6574E+002  9.5433E+002  9.4292E+002  3.9230E+002
(* output parameters
(* plot frequency tenth minutes
 10
(* tap file name
al6c3.tap
(* data file name
al6c3.dat
(* Data file output
 ON
(* Tap file output
 ON
(* Printer output
 OFF
(* Autotap switch
 ON
(* tap frequency hrs
 24
(* time to next tap hrs
 22
(* AlF3 addition frequency hrs
 24
(* time to next AlF3 addition hrs
 22
(* Anode Change frequency mins
 1920
(* Time since last anode change
 595
```

```
(* Time for anode out of bath mins
 4
(* Simulation Time hours
 1.7000E+002
(* feedtimer
 25
(* target call cm
 19
(* pad target cm
 14
```

A.2 The User Interface for the Simulation Program

Although the initialisation files allow all the parameters in the model to be initialised, it is a cumbersome method for dealing with those variables that most commonly require changing, for example feed times or target voltage. It also makes the program difficult to operate by anyone without a very detailed knowledge of the initialisation files. In order to facilitate the use of the software, a front end menu system was developed to allow the main operating parameters to be easily changed.

The menu system is accessed by function keys from the top level menu shown below.

Aluminium Reduction Cell Simulation

Control version CELTROL

Model Version SIXC

F1 Output Options

F2 Tapping Schedule

F3 Chemical Additions

F4 Control Variables

F5 Model Variables

F6 Run

F7 Quit

The version of the control algorithms and the cell model linked into the program is listed at the top of the screen for reference. The functions keys allow access to the following menus.

A.2.1 Output options

The output options menu controls the data that is stored by the program, the names of the data files used for storage and the length of the simulation. The frequency at which data is stored is controlled by the *Print Data* option which allows the data to be stored as frequently as every second. This can be used to increase the resolution of simulated events such as anode effect or to reduce the amount of data stored for longer runs.

The simulation will also produce a voltage trace with a three minute interval in the same format as that produced by Anglesey Aluminium control and datalogging system. This can be directed to a printer or to file.

```
                    Output Options

          Simulation Time                    170.0 hrs

          Metal Tap Data to Disc  ON

          Tap File is alsdata\al6d1.tap

          Cell Data to Disc  ON

          Data File is alsdata\al6d1.dat

          Print Data every  1.0 mins

          Voltage Trace to Printer OFF

   PG UP MAIN          SPACE MAIN          PG DN TAP
```

In all these menus, the variable may be changed by pressing the highlighted letter key. The **PgUp** and **PgDn** keys access the previous or next menu respectively. The **Space Bar** returns the user to the main menu.

A.2.2 Tapping schedule

The parameters pertaining to the tapping of aluminium from the cell can be specified from this menu.

Metal Tap Schedule

Metal Tap Rate	5.0 kg/s
Target **P**ad	14 cm
Automatic Tapping	ON
Tap Frequency	24 hrs
Time To **N**ext Tap	20 hrs
Target **C**all	19 cm

PG UP OUTPUT **SPACE** MAIN **PG DN** ADD

The metal tap rate specifies the rate at which the molten aluminium is removed from the cell into the crucible. The remaining parameters pertain to the automatic tapping routine. When the routine is enabled the tapping sequence will be initiated at the specified tap frequency. The amount removed is determined by the deviation of the pad depth from the target pad and is based around the target call parameter. This is the amount of aluminium that should be removed from the cell, expressed as the required depth in the crucible, if the pad depth is at the target.

A.2.3 Chemical additions

The chemical additions menu allows the user to control the amount and frequency of aluminium fluoride added to the cell to maintain the composition of the electrolyte. It is intended that this menu could be extended to include the addition of other compounds, for example lithium fluoride should this be required.

Chemical Additions Menu

Bagged AlF3 Addition **F**requency	24 hrs
Time To Next AlF3 Addition	20 hrs
Mass AlF3 Added	25.0 kg
Time Since Last Anode Change	19.92 hrs
Anode Change Frequency	32 hrs

PG UP TAP **SPACE** MAIN **PG DN** CNTRL

This menu also allows the frequency of anode change to be specified.

A.2.4 Control variables

The control variables menu is a function key driven sub menu that pertains to the control system in the program. This menu is imported from the control module and the menu items available will be specific to the version of the control system that is implemented. For example, a control system incorporating feed back control loops would include menu options for the controller settings.

Aluminium Reduction Cell Simulation

Control Variables Menu

Control version CELTROL

F1 Current and Voltage

F2 Cell Type

F3 Main Simulation Menu

In the standard CELTROL version, this menu allows access to the following sub menus

A.2.5 Current and voltage

This menu allows the line current and initial target voltage to be specified for the simulation.

Line **C**urrent	151.0 kA	
Target **V**oltage	4.39 V	
PG UP CNTRL	**SPACE** CNTRL	**PG DN** CELL

A.2.6 Cell type

The implementation of the CELTROL system is different for half-break and point feed cells. The version of the control module linked into the program therefore defines the cell type that can be simulated. The cell type is displayed for reference.

Cell Type

Cell Type is Half break	
Mass of Alumina Fed	23.0 kg/dump
Base **F**eed Time	67 mins
Time to **N**ext Feed	47 mins
Number of **B**reaks at Feed	2
Number of Dumps at Feed:	
Duct End	4
Tap End	4

PG UP VOLTS **SPACE** CNTRL **PG DN** MAIN

The basic alumina feed control parameters are also specified from this menu. The base feed time is the nominal time between feeds but this may be altered by the control system, for example during search or starve cycles.

A.2.7 Model variables

Just as the control variables sub menu is imported from the control module, so the model variables sub menu is imported from the model

module. Should features be added to the model that require user input it is then a simple matter to include additional menu items the menu system without losing the general menu structure. Only the model module need then be altered.

```
                Aluminium Reduction Cell Simulation

                        Model Variables Menu

                        Model version SIXC


                        F1  Bath Composition

                        F2  Cell Geometry

                        F3  Main Simulation Menu
```

In version SIXC of the aluminium reduction cell model, there are two menu items. These allow the following parameters to be changed.

A.2.8 Bath composition

The bath composition menu allows the initial composition of the electrolyte and the bath temperature to be specified. The alumina is specified in three states, as a weight percentage of dissolved alumina, as a mass of alumina held as agglomerates in suspension and as a mass of alumina in sludge pockets around the edge of the cell.

```
                    Initial Bath Composition

    Bath Temperature                        970.9 C

    Wt Ratio NaF/AlF3                         1.23

    Wt% Calcium Fluoride                       5.1 %

    Wt% Alumina in solution                   4.01 %

    Mass of Alumina in Suspension              0.0 kg

    Mass of Alumina as SLudge                  0.3 kg

PG UP MODEL          SPACE MODEL          PG DN GEOM
```

A.2.9 Cell geometry

The cell geometry menu allows the initial shape of the frozen sidewalls containing the electrolyte to be specified. As well as requiring the average thicknesses of the ledge in the regions of the bath and the metal pad, the depths of the electrolyte and the aluminium pad must be specified.

Auto calculation options have been included to allow the model to be initialised where the ledge data is not available. This assumes that at the start of the simulation, the cell is at steady state and a heat balance is performed to calculate the thickness of the ledges.

The final parameters on this menu are the anode cathode distance and the operating volts at the start of the simulation. These two parameters are interdependent and the user can specify which should be calculated by the program.

Initial Cell Geometry

AUTO **C**ALCULATE OPERATING VOLTS

AUTO CALCULATION OF **S**TEADY STATE LEDGES OFF

Bath Depth	18.8 cm
Pad **D**epth	12.4 cm
Ledge Thickness at Bath	8.6 cm
Ledge Thickness at **P**ad	4.6 cm
Anode to Cathode Distance	4.8 cm
Operating Voltage	4.39

PG UP BATH **SPACE** MODEL **PG DN** MAIN

Appendix B Output from the Simulation Program

In addition to continuously recording the conditions within the simulated cell in data files on the computer disc, the simulation outputs many of the parameters to the computer screen. This allows the user to follow the progress of the simulation and to make changes to some of the parameters should this be required. The format of the output screen is shown below.

```
                    Aluminium Reduction Cell Simulation
                  Model version SIXC  Control version CELTROL

    Day
    TIME  :                          DATA FILE IS alsdata\al6c1.dat
SRCH STRV AVC AET TAP
  X    X   O   X   X                  CELL TYPE            Half-Break
    TapFile alsdata\al6c1.tap         MASS OF ALUMINA FED    23.0 kg/dump
    AUTOTAP  ON                       LINE CURRENT          151.0 kA
    LAST TAP                          CALCIUM FLUORIDE       5.11 %
    TARGET PAD 14 cm                  Wt RATIO NaF/AlF3      1.23 %

 DAY  BATH  PAD TAPPED                Cell Conditions at    0: 2:38
      cm   cm  kg
                                      OPERATING VOLTS       4.39 V
                                      BATH TEMPERATURE       971 C
                                      PAD DEPTH             12.4 cm
                                      BATH DEPTH            18.8 cm
                                      PAD LEDGE              4.6 cm
                                      BATH LEDGE             8.6 cm
                                      ACD                    4.8 cm
                                      WT% AL2O3             3.95 %
PRINTER OFF AVC ON BASE TARGET VOLTAGE  4.39

ALT - A AVC  P PRINTER  Q QUIT  S SCREEN  T AutoTap  V TARGET VOLTS  F10 OTHER
```

The screen is designed to provide information that is generally available to the operators at the cell, either from the CELTROL panel or on chalkboards at the front of the cell. Some additional parameters that it

would be desirable to monitor continuously, for example the alumina content of the electrolyte, are also displayed.

In the top left hand corner of the screen, the status of the various control routines is continuously updated. Reading from left to right these are

SRCH	Search routine
STRV	Starve routine
AVC	Automatic voltage control
AET	Anode Effect Termination
TAP	Tapping routine

An X below the mnemonic indicates that the routine is inactive. In the example above, only the AVC routine is on.

It is possible to change some of the operating conditions interactively, using the keystrokes indicated on the bottom line. These allow the user to enable\disable the AVC routine, to manually tap the cell by toggling the autotap switch, to toggle output to an on-line printer and to change the target voltage for the cell.

The ability to change operating conditions during the simulation allows the user to investigate the behaviour of the cell to disturbances in the system. For example, use of the manual tapping option would allow the effect of over or under tapping to be investigated.

Appendix C. Graphical Presentation of Results

A necessary part of the simulation of a process is the ability to present the data in an intelligible format. For dynamic simulation this generally requires the process variables to be displayed graphically against time.

In the simulation of aluminium cells, the process is being investigated over a long time scale, (typically 5-15 days) and because events lasting only minutes, eg anode effect, must be logged a large amount of data is produced. As the simulation takes along time to run it is desirable to run the simulation on the fastest machine available and to post process the graphs on other available machines.

Whilst there are many sophisticated spreadsheets and graphics packages available most are unable to deal with the quantity of data produced by the aluminium simulation. In order to interpret this data it was therefore necessary to develop a graphics package capable of manipulating the data and producing high quality output. As well as being able to deal with the quantity of data generated, this approach has the advantage of producing graphs in any desired format and is not limited to the rigid types of a commercial spreadsheet or graphics package.

The program was written in Modula 2 to maintain the modular nature of the main program and also to allow the use of text and file modules previously written. Much of the interpretation of the simulation data requires the comparison of the trends of process variables at specific times throughout the simulation. The graphics package was designed to allow up to three graphs to be plotted on one page with a maximum of four data sets per graph. In order to investigate particular features of the model, areas of the graph can be zoomed into and replotted in more detail.

In order to optimise the speed of graphical analysis the program loads as much data as possible into memory and continues from disk once this memory is full. This greatly enhances the speed at which graphs are drawn as much of the time taken in plotting a graph is due to reading data from disk.

Once the required graphs have been produced and investigated on screen, hard copy may be obtained on a Hewlett Packard plotter.

References

Aarebrot, E. et al, Metall. vol 32, no 41, 1978

Abramov et al, *"Theoretical Principles of the Electrometallurgy of Aluminium"*, Moscow, 1953

Arita, Y., Urata., N. and Ikeuchi, H., *"Estimation of Frozen Bath Shape in an Aluminum Reduction Cell by Computer Simulation"*, AIME Light Metals, 1978, pp59

Asbjørnsen, O. A., Andersen, J. A., *"Kinetics and Transport Processes in the Dissolution of Aluminium Oxide in Cryolite Melts"*, AIME Light Metals 1977, pp137-152

Aylward, G. H. and Findlay T. J. V., SI Chemical Data, 2nd Edition, The Jacaranda Press, 1974

Azbel, D.S. and Lee, S.L., *"Two-Phase Momentum Heat Transfer Chemistry"*, Process Eng. Syst., vol 1, p159, 1978

Bagshaw, A. N., Kuschel, G., Taylor, M. P., Tricklebank, S. B., and Welch, B. J., *"Effect of Operating Conditions on the Dissolution of Primary and Secondary (Reacted) Alumina Powders in Electrolytes"*, AIME Light Metals, 1985, pp649-660

Belyaev et al, Izv, Vyssh. Ucheb. Zav., Tsvetn. Met., vol 4, no 3, 1961, p67

Bennet and Meyers, *"Momentum, Heat and Mass Transfer"*, McGraw-Hill, 1962

Berge, B., Grjotheim, K., Krohn, C., Naeumann, R. and Tørklep, K., *"The Influence of Operating Parameters on the Current Efficiency in the Aluminium Reduction Cells"*, AIME Light Metals, vol 1, 1976, pp23

Bersimenko et al, Tsvet. Met., vol 46, no 3, 1973, p30

Blake, S. R., *"A Model for the Variation of Alumina Concentration in Industrial Hall-Héroult Cells"*, MSc Thesis, Department of Chemical Engineering, University of Newcastle upon Tyne, June 1983

Bratland, D., Grjotheim, K., Krohn, C. and Motzfeldt, K., Journal of Metals, vol 19, 1967, pp13

Bratland, D., José del Campo, J. and Cho, K., *"Current Efficiency Measurements in Laboratory Aluminium Cells. Influence of Bath Volume, Anode Size and Anode Quality"*, AIME Light Metals, 1981, pp281-308

Bruggeman, D.A., Ann. Physik, vol 24, 1935, p632

Bullard, G., KACC Research Report, 2nd quarter, 1984

Calandra, A.J., Castellano, C.E., Ferro, C.M. and Cobo, O., *"Experimental and Theorectical Analysis of the Anode Effect in Industrial Cells"*, AIME Light Metals, 1982, pp345-358

Choudhary, G., *"Electrical Conductivity for Aluminum Cell Electrolyte between 950°–1025°C by Regression Equation"*, J. Electrochem. Soc., vol 120, 1973, pp381-383

Dewing, E.W., *"Liquidus Curves for Aluminum Cell Electrolyte v. Representation by Regression Equations"*, J. Electrochem. Soc., 117, 1970, pp780-781

Dow, D.W. and Goodnow, W.H., *"Influence of Operating Variables on Reduction Cell Bath Temperature"*, AIME Light Metals, 1972, pp3-20

Ek, A. and Fladmark, G. E., *"Simulation of Thermal, Electric and Chemical Behaviour of an Aluminum Cell on a Digital Computer"*, AIME Light Metals, 1973, pp85

Entner, P, Scmidt-Hatting, W., Mitrovic, Z., Gruber, U., Rufer, D. and Fjørnes, *"Investigation of the Dynamic Behaviour of Aluminum Pots"*, AIME Light Metals, 1984, pp701

Evans, J.W., Zundelevich, Y. and Sharma, D., Met. Trans, vol 12B, 1981

Fellner, P., Grjotheim, K. and Kvande, K., *"Model Calculations of Cryolite Melts"*, AIME Light Metals, 1984, pp805

Filimonov, S. S., Kryukova, M. G. and Teplov, S. V., Thermal Physics of High Temperatures, vol 2, no 6, 1964, pp901

Firsanova et al, Izx. Vyssh. Ucheb. Zav., Tsvetn. Met., vol 5, no 3, 1962, p52

Frovlova, E.B., Dobrokhotov, V.B. and Tsyplakov, A.M., Trudy V.A.M.I, 89, vol 36, 1971

Gerlach, J., Hennig, U. and Kern, K., *"The Dissolution of Aluminium Oxide in Cryolite Melts"*, AIME Light Metals, vol 1, 1974, pp49-61

Gjerstad et al, Symposium on Industrial Electrode Processes with Gas Evolution, Electrochem. Soc., 1966

Grjotheim K. et al, Can. Met. Quart., vol 11, 1972, p295

Grjotheim, K., Haupin, W. E. and Welch, B. J., *"Current Efficiency--Relating Fundamental Studies to Practice"*, AIME Light Metals, 1985 pp679-694

Grjotheim, K., Kvande, H. and Motzfeldt, K., *"Vapor-Liquid Equilibria in the System NaF-AlF_3-Al_2O_3"*, AIME Light Metals, 1975, pp125-137

Hashimoto, T. and Ikeuchi, H., *"Computer Simulation of Dynamic Behaviour of an Aluminum Reduction Cell"*, AIME Light Metals, 1980, pp273

Haupin, W.E., *"A Scanning Reference Electrode for Voltage Contours in Aluminum Smelting Cells"*, Journal of Metals, Oct., 1971

Haupin, W. E., *"Calculating Thickness of Containing Walls Frozen from Melt"*, AIME Light Metals, 1971, pp188

Haupin, W.E., *"Overvoltages Determined by Nonlinear Regression Analysis of Cell Volts vs. Current Density"*, AIME Light Metals, 1980, pp183-190

Haupin, W. E., *"Mathematical Model of Fluoride Evolution from Hall-Héroult Cells"*, The 4th Int. Course on Process Metallurgy of Aluminium, Trondheim, 1985

Haupin, W. E., *"The 4th Int. Course on Process Metallurgy of Aluminium"*, Trondheim, 1985

Haupin, W.E. and Frank, W.B., *"Comprehensive Treatise of Electrochemistry"*, eds. Bockris, Conway, Yeager and White, Plenum Publishing Corp., New York, 1981, p308

Hertzberg, T., Tørklep, K. and Øye, H.A., *"Viscosity of Molten NaF-AlF_3-Al_2O_3-CaF_2 Mixtures"*, AIME Light Metals, 1980, pp159-170

Hove, S.J. and Kvande, H., *"Centre-Break Alumina Feeding and Sludge Control of Prebaked Cells"*, AIME Light Metals, 1982, pp513

Jain, R. K. et al, *"Interaction of Aluminas with Aluminium Smelting Electrolytes"*, AIME Light Metals, 1983, pp609

JANAF Thermochemical Tables, NRDS, National Bureau of Standards 37

Johnston, A. R., *"Alumina Crusting and Dissolution in Molten Electrolyte"*, AIME Light Metals, 1981, pp373

Johnston, T.J. and Richards, N.E., *"Laboratory and Field Studies with an Improved Direct Reading Alumina Concentration Meter"*, AIME Light Metals, vol 1, 1974, pp94

Kachanovskaya, I. S., Osivik, V. I. and Kukhotkina, T. N., *"Phase Transformations and Alumina Dissolution in Cryolite"*, Tsvetnye Metally, No 12, 1971, pp10-23

Keller, R., *"Alumina Dissolution and Sludge Formation"*, AIME Light Metals, 1984, pp513

Kent, J. H., *"A Review of the Hall-Héroult Process"*, Aluminium and Energy, A 100 Year Partnership Conference and Exhibition, Bangor, Sept 18-19, 1986

Kvande, H. and Rorvik, H., *"The Influence of Bath Density in Aluminium Electrolysis"*, AIME Light Metals, 1985 pp671-678

Less, L. N., *"The Crusting Behaviour of Smelter Aluminas"*, AIME Light Metals, 1976, pp315

Levich, V.G, *"Physicochemical Hydrodynamics"*, Prentice Hall, New Jersey, 1962, pp690-698

Lewis, R. A., *"Technical Fundamentals of the Aluminum Reduction Cell Process"*, Reduction Division Technical Manual I, Kaiser Aluminum Internal Publication, 1973

Lillebuen, B., and Mellerud, Th., *"Current Efficiency and Alumina Concentration",* AIME Light Metals, 1985, p637

Lillebuen, B., Ytterdahl, S. A., Huglen, R., and Paulsen, K. A., *"Current Efficiency and Back Reaction in Aluminium Electrolysis"*, Electrochimica Acta, vol 25, No, 2, February 1980, p131

Maeda, H., Matsui, S., and Era, A., *"Measurement of Dissolution Rate of Alumina in Cryolite Melt"*, AIME Light Metals, 1985 pp763-780

Manaktala, S., "Process Control Techniques for Reduction Cell Operation", AIME Light Metals, 1971, pp165

Matiašovsky, K., Danek, V. and Malinovský, M., *"Effect of LiF and Li_3AlF_6 on the Electrical Conductivity of Cryolite-Alumina Melts"*, J. Electrochem. Soc., 116, 1969, pp1381-1383

Newitt, Dombrowski and Knellman, Trans. Inst. Chem. Engr., vol 32, 1954, p244

Paulsen, K.A., Huglen, R., Andersen, J.A., Lillebuen, B., and Ytterdahl, S.A., *"Variation of Side Lining Temperature, Anode Position and Current/Voltage Load in Aluminium Reduction Cells"*, AIME Light Metals, 1980, pp325-339

Peacey, J. G. and Medlin, G. W., *"Cell Sidewall Studies at Noranda Aluminum"*, AIME Light Metals, 1979, pp475

Plimley, R. E, *"Process Modelling and Optimisation"*, Electrochemical Process Engineering Course, University of Newcastle upon Tyne, 1984

Poole, R.T., Etheridge, C., *"Aluminium Reduction Cell Variables and Operations in Relation to Current Efficiency"*, AIME Light Metals, 1975, pp163-183

Qiu, Z. and Fan, L., *"The Rate Determining Step of Metal Loss in Cryolite-Alumina Melts"*, AIME Light Metals, 1984, pp789

Reynolds Metals Company, *"Alumina Concentration Meter"*, U.S. Patent 3,471,390, October 7, 1969

Richard, M. C., *"Use of a Mathematical Cell Model to Determine Cell Parameter Design Changes for Production Maximization"*, AIME Light Metals, 1975, pp95

Robl, R. F., Haupin, W. E., and Sharma, D., *"Estimation of Current Efficiency by a Mathematical Model Including Hydrodynamics Parameters"*, AIME Light Metals, vol 1, 1977, p185

Rolseth, S. and Thonstad, J., *"On the Mechanism of the Reoxidation Reaction in Aluminum Electrolysis"*, AIME Light Metals, 1981, pp289

Saksvikronnig, T., Valsvik, G., and Hove, S. J., *"Anode Effect Quenching by Anode Tilting"*, AIME Light Metals, 1982, p553-558

Schmitt, H., *"Extractive Metallurgy of Aluminium"*, vol2, Intersci. Pub., New York, 1963, p169

Sides, P.J. and Tobias, C.W., J. Electrochem. Soc., vol 129, 1982, p2715

Sidorov, L.N., Kolosov, E.N. and Shol'ts, V.B., Russian Journal of Physical Chemistry, 42, pp1382-1386, 1968

Solheim, A. and Thonstad, J., *"Heat Transfer Coefficients between Bath and Side Ledge in Aluminum Cells. Model Experiments"*, AIME Light Metals, 1983, pp425

Sulmont, B. and Hudault, G., *"Application of a Thermoelectric Model to the Investigation of Reduction Cell Thermal Equilibrium"*, AIME Light Metals, 1978, pp73

Szekér, Acta Tech. Acad. Sci. Hung., vol 10, 1955, p91

Tabereaux, A.T. and Richards, N.E., *"An Improved Alumina Concentration Meter"*, AIME Light Metals, 1983, p495-506

Thonstad, J., *"The 4th Int. Course on Process Metallurgy of Aluminium"*, Trondheim, 1985

Thonstad, J. et al, Proceedings, 3rd Czech. Aluminium Symposium, Banská Bystrica, 1976, p88

Thonstad, J., Johansen, P., and Kristensen, E. W., *"Some Properties of Alumina Sludge"*, AIME Light Metals, 1980, pp227-241

Thonstad, J., Nordmo, F. and Paulsen, J. B., *"Dissolution of Alumina in Molten Cryolite"*, Metallurgical Transactions, vol 3, February 1972, pp403-407

Thonstad, J. and Rolseth, S., Proceedings of 3rd ICSOBA Conference, Nice, 1973, p657

Thonstad, J. and Rolseth, S., *"Equilibrium between Bath and Side Ledge in Aluminium Cells. Basic Principles"*, AIME Light Metals, 1983, pp415

Thonstad, J., Rønning, S. and Entner, P., *"Formation of Bottom Crusts in Aluminium Pots. A Laboratory Study"*, AIME Light Metals, 1982, pp485

Vasiliadis, C. G., *"Mass Transfer Studies related to Aluminium Electrolysis"*, MSc Dissertation, Oct 1981, University of Newcastle upon Tyne

Vetyukov, M. M. et al, Physical Chem. and Electrochem. of Molten Salts and Slags, Kiev, 1969, pp367

Vetyukov M. M. et al, Isv. Vyssh. Uchebn. Zaved., Tsvetn. Metall., 1978, p62

Waddington, J. and Pearson, T. G., *"Electrode Reactions in the Aluminium Reduction Cell"*, Discussions, Faraday Society, 1947, vol 1, pp307-320

Welch, B.J., *"Energy Balance-Transient Thermal Effects During Cell Operation"*, The 4th Int. Course on Process Metallurgy of Aluminium, Trondheim, 1985

Wilson, C.A and Tabereaux, A.T., *"Alumina Control in Center-Break Cells"*, AIME Light Metals, 1983, pp479-493

Winkhaus, G., *"On the Dissolution Rate of Alumina in Cryolite Melts"*, 99th AIME Annual Meeting, Denver,1970, Paper A70-25

Wittner, H., *"Working Methods for High-Current Efficiency and Flexible Amperage"*, AIME Light Metals, 1975, pp139-150

Wittner, H. and Giulini, Gebr., *"How to run a Smelter with Current Efficiency higher than 90%-Scientific and Practical Basis"*, AIME Light Metals, 1977, pp153-161

Tabereaux, A.T. and Richards, N.E., *"An Improved Alumina Concentration Meter"*, AIME Light Metals, 1983, pp495-506

Zuca, S., Herdlicka, C. and Terzi, M.,*"On Porosity-Overvoltage Correlation for Carbon Anodes in Cryolite-Alumina Melts"*, Electrochimica Acta, vol 25, February 1980, pp211-216

Nomenclature

a_j	activity of species j in the electrolyte
A	area
ACD	anode to cathode distance
c_j	concentration of species j in the electrolyte
c_j^*	saturation concentration of species j
%CE	current efficiency as a percentage
C_f	friction factor
Cp	specific heat capacity
CR	Cryolite ratio = mole ratio NaF/AlF_3
C_s	factor for skewness of velocity profile
d	inter electrode distance
d_c	critical dimension for Reynolds number in the bath
D_j	diffusivity of species j in the electrolyte
D_{em}	equivalent convective diffusivity for metal species in bath
D_m	mean molecular diffusivity of metal species in bath
E	electrical potential
$E^{\varnothing}$	thermodynamic equilibrium potential for a reaction
F	Faraday's constant
f_c	fraction of anode surface covered with bubbles
F_E	mass of fluoride entrained in the pot gases per tonne of aluminium
F_G	mass of gaseous fluoride produced per tonne of aluminium
F_{vp}	mass of particulate fluoride in the pot gases per tonne of aluminium
g	acceleration due to gravity
gap	gap between banks of anodes
GE	scrubber efficiency for gaseous species
Gr	Grashof number
ΔG	Gibbs free energy
ΔH_{fus}	latent heat of fusion
$\Delta H_{R,j}$	heat of reaction j
h	heat transfer coefficient
$H_{diss,\,j}$	heat of dissolution of species j
HE	hooding efficiency
H_j^f	heat of formation of compound j
H_m	depth of metal pad

I	total current
I_j	current associated with reaction j
i	current density
i_j	partial current density associated with reaction j
κ	electrical conductivity
k	rate constant
k_j	thermal conductivity of component j
K_d	equilibrium constant for dimerisation of $NaAlF_4$ vapour
k_L	mass transfer coefficient
K_p	constant of proportionality
k_t	turbulent kinetic energy
L	physical dimension for description of system
M_j	mass of component j
n	number of anodes
N	stirrer speed
ν_f	velocity of anode gases
Nu	Nusselt number
p_j	partial pressure of species j
P_b	barometric pressure
PE	scrubber efficiency for particulates
Pr	Prantl number
P_v	total vapour pressure
q	heat flow
Q_k	volumetric flowrate of stream k
R_i	rate of reaction i
R_j	electrical resistance of component j
R	universal gas constant
Ra	Rayleigh number
rAl_2O_3	radius of Al_2O_3 agglomerate
r_{Alconv}	rate of convective transport of aluminium into the electrolyte
r_{Aldiss}	aluminium dissolution rate
R_b	weight ratio NaF/AlF_3
Re	Reynolds number
R_m	radius of rotation of metal pad
r_m	rate of convective transport of metal into the electrolyte
r_t	theoretical maximum rate of production of aluminium
Sc	Schmidt number

Sc_t	turbulent Schmidt number
S_f	fraction of feed becoming sludge
Sh	Sherwood number
T	temperature
T_0	reference temperature
t_a	thickness of bubble layer at anode
t_d	dead time
t_f	fixed feed time
t_{remelt}	time taken for electrolyte frozen onto a surface to melt
t_s	activation time for solenoids
U	overall heat transfer coefficient
u_t	turbulent viscosity
V	volume
W_j	molecular weight of species j
wt	weight percent alumina in electrolyte
x	thickness of a layer or zone
x_j	mole fraction of species j
x_a	anode width
X_{AlF3}	AlF_3 in electrolyte expressed as a weight percentage excess of that in pure cryolite
y_a	anode length
z	distance normal to the interface
z_j	Charge number
α	Tafel constant
β	Tafel constant
δ	bubble diameter
ε	gas fraction in free bubble layer
ε_{ct}	emissivity in centre trench
η	overpotential
ℓ	inter electrode gap
λ_j	latent heat of fusion of species j
μ	viscosity
ν	interfacial velocity
θ	surface coverage by bubbles at the anode
ρ	density
σ	Stefan Boltzmann constant
$\upsilon_j^{\varnothing}$	molar volume of species j

suffixes

A	Anode
ac	alumina cover
af	frozen layer at anode surface
Al	Aluminium
Al_2O_3	Alumina
Al^{3+}	Aluminium ions
AlF_3	Aluminium fluoride
As	anode surface
b	bath
ba	bath
bf	bath / frozen ledge interface
bt	bath / alumina interface
C	cathode
cav	cavity beneath shields
CO_2	carbon dioxide bubbles
conv	convective
cov	alumina cover on top of anode
ct	centre trench
d	dimer $Na_2Al_2F_8$
diss	dissolution
e	electrolyte
ex	exposed bath
ext	external
F	fluoride ions
f	freeze
g	gas
h	horizontal component
H_2O	water
HF	Hydrogen fluoride gas
hole	hole in the crust
l	liquid
m	monomer $NaAlF_4$
mf	metal pad / frozen ledge interface
$NaAlF_4$	Sodium Aluminium Fluoride
O	oxide reaction or ions
sludge	alumina as sludge at the cathode
stub	anode stub

suspn	alumina in suspension in the electrolyte
tc	centre trench / cavity interface
v	vertical component
vol	volatilisation
W	water
sat	saturation